

**HYDRO CLIMATOLOGICAL STUDIES OF GILGIT RIVER
BASIN PAKISTAN**



MUHAMMAD IRFAN

02-282142-003

Doctor of Philosophy (Environmental Science)

Department of Earth and Environmental Sciences

BAHRIA UNIVERSITY KARACHI CAMPUS

February 2024

**HYDRO CLIMATOLOGICAL STUDIES OF GILGIT
RIVER BASIN PAKISTAN**



MUHAMMAD IRFAN

02-282142-003

**A thesis submitted in fulfillment of the requirements for the
award of the degree of**

Doctor of Philosophy (Environmental Science)

Department of Earth and Environmental Sciences

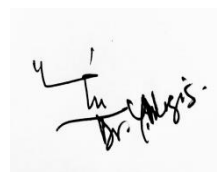
BAHRIA UNIVERSITY KARACHI CAMPUS

February 2024

APPROVAL CERTIFICATE

Scholar's Name: **Muhammad Irfan** Registration No. **27198** Programme of Study: **Doctoral Program in Environmental Sciences** Thesis Title: **Hydro Climatological Studies of Gilgit River Basin Pakistan.**

It is to certify that the above scholar's thesis has been completed to my satisfaction and to my belief, its standard is appropriate for submission for examination. I have also conducted plagiarism test of this thesis using HEC prescribed software and found similarity index 17% that is within the permissible limit set by the HEC for the PhD degree thesis. I have also found the thesis in a format recognized by the BU for the PhD thesis.



DR. YASMIN NERGIS
Professor/Principal Supervisor

Dated _____ February 2024

AUTHOR'S DECLARATION

I, **MUHAMMAD IRFAN** hereby state that my PhD thesis titled **Hydro Climatological Studies of Gilgit River Basin Pakistan** is my own work and has not been submitted previously by me for taking any degree from this university **Bahria University, Karachi Campus** or anywhere else in the country/world.

At any time if my statement is found to be incorrect even after my graduation, the University has the right to withdraw/cancel my PhD degree.



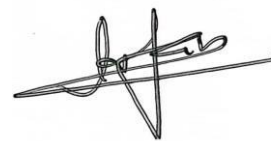
MUHAMMAD IRFAN
Dated: ____ February 2024

PLAGIARISM UNDERTAKING

I, solemnly declare that research work presented in the thesis titled **Hydro Climatological Studies of Gilgit River Basin Pakistan** is solely my research work with no significant contribution from any other person. Small contribution / help wherever taken has been duly acknowledged and that complete thesis has been written by me.

I understand the zero-tolerance policy of the HEC and Bahria University towards plagiarism. Therefore, I as an Author of the above titled thesis declare that no portion of my thesis has been plagiarized and any material used as reference is properly referred / cited.

I undertake that if I am found guilty of any formal plagiarism in the above titled thesis even after award of PhD degree, the university reserves the right to withdraw / revoke my PhD degree and that HEC and the University has the right to publish my name on the HEC / University website on which names of scholars are placed who submitted plagiarized thesis.



MUHAMMAD IRFAN

DEDICATION

To my beloved wife and late mother

Who supported and energized me to accomplish this gigantic task

ACKNOWLEDGEMENT

All praises to Almighty Allah, Who bestowed the man with intelligence, knowledge, sight to observe and mind to think and judge. Secondly, all praise to Allah for giving me strength and courage to complete this vivacious topic. Also for blessing me with great academic capabilities and supportive instructors, family and friends. Peace and blessings of Allah be upon the Holy Prophet, Muhammad (SAW), who exhorted his followers to seek for knowledge from cradle to grave. I wish to express my deepest gratitude to Dr Salma Hamza, Head of Department, Earth and Environmental Science Department, BUKC for providing encouraging environment in the department for undertaking the PhD degree. The credit of my research work goes to my most respectable professor and supervisor, Dr. Yasmin Nergis, Professor and Co-Supervisor, Dr. Mehrab Khan & Dr M Shafiq (SUPARCO) who took me out of my predicament and led to where I am now, able to present my thesis. They lent support, both spiritually and academically, in my education as well as in my thesis. They not only guided but also practically helped me in the face of all hardships. It would not be justified if I do not mention the name of Dr. Mubarik Ali, former HoD and Professor Earth and Environmental Science Department, BUKC, who guided me throughout the field and desktop works of the study. The timely execution of fieldwork would not be possible without his wholehearted and pain taking efforts. I have no doubt in mind that without his sincere interest and curiosity I would not be able to write this report. I

have no appropriate words to manifest my feelings of respect for honorable instructors who provided consistent guidance, inspiration, supervision and encouragement in different sectors during research work. I am thankful to technical staff for their assistance during laboratory/field work. Not to forget Mr. Mughal Sharif for guiding me to perform different tasks in the workstations. My special appreciations to classmates for providing zeal and encouragement throughout the course and especially during the research work. The time spent in the jovial company of Muhammad Idrees and Muhammad Farooq will remain memorable. Last but not the least my special recognition to my wife. Without her cooperation and support completion of this research work would not be an easy task.

ABSTRACT

The hydro-climatological inequalities in Gilgit drainage basin of Upper Indus basin are less technically understood due to various geography, approachability of the region and larger variations in climatic conditions. Glacier change examination and the extraction of catchments at multiple gauges are important tasks in undertaking the drainage basin management studies and are important components of two branches of hydrology viz., hydro-meteorology and snow-hydrology. Satellite remote sensing (SRS) and geographical information system (GIS) provide a very useful method to study the watersheds. In view of the facts, watershed/ natural resources management in the Gilgit river basin, application of geospatial techniques to various elevation datasets is required in order to obtain more accurate results using these elevation datasets. To achieve this goal, the topographic feature extraction has been studied in the catchment of Gilgit River using different Digital Elevation Models (DEMs) viz., Shuttle Radar Topography Mission (SRTM), Advanced Space borne Thermal Emission and Reflection Radiometer Global Digital Elevation Model (ASTER GDEM) and Global Digital Elevation Model of 30 arc sec approximately 1KM (GTOPO30). Several small watersheds for the Phakor, Karamber, East Gammu, Bhort and Bad-e-Swat glaciers were delineated for the basin definition. The delineated watersheds have been visually analyzed against the optical Landsat 8 OLI imagery for mountainous ridge matching. The results revealed that, SRTM 30m (radar based) exhibited more accuracy among these DEMs because of its precise delineation in the Gilgit sub-basin. However, it is appropriate to say that computed area from all three DEMs generally show close

agreement. Temporal analysis of Bhort, Bad-e-Swat, East Gammu, Karamber and Phakor Glaciers has been done using object based classification. Landsat Thermal Mapper, Enhanced Thermal Mapper+ and Operation Land Imagers satellite data for duration of 30 years (1988, 1994, 1999, 2014 and 2018) are used for this study. Thus comparison of glacier temporal extent has been made. It is observed that at large the glaciers in the Gilgit watershed are rather stable. The little variability of glaciers is due to their geographic condition, altitude, topography, orientation and climate conditions. The climatological data analyses of 30 years of Gilgit watershed has also been done to check the selected glaciers stability. A GPS field based land cover class comparison vs classification result for validation of the mapped glacier classes has been performed to check the accuracy assessment through an error matrix method. The kappa coefficient from the error matrix has been calculated to be 84.14%. A worthy support towards better appreciating of the watershed management and the hydrological responses in Gilgit watershed of the upper Indus catchment has been obtained through this study.

TABLE OF CONTENT

<u>APPROVAL CERTIFICATE.....</u>	<u>III</u>
<u>AUTHOR’S DECLARATION.....</u>	<u>IV</u>
<u>PLAGIARISM UNDERTAKING.....</u>	<u>V</u>
<u>DEDICATION.....</u>	<u>VI</u>
<u>ACKNOWLEDGEMENT.....</u>	<u>VII</u>
<u>ABSTRACT.....</u>	<u>IX</u>
<u>TABLE OF CONTENT.....</u>	<u>XI</u>
<u>LIST OF TABLES.....</u>	<u>XV</u>
<u>LIST OF FIGURES.....</u>	<u>XVI</u>
<u>LIST OF ABBREVIATIONS.....</u>	<u>XXIII</u>
<u>1 CHAPTER 1.....</u>	<u>1</u>
INTRODUCTION.....	1
1.1 Basic Terminologies /Concepts.....	4
1.1.2 Glacier Outlines.....	6
1.1.3 Glacier Formation.....	7
1.1.4 Glacier Mass Balance.....	8
1.1.5 Calculation of mass balance using Remote Sensing.....	9
1.1.6 Glacier’s Movement.....	10
1.1.7 Avalanche.....	11

1.1.8	Types of Glaciers by size and location.....	12
1.1.9	Types of Glaciers by Temperature.....	12
1.1.10	Debris Cover Glaciers	13
1.1.11	Supraglacial and Periglacial Debris	14
1.1.12	Morphological classification of glaciers	15
1.1.13	Types of glaciers by their frontal characteristics.....	15
1.1.14	Glacier Surges and Climate Change.....	16
1.1.15	Effect of Glaciers on Land	18
1.1.16	Glacier Speed / Glacier Velocity.....	19
1.1.17	Glacier Hazards	22
1.1.18	Importance of Glacier Mapping	23
1.2	Branches of Hydrology	28
1.3	Study Area.....	30
1.4	Aim and Objectives.....	34
1.5	Study Outcomes	35
1.6	Land Use and Land cover (LULC) in the Gilgit catchment.....	35
<u>CHAPTER 2</u>		<u>38</u>
	LITERATURE REVIEW.....	38
<u>CHAPTER 3</u>		<u>100</u>
	SATELLITE DATASETS	100
3.1	Landsat-8 OLI (Orbital Land Imager) and TIRS (Thermal Infrared Sensor).....	102
3.2	Landsat-7 ETM+ (Enhanced Thematic Mapper)	105
3.3	Landsat-5 MSS (Multi spectral scanner).....	107
3.4	Landsat-3 MSS (Multi Spectral Scanner)	108
3.5	Shuttle Radar Topography Mission (SRTM).....	109
3.6	ASTER GDEM	111
3.7	GTOPO30	113

<u>CHAPTER 4</u>	115
REMOTE SENSING METHODS	115
4.1 Watershed Delineation	115
4.1.1 Flow Direction	116
4.1.2 Flow Accumulation	117
4.1.3 Stream Link	117
4.1.4 DEM Processing and Extraction of Watershed	118
4.2 Glacier Change Analysis through Object Based Classification Method	122
4.2.1 Data Acquisition.....	126
4.2.2 Object Based Classification	126
4.2.3 Segmentation.....	127
4.2.4 Setting Parameters.....	127
4.2.5 Classification/ Glacier Change Detection	127
4.3 Remote Sensing Overview of the Glaciers Selected for Temporal Analysis	128
4.4 Kappa Coefficient	134
<u>CHAPTER 5</u>	138
CLIMATOLOGICAL DATA ANALYSIS	138
5.1 Temperature (Minimum) Profile of Gilgit watershed	141
5.2 Solar Radiation Intensity in the Gilgit Watershed.....	156
5.3 Precipitation in the Gilgit Watershed	171
5.4 Temperature (Maximum) Profile of Gilgit Watershed.....	186
<u>CHAPTER 6</u>	201
RESULT AND DISCUSSION	201
WATERSHED EXTRACTION.....	201
<u>CHAPTER 7</u>	217
RESULT AND DISCUSSION	217
GLACIER CHANGE ANALYSIS	217

7.1	Discussions on Glacier Changes	217
7.1.1	Bhort Glacier	217
7.1.2	Bad-e-Swat Glacier	222
7.1.3	East Gammu Glacier	226
7.1.4	Karamber Glacier	230
7.1.5	Phakor Glacier.....	234
7.1.6	Tabular Presentation of Clean Ice Glacier Area.....	240
7.1.7	Tabular Presentation of Debris Cover Glacier Area	242
7.1.8	Tabular Presentation of Glacier Cover Area (GCA).....	244
7.2	Accuracy Assessment on Mapping of Glaciers.....	246
7.2.1	Error Matrix	246
7.2.2	Overall Accuracy.....	247
7.2.3	Kappa Coefficient	247
<u>CHAPTER 8</u>		<u>267</u>
RESULT AND DISCUSSION		267
COMPUTATION OF GLACIER VELOCITIES		267
8.1	Bad-e-Swat Glacier	272
8.2	Karambar Glacier	274
8.3	Bhort Glacier	276
8.4	Phakor Glacier.....	278
8.5	East Gammu Glacier	280
<u>CHAPTER 9</u>		<u>283</u>
CONCLUSION		283
<u>REFERENCES</u>		<u>288</u>

LIST OF TABLES

Table 2.1 Literature review by relevance to topic	97
Table 3.1 Images used in this study	101
Table 3.2 DEM data used in the study involving the delineation of watersheds.....	102
Table 4.1. Studied glacier of Gilgit watershed.....	128
Table.4.2 Interpretation of Cohen’s kappa coefficient.....	136
Table 5.1 Yearly Low and High values for temperature in oC in Gilgit watershed.....	154
Table 5.2 Yearly Low and High values for solar radiation (in kJ m ⁻² day ⁻¹) in Gilgit watershed.....	169
Table 5.3 Yearly precipitation profile (in mm) of Gilgit Watershed.....	184
Table 5.4 Monthly Low and High values for Maximum Temperature in degree Celsius in Gilgit watershed	199
Table 6.1 Comparison analysis of DEMs	214
Table 7.1 Computed temporal glacier cover area (clean ice) in square kilometers.....	240
Table 7.2 Computed temporal glacier cover area (debris cover) in square kilometers	242
Table 7.3 Computed temporal glacier cover area (combined) in square kilometers	244
Table 7.4 Error matrix	247
Table 7.5 List of Randomly Sampled Ground Truth Reference Data Points for Bhort Glacier	252
Table 7.6 List of Randomly Sampled Ground Truth Reference Data Points for Bad e Swat Glacier	255
Table 7.7 List of Randomly Sampled Ground Truth Reference Data Points for East Gammu Glacier	258
Table 7.8 List of Randomly Sampled Ground Truth Reference Data Points for Karamber Glacier	261
Table 7.9 List of Randomly Sampled Ground Truth Reference Data Points for Phakor Glacier	264

LIST OF FIGURES

Figure 1.1 Main branches of hydrology.....	30
Figure 1.2 The Third Pole (Morello, 2012)	31
Figure 1.3 Study areas	32
Figure 1.4 Elevation distributions in the study area	33
Figure 1.5 Hypsography of the study area.....	33
Figure 1.6 Land use and land cover mapped from the Sentinel-2 satellite imagery for the whole Gilgit sub basin	36
Figure 1.7 The location of five glaciers selected for the temporal study.....	37
Figure 3.1 Artist's rendition of Landsat-8 in orbit. Copyright: NASA [Image Source https://earth.esa.int/eogateway/missions/landsat].....	103
Figure 3.2 Landsat timeline -- Since 1972, Landsat satellites have continuously acquired space-based images of the Earth's land surface, providing uninterrupted data to help land managers and policymakers make informed decisions about our natural resources and the environment [Source https://www.usgs.gov/media/images/landsat-missions-timeline]	104
Figure 3.3 Landsat-7 was launched in 1999. It carries the Enhanced Thematic Mapper Plus 8-band whiskbroom scanning radiometer instrument [Image Source https://earth.esa.int/eogateway/missions/landsat].....	105
Figure 3.4 Landsat- 5 was launched in 1984. It carried the Multi Spectral Scanner and Thematic Mapper instruments [Image Source https://earth.esa.int/eogateway/missions/landsat]	107
Figure 3.5 Landsat 3 was launched in 1978, after the successful launches of Landsat-1 and Landsat 2. These provide the longest records of the earth observation historically. [Image Source https://earth.esa.int/eogateway/missions/landsat]. ...	109

Figure 3.6 Shuttle Radar Topography Mission (SRTM) [Image Source: https://www2.jpl.nasa.gov/srtm/images/bibliography]	110
Figure 3.7 ASTER satellite sensor is one of the five state-of-the-art instrument sensor systems on-board the Terra satellite that was launched on December 18, 1999. [Source: https://www.satimagingcorp.com/satellite-sensors/other-satellite-sensors/aster] Copyright © NASA/Japanese Space Team.	112
Figure 4.1 Flow diagram	120
Figure 4.2 Workflow of the study	125
Figure 4.3 Bhort Glacier	129
Figure 4.4 Bad-e- Swat Glacier	130
Figure 4.5 East Gammu Glacier	131
Figure 4.6 Karambar Glacier	132
Figure 4.7 Phakor Glacier	133
Figure 4.8: Components of Data Research	136
Figure 5.1 Spatial distribution of monthly averaged minimum temperature (in degrees Celsius) for the month of January for Gilgit catchment	142
Figure 5.2 Spatial distribution of monthly averaged minimum temperature (in degrees Celsius) for the month of February for Gilgit catchment	143
Figure 5.3 Spatial distribution of monthly averaged minimum temperature (in degrees Celsius) for the month of March for Gilgit catchment	144
Figure 5.4 Spatial distribution of monthly averaged minimum temperature (in degrees Celsius) for the month of April for Gilgit catchment	145
Figure 5.5 Spatial distribution of monthly averaged minimum temperature (in degrees Celsius) for the month of May for Gilgit catchment	146
Figure 5.6 Spatial distribution of monthly averaged minimum temperature (in degrees Celsius) for the month of June for Gilgit catchment	147
Figure 5.7 Spatial distribution of monthly averaged minimum temperature (in degrees Celsius) for the month of July for Gilgit catchment	148
Figure 5.8 Spatial distribution of monthly averaged minimum temperature (in degrees Celsius) for the month of August for Gilgit catchment	149
Figure 5.9 Spatial distribution of monthly averaged minimum temperature (in degrees Celsius) for the month of September for Gilgit catchment	150
Figure 5.10 Spatial distribution of monthly averaged minimum temperature (in degrees	

Celsius) for the month of October for Gilgit catchment.....	151
Figure 5.11 Spatial distribution of monthly averaged minimum temperature (in degrees Celsius) for the month of November for Gilgit catchment.....	152
Figure 5.12 Spatial distribution of monthly averaged minimum temperature (in degrees Celsius) for the month of December for Gilgit catchment	153
Figure 5.13 Spatial distribution of monthly averaged minimum temperature (in degrees Celsius) – Normalized matrix of yearly profile.....	155
Figure 5.14 Spatial distribution of monthly averaged solar radiation (in kJ m ⁻² day ⁻¹) for themonth of January for Gilgit catchment	157
Figure 5.15 spatial distribution of monthly averaged solar radiation (in kJ m ⁻² day ⁻¹) for the month of February for Gilgit catchment	158
Figure 5.16 Spatial distribution of monthly averaged Solar radiation (in kJ m ⁻² day ⁻¹) for the month of March for Gilgit catchment	159
Figure 5.17 Spatial distribution of monthly averaged Solar radiation (in kJ m ⁻² day ⁻¹) for the month of April for Gilgit catchment	160
Figure 5.18 Spatial distribution of monthly averaged Solar radiation (in kJ m ⁻² day ⁻¹) for the month of May for Gilgit catchment	161
Figure 5.19 Spatial distribution of monthly averaged Solar radiation (in kJ m ⁻² day ⁻¹) for the month of June for Gilgit catchment	162
Figure 5.20 Spatial distribution of monthly averaged Solar radiation (in kJ m ⁻² day ⁻¹) for the month of July for Gilgit catchment.....	163
Figure 5.21 Spatial distribution of monthly averaged Solar radiation (in kJ m ⁻² day ⁻¹) for the month of August for Gilgit catchment	164
Figure 5.22 Spatial distribution of monthly averaged Solar radiation (in kJ m ⁻² day ⁻¹) for the month of September for Gilgit catchment	165
Figure 5.23 Spatial distribution of monthly averaged Solar radiation (in kJ m- 2 day-1) for the month of October for Gilgit catchment.....	166
Figure 5.24 Spatial distribution of monthly averaged Solar radiation (in kJ m ⁻² day ⁻¹) for the month of November for Gilgit catchment.....	167
Figure 5.25 Spatial distribution of monthly averaged Solar radiation (in kJ m ⁻² day ⁻¹) for the month of December for Gilgit catchment	168
Figure 5.26 Spatial distribution of monthly averaged Solar radiation (in kJ m- 2 day-1) normalized matrix for yearly profile for Gilgit catchment.....	170
Figure 5.27 Spatial distribution of monthly precipitation (in mm) for the month of	

January for Gilgit catchment	172
Figure 5.28 Spatial distribution of monthly precipitation (in mm) for the month of February for Gilgit catchment	173
Figure 5.29 Spatial distribution of monthly precipitation (in mm) for the month of March for Gilgit catchment	174
Figure 5.30 Spatial distribution of monthly precipitation (in mm) for the month of April for Gilgit catchment.....	175
Figure 5.31 Spatial distribution of monthly precipitation (in mm) for the month of May for Gilgit catchment.....	176
Figure 5.32 Spatial distribution of monthly precipitation (in mm) for the month of June for Gilgit catchment.....	177
Figure 5.33 Spatial distribution of monthly precipitation (in mm) for the month of July for Gilgit catchment.....	178
Figure 5.34 Spatial distribution of monthly precipitation (in mm) for the month of August for Gilgit catchment	179
Figure 5.35 Spatial distribution of monthly precipitation (in mm) for the month of September for Gilgit catchment.....	180
Figure 5.36 Spatial distribution of monthly precipitation (in mm) for the month of October for Gilgit catchment.....	181
Figure 5.37 Spatial distribution of monthly precipitation (in mm) for the month of November for Gilgit catchment.....	182
Figure 5.38 Spatial distribution of monthly precipitation (in mm) for the month of December for Gilgit catchment	183
Figure 5.39 Spatial distribution of monthly precipitation (in mm) normalized matrix of yearly profile for Gilgit catchment	185
Figure 5.40 Spatial distribution of monthly averaged Maximum Temperature (in degrees Celsius) for the month of January for Gilgit catchment	187
Figure 5.41 Spatial distribution of monthly averaged Maximum Temperature (in degrees Celsius) for the month of February for Gilgit catchment.....	188
Figure 5.42 Spatial distribution of monthly averaged Maximum Temperature (in degrees Celsius) for the month of March for Gilgit.....	189
Figure 5.43 Spatial distribution of monthly averaged Maximum Temperature (in degrees Celsius) for the month of April for Gilgit catchment	190
Figure 5.44 Spatial distribution of monthly averaged Maximum Temperature (in	

degrees Celsius) for the month of May for Gilgit catchment	191
Figure 5.45 Spatial distribution of monthly averaged Maximum Temperature (in degrees Celsius) for the month of June for Gilgit catchment	192
Figure 5.46 Spatial distribution of monthly averaged Maximum Temperature (in degrees Celsius) for the month of July for Gilgit catchment.....	193
Figure 5.47 Spatial distribution of monthly averaged Maximum Temperature (in degrees Celsius) for the month of August for Gilgit catchment	194
Figure 5.48 Spatial distribution of monthly averaged Maximum Temperature (in degrees Celsius) for the month of September for Gilgit catchment.....	195
Figure 5.49 Spatial distribution of monthly averaged Maximum Temperature (in degrees Celsius) for the month of October for Gilgit catchment	196
Figure 5.50 Spatial distribution of monthly averaged Maximum Temperature (in degrees Celsius) for the month of November for Gilgit catchment	197
Figure 5.51 Spatial distribution of monthly averaged Maximum Temperature (in degrees Celsius) for the month of December for Gilgit catchment.....	198
Figure 5.52 Spatial Distribution of Monthly Averaged maximum Temperature - Normalized Matrix for Yearly Profile.....	200
Figure 6.1 Delineated watersheds based on ASTER GDEM 30 m (a) Gilgit basin, (b) Bad-e-Swat glacier, (c) Bhort glacier, (d) East Gammu glacier, (e) Karamber glacier, (f) Phakor glacier	203
Figure 6.2 Delineated watersheds extracted from ASTER GDEM 30 m shown with Landsat-8 background False Colour Composite (FCC) images (R:G:B::7:6:4) of Bad-e-Swat glacier	204
Figure 6.3 Delineated watersheds extracted from ASTER GDEM 30 m, shown with Landsat-8 background False Colour Composite (FCC) images (R:G:B::7:6:4) of Bhort glacier	205
Figure 6.4 Delineated watersheds extracted from ASTER GDEM 30 m East Gammu glacier shown with Landsat-8 background False Colour Composite (FCC) images (R:G:B::7:6:4).....	206
Figure 6.5 Delineated watersheds extracted from ASTER GDEM 30 m Karamber glacier shown with Landsat-8 background False Colour Composite (FCC) images (R:G:B::7:6:4).....	207
Figure 6.6 Delineated watersheds extracted from ASTER - GDEM 30 m Phakor glacier shown with Landsat-8 background False Color Composite (FCC) images	

(R:G:B::7:6:4).....	208
Figure 6.7 Delineated watersheds extracted from SRTM 30 m Gilgit basin.....	209
Figure 6.8 Delineated watersheds extracted from SRTM 30 m shown with Landsat-8 background False Colour Composite (FCC) images (R:G:B::7:6:4) of Bad-e-Swat glacier	210
Figure 6.9 Delineated watersheds extracted from SRTM 30 m shown with Landsat-8 background False Colour Composite (FCC) images (R:G:B::7:6:4) of Bhort glacier	211
Figure 6.10 Delineated watersheds extracted from SRTM 30 m shown with Landsat-8 background False Colour Composite (FCC) images (R:G:B::7:6:4) of East Gammu glacier	212
Figure 6.11 Delineated watersheds extracted from SRTM 30 m shown with Landsat-8 background False Colour Composite (FCC) images (R:G:B::7:6:4) of Karamber glacier	213
Figure 6.12 Delineated watersheds extracted from SRTM 30 m shown with Landsat-8 background False Colour Composite (FCC) images (R:G:B::7:6:4) of Phakor glacier.	214
Figure 6.13 Bhort glacier – Polygons from Figure 6.3 and Figure 6.9 are combined to highlight mismatches) for the comparison of watersheds derived from SRTM (Red) and ASTER-GDEM (Black) shown with background Natural Colour Composite images of Landsat-8	215
Figure 7.1 On way to Bhort glacier (taken on 24 Oct 2020)	219
Figure 7.2 Bhort glacier temporal change extent for the years 1998, 1994, 1999, 2014 and 2018.	220
Figure 7.3 Elevation profile of Bhort glacier.....	221
Figure 7.4 Bad-e-Swat glacier and Lake (shoted on 25 Oct 2020).....	223
Figure 7.5 Bad-e-Swat glacier temporal glacier change extent for the years 1998, 1994, 1999, 2014 and 2018.	224
Figure 7.6 Elevation profile of Bad-e-Sawat glacier	225
Figure 7.7 East Gammu glacier and Lake (shoted on 25 Oct 2020).....	226
Figure 7.8 East Gammu glacier temporal change for the years 1998, 1994, 1999, 2014 and 2018.	228
Figure 7.9 Elevation Profile of East Gammu glacier.....	229
Figure 7.10 Karamber glacier (taken on 25 Oct 2020).....	231

Figure 7.11 Karamber glacier temporal glacier change extent for the years 1998, 1994, 1999, 2014 and 2018.	232
Figure 7.12 Elevation Profile of Karamber glacier.....	233
Figure 7.13 Phakor glacier (taken on 25 Oct 2020).....	235
Figure 7.14 Phakor glacier temporal glacier change extent for the years 1998, 1994, 1999, 2014 and 2018.	236
Figure 7.15 Elevation profile of Phakor glacier	237
Figure 7.16 Centre lines of 5x glaciers	239
Figure: 7.17 Glacier-wise change trends for clean ice.....	241
Figure 7.18 Glacier-wise change trends for debris covered ice	243
Figure 7.19 Glacier-wise change trends combined ice and debris cover... ..	245
Figure 8.1 Glacier velocity vectors in the Karakoram region.....	271
Figure 8.2 Glacier velocities at the marked locations of Bad-e- Swat glacier from 2015-22	272
Figure 8.3 Glacier velocities at the marked locations of Bad-e-Swat glacier from 2018-22	273
Figure 8.4 Marked locations of Bad e Swat glacier and flow direction	273
Figure 8.5 Glacier velocity at the marked locations of Karambar glacier from 2014-22.	274
Figure 8.6 Glacier velocity at the marked locations of Karambar glacier 2019 to 2022	275
Figure 8.7 Marked location of Karambar glacier and flow direction	275
Figure 8.8 Glacier velocity at the marked locations of Bhort glacier from 2014-22....	276
Figure 8.9 Glacier velocity at the marked locations of Bhort glacier 2019 to 2022.....	277
Figure 8.10 Marked locations of Bhort Glacier and flow direction.....	277
Figure 8.11 Glacier velocity at the marked locations of Phokar glacier from 2014-22.....	278
Figure 8.12 Glacier velocity at the marked locations of Phokar glacier 2019 to 2022	279
Figure 8.13 Marked location of Phokar glacier and flow direction.....	279
Figure 8.14 Glacier velocity at the marked locations of East Gammu glacier from 2014-22	280
Figure 8.15 Glacier velocity at the marked locations of East Gammu glacier 2019 to 2022	281
Figure 8.16 Marked locations of East Gammu Glacier and flow direction	281

LIST OF ABBREVIATIONS

AAR	Accumulation Area Ratio
AJK	Azad Jammu & Kashmir
ASTER	Advanced Space-born Thermal Topography Mission
ASTWBD	ASTER Water Body Dataset
AVHRR	Advanced Very High Resolution Radiometer
BII	Basal- Ice -Interface
BPI	Basal - Permafrost Interface
CFF	Cartographic Feature Files. The vector format USFS uses to publish data
DC	Debris Covered
DCW	Digital Chart of the World. A public data set published by DMA in VPF format
DAK	Data Automation Kit an ESRI software package for PC's
DEMs	Digital Elevation Models. Typically produced by USGS in 30 or 10 meter cell size
DTM	Digital Terrain Model, a generic term for software terrain modeling
DRG	Digital Raster Graphic
DBF	Data Base File, the dBase file format, used with SHP
DGN	DesiGN file, the Micro station-drawing format

DWG	DraWinG file, the AutoCAD drawing format
DXF	Drawing eXchange Format an AutoCAD exportfile
EPS	Encapsulated PoScript file a file format favoured for graphics exchange
ESRI	Environmental Systems Research Institute
E00	An ESRI export file
EIA	Environmental Impact Assessments
EOS	Earth Observing System
ETM+	Enhanced Thematic Mapper
GB	Gilgit-Baltistan
GCA	Glacier Cover Area
GCP	Ground Control Points
GDEM	Global Digital Elevation Model
GDEM 003	Global Digital Elevation Model Version 3
GIF	Graphic Interchange Format. An image format commonly used on the Web
GIS	Geographical Information System
GIT	Geographical information technology
GLIMS	Global Land Ice Measurements from Space
GLOF	Glacial Lake Outburst Flood
GRID	Global Resource Information Database
GSI	Geographical Survey Institute
GTOPO30	Global Topographic 30 Arc-Second Elevation Data
HKH	Hindu-Kush Himalaya
INEGI	Instituto Nacional de Estadística Geográfica e Informática
JPG (JPEG)	Joint Photographic Experts Group. An image format commonly used on the Web
LDCM	Landsat Data Continuity Mission
LULC	Land Use and Land Cover

MODIS	Moderate Resolution Imaging Spectroradiometer
MSS	Multi Spectral Scanner
NCC	Normalized Cross Correlation
NDSI	Normalized Difference Snow Index
NIR	Near Infrared
NIMA	National Imagery and Mapping Agency
NSIDC	National Snow and Ice Data Center
NHD	National Hydrologic Data
NSDI	National Spatial Data Infrastructure
NWI	National Wetlands Inventory
OBC	Object Based Classification.
OLI	Orbital Land Imager
PNG	Portable Network Graphic. A new format for Web graphics
RTF	Rich Text Format A generic word processing format
SDE	Spatial Database Engine, an ESRI software package for serving data
SDTS	Spatial Data Transfer Standard. The vector USGS uses for DLG version 3
SIR-C	Space borne Imaging Radar-C
SRS	Satellite Remote Sensing
SRTM	Shuttle Radar Topography Mission
SWIR	Short Wave Infra-Red
SBN	SHaPe files. One of the files that store the spatial index of the features
SBX	SHaPe files. One of the files that store the spatial index of the features
SHP	SHaPe file. An ESRI published spatial data format
SHX	SHaPe files. The file that stores the index of the feature geometry
TIRS	Thermal Infrared Sensor
TM	Thematic Mapper
TIF (TIFF)	Tag Image File Format. An image format commonly used in

	GIS
UIB	Upper Indus Basin
UNEP	United Nations Environment Programme
USAID	US Agency for International Development
USGS	United States Geologic Survey, Department of Interior
WAPDA	Water and Power Development authority
WGI	World Glacier Inventory
WRS-2	Worldwide Reference System-2
X-SAR	X-band Synthetic Aperture Radar

CHAPTER 1

INTRODUCTION

The Indus Basin Irrigation System (IBIS) consists of a number of waterways that supply water to farms and other essential purposes for human and production uses (Bhatti. et.al.2019). This system has three large storage of multipurpose reservoirs, nineteen (19) barrages and twelve (12) canals that interconnected the Indus River. Currently, the Hindu-Kush-Karakorum region of the larger Himalayas accounts for around 80% of the overall average river flows in the Indus system, with the remaining 20% coming from monsoon rain on the savannahs. Climate change may amplify variations in precipitation patterns and timing as well as durational shifts in snow and ice melt. These elements have effects on how basin water resources are managed. One of the main tributaries to the upper Indus basin (UIB) is the Gilgit river basin and therefore of paramount importance for running of IBIS and water needs of human and agricultural consumption.

Except for the Upper Indus Basin, where cool, moist conditions predominate, Pakistan receives in most cases driest and hottest weather in the region of South Asia. On the western boundary of the monsoon, the upper basin and the northern plains enjoy

rather high winter precipitation. The principle sources of water for Pakistan are Indus Basin Rivers, which are also contain headwaters from glaciers and snow fields in addition to runoff of monsoon and aquifers from percolated ground water.

Hydrology or the water pattern of Pakistan extremely depends on the freshwater supply from the Hindu Kush-Karakoram-Himalayas (HKH) through the Indus waterway framework running from north to south the nation over. Therefore, we can say with clarity that glaciers are without any doubt a significant contributor of the water cycle. Climate change phenomenon affects normal accumulation and melting of the glaciers, which in turn impact human life and economy. Mountain/Alp and polar glaciers are committed to continue melting for years or centuries as outlined in the Sixth Assessment Report-AR6 on the basis of physical science of Inter-governmental panel on Climate Change-UNIPCC (2021), contribution of working Group-I (Delmotte et al., 2021). On planet, mountain ecosystems are among the most fragile. Numerous anthropogenic and natural factors, including climate change, population increase, urbanization, economic development, and tourism have posed the serious impacts on the ranges of Hindu Kush, Karakoram, and Himalayan (HKH) mountain habitats (Coppin et al., 2004; Qamer et al., 2016). Increasing temperatures might carry large-scale drought in serious agronomic sections worldwide, risky temperature droplets in some areas and searing heat in others, and municipal turbulence and mass migrations from dispersal uncertainty about water and food provision. In parallel, KHK areas are highly vulnerable to frequent likely catastrophe such as glacier lake outburst flooding (GLOF), flash flood, landslide and debris flow, which further damages mountainous environment (Lasch et al., 2002; Yu et al., 2007; Bajracharya and Shrestha, 2011). Earth worsening in rugged catchment areas is a general happening in developing countries because of scarce planning and mismanagement of watershed belongings. The thoughtful

understanding of land cover dynamics is robust for sustainable environmental, social and economic growth. In a situation, where land and land resources are scarce due to demographic pressures and worldwide climate change, Land Change and Cover (LCC) information is very significant for planning (Shafiq et al., 2017).

Abandoning of approximately all glaciers of the world is being affected from global warming and associated incidences. Glaciers, at large, exist in remote mountainous rugged territories and henceforth are hard to monitor utilizing field apparatus. Glaciers are basically a massive substance of icy weight which moves slowly on the earth. Glaciers are present in all continents except Australia. Snow accumulates over time, solidifies into ice, and then starts to flow outward and downward under the weight of itself. This is how glaciers are created. Precipitation is a crucial component of the highly particular climate conditions needed for glacier formation. This explanation clarifies why glacier changes can be efficiently investigated using remote sensing or spatial analysis. That's what literature review exposed, numerous pixels based supervised and unsupervised classification methodology are available to demarcate the glacier ice. It has been assessed that there are around 5218 glaciers in northern Pakistan (Nabi et al., 2018).

Mostly in the world over, glaciers are the main source of supplying freshwater, exploring the attributes and progressive variations are vigorous for forecasting, progress in water asset protection, flood checking and mitigation events. Further estimated possessions comprise agronomy, improved strength and occurrence of storms, hazardous climate trials, and meal viruses like dengue and intestinal sickness fever. Some properties on together include the regular habitat and humanoid life cycle event now being ascribed to global warming. According to the IPCC 2001 statement

evacuation, sea, variations in precipitation design, enlarged strength and regularity of risky weather conditions activities, are being considered in share to global warming. Additional predictable properties contain Water scarcity, varieties in mountain snowflake, opposite wellbeing properties from hotter temperatures, and the spread of diseases. Increasing temperatures might carry huge scale dry season in serious agronomic sections worldwide, dangerous temperature drops in some areas and burning hotness in others, and municipal turbulence and mass migrations from dispersal uncertainty about water and food provisions.

Before coming to the aim and objectives of the study, it is considered prudent to briefly introduce some relevant terminologies and various relationships/ideas utilized in the research coming later in the thesis. This will surely make the readers more comfortable while studying the results and discussions in later part of the thesis.

1.1 Basic Terminologies /Concepts

1.1.1 Glaciology

Glaciers formed when during many years snow deposited is more than melting that is when accumulation exceeds ablation. If one or all of the features including debris, clouds, shadows and vegetation cover the glaciers, identification and plotting of glacial boundaries in satellite imagery is usually challenging. Debris on glaciers affects the rate of ablation.

Pakistan's Northern region is distributed into 10 important river basins. The basins include from west the rivers are Chitral River, Swat River, **Gilgit River**, Shigar

River, Hunza River, Shyok River, Shingo River, Indus River, Astore River, and Jhelum River which account for 5,218 glaciers in the ten sub-basins. It covers a total glaciated area of about 15040sq.km (ICIMOD-2005 report). This is approximately 11.7 percent of the total geographic area of the ten basins. Indus River Basin is the biggest basin in the HKH milieu of Pakistan and covers around 25 % of the area. Shingo and Astor River Basins is the littlest watershed. These glaciers and frosty lakes offer over 50% of the all-out progression of the Indus framework and are the significant wellspring of water stream for agronomic, modern, and hydro power development in the state.

The easy and increased accessibility of remote detecting equipment with suitable spatial and temporal resolution, worldwide inclusion and low monetary allow for quick, semi-automated, and cost effective assessments of variations in glacier boundaries over vast extents. The essential interpretation of glacial mass increase or decrease is glacier response to worldwide climate.

Changes in glaciers cover due to immeasurable climatic regions round the world, from the Tropics to the Poles have been observed. Impacts of climate change are prominent and noticeable especially in the high Himalaya where warming (0.6°C each ten years) has been a lot more protuberant than the worldwide average of 0.74°C throughout recent years. An advanced repository of significant information on glaciers can improve the capacity to notify strategy originators on the vulnerability, risk alleviation and activity/alteration actions. Specially, for Pakistan where water system organization of nation is vigorously reliant upon the ice melt down in summer time, exact and extensive data on glaciers is of utmost importance for water asset availability and conservation.

1.1.2 Glacier Outlines

A form of snow and ice that settled at the end of season when melt stop is basically a glacier or perpetual snow mass. What all included in it are all streams and connected tributaries that contribute ice/snow to the main glacier. Moreover all debris covered ice is also part of glacier (GLIMS, 2010).

The following outcomes and perceptions should be considered during the delineation of glacier:

- a.** Ice bodies above glaciers that are related to glaciers are to be regarded as a glacier component since it is feed ice (through avalanches) and snow (by creep flow) to the body of glacier.
- b.** A steep rock wall that does not itself hold snow but causes snow to avalanche onto a glacier itself is not regarded as a part of glacier.
- c.** An unmoving ice mass which would still be intact with body of glacier is regarded as a portion of that glacier, even if it supports a deep-rooted growing frost.
- d.** In entire region of the glacier that is covered with debris must be considered as glacier. In general, individual portions of an uninterrupted ice mass should be viewed as independent units and divided at topographic splits if there is no flow or if demarcation of the flow divides is impossible or impractical between different parts of the mass. For practical purposes, an analyst may choose to study such an ice mass as a single component.

- e. To exclude seasonal snow, only mapping to be done after the conclusion of the ablation phase, if possible in a year without snow outside of the glaciers. Then, map each and every connection to the glacier.
- f. An ice shelf has to be regarded as a separate glacier

1.1.3 Glacier Formation

An enormous quantity of snow that is aground and displays proof of existence moving or of when having moved is regarded as a glacier. The change of glaciers is currently dedicated with once again and down to earth interest for people: advances or retreat of glaciers might demonstrate early alerting of worldwide climatic changes. Glaciers occur on all mainland's, excluding Australia, and at essentially all scopes from the jungles to the chutes. High latitudes and high elevations share something common for that, both are cold. Mountain glaciers, for example, those that occur at upper altitudes in middle elevations and rainforest are especially sensitive signs of climatic variation. Glaciers don't simply freeze; they develop by a continuous change of snow into glacial mass ice. A fresh snowfall is a softened mass of irregularly crowded snowflakes, which are small, delicate ice valuable stones that fill the atmosphere. The exquisite stone becomes more solid as the ice becomes grounded for weeks or months, and this entire pile becomes crushed together into a thicker structure known as granular snow. The layer of granular snows is compacted when the snow falls and covers the old snow, forming a considerably thicker type of snow, usually a year or older, with minimal pore space. Further committal and gentle cementation (a cycle in which gems become entwined in a mosaic of buried developing ice precious stones) eventually result in the formation of rock-hard glacier ice.

The entire process could take anywhere from a few months to several years. The snow is generally several meters deep, and the lower layers have turned to ice by the interval. Once the ice has accumulated to a thickness sufficient to allow the ice to transfer gradually under its own pressure, a glacier is formed. When this threshold is reached, the ice begins to flow downwards, whether as a tongue of ice filling a valley or as a dense ice cap flowing out in all directions from the highest central point where the most snow accumulates. Ice melts and evaporates as it moves to lesser elevations in middle latitude areas like Karakorum.

1.1.4 Glacier Mass Balance

Glaciers are lasting snow or ice mass that transport. Most precisely, glaciers should have a region where snow amasses in addition to ablation. Ablation includes all methods that cut the mass of the glacier, such as melting and overflow evaporation, sublimation, and calving and wind erosion. The snow is slowly converted by compression and recrystallization into solid ice while being transferred by gravity to lower elevations where ablation surpasses mass accretion.

The accumulation region is the region on the glacial where snow cover surpasses melting throughout the summer. The ablation area is the lower elevation part of the glacier when ablation levels exceed deposit rates.

The equilibrium line is an imaginary line that connects the accumulation and ablation zones, where accumulation equaled ablation. The glacier grows in volume and generally develops when deposition exceeds ablation. When ablation exceeds deposit,

the glacier thins and/or retreats, losing mass. When ablation equals accumulation, the volume of a glacier remains constant. The difference between the two variables (accumulation and ablation) is called the mass balance.

The mass balance is on positive side and the glacial volume has increased when the amount of snowfall during the winter exceeds the amount of ice and snow melting through the summer time. If there is more of summer time snows melt over winter time snow fall, the mass balance is negative, which results in a reduction in glacier volume. Mass balance is termed in meters of Water equivalent. To determine changes in glacier size, four characteristics are measured: length, area, volume, and mass. Changes in length do not necessarily indicate a shift in mass balance. Mass balance can be determined through satellite images captured during different times throughout the year using RS and GIS techniques.

1.1.5 Calculation of mass balance using Remote Sensing

Development on using the remote detecting strategies for mass equilibrium of the Himalayan glaciers has been slow because of the absence of precise elevation information. The continued availability of present-day DEMs from stereo imagery give few valuable chances to infer mass equilibrium at more limited time scales in the Himalaya, when cautious error evaluations are done. For example, DEMs from 2004 SPOT 5 and 2000 SRTM elevation data were used to analyze mass equilibrium variations in the Indian Himalaya side.

They discovered 8 to 10 m reduction in the snow cover surface at lower elevation, including debris cover tongues, and a smaller reduction in the top portions of the frozen masses (2 m). Focuses in different regions observed a solid reliance of

glacial mass height changes with elevation, with the biggest frosty changes (diminishing) at glacier ends and less changes at higher rises (Racoviteanu et al. 2008).

1.1.6 Glacier's Movement

Glaciers can travel up to 15 meters every day (Gendreau et.al, 2022). The ice on the steeper slopes moves more quickly than the snow on the gentler slopes more down into the valley. These characteristics permit a glacier to replenish the ice lost in the left-over zone. There are two kinds of glacial movement i.e., basal sliding and Plastic flow. Due to basal sliding whole glacial travels as a solid structure. When a glacier lies on a slope, the gravity of the glacial creates pressure. A little quantity of ice melts at the bottom, generating a small film of water that acts as a lubricant, allowing the glacier to drift down the incline. Basal slip can also be caused by movable soil beneath a glacier.

Internal plastic deformation is the most classic process. The weight of the glacier becomes too great to support itself due to internal plastic deformation. This causes snow levels within the glacial to slide, causing the glacier to travel downhill as if it were a deck of cards, with the upper layers sliding faster than the bottom. The bottom strata are exposed to friction as a result of their contact with the earth that delays their mobility. The pace of plastic flow is generally faster than the amount of basal sliding. Because this sort of movement happens in response to gravity and pressure from underlying ice, thicker glacial are much more likely to shift by ductile materials than thinner glaciers. Crevasses are massive fractures on the top of glacial that often form where the glacier drifts the fastest.

Following aspects affect the flow of a glacier:

1. The roughness of the rock surface (friction)
2. The weight of the glacier
3. Ice structure (steepness, thickness)
4. Ice attributes (density, temperature)
5. Glacier slope and geometry
6. Bedrock circumstances (soft, hard, thawed bed or frozen)
7. Hydrology of sub glacial ice
8. Terminal setting (land, sea, ice shelf, sea ice)
9. Weight balance (rate of accumulation and ablation)

1.1.7 Avalanche

Avalanche occur once a large amount of ice or snow suddenly flows down through slope or cliff, occasionally at speeds greater than one hundred and sixty kilometer per hour (160 km/h). These flows consider damaging to both people and property. The most frequent avalanches occur on slopes between 30 and 45 degrees. Anything less than this does not produce sufficient down slope stress, while steeper slopes do not hold sufficient snow to produce significant avalanches. Temperature, the shearing of creeping snow masses, unexpected shocks, especially loud noises, and a combination of these trigger avalanches. Snow patrols in mountainous regions lessen the risk by setting off carefully positioned explosives that result in smaller, less damaging flows. A similar large-scale movement of rock and soil is a landslide. The avalanche is one of nature's most powerful destructive forces, at par with hurricanes, tornadoes, and earthquakes (Gillani 2013).

1.1.8 Types of Glaciers by size and location

Glaciers come in a different types of outlines and extents, ranging from the massive ice cover that spans the full island of Antarctica to little valley glaciers seen around the world. Range in size and location, they are split into many groups.

- a. Ice field, ice caps and ice sheets are the glaciers characterized in size category of glaciers.
- b. Continental, alpine, piedmont and hilly glaciers are characterized in location category.

1.1.9 Types of Glaciers by Temperature

There are two types of glaciers by temperature namely warm and cold glaciers.

a. Temperate (or Warm) Glaciers

A temperate or warm glacier is a glacier that's normally at the melting point, so liquid water present with glacier ice. Temperate glacier melt, area and volume are considerably affected by little or minor variation in temperature (www.USGS.gov). Characteristic of temperate glaciers are:

1. Glacier Ice is at the melting point throughout.
2. Ample flow is continuing character in winter days and in summer season melt water would be abundant.
3. There is a sophisticated drainage system, with moulins, ice lenses, and water pockets.
4. Most mountainous areas outside of the Arctic and Antarctic constituency.

5. The glacier is torn quickly.

b. Cold (Polar) Glaciers

The cold based glaciers also known as Polar are those glaciers at high altitude where temperature of snowfall is far less than below zero degrees. Moreover, during the entire 12 months period of the year temperature of the glacier surface remains extreme below zero degree. These glaciers consequently stay freezing to the bedrock all year and hence there is very small ice progression and ultimately slight loss of ice. Greenland and the Antarctic have cold based glaciers (www.coolgeography.co.uk). Characteristics of cold glaciers are:

1. The temperature is below freezing.
2. Due to freezing upto the bed they erode very little.
3. The polar and sub-polar zones are where they can be found (sub-polar glaciers melts at the surface only in summer days).

1.1.10 Debris Cover Glaciers

Glaciers comprise of sleet, frost, liquid, firm and rubbles material that travel gradually down to slope ward. Many highland arrays, plus the Himalayas (Fushim et al. 1980; Shroder et al. 2000; Bolch et al. 2008a; Hambrey et al. 2008; Hewitt 2009); the Andes and the Alps (Racoviteanu et al. 2008), have valley glaciers that are frequently enclosed in fluctuating volumes of rubble (also known as scree or gravel. (Paul et al. 2004, Ranzi et al, 2004, Bolch and Kamp 2006). The Himalayan glaciers are particularly vulnerable to climate forcing because of their large height range and variable debris cover. The origin of the debris on the glaciers may differ from one location to another. Mainly the happenings, which cause debris cover on glaciers, are:

1. Mass movement from next to mountain gradients
2. Windblown dust
3. Volcanic eruption
4. Salt and microorganisms from sea spray
5. Meteorites
6. Impurities

The two main processes are: first, the 9% volume expansion that occurs when water freezes, which can push the sides of a water-filled pore or crack apart and cause crack extension; and second, the capillary pressure, liquid water may enter into the freezing centers to nourish expanding lenses of isolation ice, which progressively cause the separation of the rock.

Snow and ice avalanching perform an important part in the movement of debris onto glacier surfaces, particularly in tall foothill regions like the Himalayas where heavy precipitation can lead to the accumulation of a lot of snow on precarious slopes (Raina and Srivastava (2008); Benn and Evans (1998)). Large and catastrophic avalanches caused by the collapse of these snow slopes would be sufficient to separate debris from the original rock surfaces.

1.1.11 Supraglacial and Periglacial Debris

Due to their similar spectral responses in the solar reflection zone, supraglacial debris (debris on the glacier) and nearby periglacial debris (debris outside the glacier limit) caused issues with automated mapping and inventorying of glaciers in most of the portions of world sphere (Shukla, et.al. 2010). Supraglacial debris is the glacier that is

why they are cooler than periglacial debris that is adjacent to the glacier. There is a substantial hotness variances occur amongst supraglacial and periglacial debris.

1.1.12 Morphological classification of glaciers

The morphological matrix-type classification was proposed by Muller et.al (1977) for the TTS (Temporary Technical Secretary) to the WGI (World Glacier Inventory). Each glacier is coded as a six-digit number, the six digits being the vertical columns left hand side. This scheme is a simple key for the classification of all types of glaciers all over the world.

Glacier can be written as a six-digit number. For example 520110 represents:

1. 5 for a valley glacier in the primary classification.
2. 2 for compound basins in digit 2.
3. 0 for normal/miscellaneous in frontal characteristics in digit 3.
4. 1 for even or regular in longitudinal profile in digit 4.
5. 1 for snow and /or drift snow in the major source of nourishing in digit 5.
6. 0 for uncertain tongue activity in digit 6.

1.1.13 Types of glaciers by their frontal characteristics

Following are the types of Glaciers with respect to frontal characteristics:

1. Terrestrial glaciers: Glaciers that are entirely supported by bedrock and are not in contact with the ocean or sea.
2. Grounded glaciers: Glaciers that mostly lie on bedrock but may have portions that extend into lakes or the ocean (tide water glaciers).

3. Tide water glaciers with floating tongues are known as floating glaciers.

If there is no longer topographic restrictions, their sideways borders may enlarge or adhere to the sea shore.

1.1.14 Glacier Surges and Climate Change

Abrupt activities of glaciers, called surges or heaves of glacier, happen next to lengthy phases of progressive drive. Surge may last upto three years and travel at more than six kilometers in one calendar year. Surges may be caused by growth in melting of the foundation of the glacier, allowing it to topple quickly, or inconsistent releases of ice that masses up in the middle parts of the glaciers while the lower parts are melting. Surges in the Upper Indus Glaciers are relatively recurrent and disastrous. This is not shocking, in view of the large differential in climate along the length of the glacier, because at places the elevation changes are very hasty. The Kutiah Glacier in Karakorum holds the record for the fastest glacial surge. In 1953, it moved more than 12 kilometers in three months, with an average of about 113 meters per day (Rashid 2003).

Five declared and three other conceivable frosty surges in Karakorum have happened in the previous ten years (Hewitt, 1998), potentially showing crabby reaction to environmental change.

The following significant weather systems have varying influences on the Karakorum:

1. Sub-Mediterranean system of largely winter
2. Westerly storm
3. Summer rainy season
4. Tibetan anti cyclone

Currently, glacier survival is dominated by winter snow storms. However, it has been measured that the summer months account for almost thirty three percent of the accumulation of snow at higher elevation (Hewitt, 1990). Furthermore, the region's overall patterns of advance and retreat are related to changes in the summer monsoon's strength. Other areas with advancing glaciers do not appear to be affected by the potential for such significant changes in the atmospheric bases, administration, and periodic existence of glacier nutrition. This appears to be another aim to pay closer consideration to advancing glaciers in a generally underserved area because the variability of the glaciers is affected by global heat flux.

The climate change is becoming so focused that in the Party of Conference 28 (COP28) major decisions were taken in Dubai where it held in 2023 to reduce its damaging effects on the planet. Following initiatives were taken:

- a. For low carbon climate resistant projects, private sector investment has been fortified by establishment of private market climate capital fund. An amount of \$30 billion has been estimated for contribution to this fund.
- b. To phase out fossil fuel gradually an covenant in the name of fossil fuel phase out agreement has been approved. This agreement made the parties to take out fossil fuel from the energy systems in a smooth and premeditated way. This agreement target 2050 as to have net zero emission from fossil fuel.
- c. For developing countries to cater the effects of climate change like draught, tsunami and biodiversity destructions, a loss and damage fund

has been established. This fund will support already distress countries. An amount of \$700 million initially agreed by the developed countries for this fund.

1.1.15 Effect of Glaciers on Land

Glaciers are powerful forces that shape the Earth's surface. The terrain is affected wherever glaciers flow. Icebergs take excess material as they travel and dump it far away along their pathways, leaving a number of highly recognizable traits that are typical of glaciated places (Bashir and Rasul 2010).

There are two forms of glacial erosion. The first is plucking, which involves large amounts of rocks being eroded and transported. As a glacier advances across the ground, water melts beneath it, seeping through fractures in the hard rock beneath it. This ice melts and flows, loosening the connections that keep bedrock together. These rock fragments can then be collected or ripped from their rock foundation and transported together with the glacial.

Plucking removes boulders and modifies the landscape on its own, but it also adds to the second phase of glaciation, called as abrasion. Abrasion is the process of particles scraping against one other and wearing away. The glacier's massive weight, combined with pebbles and dirt plucked up and adhered to its belly, score and cut the rock surface underneath it. It's almost as though the glacier is sanding the rocks smooth. Glacial striations are lengthy scores left behind by glaciers as they sand the rock in the line of glacial flow. These stretch marks are proof that the area was once covered by a glacier. The path of glacial motion could be extrapolated from these. The quantity of erosion is determined by volume and speed. It erodes slightly more effectively than

water.

1.1.16 Glacier Speed / Glacier Velocity

In recent past glacier / snow hydrology studies the understanding of glacier basal motion is of primary importance. In extreme cases of high basal motion, the glacier ice may decrease and may lead to diminishing. Ice flow, derived by sliding mainly at lower elevation of the glaciers is responsible for the main mass loss from the glacier in a watershed. A driving factor for the rearrangement of a glacier's ice mass, glacier surges can move at speeds of up to 10 to 40 kilometers per year. This could result in increased ice loss, erratic glacier melt, and several hazards for nearby settlements (Hewitt and Liu, 2010; Kanwal et al., 2017; Qaisar et al., 2019; Bhambri et al., 2020). Traditional Weertman sliding connections, which state that the basal shear stress is directly proportional to the sliding velocity, have typically been used to explain the sliding velocity-derived ice flow velocities. These mechanics of glacier sliding have suggested new relationships between shear stress and sliding velocity in contemporary glacier hydrology.

These connections can be categorized using three different mechanisms: (1) form drag, also known as Weertman-type connections, where shear stress rises with sliding velocity and drag is primarily brought on by the ice's viscous deformation around bed irregularities; (2) a transition regime, where shear stress gradually reaches its maximum level before starting to decline; and (3) skin drag brought on by friction between the ice and bed, where shear stress reaches an asymptote (Iverson, 2010).

Both slower-than-normal (quiescence) and faster-than-normal (surge) velocities can affect the Surge-type glaciers. In a basin area where ice flow resistance is greater

than the pushing force, the glacier increases ice mass while quiescent. When the driving force is greater than the repellent force, a surge forms, which frequently causes glacier speed to increase by an order of magnitude in comparison to quiescence speeds. This increase in speed causes an ice swell, which descends the glacier as a kinematic wave (Mayer et al., 2011). If there is a large transfer of ice from the glacier accumulation region to the ablation region, the glacier's terminal will change into the receiving area, thicken, and it may even begin to surge. Although their duration is often brief and their amplitude is relatively low (typically a 20–50% velocity increase), seasonal velocity variations can be understood as a proxy for understanding friction laws. This requires particularly high resolution and quality data. A useful tool for understanding glacier movements is satellite images. It enables monitoring in remote and inaccessible places with a broad spatial coverage and good ground resolution (Gardner et al., 2018; Gardner et al., 2019).

In some cases, the temporal resolution of remote sensing is insufficient to movement map between the acquisitions of two photos, which is often weeks to months apart. As a result, glacier velocities calculated using satellite remote sensing frequently overlook oscillations of below-month time scale, particularly at daily or hourly levels, which can occasionally be significant. Nevertheless, opportunities for glaciology studies exist thanks to developments in algorithms to model, register, and correlate optical images with a sub pixel accuracy (e.g., COSI-Corr, MicMac, ASP, CIAS, Medicis), as well as the expanding number of satellite remote-sensing datasets available (Gardner et al., 2019). Remote sensing technology has the capability to study ongoing glacier surges as well as decadal glacier dynamics and basal movements (Bhambri et al., 2020).

As per IPCC AR6 (Masson-Delmotte et.al.2021) in response to augmented

attentiveness of greenhouse gases in the troposphere the planet is warming. Due to this, glaciers and ice sheet losing great amount of ice mass and disposing of in the world oceans which ultimately raising the sea level. Solid ice discharge and accelerated melting both causing glaciers and ice sheets to lose mass. The movement of ice sheet and glacier, how they will change the sea level state probably the biggest uncertainty to estimate and approximate for the future time to come. In order to measure ice motion on continental scales, one method is to track features in repetitive satellite data (Bindschadler and Scambos, 1991). This method offers in-depth details on the methodology which cause appreciable changes in glacier movement and flow of ice.

NASA's Landsat 4/5/6/7/8, ESA's Sentinel-1 and Sentinel-2, DLR's TerraSAR-X and TanDEM-X used for surface velocities measurement of glaciers. Also using radar images surface velocities can also be derived. Synthetic Aperture Radar Interferometry (InSAR) is the most accurate technique to measure surface velocities. The ability to detect range variations from repeated pass measurements is very sensitive. False or erroneous results are obtained over fast-moving patches of ice or snow due to rapid temporal correlation, which is an issue in interferometry measurement. Offset tracking (amplitude alone) or speckle tracking (amplitude and phase), which are frequently employed in tracking for both Line of Sight (LOS) and along tracking ice movements, provide a good solution to this problem. Additionally, this method is less vulnerable to temporal correlation and phase wrapping issues.

Regional ice velocity mapping is measured by several satellites. The NASA MEaSUREs project is the main initiative to measure ice velocity. Using optical (Landsat 4/5/6/7/8 and Sentinel-2) and SAR (Sentinel-1 satellite data) measurements,

the Inter-mission Time Series of Land Ice Velocity and Elevation (ITs LIVE) generates ice velocity products (image-pair granules, regional mosaics, and data cubes) with global coverage (Gardner et.al. 2018).

A long history of producing high-quality datasets that have enabled new discoveries and aided a diverse set of ice sheet related research is included in the NASA MEaSUREs program. The NASA program included many projects in continuing building on the success of earlier NASA GO LIVE initiative, ITS_LIVE seeks to accelerate ice sheet, ice shelf and glacier science through the generation and distribution of global glacier velocities and elevation at high spatial and temporal resolution with low latency. With the passage of time the field of glaciology is fast transiting from a data sparse science to advance programs supported by numerous NASA, ESA and various international satellite missions that now allow the scientists to study in detail, the cryosphere 's response to changing environmental and basal conditions.

1.1.17 Glacier Hazards

For topographical or political reasons, it is frequently difficult to access the distant areas where glacier and permafrost risks are found (Kääb et al., 2005a). For these reasons, it is necessary to effectively analyze such threats with remote sensing techniques and DEMs of appropriate quality (e.g. Kaab et al., 2003b).

The size, mass, length, and geometry of glaciers change as a result of variations in atmospheric forces, and these changes are frequently linked to glacial risks. In addition to causing infrastructure damage, advancing glaciers can also create new

avalanche hazards by creating new avalanche scenarios. Landslides, rock collapses, and ice avalanches can all be brought on by glacier retreat.

Floods caused by glacial lake eruptions pose the greatest threat to glaciers (Richardson and Reynolds, 2000; Kääb et al., 2005a; Huggel et al., 2002). A common occurrence linked to glacier retreat is glacier lakes. (Clague and Evans 1994, Paul et al., 2007), or supraglacial ponds on flat glacial tongues coated in debris, where small ponds combine to form a lake that can span the width of the glacier (Watanabe et al., 1994, Benn et al., 2000, Komori, 2008). The importance of different mechanisms, such as a rock or ice avalanche reaching a pond and causing an overflowing of water or indeed dam destruction, that in turn makes an explosion flooding or wreckage movement, which could also contact a lesser basin or dam a river in the valley, are common hazards originating from glacier lakes (e.g. Huggel et al., 2004).

One of the primary goals of the GLIMS initiative is to use glacial assessments as support for glacial risk assessments (Kargel et al., 2005). There are a few investigations that employ glacial assessment statistics of hazard assessment.

1.1.18 Importance of Glacier Mapping

Glaciers are nature's sustainable freshwater storage system, benefiting millions of users downwards. The glacial of the Hindu Kush-Karakorum-Himalaya (HKH) region, on the other hand, have been retreating in response to rapid climate change during the middle half of the twentieth century, resulting in the formation of several glacial lakes near the glacial terminal (Mool et al., 2001). Rapid water assemblage in these ponds could cause unstable moraine dams to burst, releasing substantial quantities of water

and detritus downstream, inflicting casualties, land, and destruction of vital forested and grazing reserves, croplands, and expensive alpine structures.

Glacier and permafrost dangers begin from distant districts that are frequently challenging to entree for geographical or administrative causes (Kääb et al., 2005a). Because of these reasons, remote detecting methods and DEMs of adequate worth are expected to survey such risks (e.g.Kääb et al., 2003b).

Changes of the atmospheric forces impact the size, mass, length and math of glaciers changes that are frequently linked with glacial mass dangers. For example, thrusting glaciers can annihilate infrastructure and in other way cause new threat possibilities by bringing about new circumstances for ice avalanches. Glacier retreat can likewise cause Ice landslides, avalanches or rock falls.

The most threatening glacier danger is flooding produced by glacial lake outburst flood (e.g., Huggel et al., 2002; Richardson and Reynolds, 2000; Kääb et al., 2005a). The creation of glacier lakes is a common occurrence linked with glacial mass retreat. Glacier retreat can guide to the creation of moraine inhibited glacier lakes, which can cause outburst floods (GLOFs) upon failure of the dam. GLOF is disastrous to people existence and setup in far reaching areas. Therefore, isolating of likely lake sites and forecasting the growth of existing lakes is crucial for in time monitoring/ investigating and vindication of such threats.

Clague and Evans (1994, 2000, Paul et al., 2007) found that glacier mass ponds can occur at the front or borders of a glacier mass, or as supraglacial ponds on level,

floating debris and jetsam-covered glacier mass tongues (Watanabe et al, 1994; Komori, 2008; Benn et al, 2000).

Perils originating in glacier lakes frequently involve the interaction of multiple cycles, such as a stone or ice rainstorms slide that reaches at a lake and creates overflowing of water or even dam impairment, resulting in an eruption overflow or waste flow that may stretch to a lesser pond or dam a waterway system in the meadow (Huggel et al., 2004).

Involving glacial mass inventories as a help for glacial mass peril appraisal is, for example, among the principal points of the GLIMS drive (Kargel et al., 2005). Several investigations exist which utilized such glacier stock information with regards to glacial mass danger appraisal.

After deeply understood the terminologies and terms used in the study now come to the topic of research work. The glaciers are nature's inexhaustible storage facility of new water that paybacks to countless individuals living downstream. The glaciers of the Hindu Kush-Karakorum-Himalaya (HKH) locality, in any case, are withdrawing notwithstanding sped up a dangerous atmospheric deviation since the last part of the twentieth hundred years and have added to the production of numerous cold lakes on the new glacial mass end (Mool et al., 2001). Quick gathering of water in these lakes can prompt abrupt penetrating of the unsound moraine dams stopping colossal measures of water and trash causing misfortune life, property and annihilation of important timber land and field assets, farm lands, and expensive mountain frameworks downstream.

Rasul et al. (2011) found that the temperature increase in Pakistan over the last 40 years was 0.76 degrees Celsius, whereas the temperature rises in mountain areas with dozens of glaciers was 1.5 degrees Celsius. Variations in glacier performance have resulted in the formation of fresh ponds and the expansion of the volume and size of older ponds. Therefore, the likelihood of unexpected release of water from these ponds usually recognized as Glacial Lake Outburst Flood (GLOF) has increased which strengthens with alteration in pattern of precipitation (Awan, 2002; Din et al., 2014). Besides melting of glaciers there is evidence that further 35 glaciers of Karakorum are evolving with excellent heaves/surges (Hewitt et al., 2009).

Presently the climate monitoring facilities are meager and substantial data availability source is GIS/remote sensing. Fresh water stored in the glaciers of the Gilgit basin in the Karakorum and Hindu Kush Mountain ranges is an important source for water supply and irrigation in Pakistan, providing headwaters to the Indus River and other major rivers. Accelerating shrinkage of glaciers due to global warming will adversely affect freshwater availability. This is an important motivation for improving the observations of the climatology of the region. Due to the difficult access and the large extent of glacier regions, fields-based observations of climate parameters are difficult worldwide. Therefore, satellite-based Earth observation, providing repeat coverage at regular time intervals, is a main information source for studies and monitoring.

The typical profile of any basin drainage, quantitatively, may be studied by calculations of linear, relief and aerial aspect (Pareta, 2011). Drainage morphology of

basin as well as sub-basins in various parts of the earth has been assessed via geomorphologic orthodox tactics (Rai et al., 2017). Geographical information technology (GIT) / geographical information system (GIS) approaches with different satellite data have allowed the feasible stage for analyzing morphometric aspects and geography of a drainage set ups (Wakode et al., 2013).

Morphometric investigation of drainage organization is exceptionally valuable and plausible in appraisal of hydro-climatological varieties, flood risk the executives, watershed the board and water asset potential (Ahmad et al., 2018). In any case, it is problematic to concentrate on all left-over organizations through ground perception or from study brought about by their reach all over uneven landscape in the monstrous locality especially in rough regions (Huggel et al., 2002). Acknowledgment of seepage framework inside basin too as sub-bowl can be achieved utilizing exceptionally created methodology DEMs, such as the Shuttle Radar Topography Mission (SRTM), Advanced Space-born Thermal Topography Mission, and Global Elevation Model (ASTER-GDEM). These DEMs were utilized to divide the seepage framework, the Gilgit basin or bowl region, and the shape of very small watershed/catchments limits (Ali et al., 2017; Pareta , 2014).

In Gilgit the hydro-climatological discrepancies of watershed of Upper Indus sink aren't as much of technically implicit because of numerous inaccessibility of the area, geography and greater dissimilarities in climatic conditions. Withdrawal of catchments at numerous gauges is a significant job in endeavor the watershed administration trainings. Topographical data innovation (GIT) and satellite remote detecting (SRS) deliver an identical valuable technique to concentrate on the

watersheds. In light of the real factors, watershed normal assets administration in Gilgit waterway basin, utilization of geospatial strategies to various height datasets is fundamental in order to get additional precise outcomes by method for these upsurge datasets. To achieve this objective line, the geographical component deliberation has been considered in the watershed of Gilgit River by implies of diverse Digital Elevation Models (DEMs) viz., ASTER, SRTM, GTOPO30 and GDEM.

For the sink description, numerous small streams for the Karamber, Phakor, Bhort, East Gammu, and Bad-e-Swat glacier were reported. In contrast to the optical Landsat 8 OLI picture for hilly ridges identical, the stated watersheds have been examined. Due to its excellent results in the Gilgit sub-basin, the SRTM 30m (radar-based) DEM was found to be more accurate among studied DEMs. Nonetheless, it is reasonable to conclude that the computed parts of all three DEMs frequently show nearby contract. A better knowledge of watershed management and hydro logical results in the Gilgit watershed of the upper Indus catchment is made possible by the research which presented here. Numerous research groups have mapped the glaciers of the Gilgit watershed as a whole and computed the percentage of glacier cover. Latif et al., (2020) calculated the glacier cover to be 9%, Hasson et al., (2014) and Ali et al., (2017) calculated it to be 8%. So far, no studies have been found to investigate the change analysis at the individual glacier level.

1.2 Branches of Hydrology

The research of the occurrence, spreading, flow, and characteristics of water is known as hydrology, in all its forms, of the earth. Traditionally the science of hydrology has been understood as a science of flowing water. With the evolution of knowledge,

towards the recent era of rationalization, theorization, and computerization, the subject of hydrology became very broad and was sub-divided into further branches and sub-fields. The hydrology also includes the formation of clouds, rainfall, snowfall, snow melt and refreezing into ice. The driving forces in the hydrological sciences are sun, soil, air, and water. With its potential to improve society's ability to make decisions and solve issues, GIS is regarded as one of the most significant emerging technologies. For use in hydrologic modeling, GIS offers a digital representation of watershed properties. The fundamental benefit of GIS for very vast areas is its capacity to integrate, analyze, and manage massive volumes of data. The primary usage of GIS applications in hydrology is watershed study. Hydrological models need a large amount of input data, including information on soil cover, geography, weather, geology, and water in solid form. To assess local variations in land use, such as urbanization and large-scale agriculture GIS can be used for accurate calculation. By examining the earth's surface or atmosphere from space using satellites (space-born) or from the air using aircraft, remote sensing and GIS are inextricably linked (airborne). For the study of the ionosphere, meteorology, climatology, and wind direction and speed, weather radar is used. In Figure 1.1, the names of the hydrological branches are listed. The research in this thesis is pertinent to the sub fields of snow hydrology and glacier hydrology.

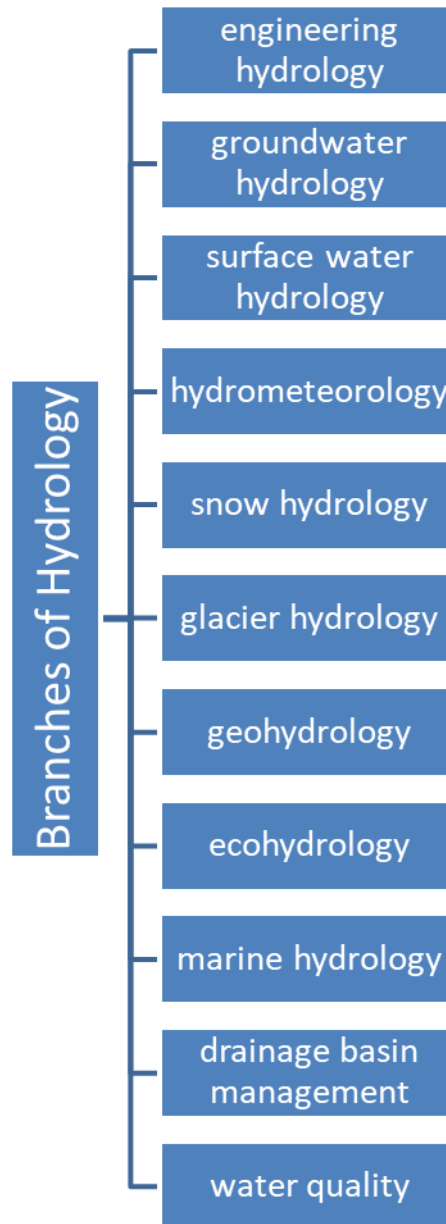


Figure 1.1 Main branches of hydrology

1.3 Study Area

Gilgit basin is a significant source of freshwater in Pakistan's HKH region, situated in the northern part of the country (Figure 1.2). The HKH region encompasses all or sections of Bhutan, Afghanistan, China, Bangladesh, Nepal, India and Pakistan, and is known as "the third pole" in South Asia (Zhen and Li, 1998). Many of Asia's major rivers, along with the Indus, Ganges, and Brahmaputra, originate in this region.



Figure 1.2 The Third Pole (Morello, 2012)

Between $72^{\circ}25'02''$ E and $74^{\circ}19'25''$ E, and $35^{\circ}46'05''$ N and $36^{\circ}51'16''$ N, the Gilgit watershed is located. The geographical watershed region is 13,552 square kilometers, with elevations ranging from 1388 to 6722 meters (Ali et al., 2017; 2019), and same is shown in Figure 1.3. Using elevation data from the Shuttle Radar Topography Mission (SRTM) at one-arc second resolution Gilgit watershed is shown in Figure 1.4 depicts the Gilgit watershed's altitude variation. Similarly, Figure 1.5 shows the hypsography of Gilgit Basin study area.

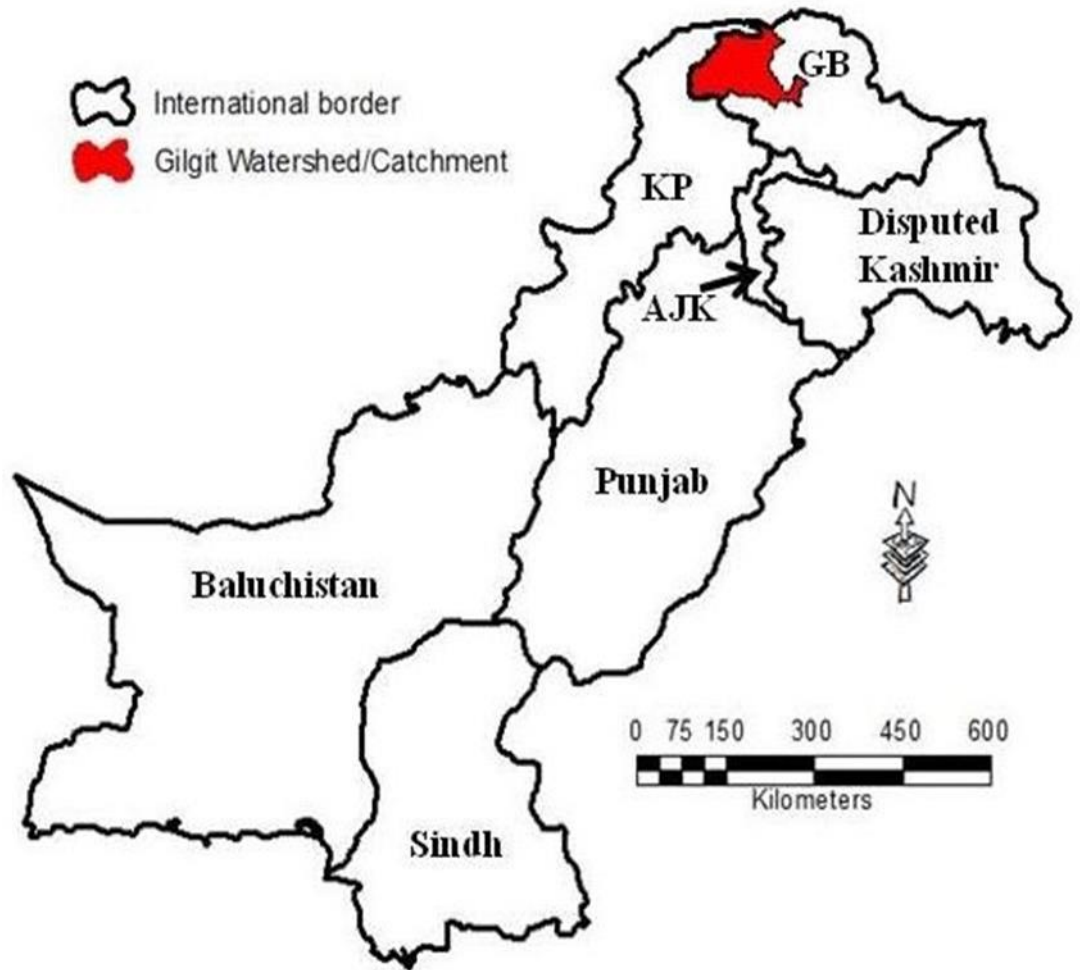


Figure 1.3 Study Area

The glaciers are mostly found between 3500 and 5500 meters above sea level. Gupis, Puniyal, Phandar, Gilgit, Ishkoman, and Yasin are among the 6 main basins in the research area. Phandar, Yasin, and Ishkoman are three small rivers/lakes that join to form the Gilgit River (Ali et al., 2019; Mukhopadhyaya and Khan, 2015). The printed publications and bibliographies are lacking in hydro-climatological studies of the Gilgit region. With just five weather stations in the territory, including Gilgit, Gupis, and WAPDA met stations at Shandure, Ushkore, and Yasin, the area is inadequately measured (Adnan et.al., 2017; Hasson et al., 2017). This facility frequency is substantially lower than that in developed countries of the world, such as Switzerland,

in which there is one temperature monitoring station per 475 square km and one precipitation station per 100 square km (Gubler et al., 2017). In general there are more weather stations density in developed countries compares to developing countries such as India, Sri Lanka, Nepal and Bangladesh.

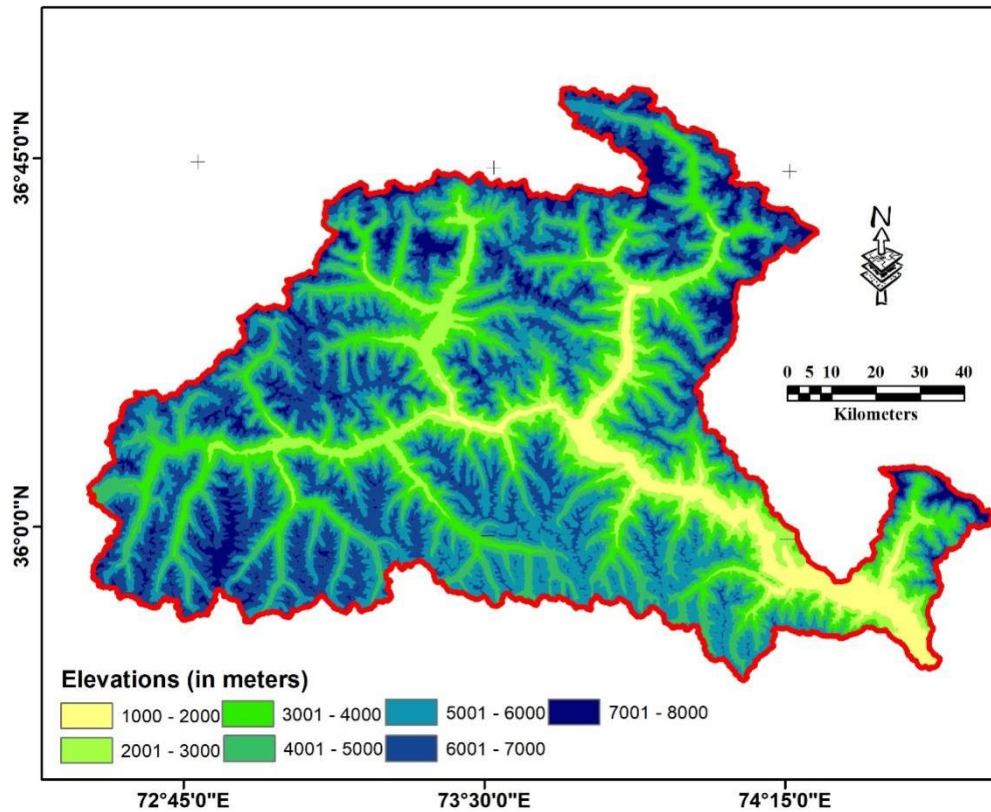


Figure 1.4 Elevation distributions in the study area

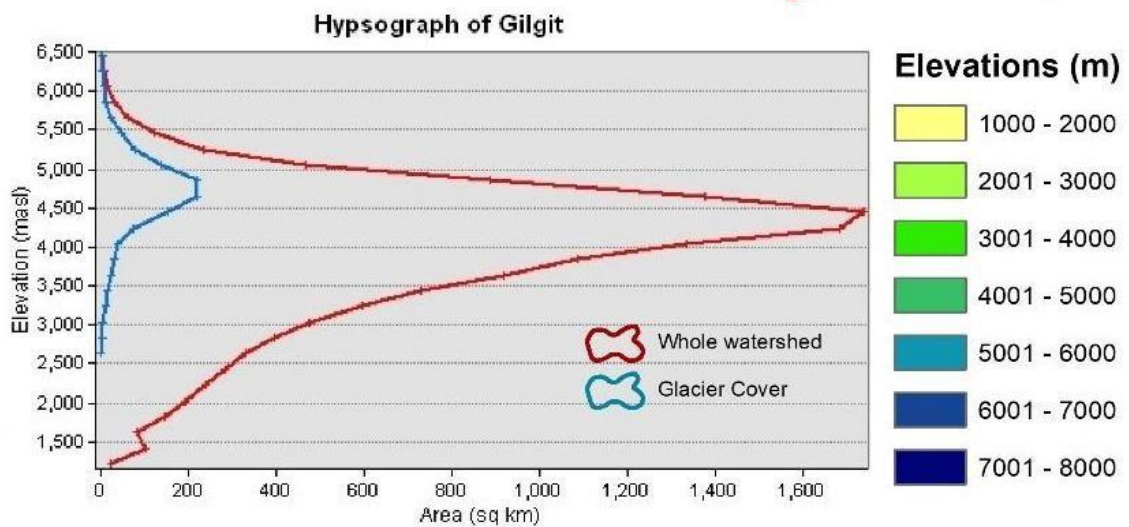


Figure 1.5 Hypsography of the study area

The Northern part of Glacier Mountains is technically less or inadequately explored due to its distance and wider fluctuations in meteorological conditions. According to the Pakistan glaciers inventory (2017) being developed by the Space and Upper Atmosphere Research Commission (SUPARCO), the Gilgit river basin has 979 minor and large glaciers with a total glacier area of 1022 square kilometers. Phakor, Karamber, East Gammu, Bhort, and Bad-e-Swat are some of the major glaciers in the Gilgit river basin. Furthermore, flash floods, supraglacial lakes, glacier lake outburst floods, and landslides are also common in Northern Pakistan (Kanwal et al., 2017; Qaisar et al., 2019; Rahim et al., 2018).

1.4 Aim and Objectives

The overall aim of this research work is to improve the knowledge of climate and hydrology of the Gilgit river basin in Pakistan and the seasonal variations of these parameters. The above aim is strategically characterized through the following objectives:

- 1.4.1** To map the five large glaciers in the Gilgit River watershed using time series of satellite remote sensing data from years 1988, 1994, 1999, 2014 and 2018.
- 1.4.2** To compare different remote sensing products / datasets by the computation of hydrological watersheds.
- 1.4.3** Image Classification and analysis of climatological data from Worldclim for the period of 1970-2000.
- 1.4.4** To evaluate the time series of areal extents of the glaciers.
- 1.4.5** To identify surge / retreat / stability of the selected glaciers.
- 1.4.6** To compare multi-sensor DEM data for the extraction of watersheds/

catchments.

1.4.7 To delineate the velocity of the selected glaciers.

1.5 Study Outcomes

The intended outcomes of the research work are:

1.5.1 Satellite derived map of study area i.e., glacier extents.

1.5.2 Glacier change analysis.

1.5.3 Time series maps of study area derived from multispectral Satellite data.

1.5.4 Analysis of climatological data.

1.6 Land Use and Land cover (LULC) in the Gilgit catchment

LULC defines the areal coverage of land forms e.g., foliage (plants, scrubs, parks, grasses), bare soil, solid surfaces (stalwarts, built up), damp areas and bodies of aquatic. The land cover mapping of the study area has been made with the use of data / imagery from Sentinel -2 satellite. The results of the land cover and the corresponding classes are shown in Figure 1.6.

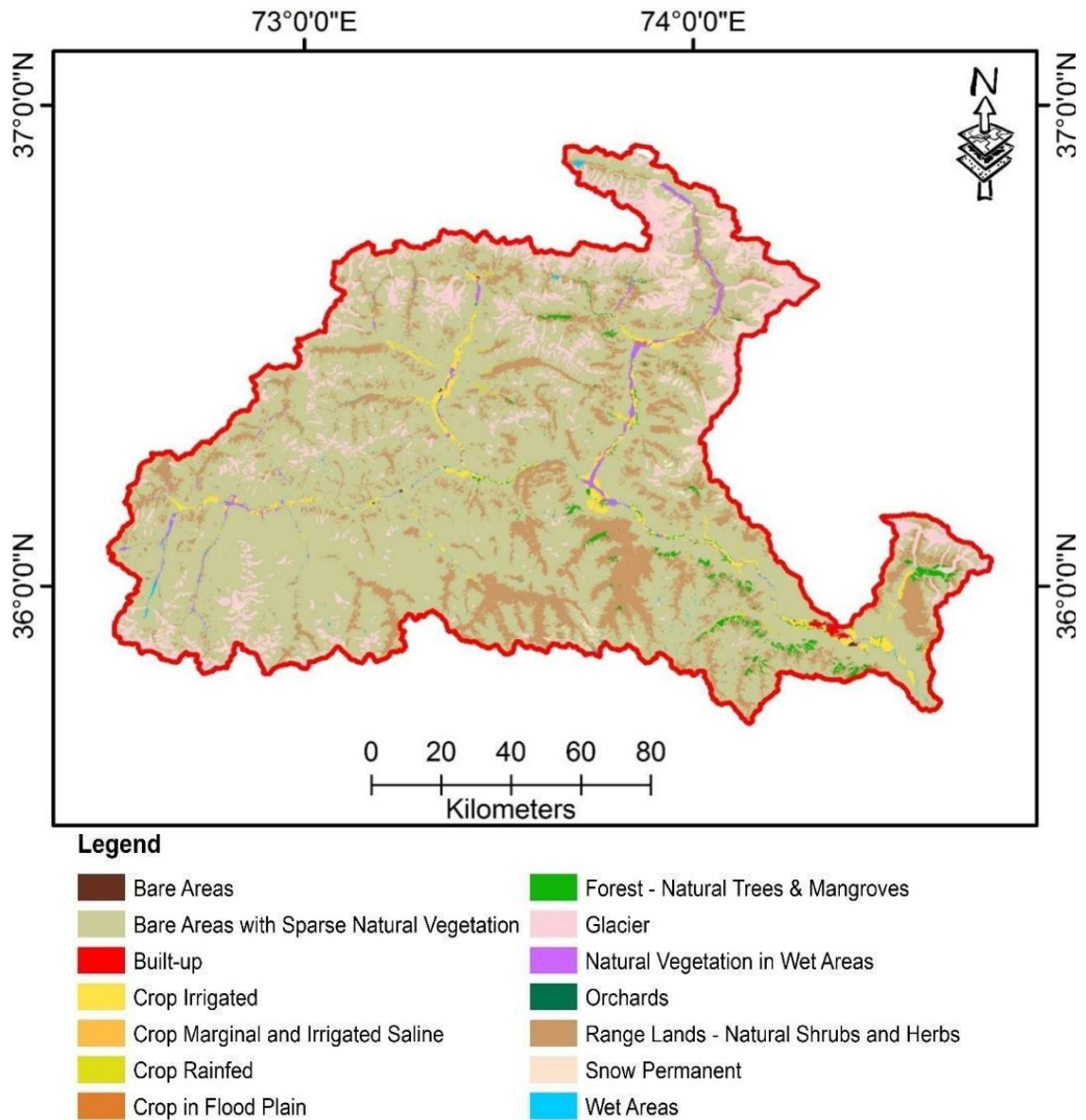


Figure 1.6 Land use and land cover mapped from the Sentinel-2 satellite imagery for the whole Gilgit sub basin

As illustrated in Figure 1.6, the large glaciers in the Gilgit river basin are the Phakor glacier, Karamber glacier, East Gammu glacier, Bhort glacier, and Bad-e-Swat glacier. The extent of the glaciers/outlines has been calculated with the methods described in details in the relevant part of thesis.

Study Area

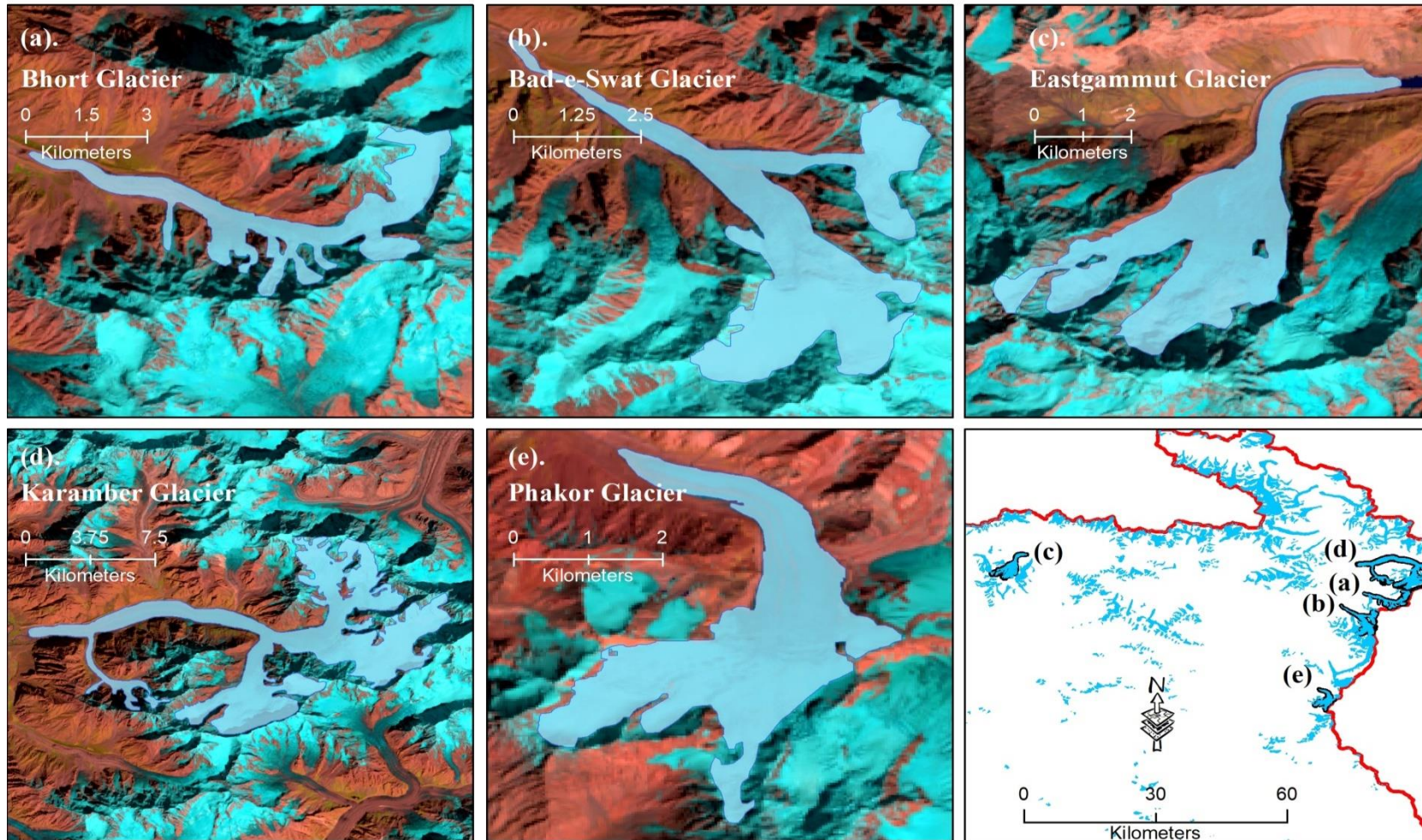


Figure 1.7 The location of five glaciers selected for the temporal study

CHAPTER 2

LITERATURE REVIEW

A literature review is a vital element of any analysis study, and it helps to establish the context for the study by identifying what is already known about the topic. By reviewing the existing literature, it has been found that the hydro-climatological variations in Gilgit watershed of Upper Indus basin are less technically agreed due to fewer studies conducted / published so far. There are rarely any studies pertaining to Glaciers in the Gilgit watershed and almost no published literature relating to glacier change analysis and the extraction of catchments.

The review of literature has been made in order to find the research gaps. There are several research groups in the domain of land use, hydrology and climatology where research in the Pakistani- part of HKH region has been conducted. It has been found that due to remoteness of glaciers and lack of road infrastructure, there are only a few studies made so far in the Gilgit Baltistan despite the signification of the hydrology especially for the Gilgit Baltistan province and generally for the entire country. In addition to remoteness, this region is less studied also partially due to rugged terrain,

scarce in-situ measurements, unfitting and unbefitting datasets and poor network of meteorological stations. Specifically, there has been no previously study made to assess the decadal or half-decadal changes of glacier cover area or investigate the watershed features of the Gilgit sub-basin.

The literature review has been divided into various categories and accordingly mentioned in upcoming paragraphs. More than 125 papers, articles and conference's conclusions have been consulted prior start of research work. Broadly these papers have been divided into 11 categories. The groups are Glaciology, climatology, combination of climatology and glaciology, combination of hydrology and glaciology, remote sensing, combination of remote sensing and glaciology, combination of remote sensing and hydrology, land use and remote sensing and combination of climatology, hydrology and glaciology. Accordingly brief of relevant significant outcomes of papers/articles/seminars has been stated in proceeding paragraphs. Same has also been listed in Table 2.1 of this chapter.

Glaciology:

Bishop et al., (1995) investigated into debris-load characteristics of Batura Glacier using high-resolution satellite imagery in the Hunza sub-basin. Vuille et al., (2000) characterized how Mean annual and seasonal patterns in the tropical Andes were defined over the past sixty years (1939– 1998) to study the seeming variation between measured glacier retreat and the published slight freezing trend in the lower tropical troposphere after 1979 in a research letter titled "Yearly average temperature trends and their vertical structure in the tropical Andes." Since 1939, the temperature in the tropical Andes has increased by 0.10°–0.11°C every decade, according to their findings. Over

the last 25 years, the warming trend has more than quadrupled (0.32° – 0.34° C/decade), with the last two years of the period, connected with the 1997/98 El Niño, being the warmest in the last six decades. Temperature effects differ with height, but show an overall decrease in warming as elevation rises. Despite the slower rate of warming, even at the highest elevations, the trend toward higher temperatures is still visible at the 95 percent confidence level. The small cooling trend reported in the tropical lower-troposphere is clearly not reflected by higher altitude land stations in the Andes.

Salomonson et al., (2004) used snow indices to quantify the fractional snow cover using coarse resolution satellite imagery at 500m spatial resolution. The estimates were then verified using Landsat 30-m observations over three diverse snow-covered areas concluding, that regression association among fractional snow shelter and NDSI is practically vigorous.

Mayer et al., (2006) investigated the ablation state of Baltoro glacier. One of the world's greatest valley glaciers, the Baltoro glacial in Pakistan's Karakoram. It drains an area of about 1500 km^2 and stretches for more than 60 kilometers. The debris type influences ice ablation on the Baltoro glacier because it is a debris-covered glacier. Stake observations of ice ablation and debris cover, together with climatological statistics from neighboring instinctive weather locations, were used to establish the local melt conditions. The findings of these computations were combined with an assessment of several kinds of surface coverage to calculate energy fluxes for the top half of the Baltoro glacier. GPS-based non - motorized transport observations along the stake network were used to investigate the glacier's dynamic state. A comparison of these short-term data with surface velocities derived from feature tracking of satellite photos

during the melt season reveals a high level of seasonal variation in ice motion. They discovered that this fluctuation can account for up to 100% of the mean annual velocity. As a result of these tests, the mass fluxes at the Concordia cross-section have been identified. This method can now be used in conjunction with ablation calculations to reconstruct the variations of glacier extent and volume in the past using easily accessible climate data from the central Karakoram. Historical data and photographs show that the Baltoro glacier's snout is moving back and forth a few hundred meters. Other than that, it doesn't seem to be responding to climate change the same way other glaciers do. Elevation changes at Concordia are often measured in tens of meters.

Anil et al., (2007) presented the glacier health condition of Himalaya which is one of the sphere's major ice and snow arenas, the Himalayas serve as a gigantic freshwater reservoir. In order to determine the reservoir's general health, the glacier must be observed. Since 1962, 466 glaciers in the Chenab, Parbati, and Baspa valleys have been monitored for their retreat. Excursions to the Chhota Shigri, Patsio, and Samudra Tapu glaciers in the Chenab basin, the Parbati glacier in the Parbati basin, and the Shaune Garang glacier in the Baspa basin were planned to find and map the glacial terminus. The glacier area has shrunk by 21% since 1962, from 2077 square kilometers to 1628 square kilometers currently, according to the study. Nonetheless, due to disintegration, the quantity of glaciers has grown. The average glacier extent has shrunk from 1.4 to 0.32 square kilometers. Between 1962 and 2001, the average glacial extent decreased from 1.4 to 0.32 square kilometers. In general, the proportion of glaciers with larger areal extent has decreased while the number of glaciers with lower spatial extent has improved throughout time. Deglaciation has been observed in smaller glaciers and ice fields. For example, 127 glacierates and ice areas less than 1 square

kilometer have receded by 38% since 1962, probably due to slow reaction times. This suggests that the influence of glacial fracturing, modest glacier retreat, and climate change is affecting the long-term viability of Himalayan glaciers.

In their article "Spatially heterogeneous wastage of Himalayan glacier," Koji Fujita and Takayuki Nuimura (2011) described volumetric development in three benchmark glaciers in the Nepal Himalayas that have been observed since the 1970s. The Himalayan glaciers, which are linked to the world average of glacier material balance, showed rapid waste in the 1970s–1990s, but similarly waste in the previous decade. In comparison to the 1970s–1990s, a glacier in an arid environment had a negative but restrained mass balance in the last decade, while two glaciers in a humid environment had quicker waste. The consequence of the observed glaciers is depicted using a mass conservation simulation with downscale gridded datasets. Even with current climatic warming, they demonstrate a spatially varied distribution of glacier loss across the Asian highlands.

Ashraf et al., (2012) provided the monitoring and quantification of the glaciated area of the Azad Jammu and Kashmir. Naeem et al. (2016) explored glacier mapping approaches and the resilience of semi-automatic methods, as well as the usage of an unsupervised classification strategy for outlining extents. Rashid et al., (2016) investigated glacier's temporal changes in Chitral region and identified the major gaps in the existing knowledge about the methodological approaches in mapping glaciers in Chitral. The mapping of the glaciers in the HKH region conducted by Bajracharya et al., (2015) was the first-time comprehensive portal released by ICIMOD which later became a reference cryospheric data set. The task now is to keep this information up to

date and expand it by expanding the temporal span as far back as current imaging allows. The study reveals that the extent of larger glaciers in Shyk and the Wakhan Corridor has not changed significantly, but smaller glaciers are melting faster. The authors outline four main areas that need to be addressed in order to formulate projections of water accessibility. (1) Address the uncertainty in spatiotemporal quantifications of the present climate (2) There aren't any highly decentralized hydrological models with enough detail to predict future changes in water supply. (3) Provide the data required to estimate a complete energy balance and melt rate, which is typically unavailable at high altitude. (4) Stranger techniques are required to calculate future glacier extent in relation to modeling forcing and land masses. Paul et al. (2017) found several glacier surging events in Karakoram Mountain range during the past decade, whereas Bolch et al. (2017) found no significant mass change (on-average) in both surge-type and non- surge-type glaciers in Karakoram, however, also initiate some specific glacier mass change rates differed considerably for the eras before and after 2000. Similarly, some researchers have claimed that the rate of retreat is declining in those glaciers of the Karakoram that are not steady or growing (Mayer et al. 2006). More interestingly, in contrary, Baig et al. (2018) establishes a declining tendency in the glacial ice-covered area of Karakoram, alongwith the lessening of 20.47% in the lower elevation bands.

Zhou et al. 2021 in their paper Glacier Velocity Changes in the Himalayas in Relation to Ice Mass Balance carried out research on surface velocity of glacier of Himalaya. Climate variability provides important information about glacier evaluation. In this study glacier velocity changes in the Himalaya were investigated and pattern of glacier flow was analyzed. In this study, 220 scenes from panchromatic Landsat-7

pictures from 1999 to 2000 and panchromatic Sentinel-2 images from 2017 to 2018 were gathered. 36,722 glaciers' surface velocities were calculated between 1999–2000 and 2017–2018 using this collection. This velocity data allowed for the early winter period's velocity fluctuations between 1999 and 2018. They thoroughly examined the movements of each glacier on this basis and found that the alterations are regionally varied. As per the data, 32% of glaciers have augmented, 24.5 percent have decelerated down, and 43.5% have persisted unchanged status. It's interesting to note that glaciers that slow down due to mass loss have amplitudes that are substantially larger than those of glaciers that accelerate. Between 1999 and 2018, the glacier surface velocity in the western Himalaya declined consistently on a regional basis. In contrast, the eastern region saw an increase in glacial surface velocity. The decadal changes in accumulation and/or melting under new climatic regimes are linked to this contrast difference. The general trend of surface velocity is determined by seasonal fluctuation. Summer time velocity variations and ice mass loss have a positive correlation. It indicates that velocity of mass loss has risen as a result. Winter time velocity fluctuations exhibit an inverse relationship. This study made a compelling case for the heterogeneity of time and space in the Himalaya's velocity fluctuations. Environmental forces and glacier dynamics are to blame for this.

Evan, et al. 2021 in paper Health and sustainability of glaciers in High Mountain Asia highlighted the importance of glaciers for the population of 250 million. The present information of glacier ablation and accumulation on annual basis depends largely on field measurement which determines the size and location of glaciers. However, very sparse research has been done due to inaccessibility to high and difficult terrains of glacier mountains. The melt water generated from the high mountain glaciers in Asia provides

livelihood to millions of people. There are 5527 glaciers which have been studied in high mountain Asia for a period from 2000-2016 through specific mass balance technique. The study outcome shows 41% of glaciers accumulated mass over only 20% of glacier covered zone. The rest 60% plus of regional annual ablation was remunerated by accumulation. Owing to present climatic geometric disparity the ice volume of Asian mountains will be lost to 21% by 2100. This will achieve even without the warning given for climate change in the 21st century. This will reduce glacier ablation into rivers by 28%. The unsustainable and lost ice volume in Himalayas and Tien Shan will reduce ice mass to at least 30% by 2100. Interestingly, the river basins of Amu Darya, Indus, Sar darya and Tarim Interior which received glacier melt remain sustainable for more than 50 % glacier ablation. Notwithstanding long term reduction in ice mass and glacier melt water source from the Karakorum is inevitable.

Nazir et al., 2021 in their paper increasing glacial lake outburst flood hazard in response to surge glaciers in the Karakoram studied the Karakoram anomaly. The Karakoram glaciers are generally found stable or even gaining ice mass on positive side. Approximately 179 glaciers lake outburst floods (GLOFs) have been studied by them spanning over a period from 1533 to 2020 in five major valleys of Karakoram. Surprisingly out of 179 GLOFs studied, 64 of them occurred after 1970. From these 64 events, 37 events recorded through remote sensing imagery. From these 37 GLOFs, 36 glaciers linked with GLOFs due to ice front advance building ice barriers in rivers. In the entire Karakoram region, 31.8% of major GLOFs occurred in Kayger and Khurdopin glaciers. They analyzed ten surge glaciers through the use of a cross correlation feature tracking technique on remote sensing imagery. From 1990 to 2019, they documented six surge events. The Khurdopin, Kyager, Shishper and Chilinji

glaciers show periodic surge cycles. On all studied glaciers, it was found that surge velocity in the mid-2010s were above that of late 1990s. To determine the magnitude and frequency of outburst flood events, the higher velocity of a glacier enhance the risk of flooding below the terminus of glaciers. This is due to transfer of an enormous ice mass downward the terminus during the surge of glaciers. The climate change and global warming affect the Karakoram glaciers in other ways. Glaciers gain mass, however thinning of ice and its advancement resulted in the formation of lake and ice dam failures. Based on this phenomenon they predicted that GLOFs occurring frequency will increase in the upcoming time period. To monitor this frequency of GLOF occurring they presented a theoretical model of ice dammed lake creation which initiate formation of GLOF in reaction to heaving of glaciers.

Sivaranjani, et al. 2021 in their paper temporal fluctuations of Siachen glacier velocity studied the glacier velocity. The health of glacier is dependent on glacier velocity. It has becoming emergent research technique in global warming among scientific communities in recent time frame. The glacier of Karakoram due to their stable and advance nature are exclusive from these warming climatic changes. Their work emphases on the temporal velocity variations of the Siachen Glacier, Shyok Basin, and Karakorum utilizing SAR datasets. Due to the challenges in measuring the glacier velocity across the remote Karakoram Mountains, this method is used. Using the DInSAR approach, 30 Sentinel-1 generated interogrammes were used to examine the 2017-2018 hydrological year in order to determine the Line-of-Sight velocities. However, a well-defined pattern inside the glaciers for the several seasons emerged as a result of the thermodynamic and orographic system over the glacier. In azimuth and range direction, a two-dimensional surface glacier's estimated annual LOS velocity was

calculated to be 103.8 ± 3.1 m/year.

Sivaranjani, et al., 2023 also studied dynamics in surface ice flow rate of glaciers in Hunza basin. They mentioned after the research on around 80 glaciers in Hunza basin that Batura, Hassanabad II, Barpu, Ghahesa, Hispar, Khurdopin, Minapin, Virjerab, Yazgil, and Ghulkin glaciers are highly susceptible to surging based on interannual surface flow rates. Along their snouts, these glaciers had advanced and surged based on the findings concluded during the research period.

Jiang et al., 2021 in their paper on Surging dynamics of South Rimo Glacier, Eastern Karakorum defined the dynamics features of glacier surge events. South Rimo Glacier (SRG), situated in the East Karakorum region, surge has been explained through surface velocities and surface elevation changes. The surging dynamics characteristics of SRG during 2018–2020 have been studied in the paper. Ice deformation during the dormant phase controlled the surface velocity variations. It was noted with confidence that ice thickness increases from cold to temperate season. During the active phase surface velocity speeded and slowed with the advancement of surge front. The latest surge was generated by the thermodynamic of the glacier and ultimately increases by the hydrological processes. 25-30 years of surge return period has been projected. Understandably, it is lengthier than for other freshly informed surges/flows in the SRG eastern Karakorum region. Accepting of surge mechanism and return period of Karakorum glaciers has been clarified by this study and provided a guideline for future research by the scientists.

David et.al. 2023 in studied the global glacier change in the 21st century based on shared socioeconomic trails calibrated with data for each glacier presented projections of global glacier, apart from the ice sheets. The paper concluded that by 2100 world glaciers are expected to drop about 52 % of their mass if temperature rises from 1.5 to 5°C. Sea level equivalent corresponds to this is 90 ± 26 to 154 ± 44 millimeters and 58 to 90% of glaciers will vanish. Temperature increase is linearly related mass loss and thus reduces mass loss related to temperature increase. By 2100 Sea level will rise by 115 ± 40 mm and will affect extensive deglaciation in most mid-latitude areas (COP26).

Afzal et.al. 2023 studied the hydrological and dynamical response of glaciers to climate change in the Hunza area. They verified that surprisingly glaciers in this region have showed abnormal outcome if relate it to the nearby region. The glaciers in this region are increasing, steady and also receding within same region (Dimri, 2021, Hewitt, 2005). Nevertheless, such studies are established on imagery of satellite, which are exposed to local glacier dynamics and shows late retort.

Climatology:

During the last century, most of the glaciers across the globe have retreated in reaction to climate variability (Chen et al., 2006; Zemp et al., 2009). However, such witnessed inclinations are not locally even (Kargel et al., 2011; Yi, Shuang, and Wenke Sun., 2010; Schmidt et al., 2012). Since the nineteenth century halfway, plenty of the glacial in the Hindu Kush-Himalaya (HKH) range have been declining and losing mass. (Azam et al., 2012; Bolch et al., 2012; Bolch et al., 2011; Bolch 2007; Zhang, Yong, et al 2011), but many of the large glaciers in the Karakorum have been stable (Farhan et

al. 2015; Mayer et al. 2010; Scherler et al. 2011) and some have even exhibited positive growth and expansion (Gardelle et al. 2012; Hewitt 2011; Hewitt 2005; Zemp et al. 2009). Azam et al. (2018) employed the geodetic measurements and establish almost balanced mass budgets for Karakorum glaciers since the 1970s.

Quincey et al., (2009) in their paper Ice velocity and climate variations for Baltoro Glacier, Pakistan described the changes in glacier ice mass. The central and eastern Himalaya is being affected by climate change badly. However, the recent dynamic behavior of Karakorum glaciers is different from it. It could be due to regional variations in precipitation and temperature trends. The inadequate quantitative data is insufficient to support this hypothesis. In this study the author took the velocity data for Baltoro glacier which is one of the largest glaciers in the Karakorum. In part of the eastern Himalaya down wasting ice being observed resultantly mountain glacier recession in response to sustained climatic warming is reported. The velocity data covered a period from 1993 to 2008. Ice velocity was determined by using cross-correction feature tracking to data from the European Remote Sensing Satellites (ERS-1 and 2), Envisat Advanced Synthetic Aperture Radar (ASAR), and differential global positioning system (DGPS) measurements. Glacier surge was observed to happen gradually in the early 2000s, especially during the winter. Through the use of multi-seasonal data gathered throughout the study period, a significant difference between summer and winter flow characteristics was found. However, this occurred only in upper ablation zone. After the significant winter snowfall in 2004, the active summer of 2005 was especially significant. This amply demonstrates how crucial basal melt water accessibility is to glacier flow. The transverse velocity profile of the Baltoro Glacier shows that throughout the summer, block flow occurs across the majority of the upper

ablation zone. This is interpreted as evidence of extensive basal sliding. DGPS data verified this sharp rise in flow that was discovered in 2005. Modeled climatic data confirm the lowering summer temperature and rising precipitation over the study area. This work contributes to the understanding of the observed dynamic fluctuations and how they differ from other Himalayan glaciers.

Shafique et al., (2018) evaluated the decadal changes of glaciers in the Hunza sub-basin using multi-temporal remote sensing images. Annual temperature rise outcomes in enhanced melting rate and vice versa. Likewise, rise in yearly rainfall consequences in growing the glaciated extent.

The association between temperature and precipitation was investigated by Sheeba and Nasir (2013). Climate evaluation entails careful consideration of rainfall and temperature outlines. As a result, there are numerous aspects to consider when studying climate. Temperature and precipitation, however, serve a critical and multifaceted role in climatic research, predominantly in the context of several environmental dangers. The goal of the plan was to create and test a predicting model that could forecast Hunza-temperature Nagar's and precipitation with precision and send out alerts in a timely manner. They used and produced a measureable therapy using various statistical techniques, including regression and time series/stochastic modeling, on a data set of temperature and rainfall (2007-2011). According to the regression analysis, rainfall increased as the temperature rose. It was also discovered that between 2007 and 2011, monthly mean maximum temperature indices increased while rainfall declined. Based on the accessible data, the AR model is the most suitable for temperature forecasting. For future investigations, these estimates will be valuable to public, corporate, and

government organizations.

Afsar et al., (2013) conducted a relative research of temperature and precipitation Variance in the Hunza-Nagar District and found that there is a clear link among temperature and precipitation, with rain cumulative as temperature increases.

Yaduvanshi and Ranade (2015) have studied the climatological physiognomies, variation topographies and intervallic phases of yearly, periodic and once-a-month precipitation change of seven river basins. With no noteworthy lasting tendency in twelve-monthly precipitation across, eastern Indo Gangetic Plains there is a substantial decrease in monsoon rainfall in past twenty years.

Usman et.al. (2015) highlighted in the article the importance of glaciers to Pakistan and huge numbers of glaciers bestowed to her by its geography. For rivers whose flows are linked to glacier melt, variations in glacier extent become extremely important. Small changes in glacier extent can cause significant changes in downstream river flows. Many studies have predicted potential flows in such catchments based on climate change scenarios. The melting of glaciers, on the other hand, is practically never based on any solid evidence. As a result, investigation is required to determine how glaciers remain operating under different temperature and precipitation conditions in order to accurately predict future flows. The Chitral watershed was carefully examined as a study area for this reason. For several years, MODIS data was used to measure the periodic variation in snow extent, which helped to identify the month with the smallest glacial extent. Unsupervised classification was used to predict the glacial size in the Chitral watershed using remote sensing. For the last decade, the results demonstrate a

good receding trend in the glacier of the Chitral region in terms of time.

The properties of WorldClim2 were discussed in the research publication "WorldClim 2: novel 1-km spatial resolution climate surfaces for global land regions" by Stephen Fick et al., (2017). They created a new monthly climate data set for global land areas that was spatially interpolated at extremely high spatial and temporal precision (about 1km²). They compiled monthly temperature (minimum, maximum, and average), rainfall, solar radiation, vapor pressure, and wind speed data from between 9000 and 60000 meteorological stations between 1970 and 2000. Thin-plate splines were used to approximate weather station data with covariates like elevation, mileage to the shore, and three satellite-derived covariates collected using the MODIS satellite platform: maximum and minimum land surface temperature, as well as cloud cover. Based on station density, interpolation for 23 zones of various sizes was completed. Temperature prediction accuracy improved by 5–15 percent (0.07– 0.17 °C) using satellite data, especially in areas with low station density, but prediction error for all meteorological parameters remained high. Satellite factors had little effect on the remaining variables, however their importance varied by region. They created the final output by selecting the highest scoring model for each region and variable, rather than utilizing a single model composed for the entire world as is often done. The worldwide cross-validation correlations for temperature and humidity were 0.99, rainfall 0.86, and gust speed 0.76. The statistic that incorporating satellite variables only slightly enhanced most of our climate surface estimates stresses the need for a more robust network of climate stations.

Gubler et al., (2017) examined relative homogenization approaches in their

study the effect of unit frequency on climate science homogenization. Relative homogenization approaches rely on extensive unit systems with a high connection since observations of surrounding sites face analogous climate signals. However, networks in third-world nations such as Pakistan and Peru frequently suffer from low station density. This research was designed to evaluate the impression of strength on homogeneity. The HOMER homogenization algorithm was used on a drastically thinned Swiss network for this.

Klare (2019) highlighted the global warming effects on water scarcity. Specific to Pakistan the Indus River water state w.r.t. weather variation have been deliberated in detail. There is no evidence that Pakistan is seen as a "state critical to US national security interests" by US security analysts, a phrase used by Defense Intelligence Agency to characterize nations of interest in the 2012 ICA on water. Pakistan is not only an important—if not always fully committed—partner in the global battle on terrorism, but it also has a large nuclear arsenal whose stability is a major concern for American policy makers.

United States, Pakistan remained susceptible to social and ethnic divisions. As farming is Pakistan's primary economic activity, maintaining access to clean drinking water is a major public and government priority. This entails, above all, controlling the Indus River, the country's primary source of water for cultivation and its primary source of electricity generation. Pakistan's booming population and metropolis, with their ring of factories, are putting excessive pressure on the Indus, resulting in rivalry among farmers, manufacturers, and urban customers. With water and electricity shortages becoming a more common occurrence, public outrage has risen across the country,

sometimes turning violent. During a lengthy power failure in June 2012, rioters set fire to trains, stopped roads, robbed stores, and vandalized banks and petrol stations in one particularly violent outburst.

Climate change is expected to make conditions in Pakistan substantially so much worse years ahead, no matter how terrible things are now. Long-term droughts, according to climate experts, will become more common, posing a serious threat to the country's agriculture industry and further lowering hydroelectric power availability.

With struggle for freshwater resources expected to intensify, and Pakistan currently split across ethnic and religious lines, extensive civil unrest may become increasingly possible, perhaps compromising the country's future.

It's difficult to say how the US would react if Pakistan's state governance system collapsed. One thing is certain: the American military could react with devastating force at the first evidence if the country's nuclear weapons were in danger of slipping into hostile hands. "U.S. forces could hurry into the state, travelling internationally, climbing down from chopper, and parachuting out of planes, so they may capture suspected of having nuclear—storage sites," the NTI stated in the case of a coup or crisis.

The possibility that India will try to use its advantageous position as the largest river basin on three significant Indus watercourses—the Ravi, the Beas, and the Sutlej to divert water for its own purposes, rejecting downstream Pakistan's need for supplies, and possibly even starting a war between the two countries—is another issue that has

some analysts concerned. In retaliation for Pakistani attacks against Indian installations in the disputed area of Kashmir, Indian politicians have vowed to dam the rivers or otherwise impede their flow into Pakistan. Analysts predict that in such a scenario, India's stronger ground troops will overrun Pakistan's equivalent forces, compelling Pakistan's leadership to authorize use of nuclear weapons against India, resulting in a regional nuclear war. According to specialists, a conflict like this would kill 50 to 125 million people and create a dust cloud that would blanket most of the globe, decimating global agriculture and having major implications for American national security.

Climatology and Glaciology:

Chen et al. (2006) used time-variable gravity measurements from the Gravity Recovery and The Greenland Ice Sheet Change Study (GRACE) satellite mission measured ice mass variations across Greenland from April 2002 to November 2005. After accounting for the impacts of spatial strain and the restricted precision of GRACE data, the overall melting ice velocity over Greenland is predicted to be -239 ± 23 cubic kilometers per year, with the majority of melting occurring in East Greenland. Derived from satellite radar interferometry data, this approximation matches with actual one current calculation of -224 ± 41 cubic kilometers per year. GRACE estimations in Southeast Greenland suggest that melting has accelerated during the summer of 2004, which is stable with the most recent remote sensing data.

Climate change and tropical Andean glaciers was the title of a paper by Mathias Vuille et al. (2008). The paper included observations on glacier extent from Ecuador, Peru, and Bolivia as well as a clear record of fast deformation of tropical Andean glacial since the Little Ice Age (LIA). However, this reduction was halted by several

periods of static or even increasing glaciers, the most recent of which was around the turn of the twentieth century. The behavior of glaciers in the inlet and outflow tropics can be compared using fresh data from more than a dozen mass balance networks. Despite diverse understandings of environmental forces like as temperature, rainfall, humidity, and so on, it seems that glacier discrepancies are quite consistent across the region. Climate change in the tropical Andes has occurred in lockstep with glacier retreat over the last 50–60 years. The average temperature in the Andes has risen by 0.1°C every century, the last 20 years with only two times temperature falling below the 1961–90 average. Rainfall in the inner tropics improved significantly in the second part of the twentieth century, but it decreased in the outside tropics. The observed alterations in the large-scale circulation are dynamically predictable with the general trend of rehydrating in the inner tropics and dryness in the subtropical Andes, implying a development of the tropical weather systems. Model forecasts of future climate change in the tropical Andes show that the tropical troposphere throughout the twenty-first century will continue to warm, with a temperature increase that is more noticeable at advanced altitudes. By the end of the century the tropical Andes could warm by 4.5–5 degrees Celsius, using the SRES A2 emission scenario. The periodic hydro logical regime in the tropical Andes will be improved by increased precipitation during the rainy season and decreased precipitation during the arid period.

Tropical glacier energy balance is much more susceptible to changes in moisture (which affects sublimation), precipitation (whose unpredictability has a positive feedback effect on albedo), and cloudiness as a result of these observed and anticipated climate changes (which controls the incoming long- wave radiation). The energy balance in the inner tropics is negatively impacted by air temperature rather than

sensible heat flow, albeit indirectly through oscillations in the rain-snow line and consequent changes in albedo and net radiation receipts.

Studies with a tropical glacier simulation reveal that, given predicted temperature changes built on numerous IPCC scenarios for 2050 and 2080, the glacier will remain to retreat. Numerous minor, low land glaciers are even now out of balance with the current climate and will disappear in the next few years. Even in catchment areas where glaciers do not completely melt, the absence of the glacial buffer would produce a considerable shift in stream flow seasonally, affecting downstream water availability.

In the brief period, when glaciers retreat and drop mass, they result in greater runoff, which downstream consumers will quickly adjust to, creating significant doubts about long-term sustainability.

Thompson (2012) paper published in Nature Climate Change journal mentioned that the Tibetan Plateau and its ambiances comprise the biggest quantity of glaciers external to the Polar Areas. Such glaciers are at the fore front of waters for numerous protuberant Asian rivers. Unfortunately, many of them are mostly facing ablation, which disturbs the water release of big rivers like that of the Indus and Brahmaputra. The resulting likely geo hazards worth a full research of glacier eminence in the Tibetan Plateau and its ambiances. Over the past 30 years by exploring the glacier status it came to know that Eighty-Two glaciers are retreating, 7,090 glaciers area have decreased and fifteen glaciers mass-balance changed. The most comprehensive shrinking in the Himalayas has the extreme reduction in glacier extent and area, as well as the largest

negative mass balance. From the Himalayas to the continental heart land, the reduction gradually decreases, with the eastern Pamir having the lowest glacier retreating, area lessens, and positive mass balancing. Additionally, rising temperatures are generating decreased rainfall in the Himalayas and higher rainfall in the eastern Pamir, both of which are influenced by different atmospheric circulation patterns.

Din et al. (2014) quantified the GLOF and its explanation in the study Temperature and Precipitation. In Gilgit- Baltistan, GLOFs are one of the most frequent climate change-related dangers. More than 35 GLOF incidents have occurred in Gilgit-Baltistan in the last 200 years, but in recent years their occurrence has grown, with five GLOF events in the Gojal Basin (Upper Hunza) in 2008. From 1990 to 2012, well-known GLOF incidents were chosen, and two types of meteorology data sets, real-time and analyzed data, were used to investigate the association among GLOF occurrences and weather conditions. Temperature and precipitation (rainfall), according to this study, play a role in raising the probability of a lake outburst resulting in a GLOF. The bulk of GLOF events in Gilgit-Baltistan were shown to be linked to extreme meteorological circumstances during the research period, such as sudden increase in temperature, heat wave, or precipitation drop a short time before or during the GLOF phenomena. GLOF dangers can be condensed and pressures to societies mitigated by constant hydro-meteorological observation of the impacted areas.

Irfan et al. (2020) found that due to the region's varied terrain, remoteness, and greater climatic change, the hydro-climatological variations in the Gilgit watershed of the Upper Indus basin are less well understood scientifically. A crucial step in carrying out the watershed management studies is the extraction of catchments at various scales.

Watershed research can be greatly aided by the use of geographical information technology (GIT) and satellite remote sensing (SRS). Keeping in assessment of the facts, watershed/natural resource supervision in the Gilgit river basin, it is required to use geospatial algorithms to a variety of elevation datasets in order to obtain more accurate results using these datasets. This has been accomplished by investigating the extraction of topographic characteristics from the Gilgit River basin using a variety of Digital Elevation Models (DEMs), including SRTM, ASTER GDEM, and GTOPO30. The basin was defined by the minor watersheds of the glaciers Phakor, Karamber, East Gammu, Bhort, and Bad-e-Swat. For the purpose of matching mountain ridges, the delineated watersheds have been optically compared to optical Landsat 8 OLI pictures. The results showed that, due to its accurate delineation in the Gilgit sub-basin, the SRTM 30m (radar-based) displayed the highest accuracy among all. However, it is accurate to claim that there is generally good agreement between the computed areas from the three DEMs. This research significantly advances our knowledge of the hydrological responses and watershed management in the upper Indus catchment's Gilgit watershed. The hydrological unit connected by drainage lying upslope from a pour point or particular departure is known as a catchment, watershed, or drainage system. The watershed extraction characteristics are essential for water resource management and hydrological analysis in GIT/GIS, including catchment delineation and stream network. For mountain ridge matching, the delineated watersheds were visually matched to optical Landsat 8 OLI images. The radar-based SRTM 30m has been found to be more accurate for this region.

Hydrology and Glaciology:

Rasul et al. (2011) studied the Indus River System's mountains and glacial lakes. The majority of glaciers in Pakistan are debris-covered (DC), and melting rates vary

determines the thickness and kinds of debris, as well as height. Pakistan saw the warmest decade on record, with a 0.93°C increase in temperature between 1971 and 2000. Because the fatness of the debris coating is inversely proportional to the rate of ice melt, high altitude glaciers have less debris covered than lower altitude glaciers.

Focusing upon the effects of yearly glacier snow liquefy on river flows across two watersheds and rivers situated in the region where monsoon is dominant in the Nepal side of Himalaya, (Adina et al. 2013) (Trishuli and Dudh Kosi basins). They applied a straight forward elevation ice ablation system founded on glacier regions from ASTER and IKONOS remote sensing data, along with hypsometry from the Radar sat Project (SRTM). Using long-term hydrologic measurements at great distances and distances from glacier outlets, the percentage role of the glacier ice melt element of the water balance in outflow was estimated. In the minor Langtang Khola watershed in the Trishuli basin (which has a 43.5 percent glacierized area), glacier ice melt produced 58.3 percent of the yearly flow, and 21.2 percent in the Hinku watershed in the Dudh Kosi basin (34.7 percent glacierized area). The presence of particulate glaciers in Langtang Khola and Hinku was responsible for 17.7% and 4.1 percent of stream flow, respectively. Glacier ice melt contributed much less to observed discharge near low-lying regions at both study sites, accounting about 9.5 percent at Betrawati (600 m) and 7.4 percent at Rabuwa Bazaar (470 m), both about 50 km from glacier termini. Further downstream in the Trishuli basin, the amount of yearly discharge from glacier ice melt was reduced to 4.5 percent (at 325 m, about 75 km from glacier termini). Debris-covered tongues made up a very minor portion of the population at low altitudes (1.1 percent and 3.0 percent, respectively, of reported flow at Betrawati and Rabuwa Bazaar stations). They independently assessed the ice ablation method by counting the influence of

diverse water sources on river flow utilizing synoptic surveying of steady water isotopes collected throughout the post-monsoon season. Mixing models revealed that groundwater is an essential element of river flow around tens of kilometers of glacier vents during the season after the monsoon.

The glaciers in the HKH region mapping was conducted by Bajracharya et al., (2015) the first-time comprehensive portal released by ICIMOD which later became a reference cryospheric data set.

The Karakoram region is too famous for its surging type glaciers e.g. Hunza watershed was imperiled to the Soil and Water Assessment Tool (SWAT) model together with a temperature table and altitude band algorithm in a study by Garee et al. (2017). The main factors influencing river flow in this region are snow and glacier melts. The combination of the SWAT and a snow melt approach makes this study distinctive (temperature index with elevation bands). The SWAT model was used in the watershed of the Upper Indus Basin, which is mostly covered by snow and glaciers, to assess the effects of climate change on future stream flow volume at the watershed's outlet as well as its contribution to the Indus River System in both space and time. Utilizing uncertainty analysis and the four suggested statistical coefficients, the model's performance is assessed (p-factor and r-factor). For the daily flow gauge, simulations produced good calibration and validation results. A thorough evaluation of the model's performance revealed a significant correlation between the simulated and actual flows. The daily flow has a Nash-Sutcliffe Efficiency index (NS) of 0.80 and a coefficient of determination (R²) of 0.82 according to the model results, with p-factor and r-factor values of 79% and 76%, respectively. The SWAT model and the three GCMs from the

IPCC's fifth report were used to evaluate the effects of climate change on the hydrological regimes in the target watershed for the years 2030–2059 and 2070–2099, respectively, using 1980–2010 as the baseline. In general, the analysis showed that the hydrology of the study region underwent fewer absolute changes near the end of the century. At the turn of the century, rising river flow (5%–10%) was accompanied by greater variability in temperature (1.39–6.58 °C) and precipitation (31%). The findings showed that the calibrated model responded to temperature, precipitation, snow-melt parameters, and Curve Number more quickly (CN2). The SWAT findings also provide trustworthy data on the response of the sub-basins daily discharge from their watersheds to shifting climatic circumstances. In order to lower flood risks and water storage in upstream reservoirs like the Diamer-Basha dam, SWAT can be used to create active approaches for long-term, workable water management in the area.

Sen's approach was used to determine the slope of tendencies that were found during four periods of varying lengths, while the Innovative Trend Significance Test (ITST) and Modified-Mann-Kendall (MMK) test were combined to look for trends (T1: 1961–2013; T2: 1971–2013; T3: 1981–2013; and T4: 1991–2013). Most sites across T1 saw significant declines in the mean summer and individual month's temperatures (June–August) (T_{mean}), whereas noteworthy upsurges were seen throughout the shorter T4. At 10 locations, the mean precipitation (P_{mean}) was found to be meaningfully negative in July; positive tendencies, however, were seen in August and September. Mean summer flows (snow melt dominant) during T1 and T2 exhibited significantly increasing trends within the glacier-fed basins of Hunza, Shigar, and Shyok; in contrast, stream flow (glacier melt dominating) during the most recent period T4 showed significantly decreasing trends in August and September. The mean summer

and individual months' temperatures (June-August) (T_{mean}) significantly decreased at the majority of sites across T1, although significant increases were found everywhere through the 10 locations, the mean precipitation (P_{mean}) was found to be significantly negative in July; positive tendencies, however, were seen in August and September.

Atif et al., (2018) investigated the hydro meteorological trends in the Hunza and Astore sub-basins in connection with the snow cover trends. It was concluded that there is a strong influence of the westerly system responsible for the falling trends of temperature and more solid precipitation hence controlling the runoff from the Hunza sub-basin. In assessment, the Astore sub-basin, which is powerfully effected by the monsoon structure, increases tendency in watery rainfall and greater hotness owing to its lesser elevation causing in higher runoff.

Bilal et al. (2019) studied on mountainous basins, such as Gilgit Baltistan's Upper Indus Basin (UIB), are reliant on glacier and snow melt during specific seasons. Monitoring the snow-covered area (SCA) is crucial for the Indus basin's total hydrology as well as for the hydro power and sustainable agriculture systems. The Moderate Resolution Imaging Spectroradiometer (MODIS) snow product was used to look for changes over the past 18 years in the snow-covered area in the UIB of GB. Five elevation zones, spanning from 877 to 8564 meters above sea level, were created in the study region (m ASL). SCA in the UIB is modestly increasing, in contrast to studies that are related to the global cryosphere. SCA research based on elevation also showed that SCA is gradually rising in each elevation zone. Nevertheless, locations above 5000 m ASL have the highest concentration of snowfall. The data on precipitation exhibit a similar pattern because of the tight link between SCA and precipitation. The climatic

data show a statistically significant rise in total monthly precipitation, relative humidity, a slight decrease in monthly mean temperature, and a scientifically substantial increase in monthly solar radiation. The main causes of the research area's slightly rising SCA are all of these changes, as well as the rising trend in global precipitation, winter westerly disturbances, and orographic precipitation. Despite the drawbacks of the brief observation time, our findings primarily aid in understanding how the snow cover and glaciers in the Hindu Kush Karakorum progress.

According to Ahmed et al., (2020) the population in several part of the sphere, plus the Hindu Kush-Karakorum-Himalayan (HKH) region, rest on snow and glacier-melt waters to farm foodstuff, produce power, and conserve water for year-round use (2020). The snow cover area (SCA), which varies annually and seasonally as a result of its response to climatic factors, has a direct impact on water availability. The current study's objective is to assess spatiotemporal patterns in the seasonal and yearly snow cover at a basin-wide scale. By displaying the tendencies in SCA in diverse elevation bands, the effect of topography on the SCA is examined. It also looks at the relationships between changes in SCA and trends in the hydro-climatic variables (temperature, precipitation, and river flows) in the Hindu Kush region's Chitral River basin. Through the use of cloud-free 8-day MODIS snow data, a rough estimate of snow cover is obtained over a 17-year period (2000–2016). The Water and Power Development Authority (WAPDA) and the Pakistan Meteorological Department both provided information on river flow (1989 to 2014), temperature, and precipitation (1965–2013) (PMD). Mann-trend In order to analyze the trends of the SCA and hydro-climatic variables, Sen's slope and Kendall's test were utilized. The outcomes demonstrate: (1) a significant increase in SCA at basin-wide scale and at all

elevation zones, from A to E (1471-7708 m ASL), with zone B (2500-3500 m ASL) being the only exception; (2) reducing and continuous patterns in average temperature and total precipitation, in both, across the same period as SCA, denoting possible causes for increasing SCA; and (3) a slight decline in mean annual and summer flow (1989-2014), probably indicating a efficiently water supplies in the research region, snow melt runoff may be calculated under future climate forecasts.

Ayub et al., (2020) performed glacier melt runoff simulations in the Gilgit sub-basin and estimated runoff from different elevation zones. It was found that major portion of runoff is generated from the 4000–5000 m elevation zone. Higher temperature scenarios predicted higher runoff. Precipitation trend analysis exhibits an increasing snow cover area.

Umar et.al (2021) did trend analysis of Hydro-meteorological parameters in the Jhelum River basin, North Western Himalaya and studied the susceptibility to flood of River Jhelum. Jhelum river basin is surrounded by Himalayan Mountain range in the Kashmir valley. Various agricultural and hydraulic structures activities management and planning are analyzed through Hydro-meteorological trend and it is very crucial for such activities administration. The tendencies in the yearly maximum and yearly average rainfall, yearly maximum, and yearly average discharge for the Jhelum River Basin have been studied and analyzed in this study. Sen's slope, Mann-Kendall (M-K), and innovative trend analysis (ITA) were used to analyze trends in a variety of hydro-meteorological data. In contrast to the considerable falling trend in annual average rainfall and discharge, the study using ITA showed a large rising trend in the annual maximum rainfall and discharge. Trend analysis, which shows deviations in hydro-

meteorological data, can be used to manage water resources in the future. It was also determined that the Jhelum River discharge fluctuations were caused by climatic changes and anthropocentric activities in the basin area.

Adnan et al. (2022) did research on the Upper Indus Basin's (UIB) stream flows are influenced by changes in seasonal snowfall and glacier ablation, which in turn disturbs the water amount in UIB's downstream regions. Studying the long-term fluctuations in runoff components as a consequence of climate change is urgently needed in this situation. Using the University of British Columbia Watershed Model, the current study examines the spatiotemporal variation in runoff and runoff components as a result of climate change to the Gilgit River stream flows from 1981 to 2020. (UBC WM). Three statistical measures were employed to compare stream flows simulated by UBC WM to actual stream flows: the Nash-Sutcliffe efficiency (NSE), coefficient of determination (R^2), and correlation coefficient (CC). According to statistical indices, the UBC WM performed well during both the standardization (1981-2000) and authentication (2001-2015) phases, with R^2 values of 0.86, 0.83, and 0.92. From 1981 to 2020, all runoff components showed a significant rise, with significant inter annual variability in their respective contributions to stream flows. Between 1981 and 2020, the Gilgit River's stream flows were anticipated to be affected by snow melt, glacier melt, rainfall-runoff, and base flow, with respective average contributions of 25%, 46%, 5%, and 24%. A seasonal study found that the Gilgit River got just 14% of its total discharge during the winter and approximately 86 percent of it during the summer (April to September) (October–March). The Gilgit River generates around 76% of its total runoff between altitudes of 3680 and 5348 m, just 19% below 3680 m, and only 5% above 5348 m, according to a more thorough analysis of runoff at the

geographical scale. Furthermore, it was shown that groundwater from the lowest zone of the earth contributed to 76% of stream flows. The results of the research may help hydrologists and water monitoring personnel handling the water supplies for domestic, industrial, and agricultural usage in areas downstream of the UIB. Approximately 70 to 80 percent of the Indus River's discharge was caused by glaciers and seasonal snow melt. Water from the Indus River basin is crucial for Pakistan's industry, livelihoods, agriculture and enormous populace. Due to its terrain and water supplies, the Gilgit River basin, which is a sub-catchment of the UIB, has recently gained increased significance.

Additionally, a number of hydro power and building projects are being carried out in this area with the support of the Chinese government, making it crucial for the development of both China and Pakistan. However, due to the high susceptibility of adversities connected to glacial retreat and detachments, landslides, rock-ice avalanches, debris flows, and GLOFs, new reservoirs must be built in the HMA. Sustainable sediment management techniques are needed to address these problems since these kinds of catastrophes produce significant amounts of residue that can fill basins/lake and perhaps lead to dam disaster.

Remote Sensing:

The benefits of Digital Elevation Models were discussed by Susan K. Jenson (1991). Digital elevation models (DEMs) can be used to generate a plethora of data on a land surface's morphology. Slope, aspect, and shaded relief data can be derived using traditional raster analysis methods; depressions, overland flow pathways, and watershed borders can be delineated using recently developed computer programmes. To establish

watershed margins for a geochemical stream sediment research, evaluate slope and flow route extraction findings from DEMs of different resolutions, and analyse the geomorphology of a Martian DEM. such methods were used.

Willhauck et al, (2000) described the most recent developments in remote sensing analysis software that enable innovative methods of integrating satellite imagery with archive data from aerial photography in their document called "Comparison of object-oriented classification techniques and standard image analysis for the use of change detection between SPOT multispectral satellite images and aerial photos" that was printed in the minutes of the XIX ISPRS congress in Amsterdam. This study demonstrates how decision-making in forestry applications in the Argentine Nothofagus woods can be aided by this inclusion. Two key elements are highlighted. The classification of SPOT multi spectral data for land cover identification in Tierra del Fuego is one example. Another is the use of aerial pictures coupled with SPOT multispectral data to detect changes using object-oriented classification. The methodological novel methodology of object-based classification has now achieved critical objectivity of comparison. In order to comprehend its use in this study, a fundamental definition of the novel idea of object-oriented classification is provided. The SPOT data categorization findings show that there are no significant differences in accuracy between the two approaches. The object-oriented strategy is preferred in terms of output map appearance. The variation finding result demonstrates that the object-oriented method opens up novel options beyond standard visual analysis of aerial photos, allowing quantitative change detection and GIS implementation utilizing automatic feature extraction.

Hayakawa et.al. (2008) made comparison between two DEMs. G-DEM, a new global elevation data set based on ASTER satellite images, is expected to be available in late 2008. At a horizontal resolution of 1 arc second, G-DEM will be the best unrestricted and publicly available global digital elevation model (DEM). They compared the value of G-DEM to the best current global elevation data set, the 3-arc-second SRTM DEM. Basic geomorphometric parameters were investigated for a pre-release edition of G-DEM and SRTM DEM for western Japan. G-DEM contains fewer misplaced cells than SRTM DEM in sharp, steep terrain. Furthermore, G-DEM depicts low lands, valleys, steep slopes, and highland ridges more consistently and accurately than SRTM DEM, which includes numerous localized spike and gaps and over values valley-floor elevation while under valuing ridge elevation. G-DEM will be widely used in geo scientific investigations due to its higher quality, fewer incomplete information, and better topographic representation than SRTM DEM.

Farr et al. (2014) in article The Shuttle Radar Topography Mission characterized the Shuttle Radar Topography Mission. The Shuttle Radar Topography Project created the world most comprehensive and high-resolution digital elevation model. NASA, the National Geospatial- Intelligence Agency, and the German and Italian Space Agencies collaborated on the project, which began in February 2000. It acquired interferometry radar data with two radar antennas and converted it to digital geographic information with a one-arc-second resolution. Consumers of this unique data collection can learn more about the innovation, general aviation, data analysis, and goods.

Four homogenization experiments were looked at, each with a distinct

homogenization methodology. Different levels of homogenization operator environment with HOMER, as well as different Meta data applications, are used in these approaches. A reference series was established by using HOMER underneath the greatest possible conditions to evaluate the efficiency of HOMER in limited networks.

HOMER reduces the accuracy of temperature data when used in fully automated mode. As a result, using HOMER automatically is not recommended. In sparse networks, the reliability of precipitation and temperature data may be enhanced if HOMER is used in cooperating mode. Breakpoints, on the other hand, must be placed cautiously. Data from Meta data should only be utilized to pinpoint the precise timing of quantitatively detected breaks. Given the high noise in sparse networks, adding extra breakpoints based purely on metadata may result in negative modifications.

Kanwal et al. 2016 employed GIS information and methodologies to quantify landslide risk in Pakistan's Shigar and Shyok Basins' harsh hilly terrain. The study area is in the Karakorum mountainous area, where earthquakes are widespread and carriage a grave hazard to ancient residents. Landslide vulnerability index maps were made by mingling 04 key indicator clusters: (1) human-induced parameters, such as Landsat 8 visuals and road location; (2) topographical specifications, such as slope, aspect, and scheme curvature; (3) hydro logical variables, such as flow power index, geomorphologic moistness index, and length from drainage; and (4) geological parameters, such as lithology and distance from lead to a significant. These layers were developed using a Geographic Information System (GIS) and a heuristic approach based on the analytical hierarchical (AHP) was used to produce the final landslide susceptibility for this early district levels landslide hazard analysis. In the area, three

main susceptibility zones have been identified. The final map was created using AHP weights with a consistency ratio of 0.04. When the distance from roads, distance from drainage, and location from significant thrusts and faults parameters were not combined in the analysis, the final landslide susceptibility map was prepared shows that the low, modest, and elevated landslide susceptibility categories cover 23.2 percent (4745 km²), 45 percent (6737 km²), and 23.2 percent (3444 km²).

Remote Sensing and Glaciology:

Tasseti et al., (2008) have provided methods and procedures for glacier mapping in the open-source environment using 3 X multi temporal Landsat scenes with sensors MSS, TM and ETM + combined with other type's information (2D, 3D and thematic data). Supplementary Refined classification methods, Principal Component Analysis (PCA) and image ratioing supported by accuracy assessment for the creation of accurate maps of glacier extension, for amendment recognition researches.

Similarly, Frauenfelder and Kaab (2009) used multi- temporal optical remote sensing data to perform glacier mapping in the Brahmaputra River basin. Raup et al., (2007) presented the international consortium on Global Land Ice Measurements from space (GLIMS) project. This project obtains global satellite images for glaciers, analyses those for glacier extent and changes as well as make assessments on change data. Paul (2000), Bolch and Kamp (2006), Paul et al., (2013), Smith et al., (2015) and Paul et al., (2016) discussed methods, algorithms and accuracy for semi- automated glacier mapping and delineating outlines and concluded that the algorithms misclassify upto approximately ten percent of the glacier area, hence, supplemented manual digitization may be used in combination with algorithm-based delineation.

Hewitt (2009) discussed the scientific explanation behind avalanche development. Rock avalanches are typically produced by disastrous rock slope instability in difficult terrain, according to his investigations. Movement over ice affects the magnitude of landslide runoff and its placement geometry when these occur in glacier basins. Glacier motion and sedimentation can be significantly altered. Ice activity causes avalanche or mudslide debris to rapidly change, transport, and spread. The structure of these relationships is shown by observations made over a 20-year period in the Karakorum's Bualtar Glacier. In August 1986, stalwart landslides swept down onto the glacier's ablation zone. Their wetness parts and outlines of deposition were exaggerated by movement over ice. Glacial motion accelerated at and just below the rock landslide deposits and the glacier surged inside within months. Two years later, there was another increase. Beyond the ice borders, significant slope collapses and debris flows were triggered, and pond melt water resulted in local outburst floods. By 2005, the avalanche sediment had travelled 9 km, or about one-third of the millage travelled during the heaves.

It was eventually completely altered to make it less distinct from other massive supraglacial detritus. A significant region of congealed ice remained where debris hindered ablation, resulting in a positive mass balance comparable to a 20% rise in monthly accumulation. Regardless, it happened as a moving ablation zone section. It had, in reality, replaced the mass transported in the surges after ten years. According to data from the mid- 1980s, rock landslides surpassed preexisting supra glacier debris by around five times, equating to over 500 years of average supra glacial transportation to the glacier boundaries over a 30-year period. Other effects of the frequency suggest that

this proportion to denudation will double.

Three more glaciers where latest rock landslides occurred, as well as twenty-one Paleolithic cave avalanches newly recognized as having scattered over glaciers, showed similar changes. Treating such phenomena as isolated extravagances, or landslides and glacial processes separately appears insufficient. They result in polygenetic deposits and morphologically diverse land forms. Individual episodes can last years to ages, and their frequency and number can override or divert geotectonic and climatic factors. They are proposed to be important, but previously misunderstood or overlooked, factors of land surface development in the Karakoram and possibly other high ranges.

Biswajit and Asif (2015) investigated the glacier melt components. The glacial melt component is underestimated by the hydrograph separation technique, which was previously developed to assess base flow; seasonal snowmelt and glacier melt constituents in river flows within the Upper Indus basin. For extensively glaciated watersheds, this is primarily a limiting factor. A further update to the approach has removed the limitation. Regardless of the fact that the revised procedure is fully sovereign of the bodily attributes of the watershed in which it is used, the consequences are quite consistent with physic-chemical characteristics such as how the findings will be shown and the extents of glaciers. Glacial melt far surpasses snow melt in the rivers that drainage the Karakorum and Zanskar ranges. Annual glacial melt in the Karakoram ranges from 43 to 50 percent, whereas snow melt varies from 27 to 31 percent. Snow melt, on the other hand, takes precedence over glacial melt in the rivers that drain the western Greater Himalayas and the Hindu Kush. At this time, the fraction of snow melt in river discharge ranges from 31 to 53 percent, whereas glacier melt ranges from 16 to

30 percent. Snow melt fraction is generally greater than glacial melt fraction in the main stem of the Upper Indus River. Snow melt percentages in the main stem range from 35 to 44 percent, whereas glacial melt percentages range from 25 to 36 percent. Annual flows in the Upper Indus River near Tarbela Reservoir are 70 percent melt water, with glacial melts accounting for 26 percent and snow-melts accounting for 44 percent. According to Biswajit and Asif, glacier melt inputs to river discharge decreased throughout with comparison to earlier decades, the latter part of the twentieth century and into the early twenty-first century. This occurrence can be explained by any recent basin-wide loss of glacial mass in the altitudes from which most glacial melt arises, or glacier stability and growth as a result of reduced fuel imports or enhanced rainfall, or together, at the tall elevation bands from which glacial melt water makes way to flow.

Smith, et al., (2015) in the article improving semi-automated glacier mapping with a multi-method approach: applications in central Asia mentioned that glacier investigations typically necessitate exact glacier outlines. Present algorithms scuffle to distinguish glacier sections with debris cover or even other asymmetrical spectral profiles, therefore in-depth human digitizing in a geographic information system (GIS) is required where these are not accessible. Various technologies have enhanced different spectral ratio identification of glacier areas, but none has gained widespread adoption due to complexity or processing power. They presented and tested a glacier plotting technique in Central Asia that can distinguish between pure glacier ice and debris-covered glacier tongues. The technique is based on glaciers' distinct velocity and topographic appearances, as well as spectral information relationship data. They discovered that, when compared to a 750-glacier control data set, the system misclassifies around 2 and 10% of glacier areas, and that it can properly categories a

particular Landsat scene in 3–5 minutes. Although the method does not completely solve the problem of recognizing glacier regions from remotely sensed data, it is a noteworthy advance over solely spectral-based classification systems such as the Landsat 7 band ratio or the Normalized Snow Index (NDSI). Individual glacier categorization errors, dependency on user involvement to distinguish related glacier sections, and reliance on the correctness of the entering Landsat data are among the algorithm's major faults.

Yaduvanshi and Ranade (2015) in the paper Effect of Global Temperature Changes on Rainfall Fluctuations over River Basins across Eastern Indo-Gangetic Plains described the weather cycle of India. India's annual weather cycle is dominated by rainy and parched seasons, through monsoonal rains being one of the most notable raining days. Monsoon rainfall over India reveals significant spatiotemporal differences and huge deviations from average values. This research was aimed to examine climatological traits, oscillation patterns, and episodic sequences in annual, seasonal, and once-a-month precipitation data from seven river basins covering the Eastern Indo-Gangetic plains (EIGP) between 1829 and 2007.

Its links with global tropospheric temperature changes and El Nino-La Nina cycles are also investigated. The Subarnarekha River basin receives an average annual rainfall of 1070.5 mm (216.8 mm) in Tons and 1508.6 mm (205.2 mm) in the Subarnarekha River basin. The EIGP receives the most rainfall during the monsoon season (1188115.4 mm) and in July (372.656.3 mm). Apart from post-monsoon and winter, yearly and monsoonal precipitation is evenly distributed over all river basins. Precipitation variations exhibited 2-to-3 trends in a mixture of increase, drop, and usual

across the time covered by the records that are currently accessible. Although there is no discernible enduring pattern in the annual rainfall in any of the river basins, there is a tendency in the monsoonal rainfall in the Brahmani, Sons, Mahanadi, and EIGP. In all river basins, monsoonal rainfall has decreased over the last 20 years. All precipitation series have significant, recurrent spikes in their power spectra at wavelengths of 3-5 years, 10-20 years, 40 years, and >80 years. The greatest of the variance in average rainfall (77.6%) is due to short-term fluctuations of fewer than ten years, followed by inter annual variations of 10-30 years (13.1%) and long-term trends of more than 30 years (9.3 percent). Inter annual fluctuation appears to be linked to various climatic signals, whereas long-term variations are caused by asymmetry in global tropospheric warming.

Nahida (2016) used SRTM DEM to delineate the Konya Basin. The Himalayas have the extreme reduction in glacier extent and area, as well as the largest adverse mass balance. From the Himalayas to the continental heartland, the reduction gradually decreases, with the eastern Pamir having the lowest glacier retreating, area lessens, and positive mass balancing. Additionally, rising temperatures are generating decreased rainfall in the Himalayas and higher rainfall in the eastern Pamir, both of which are influenced by different atmospheric circulation patterns. A spatial hydrology model uses GIS data to pretend water flow and transport on a definite section of the earth, with the region's boundary represented by a polygon, such as a river basin or aquifer frontier. The outcomes show that watershed boundaries in the Konya city basin and sub basin may be determined using the ArcGIS watershed function. This project primarily serves as a demonstration of how to utilize GIS to define watersheds and abstract drainage. Hydrology Tool was used to establish the watershed border, flow direction, flow

accumulation, flow length, and stream ordering; and Surface Tool was used to generate the contour in ArcGIS-10.3.1 software and DEM, and then build a model for these processes in Arcsine. According to Konya Wikipedia, the entire size of the catchment deliberate from the watershed layer is around 40233.94 km².

In their article titled "Reconstructing the progression of a deep underlying rock fall (Marzell) and its responding to glacial retreat based on historic and remote sensing data" Fey et al. (2017) used a mixture of multiple topographic maps from old topographic maps and remote sensing to recreate and display the behavior of the topped mountain ice contact rock slide system Marzell and its reaction to glacial retreat. Geodetic measurement, terrestrial laser scanning, and UAV imaging campaigns were used to transform information from noticing activities into spatial images and/or elevation data. The information has been gathered and analyzed since 1951 with the goal of reconstructing the range, width, and compaction of the glacier since 1893, as well as analyzing the expansion of rock slide deformations by getting data about dispersion path, dip angle, velocity, and incomplete letdown of rock slide slabs. The rock slide is made up of several different slabs that move downstream as stiff blocks along basal shear zones. The study's and analyses' conclusions led to rotational rock slide failure tools. The ice volume loss in the glacier's proximity coincides with the rock slide activity. Annual average rock slide action was around 0.05 m/a between 1971 and 1997, whereas yearly total ice thickness loss was around 0.05 and annual average ice fatness was 0.1 m/a. The annual average ice thickness loss has augmented rapidly to 5 m/a since the turn of the century. The rock slide activity increased at that time. The peak of rock slide action (up to 1.5 m/a) occurred in the year 2000, when glacier retreat exposed 50% of the slope toe. A slowdown of the rock slide has been seen since 2010.

Between 1893 and 2014, the glacier near the rock slide almost disintegrated, losing 99.88 percent of its ice volume. The geomorphic and geological data collected on the rock slide progression and glacial retreats from the base will be used in future rock slide investigations, as well as to analyze and model the effect of glacial debuitressing.

Remote Sensing and Hydrology:

With a pixel size of 30 arcs second, Hijmans et al. (2005) created interpolated climatic surfaces for all land areas on the planet (apart from Antarctica). The climate variables examined included mean, minimum, and maximum monthly precipitation. Data was collected from a number of sources and, where possible, was limited to records from the 1950s to 2000s. They used the ANUSPLIN package's thin-plate smoothing spline technique for interpolation, with latitude, longitude, and height as independent variable. At high latitudes, elevation bias was detrimental (stations were lower than expected), while in the tropics, it was beneficial.

Mountainous and sparsely sampled places have the highest level of uncertainty. Data partitioning revealed substantial surface uncertainty on inaccessible islands, such as those in the Pacific. Combining elevation and climate data to a resolution of 10 arc minutes revealed massive variance within grid cells, demonstrating the significance of high-resolution surfaces. A study using two high-resolution data sets for the United States found places with considerable local metamorphoses, mostly in mountainous locations. Interposed climate surfaces for global land areas developed have the following advantages over previous global climatologists: the data have a higher spatial resolution (400 times or more). Due to the limited density of available climate stations, estimated climate representations for global areas of land do not represent all variability

that might also happen at a resolution of 1 km, predominantly rainfall in hilly zones. Knowledge-based approaches and the incorporation of supplemental co-variants, such as remote sensing layers, could be used to include these distinctions in future study.

Hemant et al., (2013) highlighted how morphometric analysis of the upper catchment of the Kosi River using GIS techniques. They noted how Geographic Information System (GIS) has proven to be an effective instrument in the demarcation of drainage outline for water resources management and planning. In this work, the researchers examined the characteristics of the upper Kosi River basin and identified morphological traits using GIS and image processing techniques (flows through Tibet, Nepal and India). The high-altitude Himalayan Mountains, which include Mount Everest and Kanchenjunga, are part of the basin area. This basin was a major contributor to India's Bihar state's severe floods in 2008. Arun, Sunkosi, and Tamur are the three sub-catchments that make up the catchment. By relating the features of these three sub-catchments, a morphometric study reveals the environment of drainage in the upper catchment of the Kosi River, as well as some of the causes of high-intensity floods. It shows that the highest-order drains are present in both Arun and Sunkosi, and that the first-order drains are quite long (6,088 km) because of the nonappearance of vegetation and the rocky/barren surface, both of which have a large amount of runoff potential. Tamur sub-basin has the highest flow kinetic velocity because it has the largest mean channel gradient when compared to the other sub-basins. The Arun sub-catchment has the greatest potential for runoff and sediment production, according to the data. The fact that the sub-catchments Arun and Sunkosi contribute their peak floods at the same time, essentially doubling the flood concentration, is one of the key reasons of the high intensity of the torrents.

In their paper A GIS-based strategy in drains morphometric analysis of Kanhar River Basin, India, , Parveen et al. (2017) stated that using a Geographic Information System (GIS) to analyse morphometric parameters would be a practical method of characterizing the watershed's hydro logical response behavior. Satellite remote sensing data was widely regarded as the most effective, time- saving, and exact approach for morphometric basin investigation. ASTER (DEM) in association with satellite remote sensing information (Landsat ETM+, 2013 and geospatial survey of Indian toposheet, 1972) was proven to be useful for the drawing out of river basins and their stream webs. The Kanhar basin channels of the Son River were chosen for extensive morphometric examination in this study. Within this basin, seven sub- watersheds were also defined in order to calculate the morphometric factors. Water ordering, stream segments, branching ratio, drainage network, stream length, sleek design, circulatory ratio, and other morphometric characteristics were calculated. The basin's drainage area is 5,654 square kilometers, with a sub-dendritic to dendritic watershed. The basin's stream order was mostly determined by the area's physiographic and lithological conditions. The research region was classified as a seventh-order basin, with a drainage density of 1.72 km/km². The transition from lowest to the highest order in main channel ratio indicates that the studied area has achieved a stable geomorphic stage.

Climatology, Hydrology and Glaciology:

Hasson et.al. (2017) highlighted the importance of melt water from glaciers and its effects on low laying areas of Pakistan. The Hindu Kush– Karakorum–Himalaya melt water is the primary supply of water for about two-thirds of Pakistan's population. Water removals from Pakistan's upstream Indus Basin (UIB) contribute for 50 % of the

country's available surface water, which is crucial for crop yields, household and commercial usage, and hydro power generation. Despite this, comprehensive analyses of the current situations of major meteorological elements that influence water supply are scarce. This research examines changes in highest, lowest, and median temperatures, as well as 24-hour thermal gradient and rainfall, from 18 stations (1250–4500 m a.s.l.) during their respective record periods (1995–2012) and six stations for their long-term records (1961–2012). The presence of a trend is detected using a Mann–Kendall test on sequentially independent time series, whereas the true slope is determined using Sen's slope method. Furthermore, within the UIB's ten sub regions, locally recognized climatic trends are statistically quantified for their spatial-scale implications, and the geographically (field) important climate trends are qualitatively contrasted with changes in release out of corresponding sub regions. Over the recent time (1995–2012), they detected spring warmth and dryness (field-significant in March) as well as rising early melt season flow from most of the sub regions, probably due to rapid snow melt. During the monsoon season (particularly in July and September), however, most sub regions undergo field-significant cooling, which corresponds with the primary glacier melt period. As a result, during the mid to late melt period, the related sub regions discharge diminishes or grows only slowly (particularly in July). These patterns, which are mostly similar with long-term trends (1961–2012), most probably reflect nival dominance but repression of glacial melt command, which could have an impact on the UIB's total hydrology in the future. Despite the modest number of observations, these findings contribute to understanding the UIB melt runoff dynamics and to provide a hydro climatic hypothesis for the Karakoram Anomaly.

Adnan et al. (2017) studied the Himalayan, Karakorum, and Hindu-Kush

Mountain ranges, which make up the bulk of Pakistan's water possessions, are three of the greatest mountain ranges in the world. This study calculated the Gilgit River's (snow+glacier) and rainfall runoff, which originates in Pakistan's UIB and is one of the river's largest tributaries. The snow melt runoff model (SRM), which was developed using cryospheric data from the MODIS, was used to forecast the daily flows of the Gilgit (moderate resolution image spectroradiometer). Once the SRM was properly regulated, the replication was run from 2005 to 2010 with a coefficient of model efficiency ranging from 0.84 to 0.94. The SRM provided an average of 78.35% of the (snow+glacier) and 21.65% of the rainfall contributions to the Gilgit stream flows from 2001 to 2010. Using the representative concentration path ways (RCP) 4.5 and 8.5 scenarios from the Fifth Assessment Report of the Inter-governmental Panel on Climate Change (IPCC) the consequences of temperature changes on the climate of the Gilgit watershed were investigated. Under the RCP 4.5 scenario, the amount of precipitation will only slightly increase but Gilgit's air temperature will increase by 3°C. Between 2010 and the end of the 21st century, the RCP 8.5 scenario (overshooting scenario) predicts a 10.7°C increase in air temperature in the Gilgit watershed, but a decrease in precipitation. By the end of the twenty-first century, the average annual runoff in the Gilgit will increase by 67.03 and 177.5%, respectively, in comparison to the observed runoff, based on the use of the RCP 4.5 and 8.5 mean temperature situations in the SRM, with rises in mean temperature 3.02°C and 10.7°C, respectively. Utilizing the greater surface overflow brought on by snow/glacier melt may be achievable by creating fresh stowage sites in advantageous locations.

Hussain et al. (2019) remote sensing with MODIS to investigate the spatiotemporal dynamics of snow cover and its interactions with climate change and

stream flow, data from SCA (Snow Covered Area) and hydro- meteorological ground stations were studied. Except during the fall period, which displays a substantial falling tendency for the Gilgit River Basin, the SCA values show a statistically non-significant decreasing inclination. The fact that spring has more SCA may be the cause of the altered snowfall pattern. SCA variation is a sign of the changing climate, which has an impact on the timing and volume of snowfall in the basin. Winter temperatures are rising, which might cause solid precipitation to turn into liquid close to freezing. Additionally, according to the Pearson correlation coefficient of annual and seasonal temperatures, SCA has a very negative link with the summer time temperature. Snow cover changes have a significant impact on river runoff, so determining the winter snow accumulation is crucial to predicting the summer peak flow for improved water resource management. The SCA and stream flow in the basin have just a slender association with precipitation. The majority of climate stations are located in valleys, whereas high-altitude stations have persistent flaws in their precipitation gauges, so the current rainfall record of climate posts is not an accurate picture. However, to contribute to the analysis of snow cover is one of the most significant river basins of UIB, where the effects of global warming would have implications for water balance and, consequently, impact the sustainable management of water resources, this is the first study.

Remote Sensing and Land Use:

Land use land cover variations have emerged as pressing problem around the globe during the recent decade since these fluctuations are mainly unplanned and evident in the form of environmental degradation, water scarcity and deteriorating food security (Ali et al., 2019; Rasul et al., 2021). LULC is a dynamic process and driven by

natural phenomenon concomitant with anthropogenic interventions (Rather et al., 2020). LULC changes have a significant influence on weather, hydrology and biogeochemical cycles which results in hostile ecological problems if spread unencumbered (Bhat et al., 2016). LULC have become a crucial variable in altering regional climate, owing to which monitoring and assessment of LULC studies are impertinent and provide significant input to environmental decision-making (Ahsan et al., 2021; Meraj et al., 2018).

Land use refers to how people and their habitats use the land, with stress on the land useful role in pecuniary activities, whereas land cover states to the bodily features of the earth's surface (Mariye et al., 2020). Land usage land cover (LULCs) technique is most widely used method for determining in what way the land has been used earlier, type of discoveries can be expected in the future, as well as the dynamic force and process behind these variations (Ebabu et al., 2019; Fenta et al., 2017; Maitima et al., 2009). Similarly, land use land cover (LULC) changing aspects are a recognized, quickening and considerable method, typically ambitious by people deeds that is contributing ominously to forest destruction, land dilapidation and biodiversity damage and is mostly driven by human activities (Dagnachew et al., 2020). Climate, rainfall, foliage cover, land surface temperature, municipal structure and composition factors are affected by LULCC (Aboenour et al., 2018; Findell et al., 2017).

Aboenour et al., (2018) has experienced rapid urban growth and extensive development in recent years in Egyptian cities. As a outcome of these expansions, this region faces a variety of environmental issues. To attenuate such magnitudes, it's necessary to investigate the temporal change used to quantify the GCR's urban length,

as well as its impact on land surface temperature (LST). In the research, maps of land use/land cover (LULC) were created using data from Landsat 5 TM for 1990 and 2003 and Landsat 8 OLI for 2016. Effective LST analysis was achieved by combining a web-based atmospheric correction model and a spectral radiance model with Landsat thermal bands. The total accuracy of Landsat generated land use data was 90.3 percent, 96.5 percent, and 94.9 percent in 1990, 2003, and 2016, respectively. Within a 26-year period, the LULC change analysis showed a 7.73 percent loss of vegetation to urban land and an 8.70 percent loss of barren lands to urban usage (1990- 2016). Rapid urbanization threatens to diminish vegetation areas, boosting LST and altering the urban microclimate. The conclusions of this study will help policymakers describe the future trajectory of urban construction. Important information about the natural environment and human activities on the earth's surface is provided by land use and land cover. (Gong et al., 2011; Rather et al., 2020). Many researchers have been used multi spectral satellite images that have been used for sensing and calculating the spatial and temporal dynamics of forestry cover change (Aroengbinang et al., 2015). GIS and remote sensing statistics provide information for land use change investigation, modeling and administration. It is a cost-effective, quick and precise method of LULCC measurement (Herold et al., 2007; Jallat et al., 2021). Remote sensing data has been widely used in land use and land cover over the last few decades, providing information on forest and wetlands degradation, urbanization, agricultural activity rates, and human activities. High-resolution satellite systems including IKONOS, Quick Bird, and SPOT-5 imagery have just been available. High-resolution satellite imagery is more accurate than traditional satellite imagery (Rasul et al., 2021; Yang et al., 2011). Moreover, land use and land cover classifications are expensive and prolonged processes but there are many methods that can be used in the collection, analysis and presentation of resource

data such as geographic information system and remote sensing that can facilitate the process (Dagnachew et al., 2020; İkiel & Ustaoglu, 2011).

According to Ali et al. (2019), the mountainous regions of Northern Pakistan are full of biodiversity, home to glaciers, and a significant Indus River basin, all of which offer ecology services for the local population. Since these areas have undergone extensive deforestation and are currently susceptible to fast changes in land cover, an accurate valuation and observation are essential to halting such changes. In this study, the observed changes in land cover during a thirty-nine-year period—divided into three stages were studied. The stages were 1976–1999, 1999–2008, and 2008–2015. Land cover change was detected using four images from the Landsat 2 Multispectral Scanner System (MSS), Landsat 5 Thematic Mapper (TM), Landsat 7 Enhanced Thematic Mapper, and Landsat 8 Operation Land Imager data. To identify apparent land cover changes in Pakistan's Gilgit River Basin, the supervised classification-maximum probability technique in ERDAS envision has been utilized. Range land, glaciers, aquatic bodies, and built-up/agricultural cover are the primary classifications that have been altered by natural and anthropogenic actions, according to the assessments. In 1976, there were 1.13 percent built up/agricultural land, 45.3 percent 0.66 percent rangeland, water bodies, and 13.2 percent glacier cover, respectively. While in 2015, the proportions of built-up area, agricultural land, rangeland, water bodies, and glacier cover were 3, 25, 12, 7, 0, 91, and 8, 2 respectively. These changes to the land cover posed a serious threat to watershed assets. Therefore, effective management of the watershed resources is essential; otherwise, they will quickly deplete and lose their capacity to contribute to the region's socioeconomic and environmentally sound development.

In order to effectively manage water resources, surface runoff must be evaluated in connection to climatic and land-use changes, claim Haleem et al. (2022). Future land-use change was mainly ignored as the majority of the study focused on predicted properties of climate change on surface runoff. With a focus on the Upper Indus Basin in Pakistan, the main objective of this study is to use the Soil and Water Assessment Tool (SWAT) to differentiate between the effects of anticipated climatic and land-use changes on surface runoff. Four bias-corrected general circulation models and cellular automata artificial neural networks are used, respectively, to forecast future scenarios of land use and climate change. The calibration era (2000–2008) and the validation period (2009–2013) were separated from the historical record (2000–2013). The simulated outcomes showed that the SWAT concept worked effectively. According to the data collected between 2000 and 2013, climate change has a greater impact on river discharge (61.61%) than land use change (38.39%). Upcoming overflow deepness in this basin is predicted to rise as an outcome of both climate and land-use variations. Land-use change (0.37-1.1%) has less of an impact than climate change (12.76-25.92%). In areas without access to conventional gauges, modeling hydro logical reactions using global weather data is a suitable option. The paper analyses how changing land use and climate affect runoff depth and offers advice for water resource managers to improve the sustainability of the aquatic ecosystem. The following can be said to sum up the findings: The simulated results demonstrated that both during calibration and validation, the SWAT model generates accurate statistical findings (NSE = 0.69, R2 = 0.7, RSR = 0.56 and PBIAS = 9.7). The SWAT model was used to separate the effects of climate and land-use change on river runoff in the upper portion of the Indus River basin, Doyain station at Astore River, where the contribution rates of climate and land-use changes on surface runoff were 61.61 and 38.39%, respectively.

The CMIP5-based GCMs (CanESM2, GFDL-ESM2G, MIROC5, and HadGEM2) have significant application for predicting future climate change in the research domain. The average annual river runoff increased across the simulation periods of 2007–2020, 2021–2034, 2035–2048, and 2086–2099 using the calibrated model. The CA-ANN model's projection of land usage for the year 2050 showed that river runoff would be on the rise by 1.1%.

According to Dehri et al. (2021), one of the main issues facing humanity in the twenty-first century is Climate change. The high-altitude Indus basin's historical climatic and hydro logical regimes, as well as extreme climate projections for the twenty-first century, were examined in this study. Improved temperature and precipitation records were made and entered into a completely distributed physically based energy-balance Variation Infiltration Capacity (VIC) hydrological model in order to reproduce the fluid balance at the regional and sub-basin scales. In comparison to the historical baseline, the data revealed two distinctly different signals of changes in the hydrological and climatic regimes. By the end of the twenty-first century, the median annual air temperature is predicted to rise by another 0.8 to 5.7 °C, compared to an increase of 0.6 °C over the previous 40 years. Similar to the yearly precipitation, which has decreased by 11.9%, future predictions are highly ambiguous and spatially inconsistent. While decreasing in the SW Hindu Kush and some sections of the Western Himalayan region, precipitation is predicted to increase in the Karakoram region. The Model for Inter disciplinary Research on Climate version-5 (MIROC5) generally initiatives rises while the Max Planck Institute Earth System Model at available for treating (MPI-ESM-LR) typically projects decreases in precipitation and river inflows under three Typical Concentration Pathways (RCPs) of 2.6, 4.5, and 8.5. The Indus-

Tarbela inflows are more likely to increase as compared to inflows into the Chenab, Jhelum, and Kabul rivers. For all river gauges, significant increases in peak flow magnitudes and one-month earlier achievement are anticipated. In the majority of scenarios, high flows are expected to rise, whilst low flows may fall for MPI-ESM-LR in the Jhelum, Chenab, and Kabul River basins. Therefore, it is anticipated that hydrological extremes will intensify. In order to manage water resources in the basin as effectively as possible, significant adjustments will be needed to the strategies and action plans for hydropower production, storage reservoir building and operation, irrigation withdrawals, flood control, and drought management.

Khattak et al. (2011) evaluated changes in a variety of hydro- meteorological variables in Pakistan's upper Indus River basin (UIRB). In order to represent the variety of hydro-meteorological conditions in the basin, mean monthly usage from 20 meteorological and 8 hydrometric channels were investigated for patterns that use the non-parametric Mann-Kendall test in combination with the trend-free pre-whitening approach for attempting to correct time series data sets for serial correlation. The size of trends was assessed using Sen's slope method, a non-parametric method for computing a slope for a uni-variant time series. They took into account three meteorological variables: lowest temperature, maximum temperature, and precipitation. They also took into account stream flow as a hydrological variable. Many more trends were found for several of the variables than would be anticipated to happen by chance. In the upper, middle, and lower regions, respectively, the maximum winter temperatures showed increasing trends with trend in slopes of 1.79, 1.66, and 1.20°C per 39 years. Trends in precipitation were erratic and without any clear pattern. Increasing trends in mean maximum temperature were shown to be correlated with trends in stream flow,

particularly in the winter and spring. Stream flow in the winter and spring is predicted to increase with higher winter temperatures. Summer stream flow decreases water availability in the Tarbela Dam, necessitating adjustments to the reservoir operating strategy for more effective management of the available water.

According to Farhan et al. (2020), climate change has a substantial consequence on the thermal and hydrologic systems of rivers fed by snow and glaciers in addition to having an immediate impact on freshwater accessibility, environments, and household water use. In general, river flow is regarded as a representative of hydro logical processes and, hence, as a precise reflection of climatic changes in any given catchment. As a result, we examined the historical trends of the Astore and Hunza river flows as well as the effects of climate variability in this study. Long-term in-situ hydro-meteorological data are mostly used to derive the conclusions from this study. According to the study, climate change is considerably affecting and changing this region's characteristics and hydro logical resources. In both the Hunza and the Astore Basins, the high- and low-altitude stations consistently experience summer cooling and winter and spring warming, however the strength of these shifts was not found to be the same in any basin. Additionally, it was discovered that the Astore Basin's modest increase in total annual precipitation was incomparable to the Hunza Basin's precipitation, which exhibits a rather strong increasing tendency. Furthermore, similar temperature increases were seen at both low and high elevation postings. In contrast, the rainfall patterns at high- altitude Astore stations showed significantly increased winter precipitation, which contrasted with the precipitation seen at low-altitude stations. It was discovered that summer cooling, slower glacial ablation, and ultimately a considerable decline in Hunza River discharge were the main contributors to the

significant reduction in river flows during the glacier-melt period, notably in the Hunza basin. The Astore basin experienced a small increase in discharge but a slight decrease in temperature during the glacier-melt season. It is difficult to forecast how weather variation may influence glacier-melt patterns using hydro logical feedback due to the lack of any in-situ data on evaporative losses and the negative correlation among temperature and discharge in snow-fed catchments. It is therefore advised to conduct thorough investigations to determine how current climate change is affecting the regional hydro logical cycles in snow and glacier fed basins. It was discovered that summer cooling, slower glacial ablation, and ultimately a considerable decline in Hunza River discharge were the main contributors to the significant reduction in stream flow during the glacier melt season, notably in the Hunza basin. The Astore basin experienced a little rise in discharge but a slight reduction in temperature during the glacier-melt season.

Adnan et al. (2017) expressed major concerns about rising temperatures over the snow and glacierized Himalayan region, which could disrupt future river streams of the Indus River system. They also forecast how snowfall and glacial melt flows will manage the Upper Indus Basin's future water resources (UIB). In their study/analysis, they employed a snowmelt runoff model (SRM) combined with MODIS remote sensing data to forecast diurnal discharges of the Gilgit River in the Karakoram Range. The SRM was successfully regulated, and then imitation was carried out across four years, from 2007 to 2010, with model efficiency coefficients of 96 percent, 86 percent, 90 percent, and 94 percent, respectively. Precipitation and mean temperature data from the regional climate model PRECIS were utilized in the SRM model to anticipate future Gilgit River flows. By the end of the twenty-first century, a 3°C rise in average annual

temperature might result in a 35– 40% increase in Gilgit River flow. In the future, the predicted increase in surface runoff from snow and glacier melt would necessitate greater water protection and sustainable in the Indus basin for agriculture and hydro power generation.

Rasul, et al., (2011) in their paper "Glaciers and glacial lakes under changing climate in Pakistan," mentioned that solid water resources have been losing their ice assets at an astronomical rate as a result of global warming. This has led to both an increase in the number of glacial lakes as well as a decrease in Mountain risks known as Glacial Lake Outburst Floods (GLOFs) have been occurring more frequently in recent years. They are terrible. Over the previous decade, a concerning compounded temperature drift in Pakistan's northern regions has expedited the melting of snow and ice, causing in the creation of lakes, some of which are potentially harmful to overflow. The snowline has risen because to rising temperatures, prompting wildlife to relocate and lower elevation glaciers to melt more quickly. Snow used to fall late in the winter and disappear in the early summer, cutting down on the time it took to undergo metamorphic alterations and convert to ice. Ponding of melt water below and around the terminal moraine need ongoing monitoring in order to fully comprehend their supraglacial performance and to calculate the likelihood of an outburst on a methodical basis in order to develop an early warning system. The Mountain Institute's (TMI) collaboration with ICIMOD on the Global Glacial Lake Partnership is a step forward in establishing such lakes and mitigating the potential losses from their eruption.

They also pointed out in an article in 2011 titled "Effect of Temperature Increase on Crop Growth & Productivity" that crop development and growth is mostly a function

of temperature if water is available to the optimal satisfaction. Though weather patterns have never been consistent, with positive and negative swings occurring on a regular basis, recent atmospheric warmth has been remarkable. A growing overall warming inclination underway in 1940s after industrialized revolution and it is continuing at present also with more generation of things for human ease and comfort. The temperature rise over the twentieth century was roughly 0.7°C, however, after ten years of the 21st century the world saw an average global rise of about 1°C. Furthermore, it was the warmest period ever recorded on Earth's surface, resulting in numerous anomalies in climate system processes such as repeated flooding, famines, heat/cold waves, restricted torrential rainstorms, and exceedingly unstable climate patterns in different parts of the globe. Pakistan is also harmed by similar actions, which occurred mostly as a result of rising temperatures, which posed serious issues for maintaining food production. Temperature in Pakistan has risen significantly day and night during the previous 50 years, causing increased heat strain on plant growth. Increased exhalation has resulted from higher night temperatures, diminishing the net benefit in the shape of grain crop. Unexpected increases in air temperatures in early spring, when wheat and other winter yields were in the reproductive stage of their life cycle, resulted in significant grain yield reductions, despite the crops' apparent health. The current temperature rise is likely to continue into the twenty-first century, and extreme events linked with it are projected to increase in frequently, intensity, and duration, posing a threat to long-term harvest output. In an exceedingly hostile climate, Pakistan must produce more by employing a multidisciplinary way to addressing the food demand of an ever-increasing population with limited land and water resources. Increased temperature will alter the physiological mechanisms required for crop production, and crop yields would most likely fall below current levels. Climatic abnormalities will play

a big influence in raising crop production suspicions.

The purpose and relevance of Global Land Ice Measurements from Space (GLIMS) were outlined by Raup et al. (2007) in their research article "Remote sensing and GIS technologies in the Global Land Ice Measurement from Space (GLIMS) Project". It is a worldwide consortium formed to gather satellite photographs of the world's largest glaciers, evaluate them for changes in glacier range, and assess the information in form of forcing. The collaboration has been divided into Regional Centers, each of which is in charge of glaciers within its specialized area. In a distributed analytic setting, the glacier mapping software needed includes the ones listed below: Snow, ice, water, and mixtures of ice with rock debris are highlighted in the terrain categorization process, and modifications to accurate identification, imaging of images and derived data, clarification of derived data, archiving of derived data, and examination to ensure consistency of results from various Regional Centers are also included. A global glacier database was planned and created at the National Snow and Ice Data Center (Boulder, CO); parameters were expanded from those of the World Glacier Inventory (WGI), and the database was built to be compatible with (and to incorporate) WGI data. The US Geological Survey (Flagstaff, AZ) spearheaded the project's overall development and coordination, as well as the construction of a collaboration platform for automated analysis and manual modification of glacier pictures and derived data (GLIMSVIEW). In this study, the objectives of this dispersed project are addressed using satellite remote and Geo information Science methodologies established within the scope of GLIMS. Sample applications that demonstrate the proposed methodologies are also made available.

Shafiq et.al (2011), in a paper presented at the 62nd International Astronautically Congress, Cape Town on Enhancing Global Climate Data Exchange to better Monitor Climate Change and Empowering Policymakers, Scientists, and the Community underlined that changing climate is one of humanity's most pressing global concerns.

Its nature, evolution, and significance have yet to be fully understood. Because of the complexity of the phenomena disrupting the climate system, gaps in knowledge and comprehension of climate science are remarkable. Earth observation (EO) data can aid in the observation and forecasting of climatic fluctuations, as well as the investigation of what can be done to mitigate the negative consequences of these oscillations. Climate researchers do not have access to open and shareable data and information. Different satellite systems from different countries produce EO data, which they collect, process, and distribute using different standards. They investigated the economic and political factors that contribute to the difficulties of creating a proper data sharing framework in their article. As a result of the global effect of climate change, the study gives new viewpoints based on technological evidence that re-evaluate the current political-economic pattern of data management and recommend a new perspective that could help solve current data sharing challenges. These views and proposals are based on talks among young professionals and university students at Space Generation Congress 2010's climate session. Because the parameters used to monitor global warming diverge from those used for reconnaissance or meteorological applications, and information in use for basic science investigation has diverse demands than data needed for economic or political studies, the paper concludes by recommending a series of initiatives that could aid in the improvement of a full data sharing regime and the creation of a global data sharing community that includes many more than just

established suppliers.

Characteristics of ASTER GDEM read at IEEE International Geoscience and Remote Sensing Symposium conducted in Canada by Tachikawa et al. (2011) outlined the specifics of version 2. In May 2009, the Advanced Space borne Thermal Emission and Reflection Radiometer (ASTER) Global Digital Elevation Model (GDEM) was made available to the general public. The GDEM version 2 is in the works and employs an improved methodology to replicate recent ASTER data collected after September 2008. Authentication research of the trial and beta versions of GDEM version 2 was carried out to investigate its properties, such as geo-location error, elevation error, and horizontal resolution. The study's findings revealed that in version 2, the elevation offset and horizontal resolution will be considerably enhanced, with the improved horizontal resolution helping to lower the standard deviation of altitude and geo-location inaccuracy.

A summary of all the articles and papers consulted and referred during the course of research work is appended in Table 2.1 below:

Table 2.1 Literature review by relevance to topic

NO.	AUTHOR (s)	YEAR	AREA OF RESEARCH & TITLE ON PAGE NO IN REFERENCES
1	By Susan K. Jenson	1991	Remote Sensing. 299
2	By Bishop et al.	1995	Glaciology. 292
3	By Paul	2000	Remote sensing and Glaciology. 302
4	By Vuille et al.	2000	Glaciology. 306
5	By Willhauck et al.	2000	Remote Sensing. 306
6	By Salomonson et al.	2004	Glaciology. 304
7	By Hewitt	2005	Climatology. 298
8	By Hijmans et al.	2005	Remote Sensing and Hydrology. 298
9	By Chen et al.	2006	Climatology and Glaciology. 293
10	By Mayer et al.	2006	Glaciology. 293
11	By Bolch and Kamp	2006	Remote sensing and Glaciology. 293
12	By Herold et al.	2007	Land use and RS. 297
13	By Bolch	2007	Climatology. 292
14	By Raup et al.	2007	Remote sensing and Glaciology. 304
15	By Rajeevan et al.	2007	Remote sensing. 290
16	By Tasseti et al	2008	Remote Sensing and Glaciology. 305
17	By Vuille et al.	2008	Climatology and Glaciology. 306
18	By Hayakawa et al.	2008	Remote Sensing. 297
19	By Maitima et al.	2009	Land use and RS. 300
20	By Zemp et al.	2009	Climatology. 306
21	By Quincey et al	2009	Climatology. 303
22	By Frauenfelder and Kaab	2009	Remote sensing and Glaciology. 296
23	By Hewitt	2009	Remote Sensing and Glaciology. 295
24	By Yi, Shuang, and Wenke Sun	2010	Climatology. 306
25	By Mayer et al.	2010	Climatology. 301
26	By Shafiq et al.	2011	Climatology. 304
27	By Tachikawa et al.	2011	Remote Sensing. 305
28	By Rasul et al.	2011	Hydrology and Glaciology. 303
29	By Koji Fujita and Takayuki Nuimura	2011	Glaciology. 296
30	By Khattak et al.	2011	Climatology and hydrology. 300
31	By Bolch et al.	2011	Climatology. 292
32	By Zhang, Yong, et al	2011	Climatology. 307
33	By Hewitt	2011	Climatology. 298
34	By Yang et al.	2011	Land use and RS. 306
35	By İkiel & Ustaoglu	2011	Land use and RS. 299
36	By Kargel et al.	2011	Climatology. 296

37	By Gong et al.	2011	Land use and RS. 296
38	By Schmidt et al.	2012	Climatology. 300
39	By Azam et al.	2017	Climatology. 290
40	By Bolch et al.	2012	Climatology. 292
41	By Thompson	2012	Climatology and Glaciology. 305
42	By Ashraf et al.	2012	Glaciology. 290
43	By Gardelle et al.	2012	Climatology. 295
44	By Sheeba and Nasir	2013	Climatology. 288
45	By Hemant et al.	2013	Remote Sensing and Hydrology. morphometric analysis of the upper catchment of the Kosi River using GIS techniques
46	By Paul et al.	2013	Hydrology and Glaciology. 301
47	By Paul et al.	2013	Remote sensing and Glaciology. 301
48	By Afsar et al.	2013	Climatology. 288
49	By Din et al.	2014	Climatology and Glaciology. 293
50	By Farr et al.	2014	Remote Sensing. 294
51	By Yaduvanshi and Ranade	2015	Climatology. 305
52	By Biswajit and Asif	2015	Remote Sensing and Glaciology. A re-evaluation of the snowmelt and glacial melt in river flows within Upper Indus Basin and its significance in a changing climate
53	By Smith et al.	2015	Remote Sensing and Glaciology. 304
54	By Yaduvanshi and Ranade	2015	Remote Sensing and Hydrology. 302
55	By Smith et al.	2016	Remote sensing and Glaciology. 304
56	By Aroengbinang et al	2015	Land use and RS. 289
57	By Farhan et al.	2015	Climatology. 294
58	By Bajracharya et al.	2015	Glaciology and hydrology. 290
59	By Usman et al.	2015	Climatology. 301
60	By Bhat et al.	2016	Land use and RS. 288
61	By Kanwal et al.	2016	Remote Sensing. 296
62	By Nahida	2016	Remote Sensing and Climatology. 289
63	By Naeem et al.	2016	Glaciology. 302
64	By Rashid et al.	2016	Glaciology. 302
65	By Paul et al.	2016	Remote sensing and Glaciology. 303
66	By Fenta et al.	2017	Land use and RS. 294
67	By Parveen et al.	2017	Remote Sensing and Hydrology. 290
68	By Stephen Fick et al.	2017	Climatology. 295
69	By Gubler et al.	2017	Climatology. 297
70	By Hasson et al.	2017	Climatology, Hydrology and Glaciology. 297
71	By Adnan et al.	2017	Climatology, Hydrology and

			Glaciology. 289
72	By Fey et al.	2017	Remote sensing and Glaciology. 296
73	By Adnan et al.	2017	Hydrology and Glaciology. 288
74	By Paul et al.	2017	Glaciology. The 2015 surge of Hispar Glacier in the Karakoram
75	By Bolch et al.	2017	Glaciology. 294
76	By Garee et al.	2017	Hydrology and Glaciology. 297
77	By Findell et al.	2017	Land use and RS. 296
78	By Meraj et al.	2018	Land use and RS. 302
79	By Aboelnour et al	2018	Land use and RS. 289
80	By Azam et al.	2018	Climatology. 292
81	By Baig et al.	2018	Glaciology. 290
82	By Atif et al.	2018	Hydrology and Glaciology. 292
83	By Shafique et al.	2018	Remote Sensing and climatology. 305
84	By Ebabu et al.	2019	Land use and RS. 295
85	By Klare	2019	Climatology. 301
86	By Bilal et al.	2019	Hydrology and Glaciology. 291
87	By Hussain et al.	2019	Remote Sensing, Climatology and Hydrology. 300
88	By Ali et al.	2019	Land use and RS. 289
89	By Rathor et al.	2020	Land use and RS. 304
90	By Mariye et al.	2021	Land Use and RS. 299
91	By Dagnachew et al.	2020	Land use and RS. 293
92	By Dagnachew et al.	2020	Land use and RS. 293
93	By Irfan et al.	2020	Climatology and Glaciology. 299
94	By Ahmed et al	2020	Hydrology and Glaciology. 291
95	By Farhan et al.	2020	Climatology and Hydrology. 294
96	By Ayub et al.	2020	Hydrology and Glaciology. 291
97	By Rasool et al	2023	Land use and RS. 303
98	By Ahsan et al.	2021	Land use and RS. 289
99	By Jallat et al.	2021	Land use and RS. 299
100	By Rasool et al.	2021	Land use and RS. 303
101	By Dehri et al.	2021	Climatology and hydrology. 294
102	By Zhou et al.	2021	Glaciology. 301
103	By Umar et al.	2021	Hydrology and climatology. 305
104	By Sivaranjani, et al.	2023	Glaciology. 305
105	Afzal, Muhammad Mannan, et al.	2023	Glaciology. 289
106	By Evan, et al.	2022	Glaciology. 293
107	By Nazir et al.	2021	Glaciology. 291
108	By Haleem et al.	2022	Hydrology and Land use. 297
109	By Adnan et al.	2022	Hydrology and Glaciology. 288
110	By David et.al	2023	Climatology. 304

CHAPTER 3

SATELLITE DATASETS

Due to topographical and may be political reasons in remote regions where glaciers normally located are difficult to access. Because of these handicaps, glacier and permafrost hazards are assess worldwide through remote sensing techniques and DEMS of good quantity and quality. Landsat TM, ETM⁺ and OLI satellite Images of Gilgit Basin for 30 years period (1988, 1994, 1999, 2014 and 2018) have been obtained from earth explorer portal. The glacier changes had been extracted from the Landsat imageries presented in the Table 3.1. It is very true and common that satellite images of Northern areas of Pakistan generally have cloud cover (CC) issues. This pose a very serious limitation for any remote sensing based study in the mountainous region especially the Northern regions of Pakistan. For this reason, the satellite imagery was selected with a criterion of scene cloud cover of less than 5%. All the scenes with +5% CC were eliminated in the first round of selection of the satellite imagery for this study.

Table 3.1 Images used in this study

Satellite /Sensor	Year	Scene ID	Path	Row	Cloud Cover	Acquisition Date
Landsat-5 TM	1988	LT05_L1TP_150035_19881027_20170205_01	150	35	3%	1988-Oct-27
Landsat-5 TM	1994	LT05_L1TP_150035_19940708_20170113_01	150	35	4%	1994-Jul-08
Landsat-7 ETM ⁺	1999	LE07_L1TP_150035_19990916_20170217_01	150	35	1%	1999-Sep-16
Landsat-8 OLI	2014	LC08_L1TP_150035_20140917_20170419_01	150	35	1.25%	2014-Sep-17
Landsat-8 OLI	2018	LC08_L1TP_150035_20180912_20180927_01	150	35	1.41%	2018-Sep-12

Ideally satellite imagery should be of the same month and day but due to the constraints it is not possible. Moreover, this is to state that the satellite imagery obtained after the snowmelt summer season is better suited, again on a glacier-to-glacier basis. The imagery has to be visually inspected before a decision on its use is made. The suitable window for glacier-based studies is from July to end-Oct till the start of winter season snowfall.

The satellite photos were subjected to operations in order to remove inaccuracies caused by the atmosphere. The photos were also subjected to the following classification algorithms.

Table 3.2 DEM data used in the study involving the delineation of watersheds

Sr	Imagery ID	Sensor	Date of Acquisition	Row/ Path	Resolution	Publication reference
1	SRTM1N35E074V3	SRTM	23-SEP-14	35, 74	1 arc sec ~30 m	JPL-NASA (2014) Farr et al., (2007)
2	ASTGTMV003_ N35E074	ASTER GDEM	01-03-2000 to 30-11-2013	35, 74	30 m	Tachikawa et al., (2011)
3	GT30E060N40	GTOPO30	1-12-1996	15, 80	30 arc sec ~1000 m	Denker (2005) USGS-EROS (1996)

The province of Gilgit Baltistan has been divided into 10-hydrological watershed viz., Indus, Shingo, Jhelum, Shyok, Astore, Shigar, Swat, Chitral, Hunza, Gilgit and River.

3.1 Landsat-8 OLI (Orbital Land Imager) and TIRS (Thermal Infrared Sensor)

Landsat 8 is a collaborative project of NASA and USGS to offer adequate resolution global measurements in visible, near infrared, short wave infrared, and thermal infrared. With a 40-years Landsat data set, Landsat 8 ensures continuity. The Landsat data series, which began in 1972 and is the only satellite system designed to make recurring surveys of land, from space it looks like the lengthiest nonstop record of changes in Earth's surface. Easily accessible Landsat data deliver an exclusive reserve study areas like geology, agronomy, forestry, provincial development, edification, mapping, and global variation study. Two research tools on board the Landsat 8 satellite are the Operational Land Imager (OLI) and the Thermal Infrared Sensor (TIRS). Regularly covering the entire continent, these two sensors have spatial resolutions of 30 m (visible, NIR, SWIR), 100 m (thermal), and 15 m (thermal) (panchromatic). The

precision, dynamic range and precision of the spectrum data and radiometric presentation are intended to identify and illustrate multi-decadal land cover change. The Landsat 8 panorama is 185 kilometers long by 180 kilometers wide. The spacecraft is at a height of 705 kilometers.



Figure 3.1 Artist's rendition of Landsat-8 in orbit. Copyright: NASA [Image Source <https://earth.esa.int/eogateway/missions/landsat>]

Landsat 8 satellite has two devices: the Operational Land Imager (OLI) and the Thermal Infrared Sensor (TIRS). It first went up in February of 2013. With a 16-day repeat cycle, the satellite obtains images of the Earth that are connected to the Global Referencing System-2.

The OLI and TIRS sensors are normally combined in Landsat 8 Level 1 data products; nevertheless, the USGS archives may include OLI-only and/or TIRS-only scenes. The first two elements of the Landsat 8 scene ID identify the data provided in each scene:

1. **LC08_L1TP_003055_20170207_20170216_01_T1** = Combined

(both OLI and TIRS data)

2. **LO08_L1TP_021047_20150304_20170227_01_T1** = OLI data only
3. **LT08_L1GT_137206_20170202_20170215_01_T2** = TIRS data only

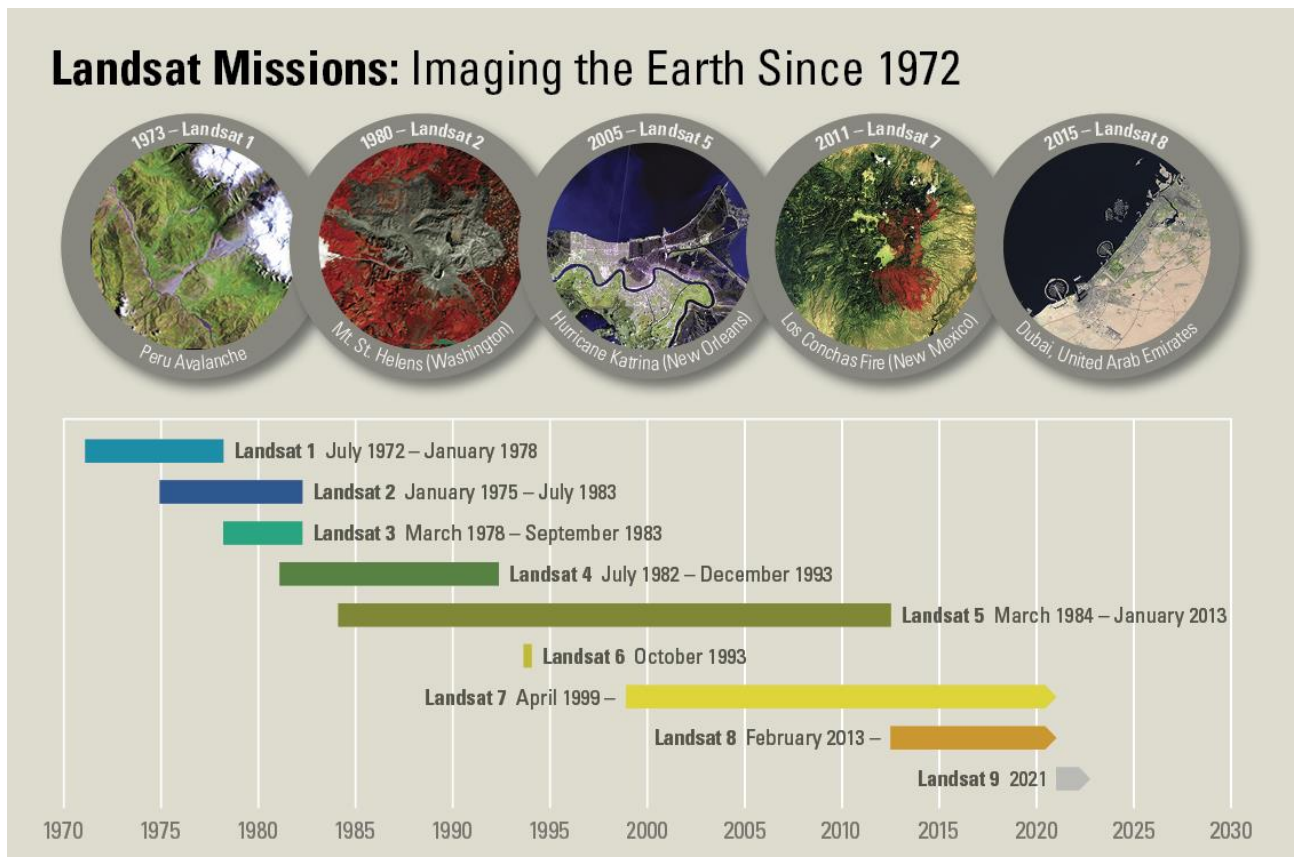


Figure 3.2 Landsat timeline - Since 1972, Landsat satellites have continuously acquired space-based images of the Earth's land surface, providing uninterrupted data to help land managers and policymakers make informed decisions about our natural resources and the environment [Source <https://www.usgs.gov/media/images/landsat-missions-timeline>]

The document includes bit evidence about variables like clouds, water, and snow that potentially affect a pixel's precision and usage. Approximately 10,000 scenes were captured between launch and April 10, 2013, before the satellite entered operational orbit. The first images are nothing more than TIRS data. On Earth Explorer as portion of the Landsat 8 OLI/TIRS C1 Level-1 data bundle this type of data are available. While the quality and geometric accuracy of these photos are at par with

those captured after reaching functional orbit, each image's geographic coverage will vary. The majority of the sceneries will receive full terrain recovery with a 30-metre pixel resolution. The results could slightly alter as a result of the telescope's temperature variations.

3.2 Landsat-7 ETM+ (Enhanced Thematic Mapper)

On April 15, 1999, Landsat-7 was propelled from Vandenberg Air Force Base in California using a Delta-II expendable launch vehicle. Landsat -7's Expanded Thematic Mapper Plus (ETM+) technology duplicates the capabilities of Landsat 4 and 5's extremely successful Thematic Mapper instruments.

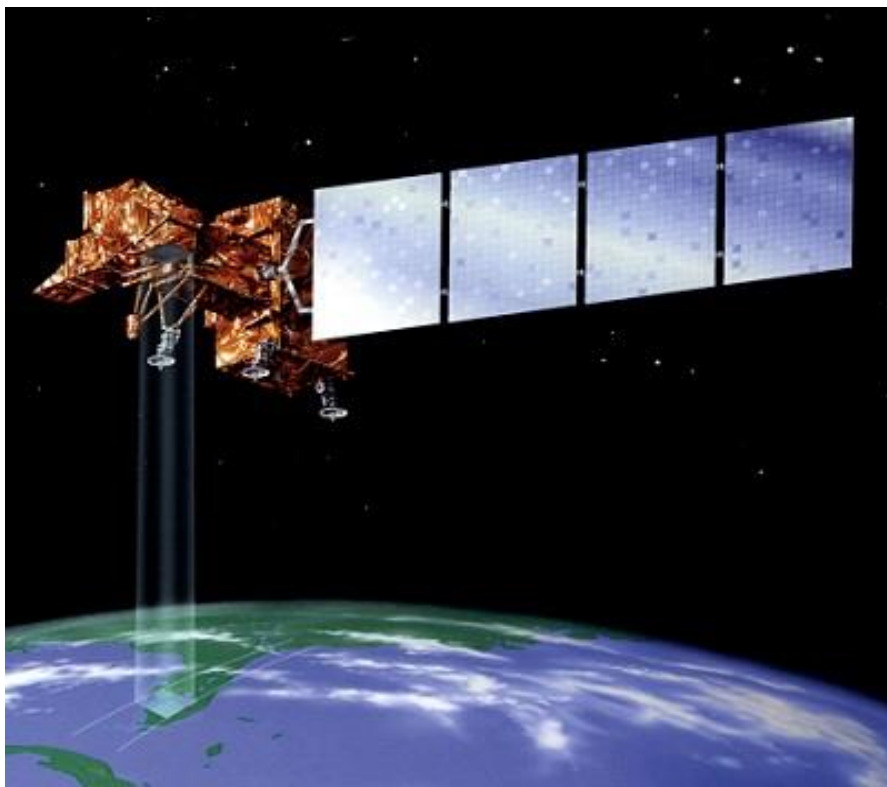


Figure 3.3 Landsat-7 was launched in 1999. It carries the Enhanced Thematic Mapper Plus 8-band whiskbroom scanning radiometer instrument [Image Source <https://earth.esa.int/eogateway/missions/Landsat>]

In terms of international updating, land cover observing and evaluation, and enormous - area charting, ETM+ possesses properties that make it more adaptive and economical than its predecessors. Landsat 7's main goal is to refresh the world's satellite photo bank, delivering fresh and cloud-free views. The Landsat program is accomplished and maintained by the United States Geological Survey (USGS), which also gathers and distributes Landsat 7 data. Among the features are an onboard chromaticity band with 15m pixel size, full apertures, 5% absolute radiological calibrating, a thermal IR band with 60m pixel size, and an onboard data recorder.

Landsat 7 is the greatest precisely standardized Earth-observing satellite, which means its readings are exceptionally precise when associated to ground-based measurements.

"The steadiest, best described Earth reflection device ever mounted in orbit," according to Landsat 7. Many coarse-resolution sensors use Landsat 7 for validation because of its stringent calibration standards. The USGS made all Landsat 7 data available to the general community in October 2008, resulting in a sixty- fold increase in data downloads and a significant shift in satellite research.

Approximately after 120 days, all Landsat data was made available free of cost. ETM+ (Enhanced Thematic Mapper Plus) is a feature on Landsat 7 that allows for a ground survey in four modes: VNIR (Visible and Near Infrared), SWIR (Shortwave Infrared), PAN (Panchromatic–Panchromatic range), and TIR (Thermal infrared – Thermal infrared range).

3.3 Landsat-5 MSS (Multi spectral scanner)

On March 1, 1984 Landsat-5 was propelled. It was expected to work for three and half years but remained in service for more than 29 years. Its payload included Multispectral Scanner (MSS) and the Thematic Mapper (TM). Close to the end of its mission, Landsat 5's use was hindered by equipment failures, and Landsat 7 and Landsat 8 mainly outdated it. During its operational phase, it took 2.5 million images of earth surfaces.



Figure 3.4 Landsat- 5 was launched in 1984. It supported the Multi Spectral Scanner and Thematic Mapper instruments [Image Source <https://earth.esa.int/eogateway/missions/landsat>]

The Landsat - Five orbits the earth in a sun-synchronous, near-polar orbit at a

height of 705 km (438 mi), tilted at 98.2 degrees. The satellite had a 16-day repetition cycle and crossed the equator at 9:45 a.m. plus or minus 15 minutes. Data from Landsat5 were collected using the WRS-2 path-row method, with swath overlapping ranging from 7% at the equator to about 85% at the poles. The Landsat-5 satellite had seven spectral bands.

3.4 Landsat-3 MSS (Multi Spectral Scanner)

Three years after Landsat 2, on March 5, 1978, Landsat-3 was launched. The imagery era began by Landsat -1 and Landsat -2 was meant to be supplemented by Landsat 3. On March 31, 1983, the satellite was placed in reserve way, and on September 7, 1983, it was neutralized. Landsat 3, similar to its predecessors, featured the Returned Beam Videocon (RBV) and the Multispectral Scanner (MSS) (MSS). The RBV sensor on Landsat 3 had a greater ground resolution of 38 m and used two RCA cameras that scanned in a single broad spectral domain rather than three discrete bands (green, red, and infrared) alike its predecessors.

Landsat 3 orbited the Earth in a sun-synchronous, near-polar orbit (99.2 degrees inclination) at an altitude of 917 km, performing 14 orbits every day. The satellite had an 18-day repeat cycle and crossed the equator at 9:30 a.m. mean local time (+/-15 minutes). In addition, the Landsat 3 Multispectral Scanner System (MSS) sensor was improved to include a thermal infrared band, though the thermal band unsuccessful shortly after launch. The Landsat Multispectral Scanner (MSS), which was carried on Landsat 1 through 5, absorbed four spectral bands of radiant energy from the earth's surface. The MSS sensor's wavelength range spans the visible to near-infrared portions

of the electromagnetic spectrum.



Figure 3.5 Landsat 3 was launched in 1978, after the successful launches of Landsat-1 and Landsat 2. These provide the longest records of the earth observation historically. [Image Source <https://earth.esa.int/eogateway/missions/landsat>]

3.5 Shuttle Radar Topography Mission (SRTM)

The Shuttle Radar Topography Mission (SRTM) is a unique NASA and NGA product developed in collaboration with German and Italian space companies. The Endeavor space shuttle began a unique mission in February 2000 (Farr et al., 2007; JPL-NASA 2014). The mission's goal was to collect elevation data on a worldwide basis. The earlier Space borne Imaging Radar-C/X-band Synthetic Aperture Radar (SIR-C/X-SAR) radar structure was employed on the Shuttle in 1994. Two radar probes were

incorporated within the SRTM payload to get topographic records. The SIR-C/X-SAR probe was in the payload bay, while the other, a precarious modification from the SIR-C/X-SAR that allowed single-pass interferometry, was on the end of a 60-meter (200-foot) pole that protruded from the payload bay when the Shuttle was in space. Each tile spans one degree of latitude and one degree of longitude, and is marked as per its southwestern angle. "n45e006," for example, covers 45°N 6°E to 46°N 7°E, while "s45w006" covers 45°S 6°W to 44°S 5°W (Farr et al., 2007; JPL-NASA 2014). The strange statistics have a resolution of one arc-second (30 meters along the equator). For the rest of the world, only three arc-second (90 m along the equator) data are available. Each one arc-second tile has 3,601 rows and 3,601 16-bit bigendian cells.

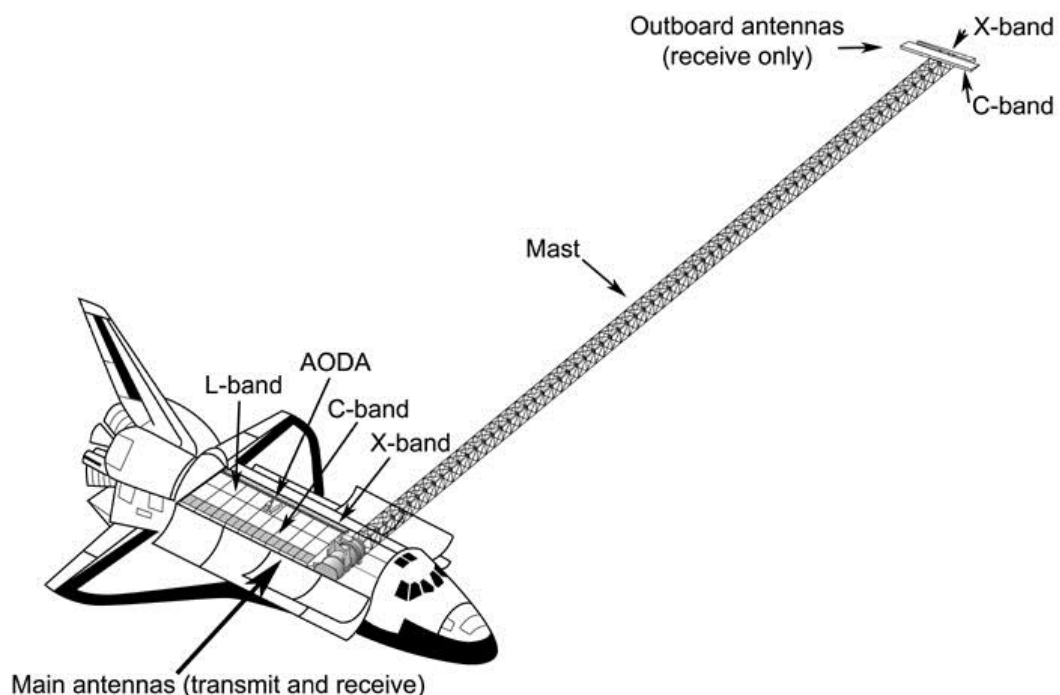


Figure 3.6 Shuttle Radar Topography Mission (SRTM) [Image Source: <https://www2.jpl.nasa.gov/srtm/images/bibliography>]

The magnitudes of the three-arc second tiling are 1201 1201. To convert all of the released products to EGM 96, the initial SRTM altitudes were computed according to the WGS84 ellipsoid, and then the EGM 96 geoid separating ratios were applied.

The space shuttle attempt orbited the Earth 16 times during its 11-day mission. Its primary objective and task was to map Earth's topography at 1 arc-second (30 meters) over roughly 80% of the planet's surface. SRTM has collected one of the most precise digital elevation models of Earth using synthetic aperture radar and interferometry. This information is now easily accessible on the USGS Earth Explorer website.

3.6 ASTER GDEM

ASTER (Advanced Space borne Thermal Emission and Reflection Radiometer) is a NASA Terra satellite instrument that was flung in December 1999 and is used to make comprehensive drawings of land surface reflectance, temperature, and height (Tachikawa et al., 2011).

The EOS satellites' coordinated schemes with Terra are a key component of NASA's Science Operation Board and Earth Science Division. NASA Earth Science's goal is to improve our technical considerate of the Earth as a complex system and its response to change. The Japanese Ministry of Economy, Trade, and Industry (METI) and NASA together declared the discharge of the ASTER Global Digital Elevation Model Version 3 (GDEM 003) and the ASTER Water Body Dataset (ASTWBD) on 05, August 2019,. In June 2009, the first unconstrained description of the ASTER GDEM was created using stereo-pair photos. ASTER GDEM data covers virtually all of Earth's landforms, from 83 degrees north to 83 degrees south latitude (Tachikawa et al., 2011).



Figure 3.7 ASTER satellite sensor is one of the five state-of-the-art instrument sensor systems on-board the Terra satellite that was launched on December 18, 1999. [Source: <https://www.satimagingcorp.com/satellite-sensors/other-satellite-sensors/aster>] Copyright © NASA/Japanese Space Team.

The newly created GDEM V3 provides more stereo-pairs, enhancing exposure and decreasing artifacts. The advanced invention algorithm provides improved horizontal and vertical accuracy, as well as improved spatial resolution. With 30-meter posts and 1 x 1-degree tiles, the ASTER GDEM V3 keeps the GeoTIFF arrangement and the similar gridding and tile arrangement as V1 and V2. Version 3 exhibits noteworthy developments done the earlier announcement. Consumers are warned, however, that the statistics comprises abnormalities and artifacts that will prevent it from being useful in specific applications.

A new global product in the ASTER GDEM, the ASTER Water Body Dataset,

is now available (ASTWBD). In this raster file, every water frame is categorized as a sea, stream, or pond. Each GDEM tile corresponds to a Water Body tile. The ASTWBD and GDEM are both downloadable from NASA Earth Data and Japan Space Systems. Anyone can use the ASTER product for free thanks to a partnership between METI and NASA.

3.7 GTOPO30

GTOPO30 is a worldwide arithmetical elevation model (DEM) with a 30 arc second (1 km) horizontal grid spacing. GTOPO30 is the outcome of a number of raster and vector topographic data sets (Denker 2005). GTOPO30 has been separated into tiles for easy distribution, which can be chosen from the plot overhead. GTOPO30 was established over a three-year period by employees at the United States Geological Survey's Center for Earth Resources Research and Science (ERS) (USGS-EROS 1996).

GTOPO30 was created using topographic data from a variety of raster and vector sources. GTOPO30 has been broken into tiles that might be nominated from the plot for simpler distribution. The USGS website has comprehensive material on the features of GTOPO30, comprising the statistics delivery arrangement, statistics bases, manufacture methods, correctness, and user tips.

GTOPO30 is a global data set that spans the entire latitude range of 90 degrees south to 90 degrees north, as well as the entire longitude range of 180 degrees west to 180 degrees east. The DEM has 21,600 rows and 43,200 columns, with a horizontal grid spacing of 30-arc seconds (0.00833 degrees).

WGS84 decimal degrees of latitude and longitude are used in parallel coordinate system. In meters, the vertically units reflect elevation above sea level. The altitude varies from -407 to 8,752 meters. Ocean regions in the DEM have been given the value 9999 and labeled as "no data." Since low lands coastlines have a least altitude of 1 meter, the land boundary portrayal will be kept if the ocean value is changed from -9999 to 0. Due to the raster layout of the DEM, tiny isles in the sea or less than 1 square kilometer could be characterized.

GTOPO30 has been broken up into 33 minuscule pieces, or tiles, to facilitate electronic distribution. From 60 degrees south to 90 degrees north latitude and 180 degrees west to 180 degrees east longitude, each tile covers an area of 50 degrees latitude and 40 degrees longitude. Each tile spans 30 degrees latitude and 60 degrees longitude, covering Antarctica from 90 degrees south to 60 degrees south latitude and 180 degrees west to 180 degrees east longitude. The longitude and latitude of the tile's top most (northwest) corner are used to name the tiles. Tile E020N40, for example, is located at 20 degrees east longitude and 40 degrees north latitude. Another tile has information in a polar three-dimensional projection that spans the entire continent of Antarctica.

CHAPTER 4

REMOTE SENSING METHODS

To compare different DEMs data of selected glaciers for the delineation of the watershed is an important part of the main objectives set in this study. This is done by utilizing various tools under the toolbox of Spatial Analyst in ArcGIS. For this, various upstream points and flow direction in GIT/GIS environment for each grid point in a DEM to determine the delineation of watersheds. Formation of shape file of pour point and snapping of pour points has been done by reconditioning of DEMs in different phases plus watershed delineation.

4.1 Watershed Delineation

A piece of land that collects water is known as a watershed. Surface water from the watershed enters a common exit as either a body of water i.e., stream, lake, or marsh and groundwater infiltration. A watershed, then, is a region that allows surface water to flow from a high altitude to a lower height. The watershed is a unit that is showed in hydrology as well since it is essential to design hydrology and is applicable to help with

the investigation of water distribution, movement, quantity and quality in a region. Briefly, the preservation, planning and administration of the natural assets of the earth verily dependent on techniques use for watershed analysis.

The watershed is formed manually from topographic maps by locating the water split. ArcGIS used to delineate watershed by the use of spatial analyst extension tool and hydrology tool. To create watershed boundary various steps are involved. Work with Raster DEM of the concessional study area is done to delineate the watershed. After obtaining the raster DEM, it has to be ensured that it is depression free which is also called sinks. These depressions could be produced during the interpolation step in the construction of a DEM and are normal in nature. In the DEM, a depression is defined as a cell that has a very low elevation in relation to a neighboring cell and that prevents water from flowing downward. By enhancing its cell values to the lowest runoff point, the low elevation cells can be eliminated. In ArcGIS Fill tool is used to remove the depression of raster DEM in watershed delineation.

4.1.1 Flow Direction

The subsequent stage is to build a raster grid holding the data regarding flows directions once the depression has been removed. The flow direction instrument is a part of the hydrology tool. The height of neighboring cells in the DEM is utilized by this tool to locate drainage networks and drainage divides. The GIS model implies there are no sinks, and the water may only be flow into one cell. If this is not the case in the output grid, sinks exist in the raster DEM. Since it specifies route of flow for each cell in the land topography, flow direction is crucial in the process of hydrologic modeling. The D8 flow algorithm is the foundation of the raster grid produced by the tool of flow

direction.

4.1.2 Flow Accumulation

The Flow Accumulation function must be run after establishing the watershed since it helps determine how much of a watershed sends overflow to a particular cell and helps build the drainage system. As a result, the final flow path need to be established built on the flow direction of each cell in the topography grid. In order to build high flow cells network, the flow accumulation chooses the cells with the highest accumulation flow. The locations of high flow cells must be in the valley floor and along stream channels. Stream flow is represented by cells with accumulation values greater than "1," whereas ridgelines are represented by cells with accumulation values of "0".

4.1.3 Stream Link

Each stream sector of the raster stream is given distinct number, such as 1, 2, or 3, after flow accumulation established the stream network. The streams' intersections resemble nodes, and the sections of the streams resemble arcs. We must choose pour point (i.e., an outlet cell)), the lowest point stream where all flow is directed in the watershed, in order to define a watershed. Any point of importance, including a gauge station, a dam, a sampling site, the amalgamation of a main stream with a tributary, or a sampling location, is regarded as a pour point. A raster or vector could be the pour point. The pour point should be located along the stream trail having the highest flow accumulation values in the flow accumulation raster in mandate to obtain the watershed. The watershed tool can also be used to extract a single watershed for a particular stream or tributary or the entire watershed polygons for the pour locations. Our raster

watershed can finally be converted to a vector format so that we can easily assimilate and bring into line with the rest of digital data.

Georeferencing is crucial for extracting watershed data. By using actual geographic coordinates, the raster dataset is positioned on the ground in accordance with georeferencing. Maps can be scanned, or you can gather satellite imagery and aerial photos to create raster data. With aerial photography and satellite imaging, these data sets occasionally come with insufficient location information, and the data does not properly align with other data you may already have. These data sets do not typically contain spatial reference information.

When georeferencing a raster data collection, the data frame's coordinate system and used map coordinates to identify the position is provided. Raster data may be seen, searched, and analyzed with other geographic data courtesy to georeferencing. Georeferencing comes in two categories i.e. Relative georeferencing and absolute georeferencing.

4.1.4 DEM Processing and Extraction of Watershed

High resolution SRTM, ASTER GDEM and coarse resolution GTOPO30 DEMs have been used in this study. Watersheds have been delineated from different methods in this study. One of the main and best methods is hand delineation which is based on knowledge obtained from contours which found on the topographic maps (Al-qaysi, 2016). Literature reviews concluded that various modern techniques in GIT (or GIS technology), however, this hand delineation method is still the best and used to proceeding and creating a digital watershed dataset. In the study area prior to watershed basin processing and delineation, preprocessing of land has been accepted.

The operational framework in successive manner includes a). DEM processing for Gilgit region, b). Extraction of DEM for Gilgit study area, c). Filling voids/DEM gaps, d). Extraction of flow directions, e). Extraction of flow accumulations, f). Catchment grid delineation, g). Catchment polygon conversion, h). Neighboring catchment processing and i). Computing watershed area. The methodological framework in a sequential order is shown in Figure 4.1.

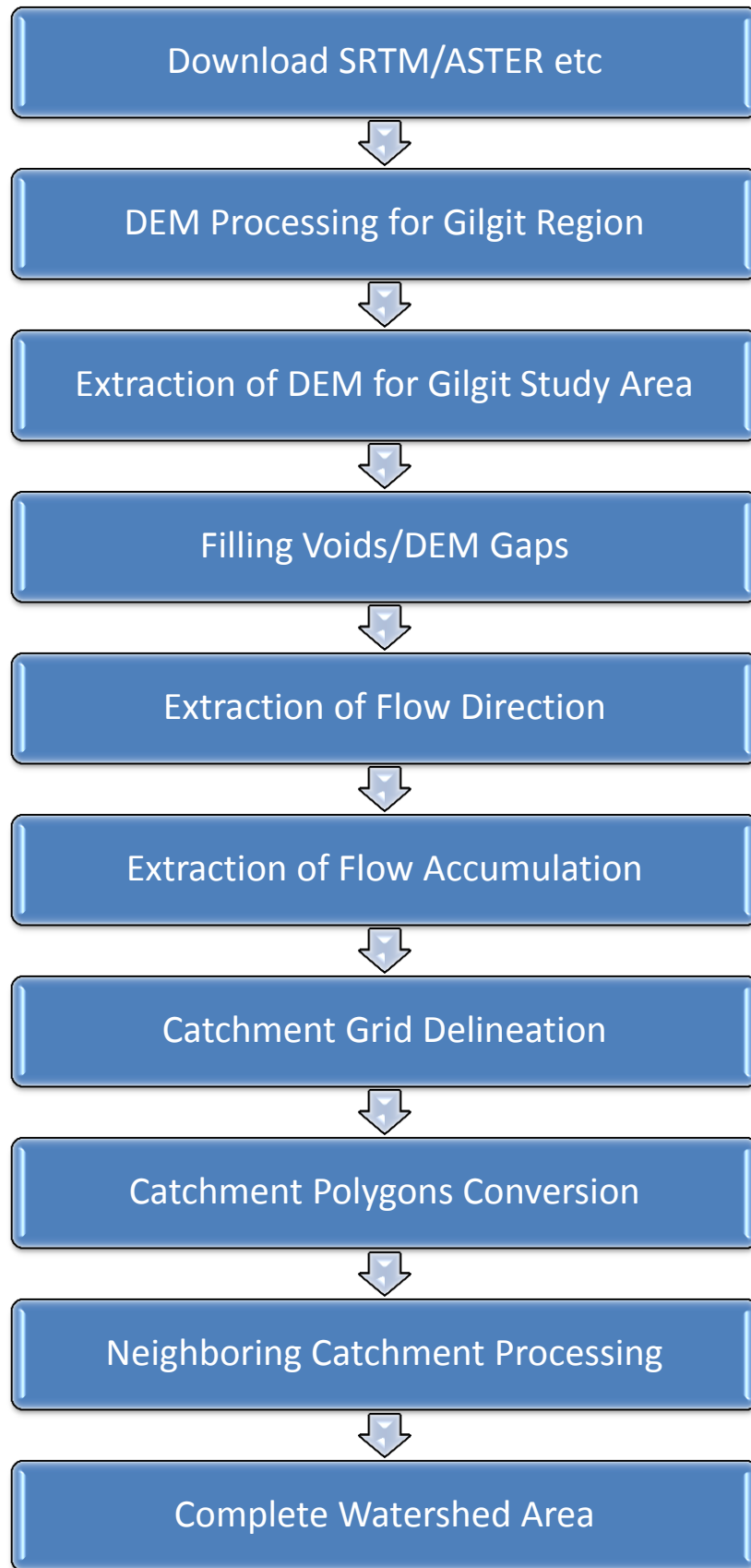


Figure 4.1 Flow diagram

For watershed delineation the basin and watershed functions are used to evaluate flow direction of a DEM. Neighborhood tool in several raster procedure system and point of inflection are used in orthodox method which encompasses of estimate aspect, slope and shaded relief respectively. Overland flow and watersheds are closely related to aspect, slope and inflection information, finding direction of flow in large flat region non-neighborhood limitations is occurred. (Jenson and Domingue, 1988; Jenson, 1991; Taylor, 2016).

To delineate watershed or basin the topographic evaluation is necessary. To get terrain information in a group of applications including landslides, surface analysis for hazards, glacier change analysis, creation of relief maps, glacier monitoring and mapping, avalanches, damage and risks evaluation and for many other studies this topographic information 's which are very useful and are acquired from DEMs.

To generates a depression less DEM the first reconditioned DEM of Gilgit river basin was done by filling the depressions in DEM. Calculation of the flow from the direction of every cell in depression on less DEM is the second stage. By using D-8 method the flow direction indicated the path where water runs from a cell is calculated.

Flow accumulation is the third stage of DEM which is to be calculated for every cell. Along with this to find the flow direction accumulation of DEM in each down slope cell evaluation for the estimated flow accumulation has been done. By this way references on the quantity of upstream cells flow is estimated. Zero value of flow accumulation of cells shows that, no other cell flow with the related cell, which characterized the pattern ridges.

4.2 Glacier Change Analysis through Object Based Classification Method

This technique precedes the form of the article and its spectral designs. In this technique, the appearance is primarily separated minor sections and these sections are categorized. Separation means the alignment of picture components of uniformity (Willhauck et al., 2000). In order to perform separation, three procedures are important specifically: thresholding/clustering, area based, and edge based. Two classes form and spectral design were used for object separation. Spectral design was allocated extra weightage (70%) related to shape (30%) as it increases the accurateness of separation. Work flow of the study is shown in Figure 4.2.

Since this software (e-Cognition) has been used for glacier-changed analysis, a brief description of software will enable to understand as how object-based classification of glaciers has been achieved. GIS professionals, remote sensing experts, and data scientists use Trimble eCognition software to automate geographic data analytics. It is advanced analysis software which is available for development of environment for geospatial applications. Users can create feature extraction techniques that turn geo data into information. The options are limitless. This software takes the real image of a selected raster and bifurcate it to Image data, elevation data, land cover map, impervious map and to tree map.

Because of its capacity to follow the human mind's cognitive powers and combine geospatial input data, eCognition differs significantly from traditional techniques to data analysis. The Trimble has developed a reliable way of presenting

knowledge in a semantic network using patented segmentation and classification processes. The technique evaluates pixels/points in context rather than in isolation. It iteratively constructs an image, recognizing clusters of pixels as objects. It draws the same conclusions and deductions as an expert analyst using color, form, quality, and size of substances, as well as their setting and associations, but with the added benefits of automation and standardization.

eCognition classifies and analyses pictures, vectors, and point clouds, taking into account all relevant semantic information. Rather of looking at individual pixels or points, it extracts meaning from the object's meanings and interrelationships, not just with surrounding objects but also with other input data. It does, however, recognize pixel information. Deep learning and machine learning techniques are simple to include into automated procedures. It adds significant value to this data, however, by building a powerful cognitive network through a series of iterative segmentation and classification procedures. This significantly boosts the value of intelligence and information extracted from data. Furthermore, the gathered data is thoroughly quantified and qualified to fulfill the needs of the user.

To put together an investigation plan, you can skillfully combine image translation steps like article creation (division), object grouping (information-based, fluffy rationale, AI), object location (format coordinating), and object change (melding, smoothing, orthogonalization, disentanglement) into a Rule Set or even another application (Rule Set with UI). The result is a spectacular approach to convert PC reasonable code (Rule Set) or an individual/tweaked program to interpret mental models (why a human translator can see the objects, alterations, or elements in geospatial

information). eCognition can meld a variety of geospatial information, for example, ghastry raster information, 3D point cloud information and tropical information from GIS vector layers. Pictures can address point mists, vectors to pictures and every one of the three to each other. Client can use the full force of their feedback information autonomous of information type and source.

Trimble eCognition is geospatial investigation programming that has advanced application. It is planned to better, speed up, and automates the translation of a variety of geographic data, as well as gives clients the ability to configure highlight extraction of progress discovering solutions for changing geo-data into geo-information. The eCognition Suite includes three components that can be used separately or in combination to solve even the most difficult image research tasks. These three sections are listed below:

1. eCognition Developer is a strong object-based image analysis development environment. It's utilized in earth sciences to create rule sets (or eCognition Architect apps) for automatic remote sensing data interpretation.
2. The eCognition Server software offers a batch processing environment as well as expedited rule set development and transferability testing.
3. Non-technical specialists such as vegetation mapping experts, urban planners, and foresters can use eCognition technology thanks to eCognition Architect. eCognition Developer allows users to simply build, calibrate, and perform image analysis workflows.

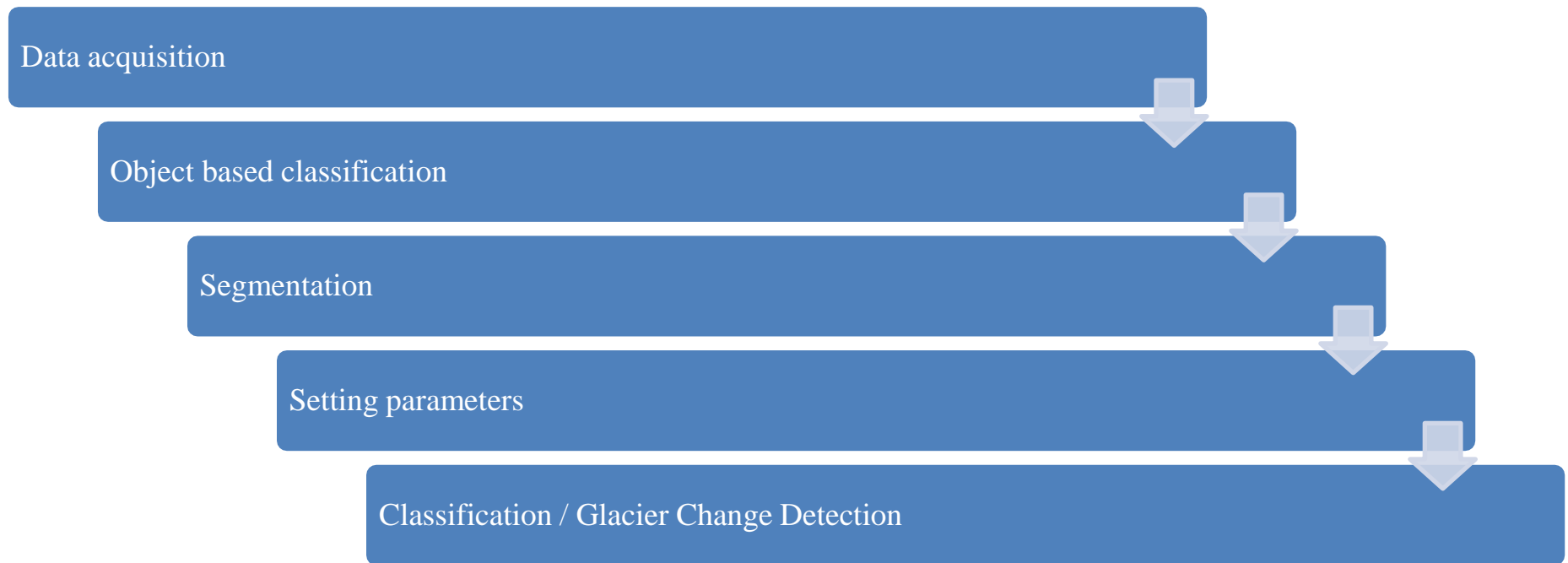


Figure 4.2 Workflow of the study

The phases involved in glacier change analysis have been discussed in ensuing paragraphs.

4.2.1 Data Acquisition

Landsat satellites have the ideal ground resolution and spectral bands to expertly trail land use and to article land alteration due to climate change, urbanization, dearth, wildfire, biomass changes (carbon assessments), and a host of other natural and human-caused changes. Landsat descending (daytime) acquisitions run from north to south; they cross the equator between 10:00 am and 10:25 am local time on each pass to provide maximum illumination. Hence the best time to acquire data is when clear sunlight is accessible.

4.2.2 Object Based Classification

In Walter and Fritsch (2000) paper, an idea for the programmed revision of geographical information system (GIS) databases by multi spectral remote sensing data was presented. This method can be sectioned into two stages. In a first phase, remote sensing data are categorized with a supervised maximum probability classification into different land use classes. The training areas are taken from an already current GIS database in order to evade the laborious duty of physical achievement. This can be done if it is presumed that the number of changes in the real world is very minor matched with the number of all GIS items in the database. This statement is vindicated because we want to realize update cycles in the range of numerous months. The classified remote sensing data have to be matched with the existing GIS objects in the second step to find those objects where a change occurred, or which were collected wrongly. This

task was solved by gauging per object the fraction, similarity, and type of the pixels, which are categorized to the same object class as the respective object stored in the record (Walter, 2000). All items are categories into the classes completely confirmed, partially confirmed, and not found by using thresholds that can be demarcated mutually by the user.

4.2.3 Segmentation

Image segmentation is the method of separating digital images into spatially unified units, or "regions." These areas represent distinct items or areas in the image. Segmented images are valuable in numerous ways, chiefly by provided that basic units used in maps when discrete pixels in the image are too minor to use for this determination. Also, segmented images can be easier to understand, by weighing precise items in the image. However, automating image segmentation has proven tough. The human mind segments images instinctively as it shares the data perceived through the eyes. To get a computer to effectually screen images has proven to be a difficult task (Haralick and Shapiro 1985).

4.2.4 Setting Parameters

Geospatial analysis processes used the rules which are setup by the eCognition developer software. A wide-ranging assemblage of algorithms can be animatedly combined ensuing in a custom application which replicates the user's anticipated analysis tactic and needs.

4.2.5 Classification/ Glacier Change Detection

Sub pixel-based classifications are used merely as it has complications in

taking out the object of desire quality and also yield a substantial amount of unpredictable classification outcomes. A new object based technique came into interference because of this. This algorithm is essentially reliant on creation of segments for the image from which the requisite object is to be taken out. Supplementary evidence like written or contextual is also compulsory which advances the classification outcomes (Rahul et.al, 2016). Segmentation is reinforced at various resolutions to differentiate diversity of objects.

4.3 Remote Sensing Overview of the Glaciers Selected for Temporal Analysis

Five renowned glaciers selected for research work in Gilgit Baltistan are listed in Table 4.1 below alongwith their latitude and longitude. The satellite pictures of delineated watershed of selected glaciers are also shown in Figures 4.3 to 4.7. These watersheds were delineated through SRTM and ASTER GDEM.

Table 4.1. Studied glacier of Gilgit watershed

Name of glacier	Latitude	Longitude
Bhort	36.55	74.09
Bad-e-Swat	36.52	74.05
East Gammu	36.64	73.38
Karambar	36.62	74.10
Phokar	36.34	74.00

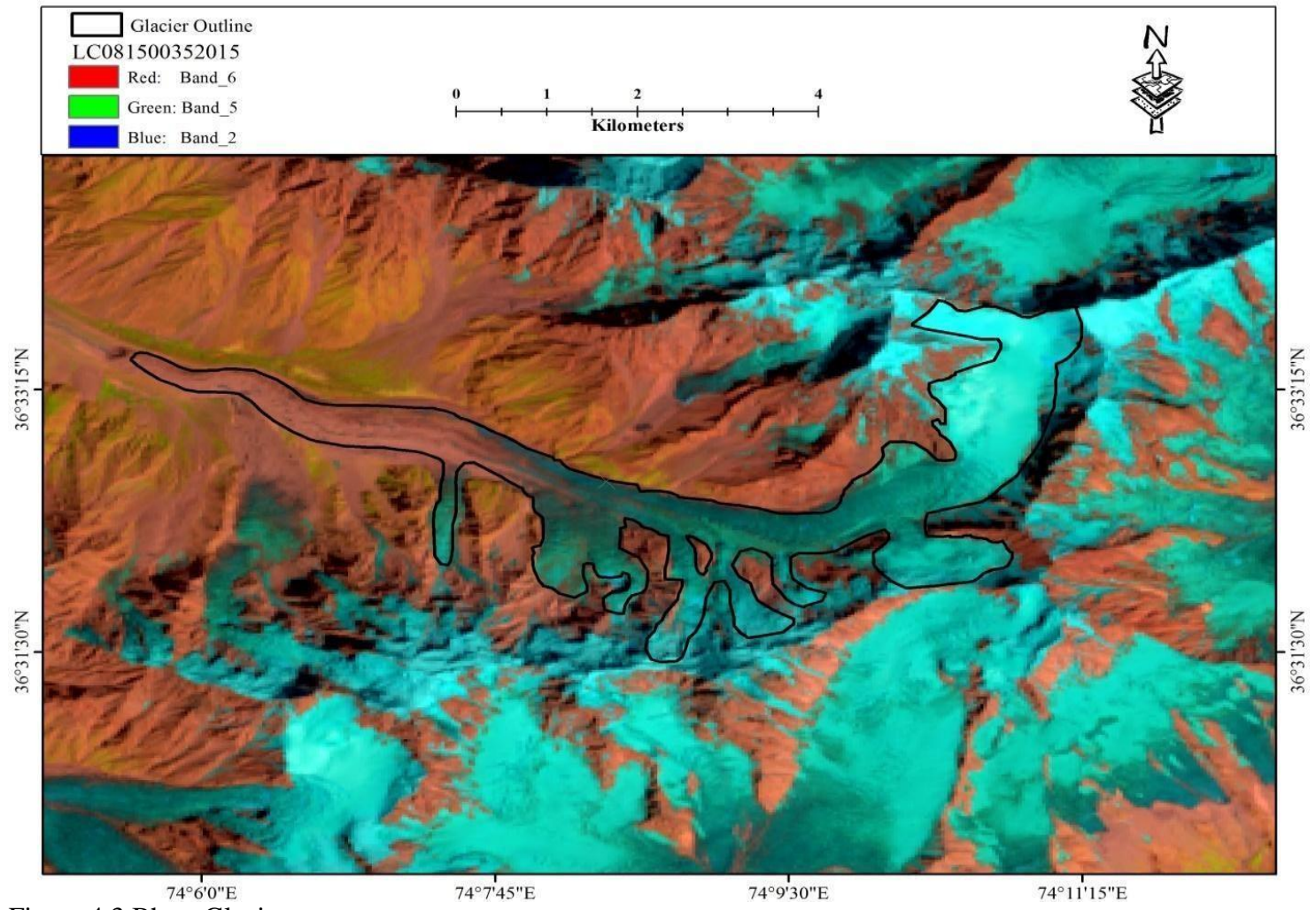


Figure 4.3 Bhort Glacier

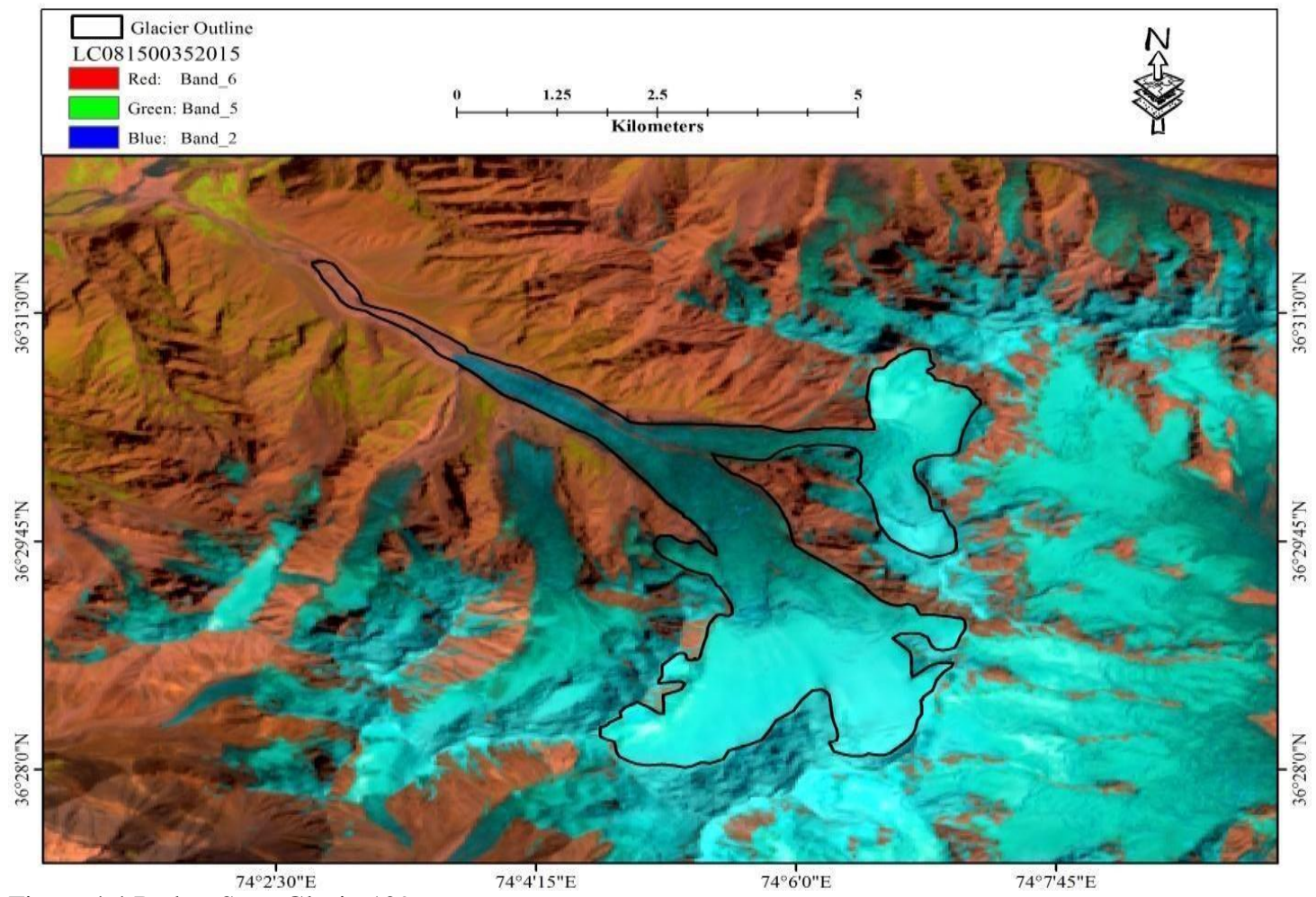


Figure 4.4 Bad-e- Swat Glacier129

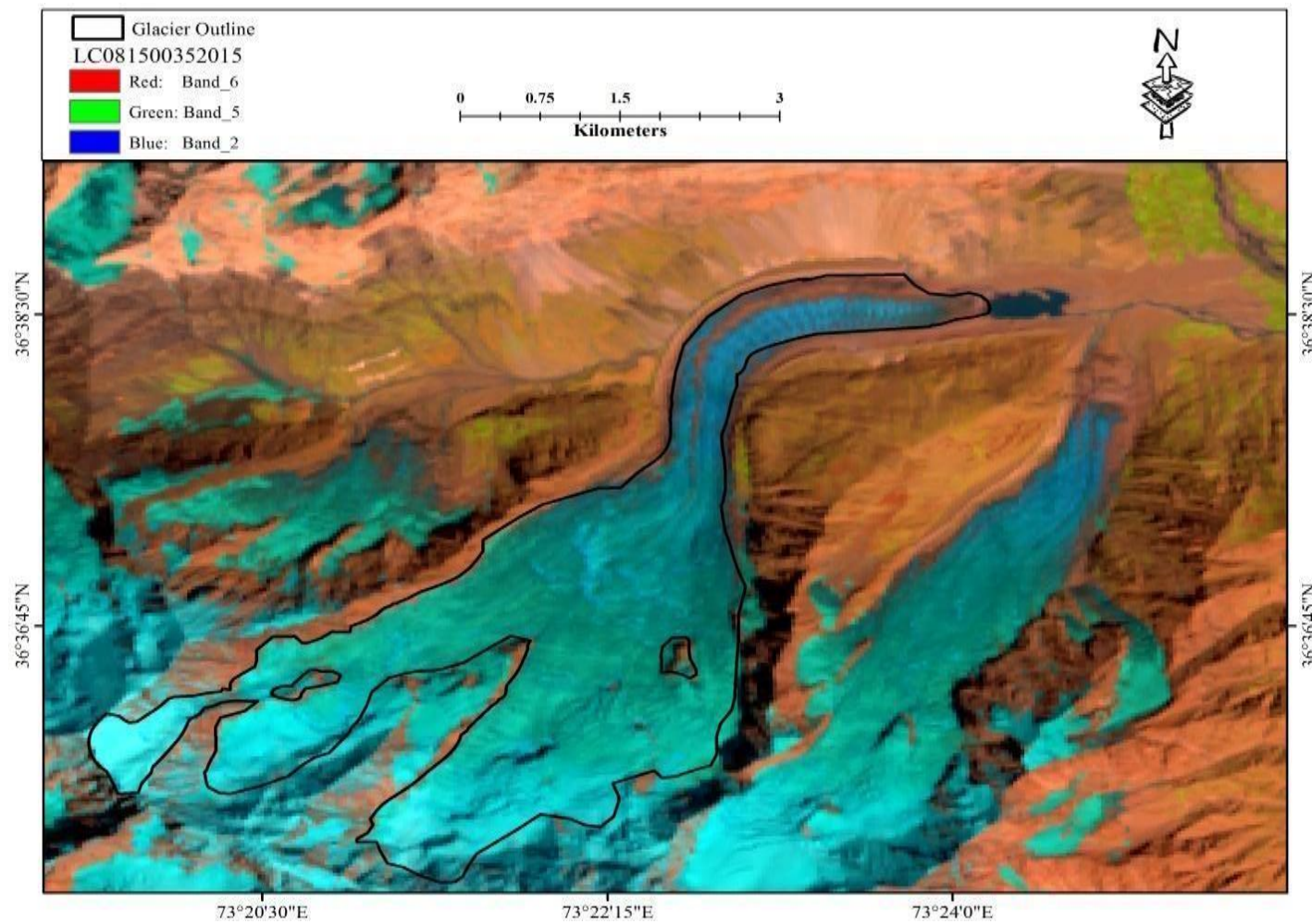


Figure 4.5 East Gammu Glacier

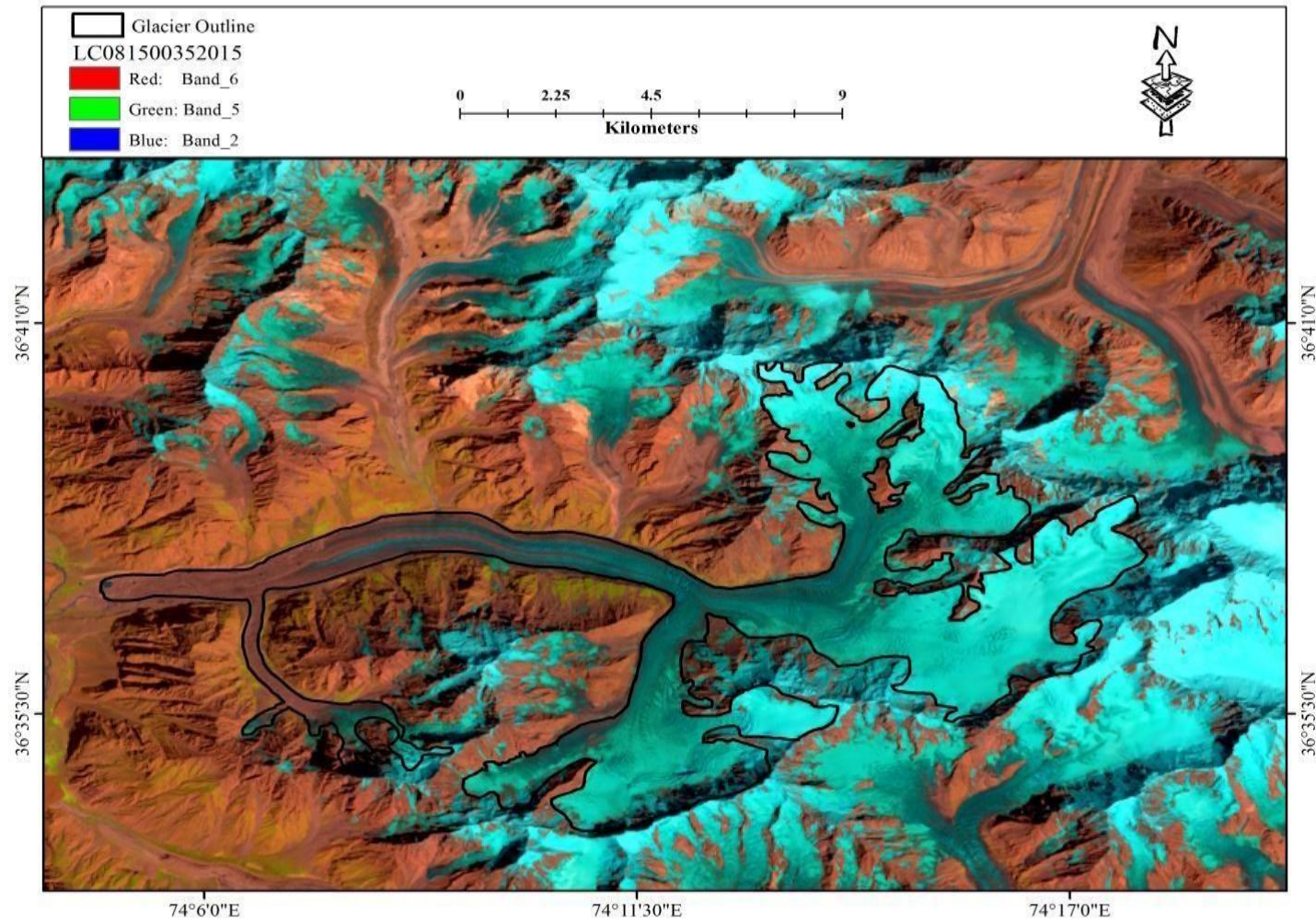


Figure 4.6 Karamber Glacier

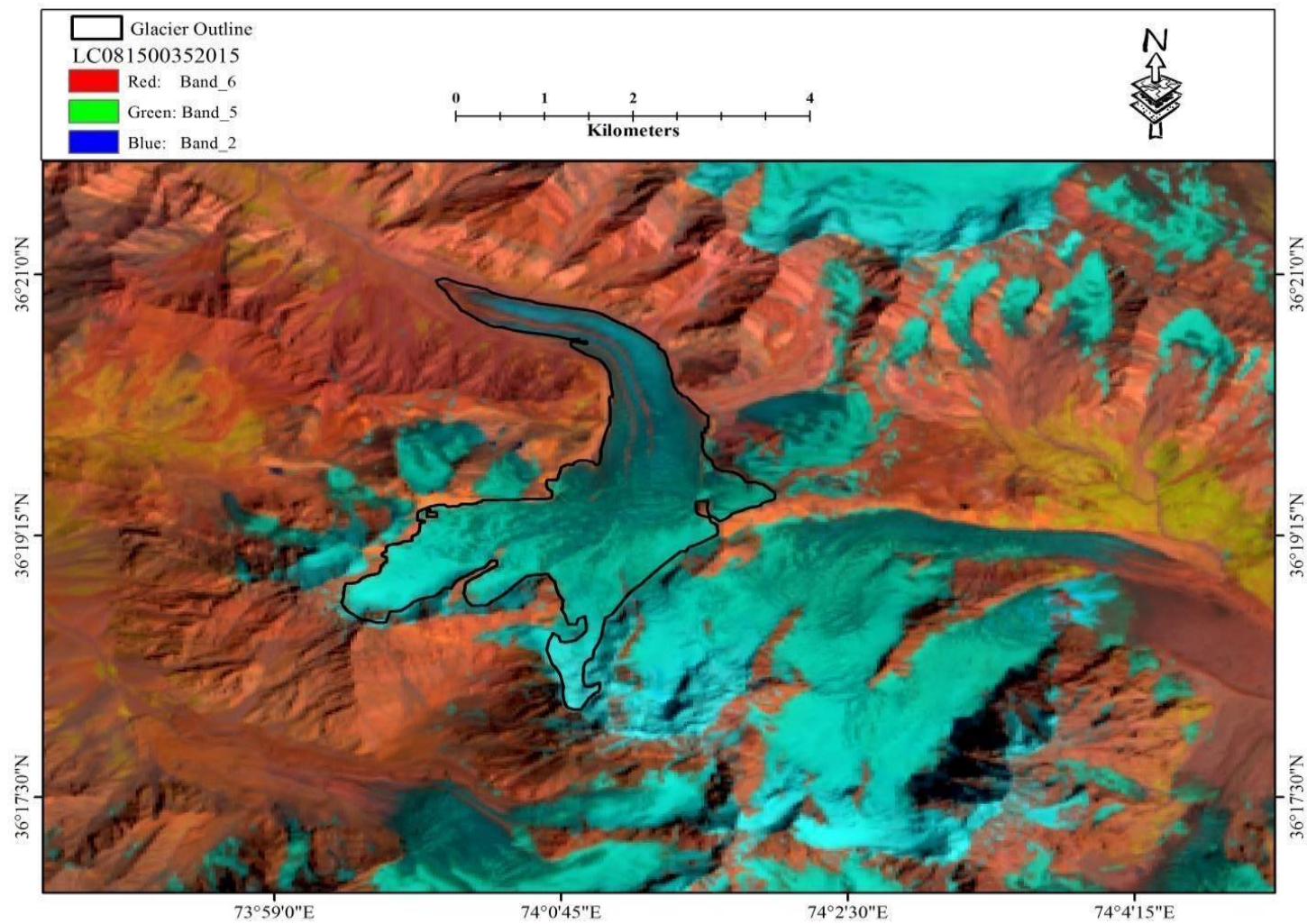


Figure 4.7 Phakor Glacier

4.4 Kappa Coefficient

For qualitative (categorical) items, Cohen's kappa coefficient (K) is a digital tool that is utilized to assess inter-rater dependability as well as intra-rater reliability. K takes into consideration the probability that the agreement could have happened by chance, making it typically considered to be a more reliable measurement than a simple % agreement estimate. Cohen's kappa is controversial because it might be challenging to understand the indices of agreement. According to some academics, conceptually evaluating disagreement between things is simpler.

The agreement between two raters who each assign N items to C mutually incompatible categories is measured by Cohen's kappa. The meaning of this:

$$K = \frac{pr_a - pr_e}{1 - pr_e}$$

Using the observed data to fix the odds of each witness randomly observing each category, Pr_e indicates chance agreement and Pr_a reflects the actual observed agreement.

Cohen suggested the following interpretation for the Kappa result:

Values of 0 signify no agreement, 0.01 to 0.20 signify agreement to a minor degree, 0.21 to 0.40 signify reasonable settlement, 0.41 to 0.60 signify modest settlement, 0.61 to 0.80 signifies strong settlement, and 0.81 to 1.00

signify almost perfect settlement.

Even a relatively low level of inter-rater agreement can be referred to be "substantial" under this interpretation. 61% agreement is immediately regarded as bad in terms of percent agreement. Some lowering of requirements from percent agreement seems logical given the frequent decline from percent agreement in kappa results. Accepting the range of 0.40 to 0.60 as "moderate" would mean that the lowest value (0.40) still indicates a high enough degree of agreement. Here is a more logical justification.

Any kappa value below 0.60 denotes poor inter rater reliability, and little trust should be placed in the study's findings. Table 4.2 illustrates the idea that research datasets might contain both accurate and inaccurate data. Although it is unusual for Kappa values below zero to appear in study data, when they do, it is a sign of a major issue. A negative kappa indicates agreement that is less favorable than anticipated or disagreement. Low negative readings (between -0.10 and -0.1) are typically taken to mean "no agreement." The degree of disagreement among raters is indicated by a big negative kappa. When raters are in such disagreement, the data collected is meaningless. Rather of being carefully gathered research data or high-quality clinical laboratory values, they are more like to random data. Those data (whether scientific or clinical) are unlikely to accurately reflect the circumstances in any significant way. Such a discovery necessitates either redesigning the experiment or retraining raters.

Table.4.2 Interpretation of Cohen’s kappa coefficient

<u>Value of Kappa</u>	<u>Level of Agreement</u>	<u>% of Data that are Reliable</u>
0 –.20	None	0 – 4%
.21–.39	Minimal	4 – 15%
.40 –.59	Weak	15–35%
.60 –.79	Moderate	35–63%
.80 –.90	Strong	64–81%
Above .90	Almost Perfect	82–100%

Components of data in research data set are explained diagrammatically in Figure 4.8



Figure 4.8: Components of Data Research

A type of correlation coefficient is the kappa. Although correlation coefficients cannot be understood directly, the coefficient of determination (COD), which is the square of the correlation coefficient, can. The COD can be defined as the percentage of variance in the dependent variable that the independent variable can account for. While the true COD can only be computed using the Pearson r , any correlation statistic can have its variance accounted for estimated by squaring the correlation rate. In turn, squaring the kappa theoretically equates to the degree of correctness (i.e. the opposite of error) in the data as a result of arrangement between the statistics gatherers.

CHAPTER 5

CLIMATOLOGICAL DATA ANALYSIS

Climate and physical circumstances affect the health of glaciers (Riedel and Burrows, 2005; Knight, 1999). Temperature and rainfall are the most important climatic variables for glacier growth and survival in most circumstances. The greatest mass intake into a glacial often comes from direct snowfall on the glacier. Wind drift and avalanching; on the other hand, can be quite essential in particular parts. Solar irradiance (a gauge of solar energy reaching a specific surface) and wind are two other environmental factors that influence glacier formation. **Air pollution is also an important parameter to assess the impact on glacier melt. However, it is not part of the objectives set for the climatological analysis, hence air pollution and tourism impact on the glacier retreat and advancement not studied and discussed in the thesis.**

Winter snowfall dominates glacier nourishment in Karakoram. However, nearly thirty three percent of high altitude snowfall amassing happens in summer (Hewitt, 1990). The likelihood of such huge swings in the atmospheric sources, regime and seasonal occurrences of glacier sustenance, this factor does not seem to be in other

regions where glaciers are surging. Glaciers fluctuation is subjected to worldly wise heat flux one can assess in study area of Karakorum.

Temperature and precipitation are the prime signs of climate change which are effectively contributing for global climate system and energy cycle (Guan et al., 2017). The Upper Indus Basin (UIB) is generally known as the Asia 'tower of solid water' as it comprises the biggest number of glaciers separate the polar region that stores water in the drainage of ice and snow (Dahri et al., 2016). The glaciers of Karakoram are mostly debris covered and hence they show a distinctive behavior of average neutral mass balance compare to the worldwide glaciers (Lutz et al., 2016). This stability is termed by many researchers as Karakoram Anomaly (Farinotti et al., 2020).

The Indus basin watershed consists of ten distinct river basins, namely Indus, Jhelum, Shyok, Shingo, Shigar, Swat, Astore, Chitral, Hunza, Gilgit (Bashir and Rasul 2010). One of the sub-basins of UIB in HKH region is our area of interest for this particular study is Gilgit basin or catchment. As per SRTM 30m digital elevation model (DEM), the basin situated among the longitudes of 35°46'05" to 36°1'16" N and latitudes of 72°25'02" to 74°19'25" E covering an approximate area of 12,726 km² with a mean altitude of 4054 m.a.s.l (Nazeer et al., 2022).

The UIB is a crucial climatological study area because it is influenced by diverse climatic controls like: the western winds, summer monsoon, and anti-cyclonic clear climate outline (Fowler and Archer 2006). Mountainous region requires a sufficient amount of data gauging instruments and data itself than the flat lands to achieve the same reliability, therefore the mean maximum temperature was calculated for duration of 30 years for the proposed study area.

It is helpful to make a distinction between changes that may be caused by variations in precipitation and those connected to changes in temperature aimed for the tenacity of evaluate the possible influence of climate change scenarios on stream flow in UIB. Variations in winter precipitation, which largely consists of snowfall in glaciated places, will impact the amount of flow from winter snowmelt. In parallel, during the melt season at the glacier surface, the amount of water that glaciers produce as they melt will vary with the amount of energy available (change in temperature, primarily during summer). The melting of glaciers dominates the flow of the Gilgit River. The summer flow has two important factors that is winter precipitation and summer temperatures. The summer temperatures (as well as annual) long term record from 1961–2000 indicate a cooling trend by -0.38°C (-0.13°C per decade). The winter temperatures show a warming up trend by $+0.17^{\circ}\text{C}$ per decade (Fowler and Archer 2005; Adnan et al., 2017).

For numerous uses, records with a high (1 km^2) spatial resolution are preferred because they detect ecological deviations that are misplaced at lesser spatial resolutions, especially in hilly and further regions with strong climate inclines. Climate surfaces, or spatially interpolated gridded climate data, are utilized in a variety of applications, primarily in the agricultural, environmental, and biological disciplines. Hijmans et al. (2005) delivered WorldClim version 1 climate database for 1970-2000, for global land areas, comprising of continuing normal monthly temperature and rainfall (Fick and Hijmans 2017), being used here to study the deviations of lowest and extreme temperature, solar energy and rainfall by means of preparation of sub-set from the original global grids. Over the earlier period, there has been an escalation in the digit of

climate locations for which statistics is accessible, with a figure of stations situated at high latitudes and elevations. Additionally, although the innovative dataset was restricted to monthly rainfall and temperature (New et al., 2002), solar radiation on monthly basis also incorporated for realistic climatological data analysis.

5.1 Temperature (Minimum) Profile of Gilgit watershed

The lowest temperature of the day is called as minimum temperature. The global grids of monthly averaged 30-year data were obtained and the subset of the study was extracted to obtain the regional temperature values. The interpolated minimum surface temperature processed from the point data from local stations portrays a high value of -0.2 degree Celsius and a low value of -35.1 degree Celsius for the month of January. The low values of temperature are mainly observed at higher altitudes on Northern side and high values of temperature on the lower altitudes on southeast of Gilgit watershed, respectively. The scale range is 60 km as shown in all Figures. Moreover, January being the severe winter month has a more projecting T_{\min} (low) as compare to T_{\max} (high). January is the frosty winter coldest month in Gilgit.

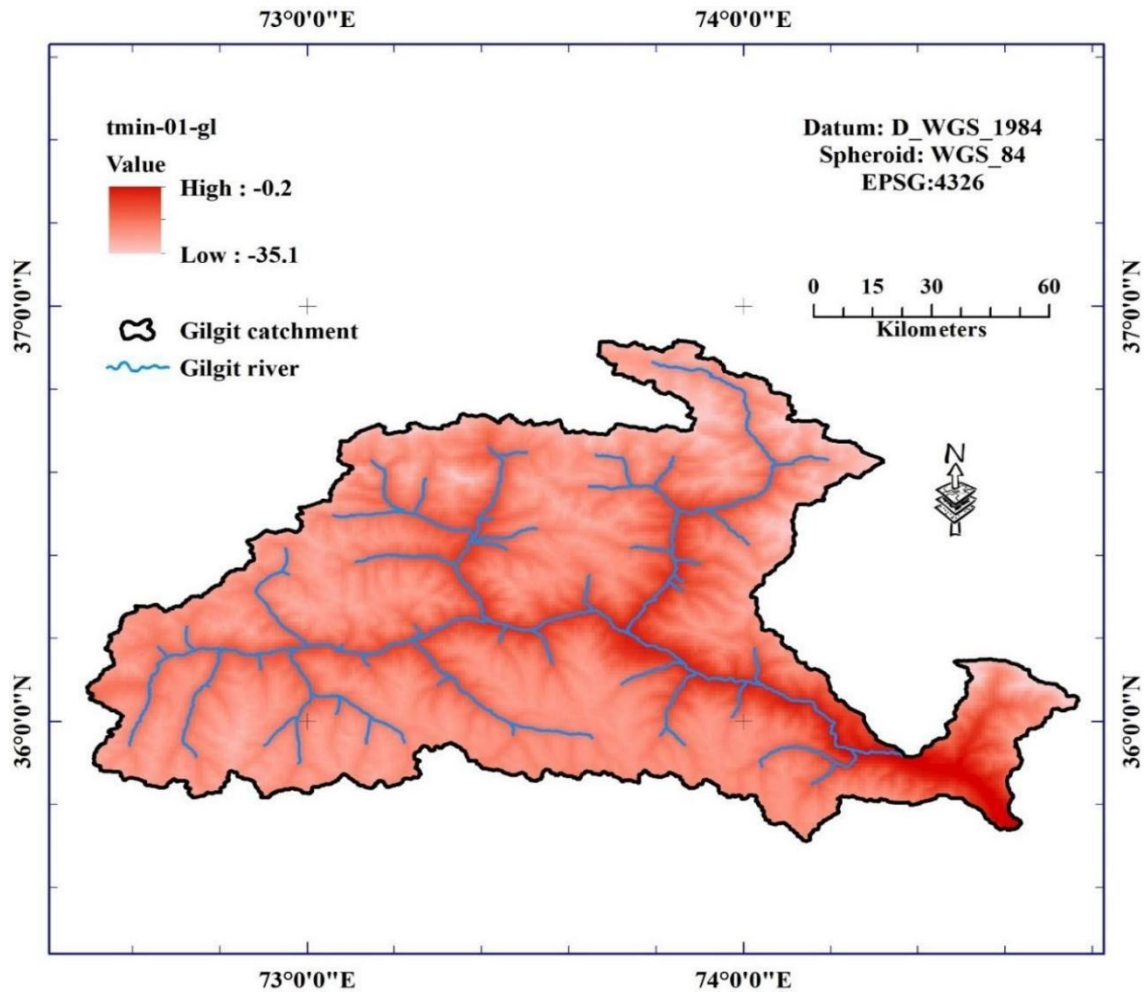


Figure 5.1 Spatial distribution of monthly averaged minimum temperature (in degrees Celsius) for the month of January for Gilgit catchment

The interpolated minimum surface temperature processed from the point data from local stations, monthly average of 30 years portrays a high value of 2.8 degree Celsius and a low value of -36.4 degree Celsius for the month of February. The low values of temperature are mainly observed at higher altitudes on Northern side and high values of temperature on the lower altitudes on southeast of Gilgit watershed, respectively. Moreover, February being the winter month has a more projecting T_{\min} (low) as compare to T_{\max} (high). The average high- temperature remains on lower side in February.

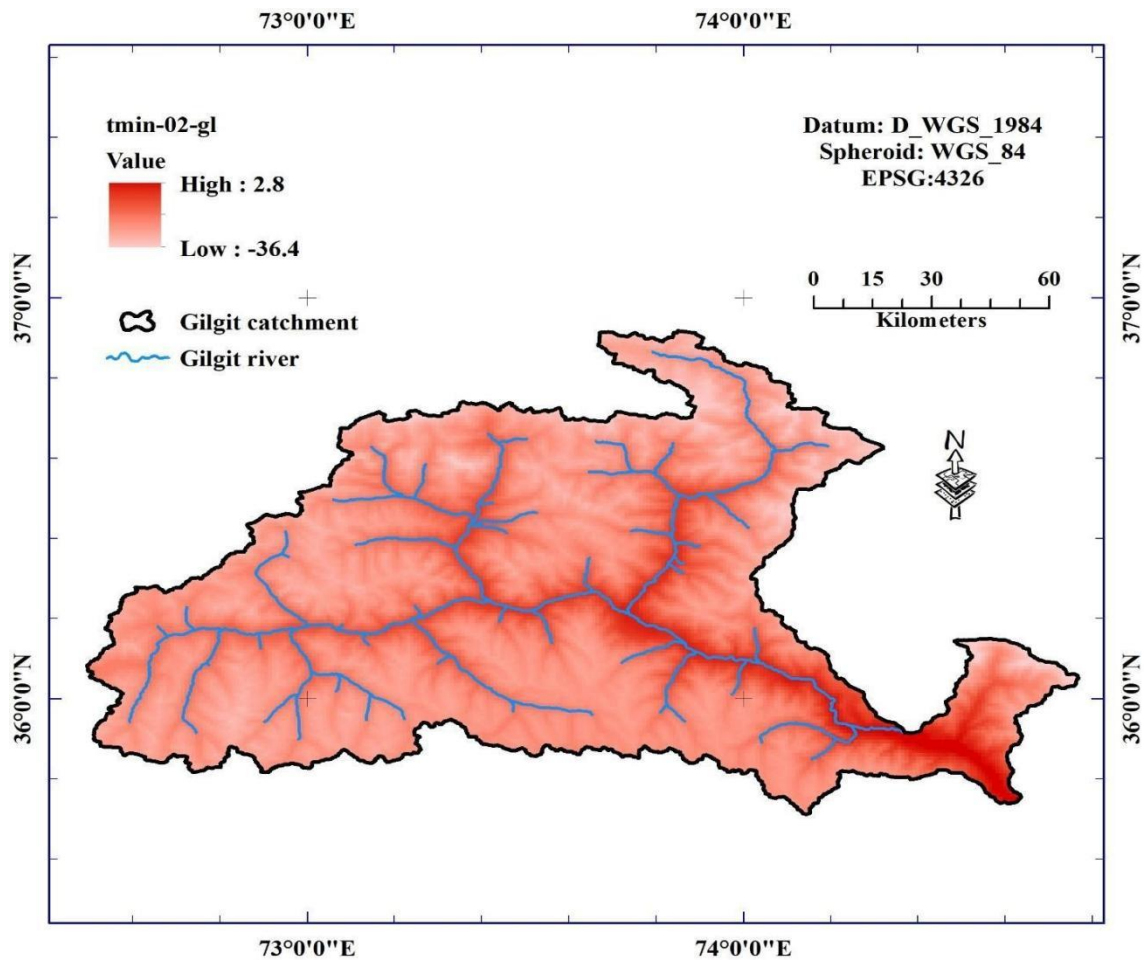


Figure 5.2 Spatial distribution of monthly averaged minimum temperature (in degrees Celsius) for the month of February for Gilgit catchment

The interpolated minimum surface temperature processed from the point data from local stations, monthly average of 30 years portrays a high value of 6.8 degrees Celsius and a low value of -33.4 degree Celsius for the month of March. The low values of temperature are mainly observed at higher altitudes on Northern side and high values of temperature on the lower altitudes on southeast of Gilgit watershed, respectively. March is the first month of the spring, a relaxed month in Gilgit by average temperature ranging between -13.3 degree Celsius and max 6.8 degree Celsius. In Gilgit, the average high-temperature rises in March.

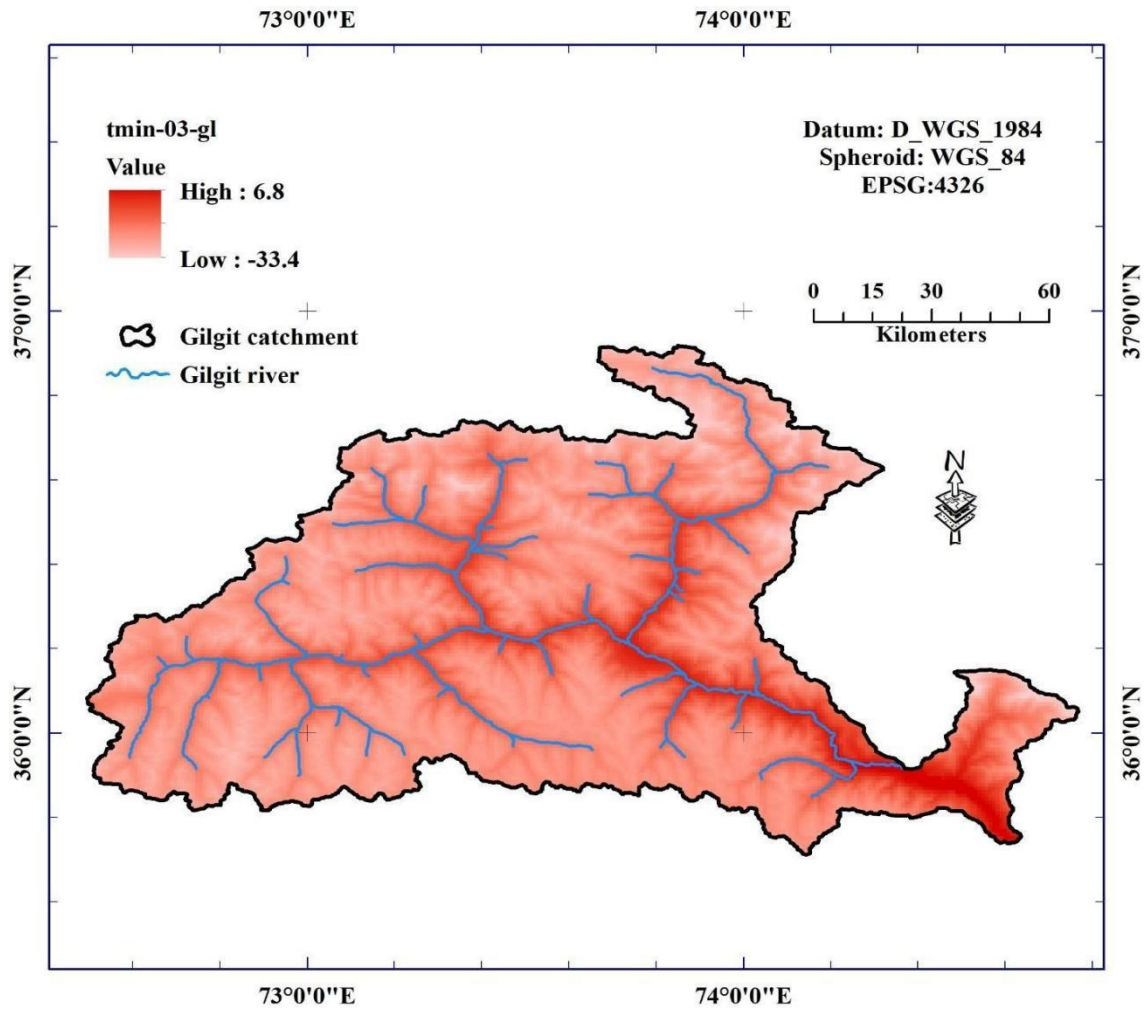


Figure 5.3 Spatial distribution of monthly averaged minimum temperature (in degrees Celsius) for the month of March for Gilgit catchment

The interpolated minimum surface temperature processed from the point data from local stations, monthly averaged of 30 years portrays a high value of 11.4 degrees Celsius and a low value of -25.7 degree Celsius for the month of April. The low values of temperature are mainly observed at higher altitudes on Northern side and high values of temperature on the lower altitudes on southeast of Gilgit watershed, respectively. April is a slightly hot spring month in Gilgit by average valley temperature changing at -7 degree Celsius. In April, the average high-temperature rises.

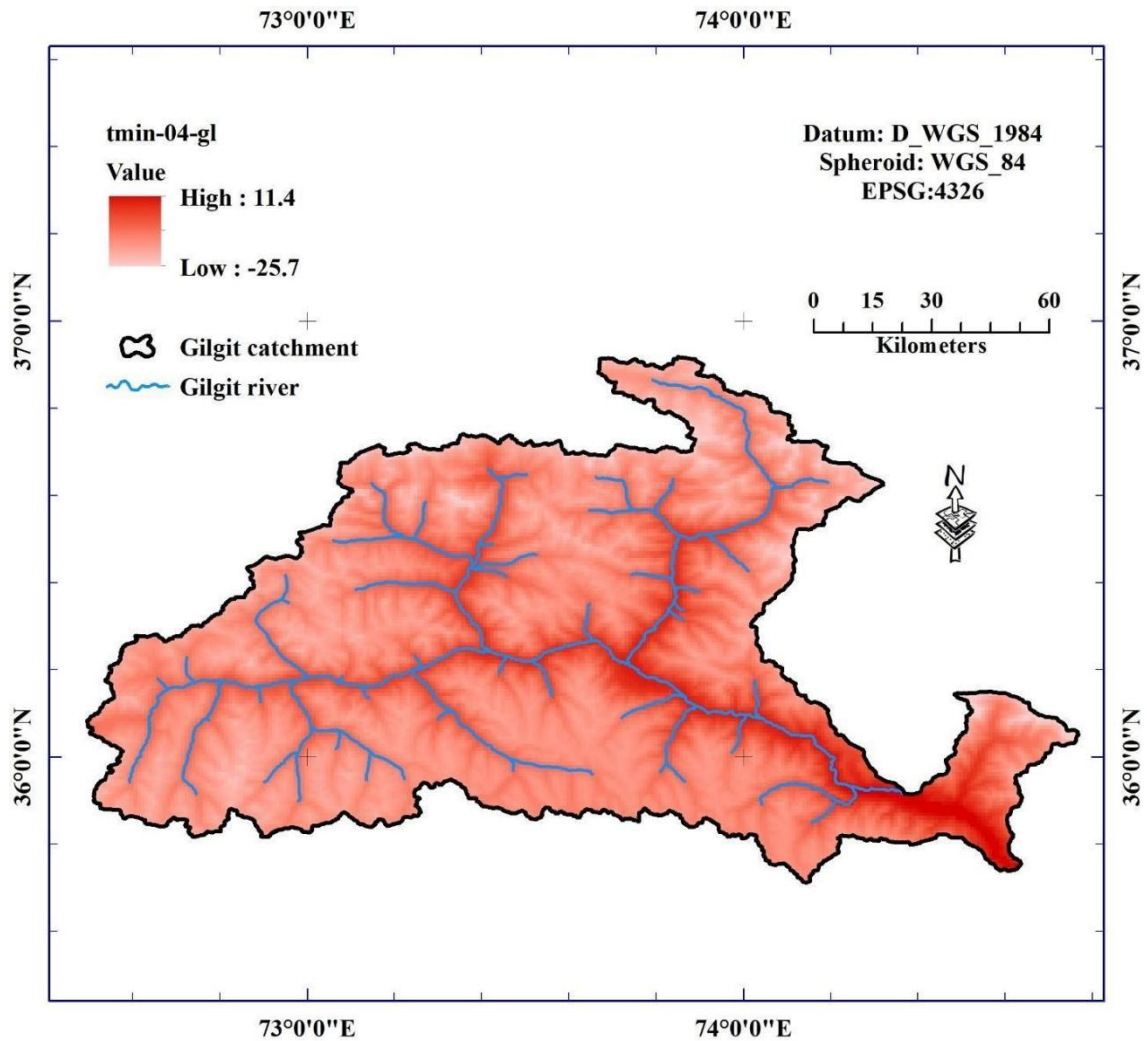


Figure 5.4 Spatial distribution of monthly averaged minimum temperature (in degrees Celsius) for the month of April for Gilgit catchment

The interpolated minimum surface temperature processed from the point data from local stations, monthly averaged of 30 years portrays a high value of 15.1 degrees Celsius and a low value of -20 degree Celsius across watershed for the month of May. The low values of temperature are mainly observed at higher altitudes on Northern side and high values of temperature on the lower altitudes on southeast of Gilgit watershed, respectively. May, the preceding month of the spring in Gilgit is one more warmer month from April with normal valley temperature variable at ~ 8 degree Celsius. The average high- temperature slightly rises from a soberly warm in April to a still warm May.

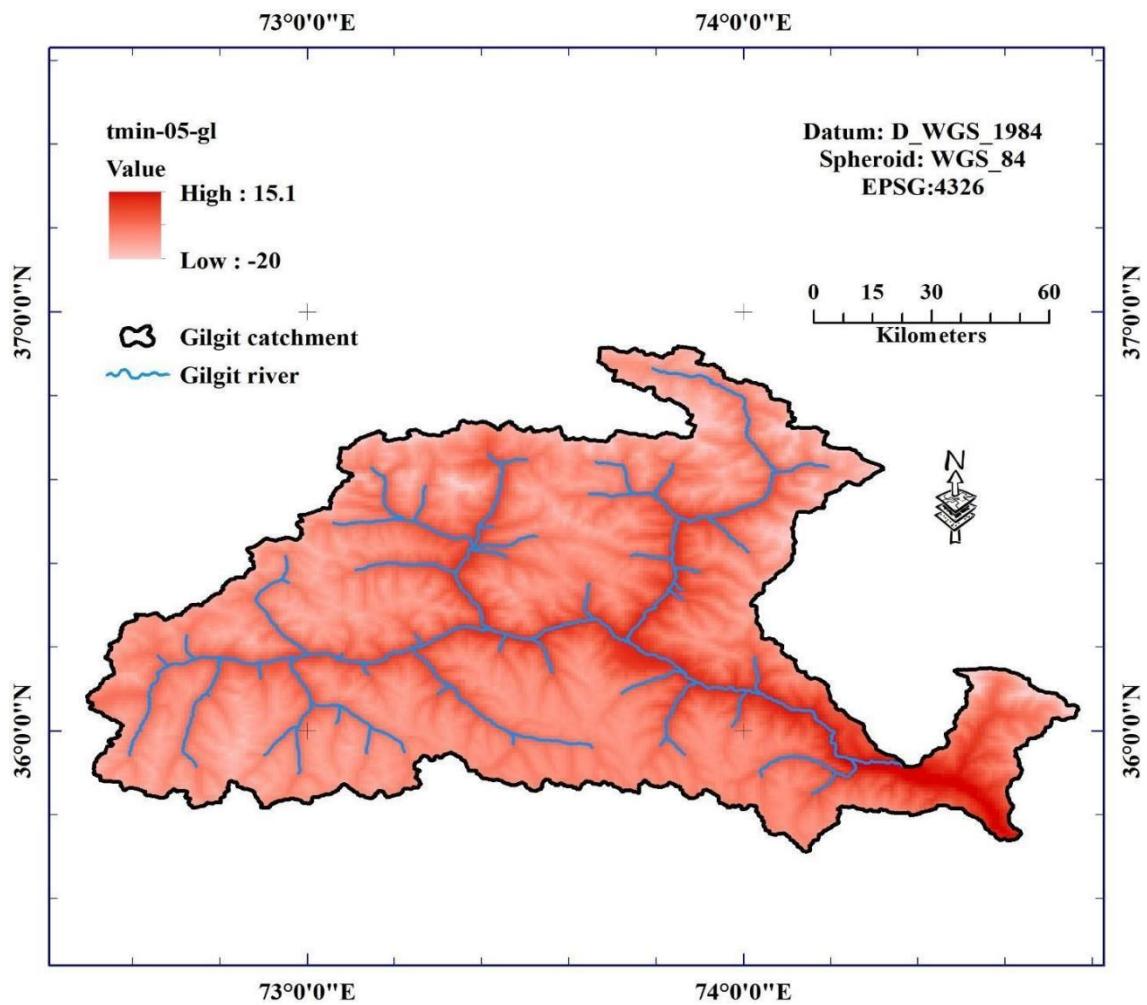


Figure 5.5 Spatial distribution of monthly averaged minimum temperature (in degrees Celsius) for the month of May for Gilgit catchment

The interpolated minimum surface temperature processed from the point data from local stations, monthly averaged of 30 years portrays a high value of 19.2 degrees Celsius and a low value of -16.3 degree Celsius across watershed for the month of June. The low values of temperature are mainly observed at higher altitudes on Northern side and high values of temperature on the lower altitudes on southeast of Gilgit watershed, respectively. June, the leading month of the summer, in Gilgit, is a searing month

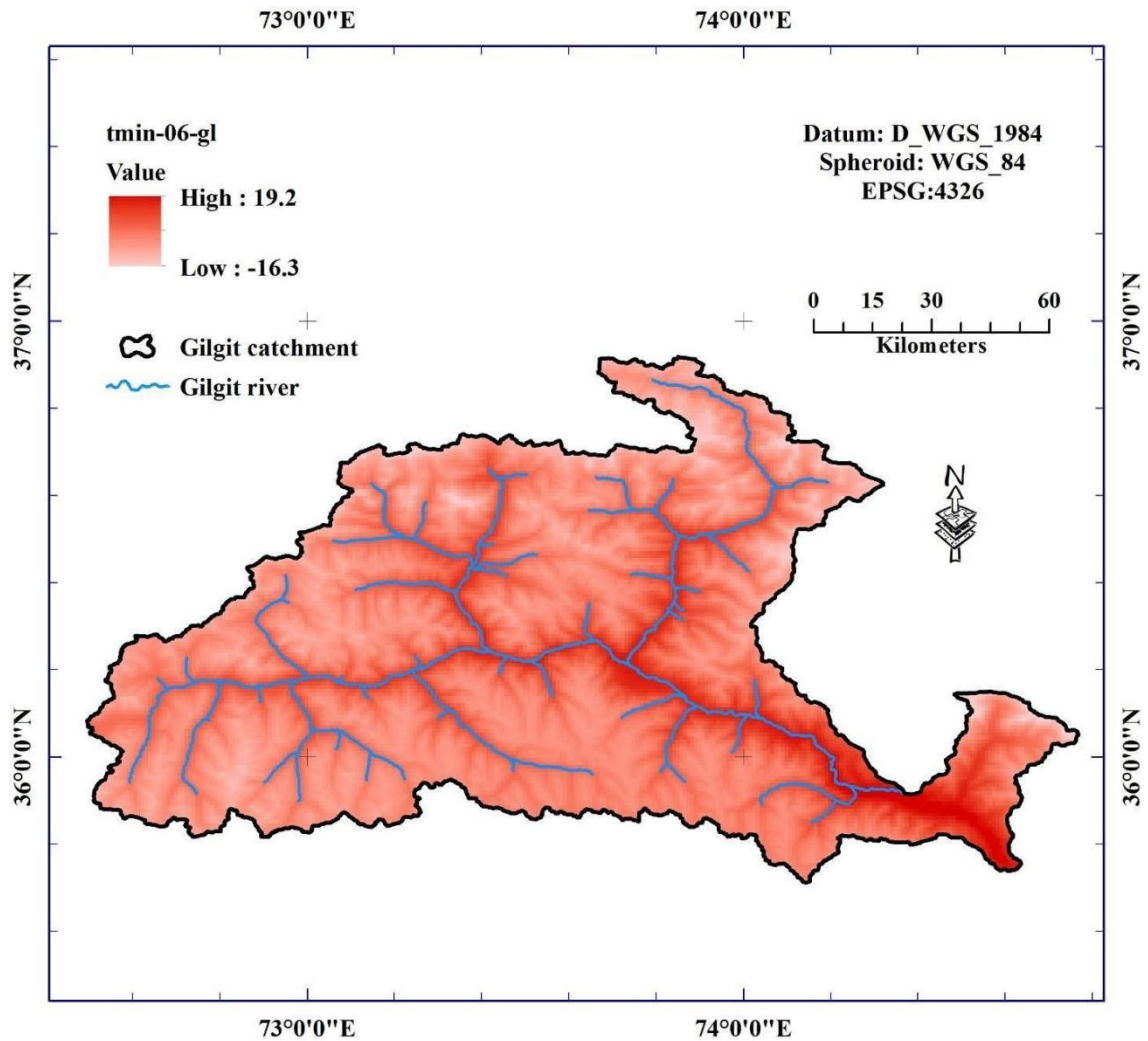


Figure 5.6 Spatial distribution of monthly averaged minimum temperature (in degrees Celsius) for the month of June for Gilgit catchment

The interpolated minimum surface temperature processed from the point data from local stations, monthly averaged of 30 years portrays a high value of 22.5 degrees Celsius and a low value of -13.1 degree Celsius across watershed for the month of July. The low values of temperature are mainly observed at higher altitudes on Northern side and high values of temperature on the lower altitudes on southeast of Gilgit watershed, respectively. July is a sweltering summer month in Gilgit.

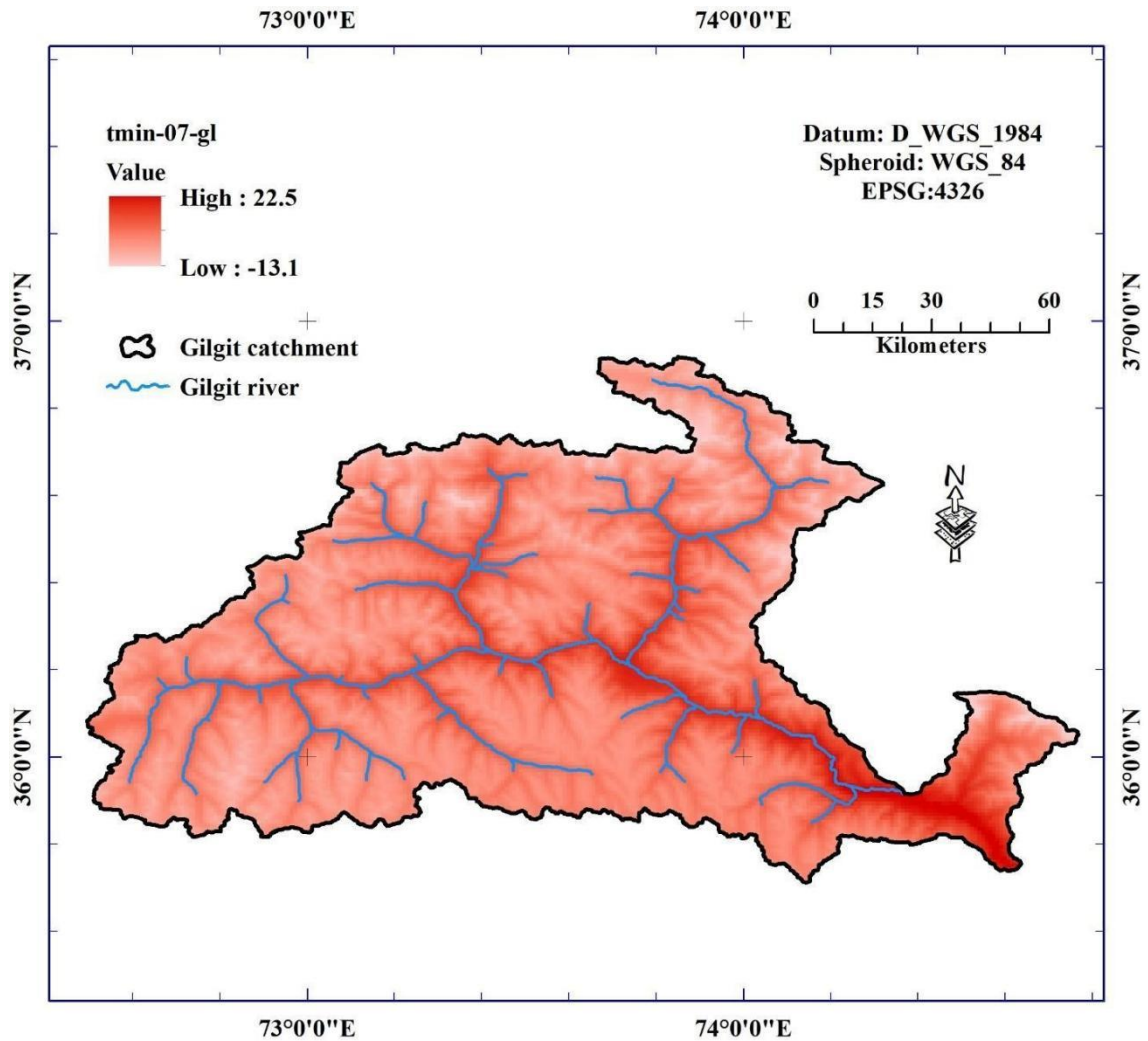


Figure 5.7 Spatial distribution of monthly averaged minimum temperature (in degrees Celsius) for the month of July for Gilgit catchment

The interpolated minimum surface temperature processed from the point data from local stations, monthly averaged of 30 years portrays a high value of 22.3 degrees Celsius and a low value of -12.7 degree Celsius across watershed for the month of August. The low values of temperature are mainly observed at higher altitudes on Northern side and high values of temperature on the lower altitudes on southeast of Gilgit watershed, respectively. The end month of the summer, August, is one more very hot month in Gilgit.

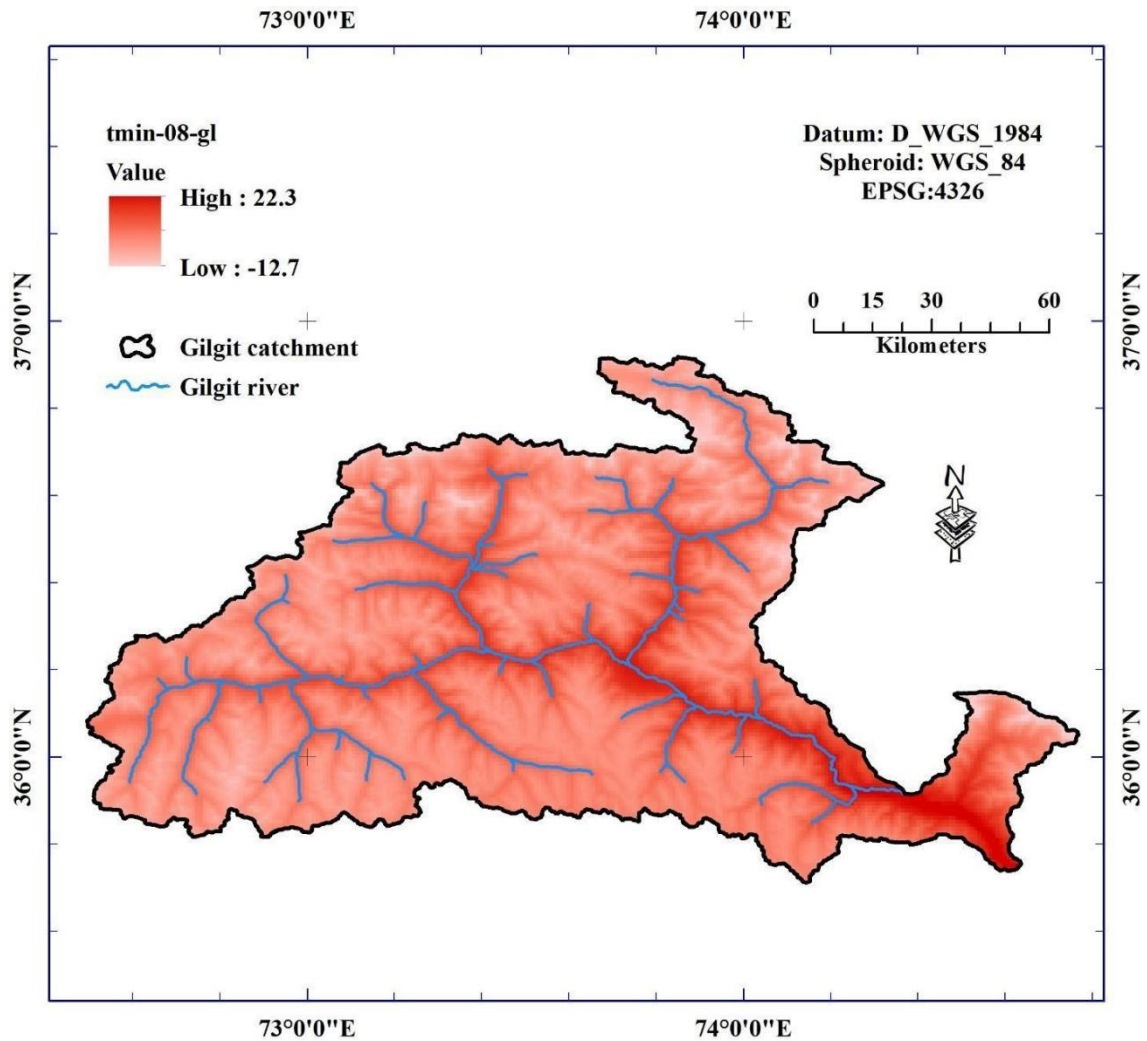


Figure 5.8 Spatial distribution of monthly averaged minimum temperature (in degrees Celsius) for the month of August for Gilgit catchment

The interpolated minimum surface temperature processed from the point data from local stations, monthly averaged of 30 years portrays a high value of 17.4 degrees Celsius and a low value of -16.6 degrees Celsius across watershed for the month of September. The low values of temperature are mainly observed at higher altitudes on Northern side and high values of temperature on the lower altitudes on southeast of Gilgit watershed, respectively. September is the first month of the autumn and is still feeling like a slight hot month.

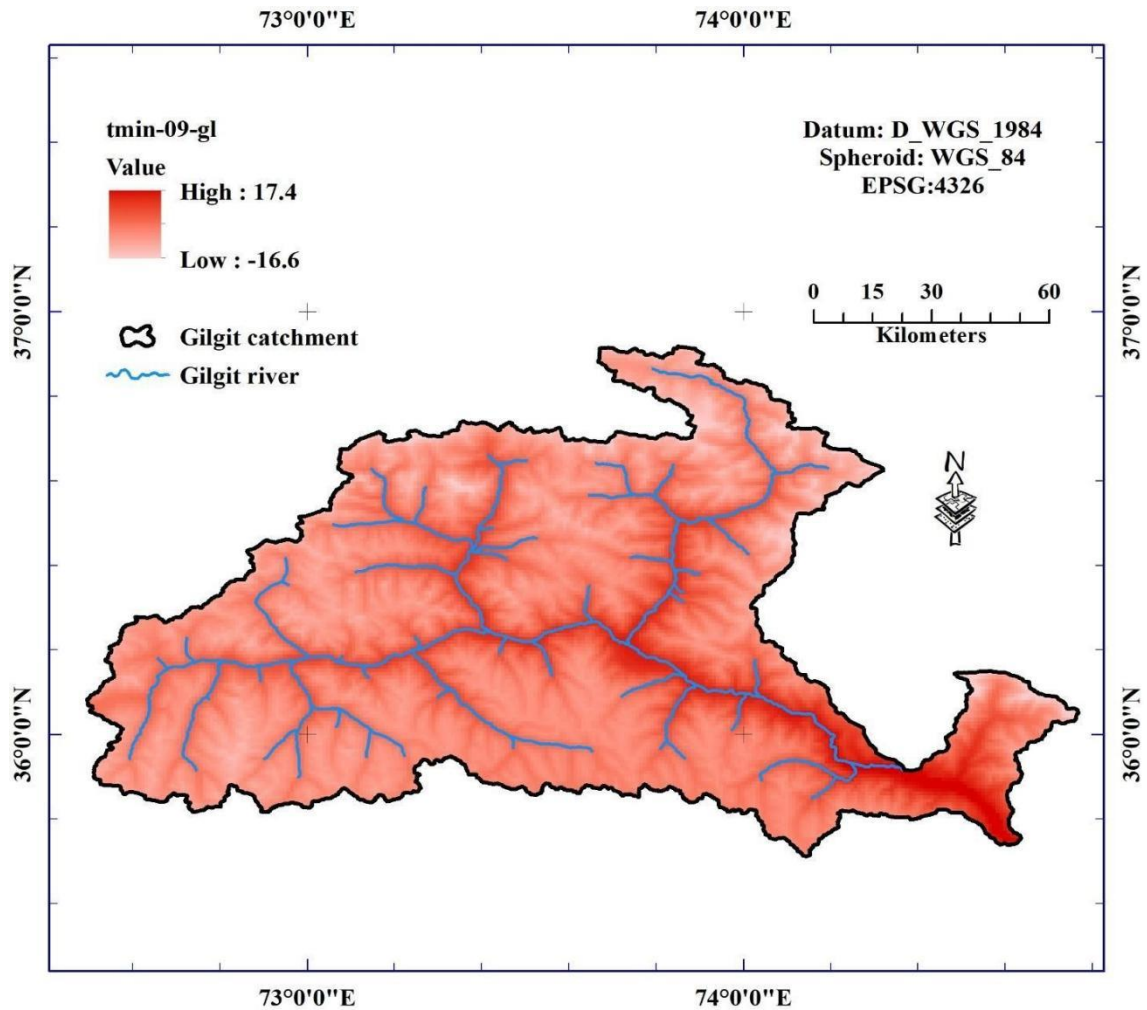


Figure 5.9 Spatial distribution of monthly averaged minimum temperature (in degrees Celsius) for the month of September for Gilgit catchment

The interpolated minimum surface temperature processed from the point data from local stations, monthly averaged of 30 years portrays a high value of 11 degrees Celsius and a low value of -21.3 degrees Celsius across watershed for the month of October. The low values of temperature are mainly observed at higher altitudes on Northern side and high values of temperature on the lower altitudes on southeast of Gilgit watershed, respectively. October, like September, in Gilgit is one of warmer fall month.

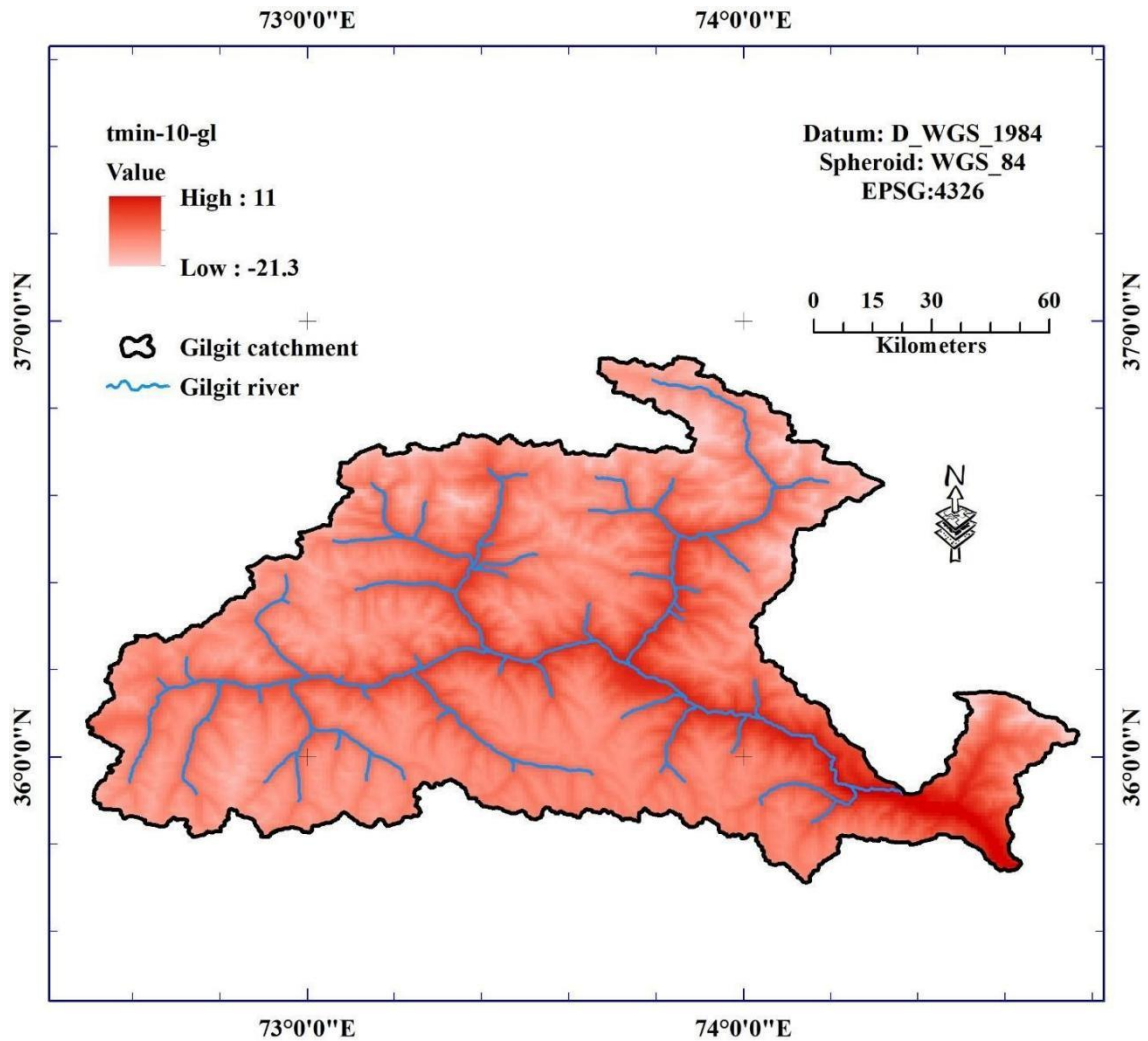


Figure 5.10 Spatial distribution of monthly averaged minimum temperature (in degrees Celsius) for the month of October for Gilgit catchment

The interpolated minimum surface temperature processed from the Point data from local stations, monthly averaged of 30 years portrays a high value of 4.7 degrees Celsius and a low value of -27.9 degrees Celsius across watershed for the month of November. The low values of temperature are mainly observed at higher altitudes on Northern side and high values of temperature on the lower altitudes on southeast of Gilgit watershed, respectively. November is the last month of the fall, in Gilgit and is one more weatherly relaxed month.

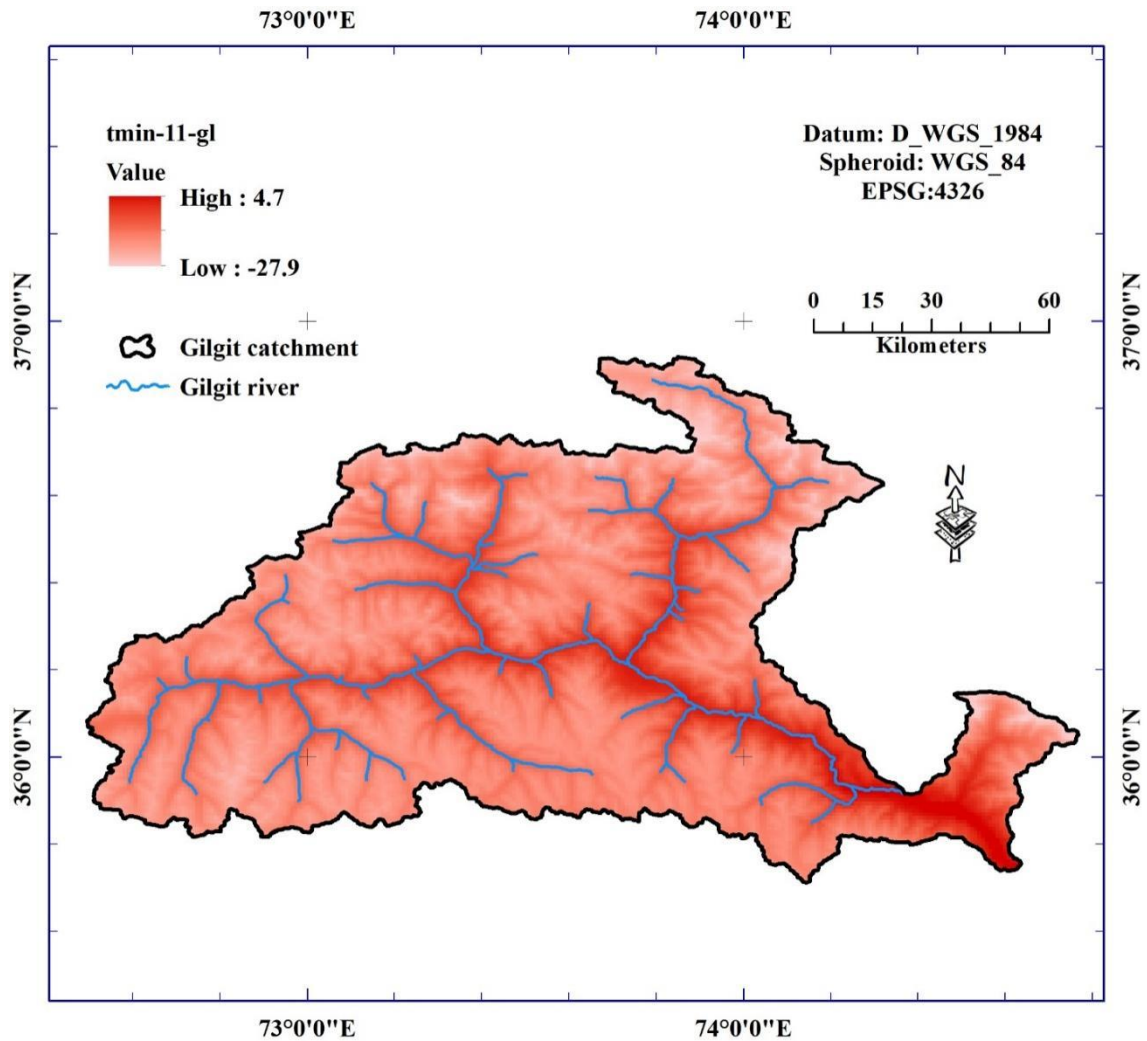


Figure 5.11 Spatial distribution of monthly averaged minimum temperature (in degrees Celsius) for the month of November for Gilgit catchment

The interpolated minimum surface temperature processed from the point data from local stations, monthly averaged of 30 years portrays a high value of 1.2 degrees Celsius and a low value of -33.2 degrees Celsius across watershed for the month of December. The low values of temperature are mainly observed at higher altitudes on Northern side and high values of temperature on the lower altitudes on southeast of Gilgit watershed, respectively. December is a full winter month in Gilgit by average min temperature fluctuating at -16 degree Celsius.

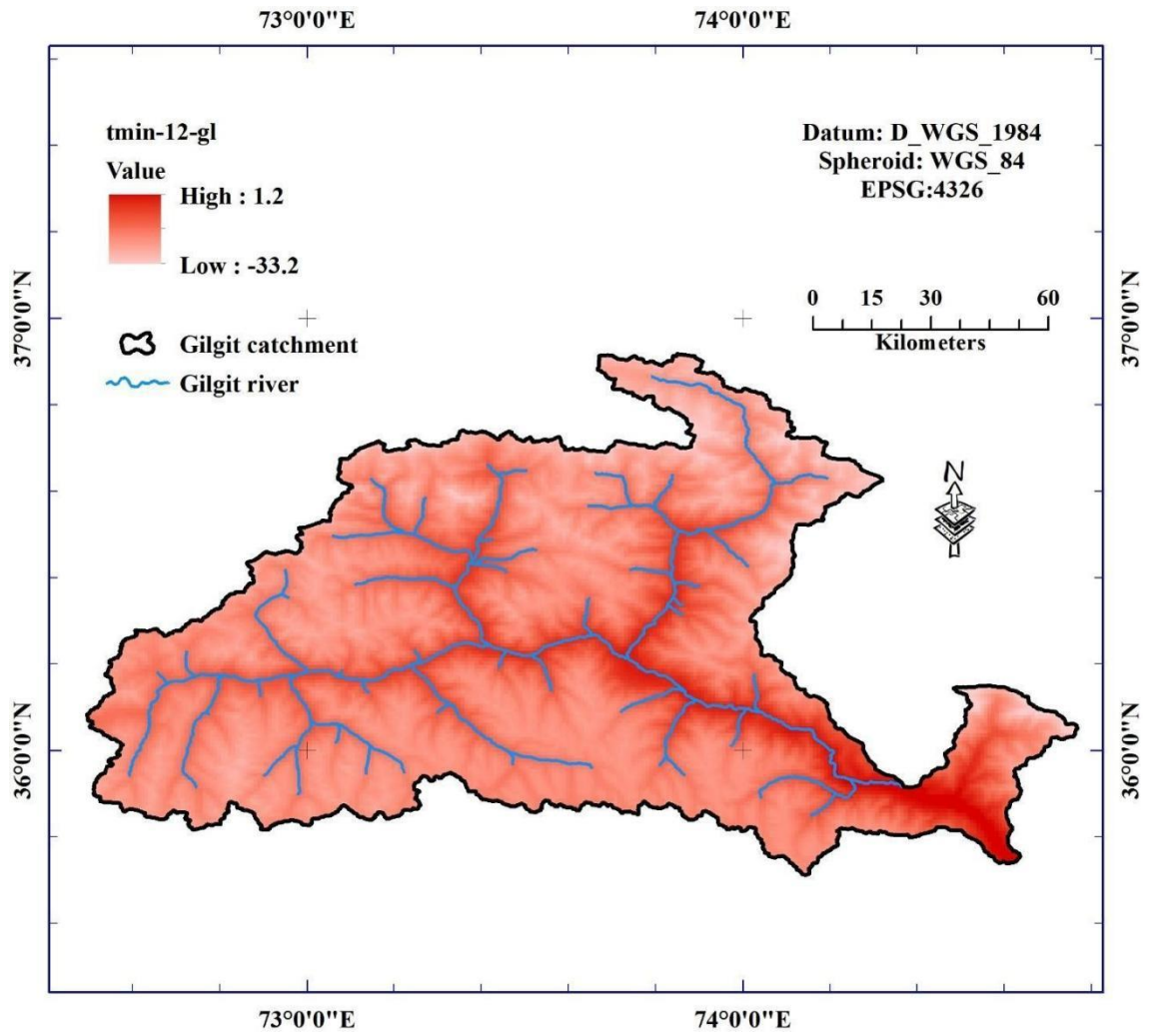


Figure 5.12 Spatial distribution of monthly averaged minimum temperature (in degrees Celsius) for the month of December for Gilgit catchment

Table 5.1 Yearly Low and High values for temperature in °C in Gilgit watershed

Sr.	Month	T_{Min} (Low)	T_{Min} (High)	T_{Min} (Ave)
1	January	-35.1	-0.2	-17.65
2	February	-36.4	2.8	-16.8
3	March	-33.4	6.8	-13.3
4	April	-25.7	11.4	-7.15
5	May	-20	15.1	-2.45
6	June	-16.3	19.2	1.45
7	July	-13.1	22.5	4.7
8	August	-12.7	22.3	4.8
9	September	-16.6	17.4	0.4
10	October	-21.3	11	-5.15
11	November	-27.9	4.7	-11.6
12	December	-33.2	1.2	-16

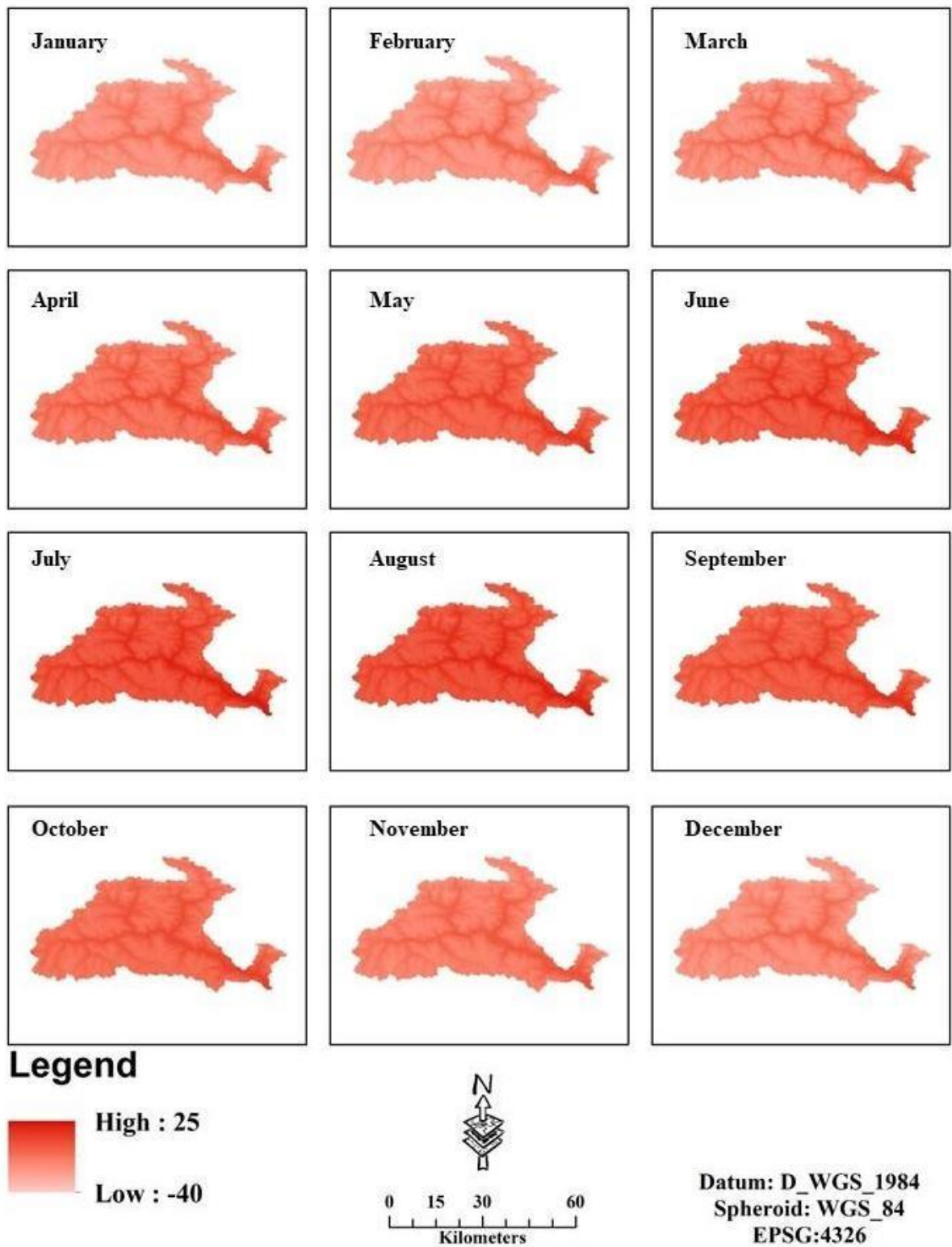


Figure 5.13 Spatial distribution of monthly averaged minimum temperature (in degrees Celsius) – Normalized matrix of yearly profile

5.2 Solar Radiation Intensity in the Gilgit Watershed

The energy accessible for removal of a glacial not set in stone by the energy spending plan of the glacier surface. Sun based radiation (daylight) conveys energy to the glacial mass surface. The sun's radiation is consumed in part, and the rest is reflected.

Precipitation and removal affect the piece reflected (called the albedo), with new snow being more intelligent than old snow or removing ice. Precipitation aids net aggregation significantly more through its albedo effect, which reduces removal, than it does through the mass added straight by snowfall. This means that precipitation affects are determined by the frequency of precipitation as well as the annual total.

It is, thus, vital to take note of the varieties in the sun oriented radiation power. Energy from the sun is the principle well spring of energy for the Earth's temperature framework. Disparities in the Earth's circle round the sun cause contrasts in the cyclical circulation and measure of sunlight based radiation arriving at the earth.

Chronicles of past environment show that there is a connection between these varieties and long haul environment changes. Interglacial conditions start with expanding mid-scope summer insolation and end as mid-scope summer insolation diminishes. Normal sunlight in March in Gilgit is 12 hours. The month with the lengthiest days is June (Normal sunlight: 14.6h). The month with the briefest days is December (Average light: 9.8h). Normal daylight in March is 6h while the month with the most daylight is June (Average daylight: 10h). Months with the least daylight are January, February and December when the typical daylight is 5 hours.

The introduced sun powered radiation information handled from the point information from neighborhood stations, month to month arrived at the midpoint of 30 years, depicts a high worth of $7545 \text{ kJ m}^{-2} \text{ day}^{-1}$ and a low worth of $5641 \text{ kJ m}^{-2} \text{ day}^{-1}$ across watershed for the long stretch of January. The low upsides of sun powered radiation at the higher heights on Northern side might be related with the huge measure of overcast cloud cover frequently present at high mountains. Ordinarily, under clear sky conditions the sun oriented radiation increments with height. This is known as the height impact. The angle values are $\sim 8\%$ per 1000m of height.

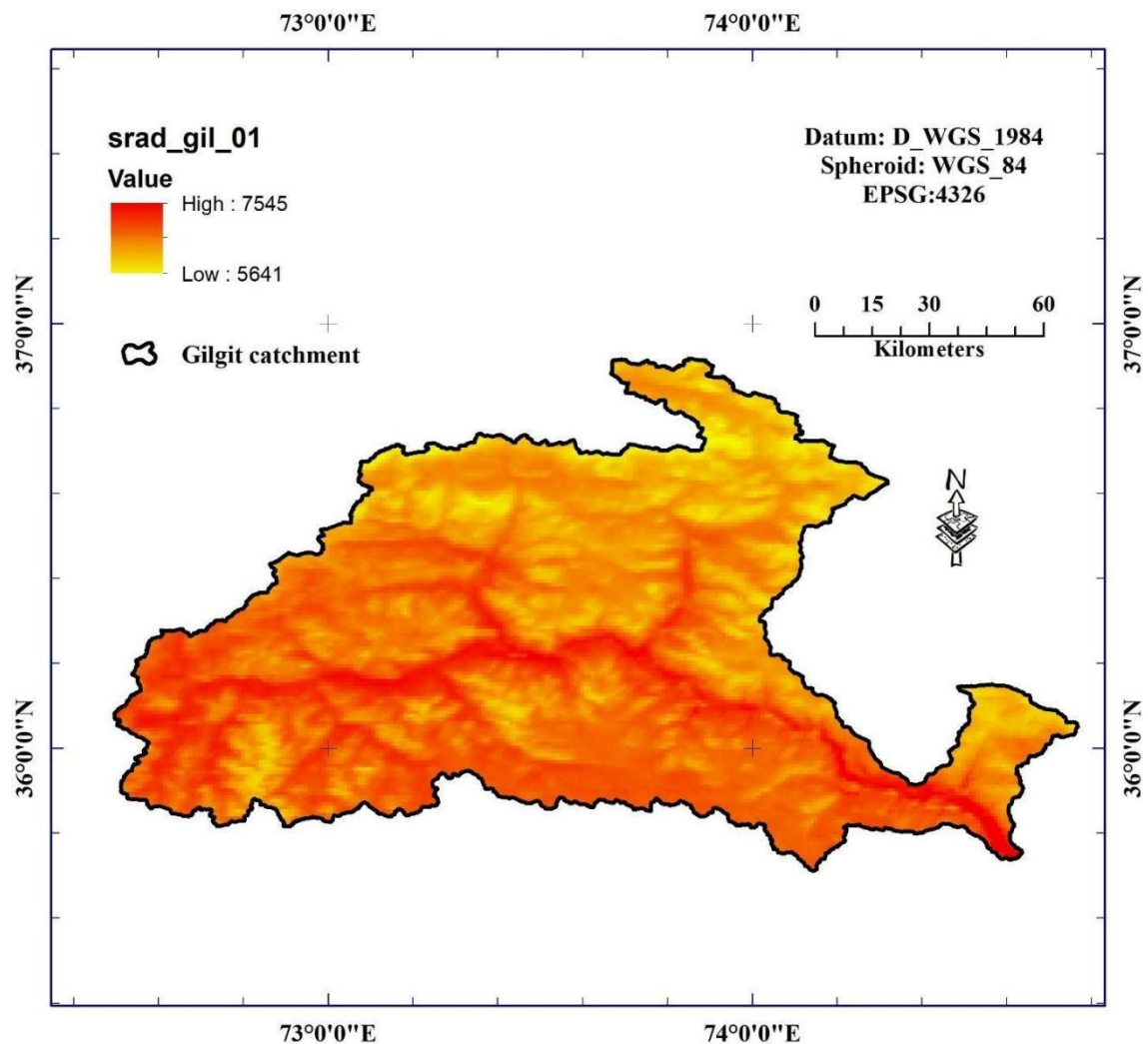


Figure 5.14 Spatial distribution of monthly averaged solar radiation (in $\text{kJ m}^{-2} \text{ day}^{-1}$) for the month of January for Gilgit catchment

The interpolated solar radiation data processed from the point data from local stations, monthly averaged of 30 years, portrays a high value of $10093 \text{ kJ m}^{-2} \text{ day}^{-1}$ and a low value of $8176 \text{ kJ m}^{-2} \text{ day}^{-1}$ across watershed for the month of February. Normally higher latitudes receive less solar radiation. Hence, the values at 36°N are higher than those at 37°N as shown in the following figure 5.15. The low values of solar radiation at the higher altitudes on Northern side may also be associated with the significant amount of cloud cover often present at high mountains. Normally, under clear sky conditions the solar radiation increases with altitude.

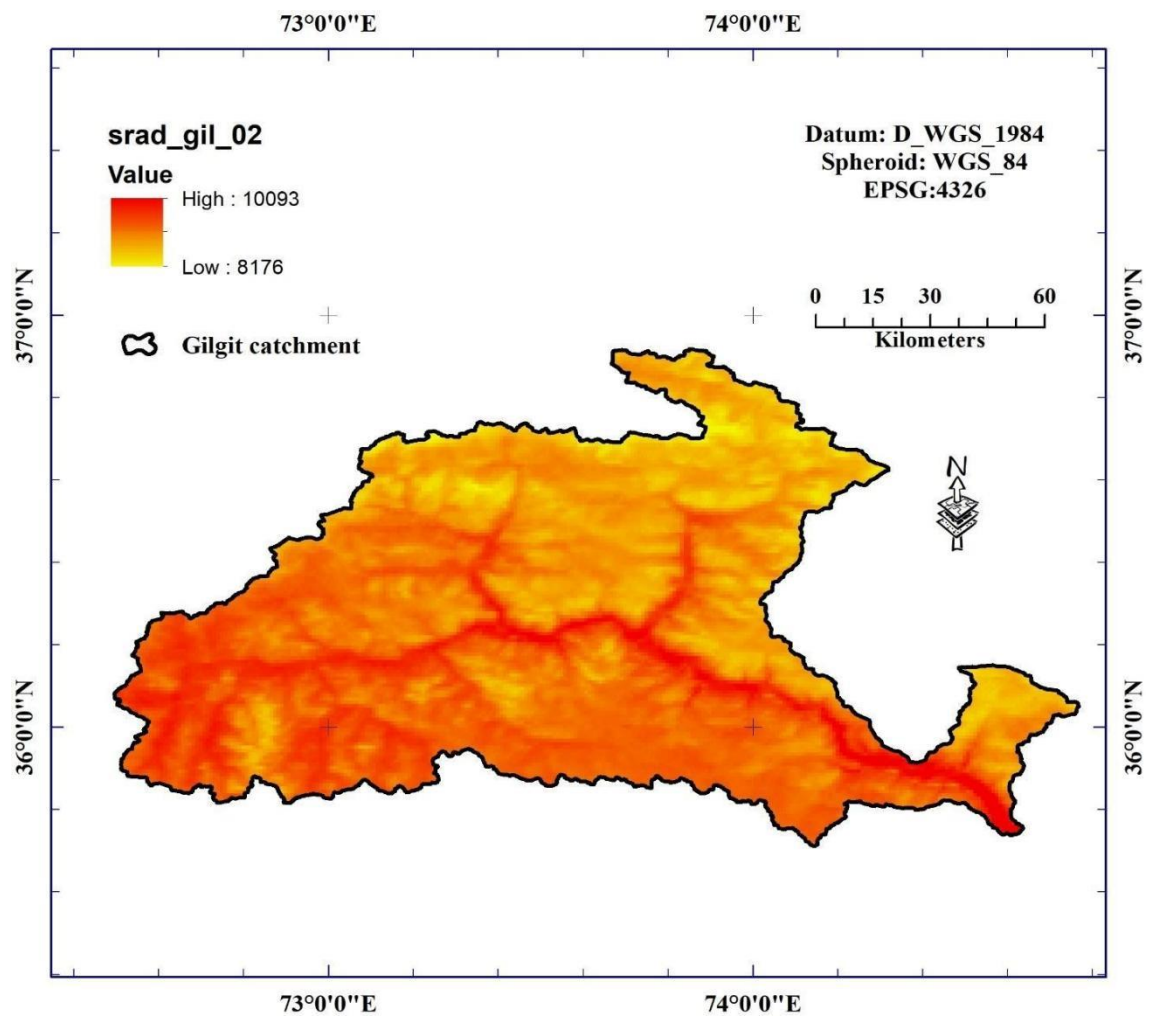


Figure 5.15 spatial distribution of monthly averaged solar radiation (in $\text{kJ m}^{-2} \text{ day}^{-1}$) for the month of February for Gilgit catchment

The interpolated solar radiation data processed from the point data from local stations, monthly averaged of 30 years, portrays a high value of $14075 \text{ kJ m}^{-2} \text{ day}^{-1}$ and a low value of $11721 \text{ kJ m}^{-2} \text{ day}^{-1}$ across watershed for the month of March. Normally higher latitudes receive less solar radiation. Hence, the values at 36°N are higher than those at 37°N as shown in the following figure 5.16. The low values of solar radiation at the higher altitudes on Northern side may also be associated with the significant amount of cloud cover often present at high mountains. Normally, under clear sky conditions the solar radiation increases with altitude.

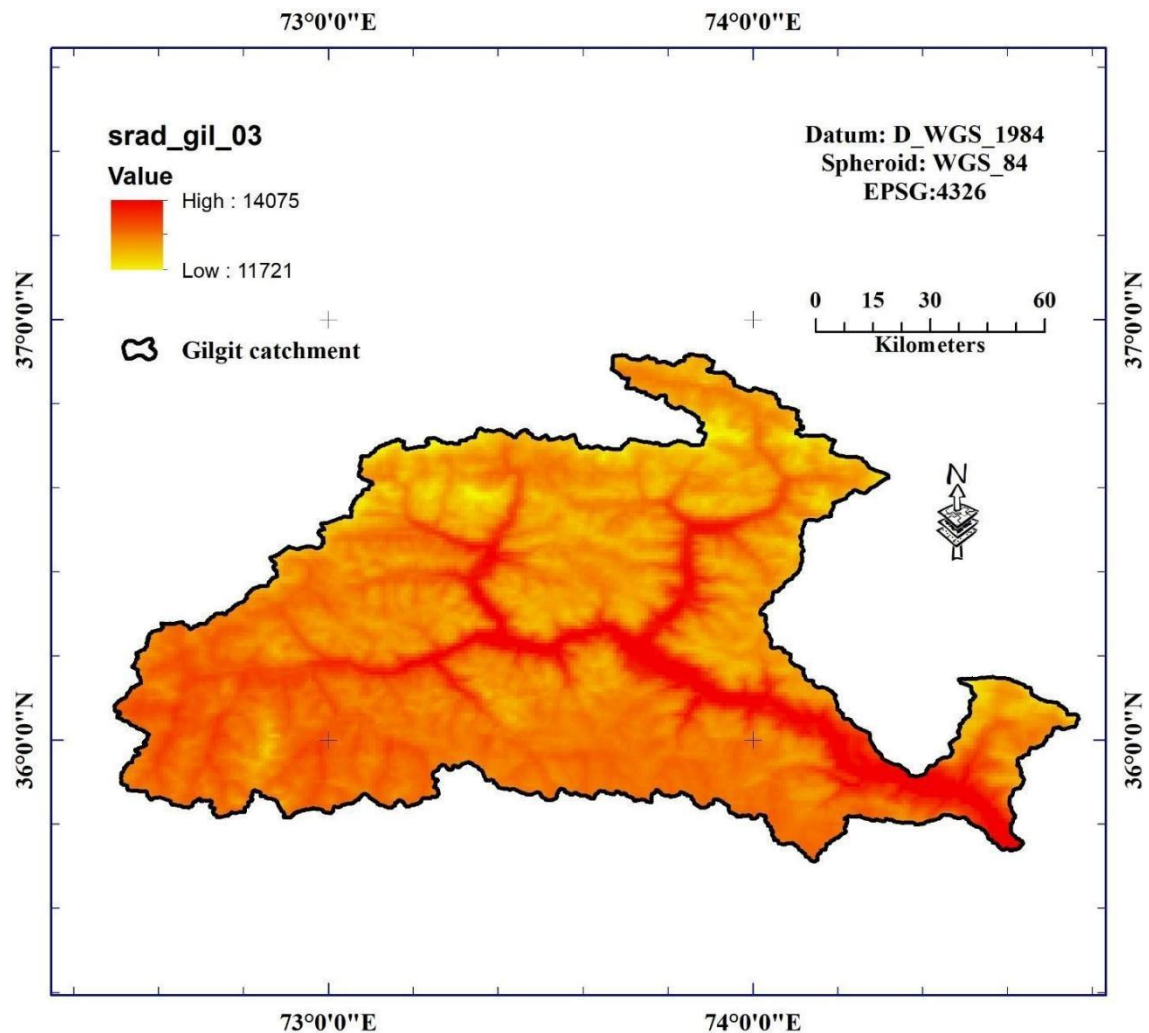


Figure 5.16 Spatial distribution of monthly averaged Solar radiation (in $\text{kJ m}^{-2} \text{ day}^{-1}$) for the month of March for Gilgit catchment

The interpolated solar radiation data processed from the point data from local

stations, monthly averaged of 30 years, portrays a high value of $18065 \text{ kJ m}^{-2} \text{ day}^{-1}$ and a low value of $16793 \text{ kJ m}^{-2} \text{ day}^{-1}$ across watershed for the month of April. Normally higher latitudes receive less solar radiation. Hence, the values at 36°N are higher than those at 37°N as shown in the following figure 5.17. The low values of solar radiation at the higher altitudes on Northern side may also be associated with the significant amount of cloud cover often present at high mountains. Normally, under clear sky conditions the solar radiation increases with altitude.

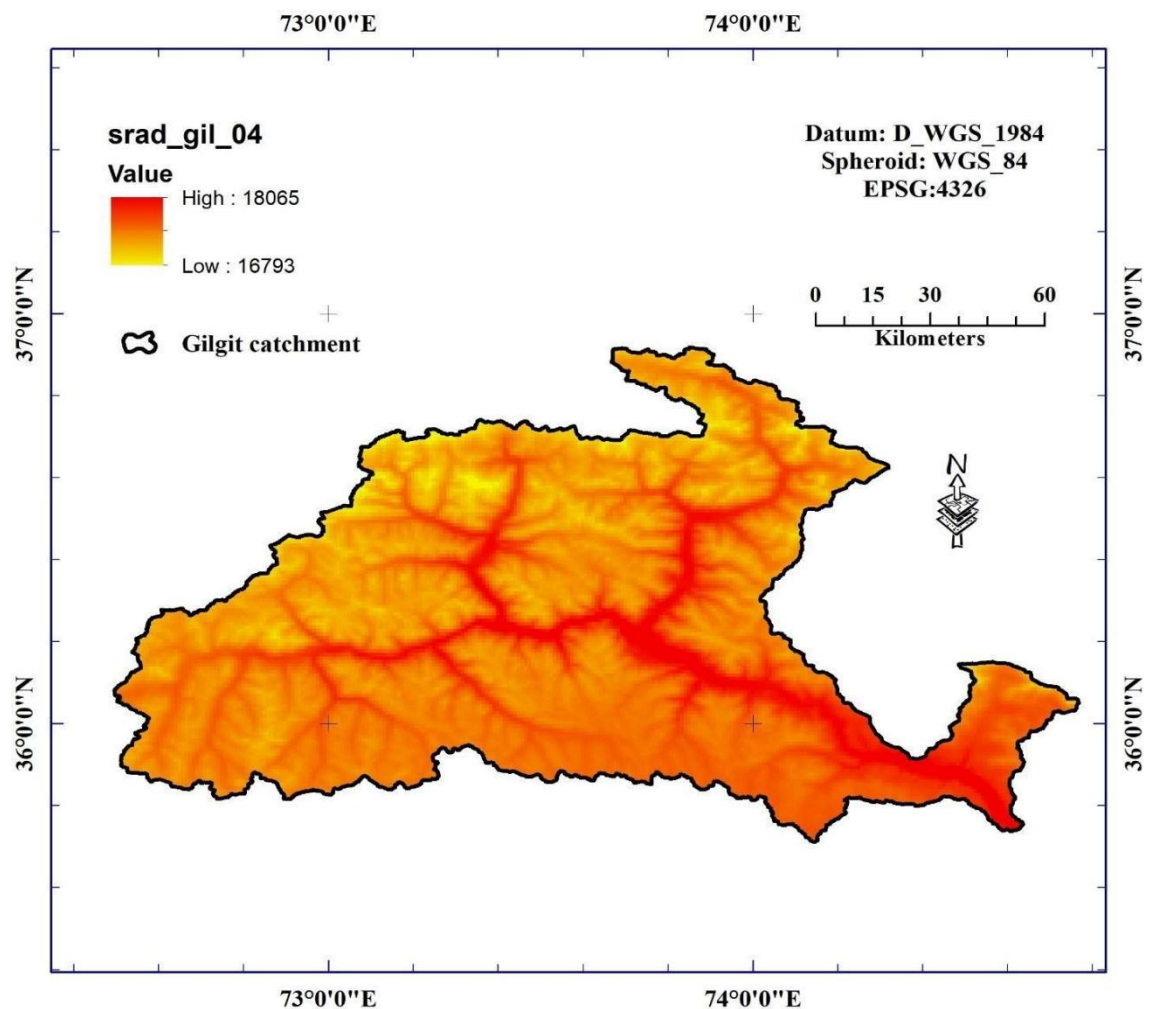


Figure 5.17 Spatial distribution of monthly averaged Solar radiation (in $\text{kJ m}^{-2} \text{ day}^{-1}$) for the month of April for Gilgit catchment

The interpolated solar radiation data processed from the point data from local stations, monthly averaged of 30 years, portrays a high value of $21560 \text{ kJ m}^{-2} \text{ day}^{-1}$ and

a low value of $20422 \text{ kJ m}^{-2} \text{ day}^{-1}$ across watershed for the month of May. Normally higher latitudes receive less solar radiation. Hence, the values at 36°N are higher than those at 37°N as shown in the following figure 5.18. The low values of solar radiation at the higher altitudes on Northern side may also be associated with the significant amount of cloud cover often present at high mountains. Normally, under clear sky conditions the solar radiation increases with altitude.

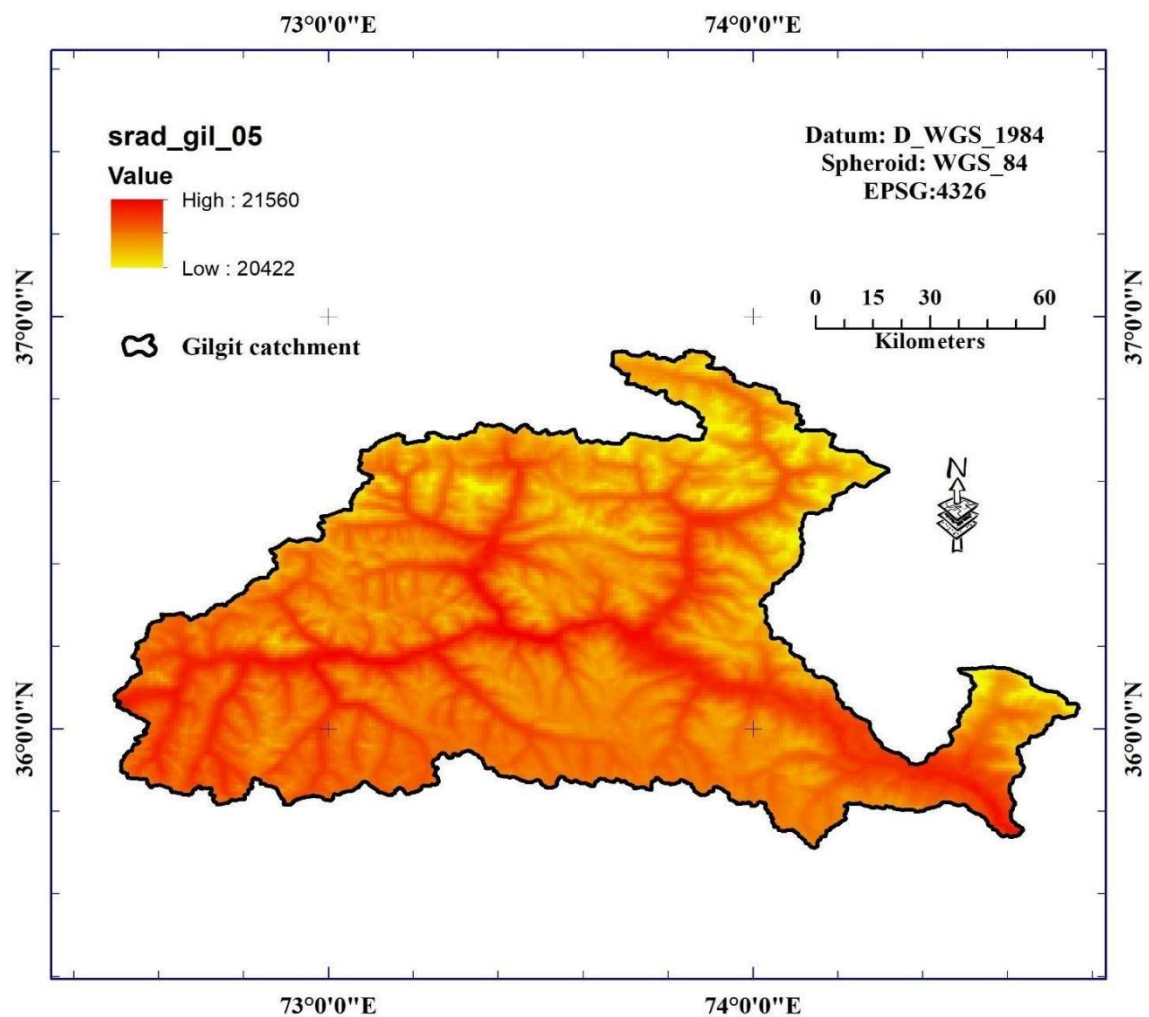


Figure 5.18 Spatial distribution of monthly averaged Solar radiation (in $\text{kJ m}^{-2} \text{ day}^{-1}$) for the month of May for Gilgit catchment

The interpolated solar radiation data processed from the point data from local stations, monthly averaged of 30 years, portrays a high value of $24790 \text{ kJ m}^{-2} \text{ day}^{-1}$ and a low value of $21927 \text{ kJ m}^{-2} \text{ day}^{-1}$ across watershed for the month of June. Normally

higher latitudes receive less solar radiation. Hence, the values at 36°N are higher than those at 37°N as shown in the following figure 5.19. The low values of solar radiation at the higher altitudes on Northern side may also be associated with the significant amount of cloud cover often present at high mountains. Normally, under clear sky conditions the solar radiation increases with altitude.

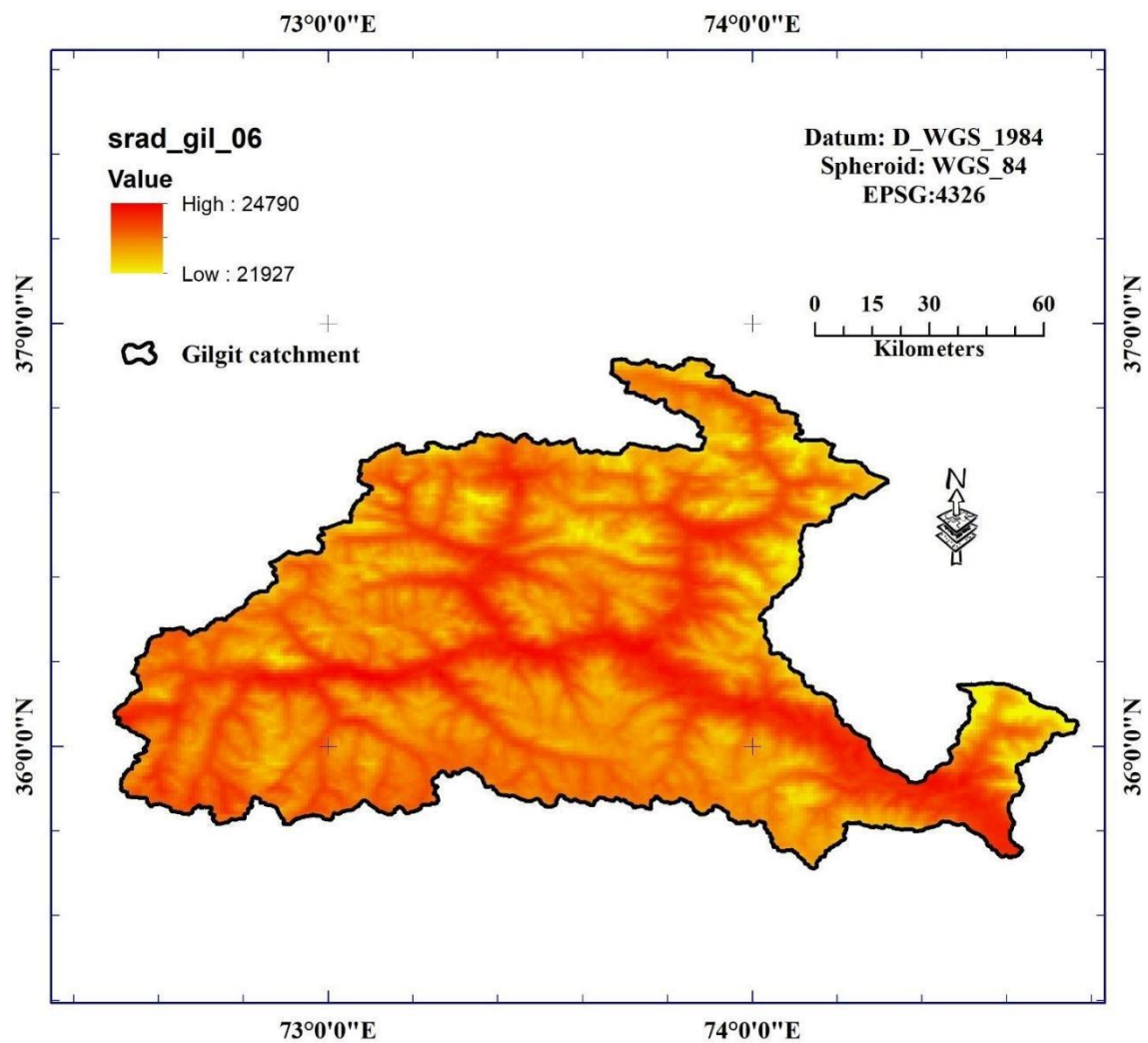


Figure 5.19 Spatial distribution of monthly averaged Solar radiation (in kJ m⁻² day⁻¹) for the month of June for Gilgit catchment

The interpolated solar radiation data processed from the point data from local stations, monthly averaged of 30 years, portrays a high value of 22605 kJ m⁻² day⁻¹ and a low value of 18612 kJ m⁻² day⁻¹ across watershed for the month of July. Normally

higher latitudes receive less solar radiation. Hence, the values at 36°N are higher than those at 37°N as shown in the following figure 5.20. The low values of solar radiation at the higher altitudes on Northern side may also be associated with the significant amount of cloud cover often present at high mountains. Normally, under clear sky conditions the solar radiation increases with altitude.

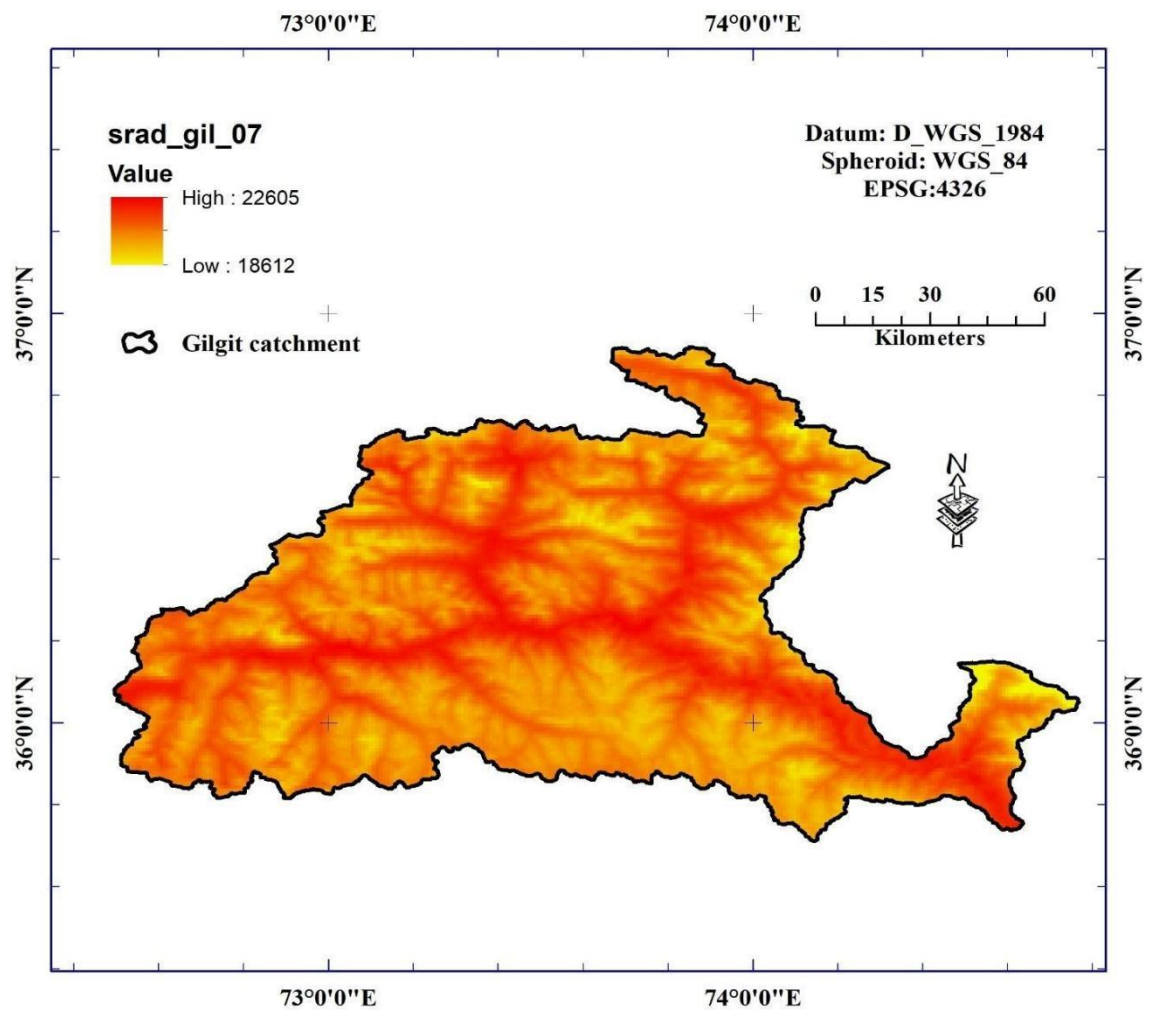


Figure 5.20 Spatial distribution of monthly averaged Solar radiation (in kJ m⁻² day⁻¹) for the month of July for Gilgit catchment

The interpolated solar radiation data processed from the point data from local stations, monthly averaged of 30 years, portrays a high value of 21226 kJ m⁻² day⁻¹ and a low value of 17000 kJ m⁻² day⁻¹ across watershed for the month of August. Normally higher latitudes receive less solar radiation. Hence, the values at 36°N are higher than

those at 37°N as shown in the following figure 5.21. The low values of solar radiation at the higher altitudes on Northern side may also be associated with the significant amount of cloud cover often present at high mountains. Normally, under clear sky conditions the solar radiation increases with altitude.

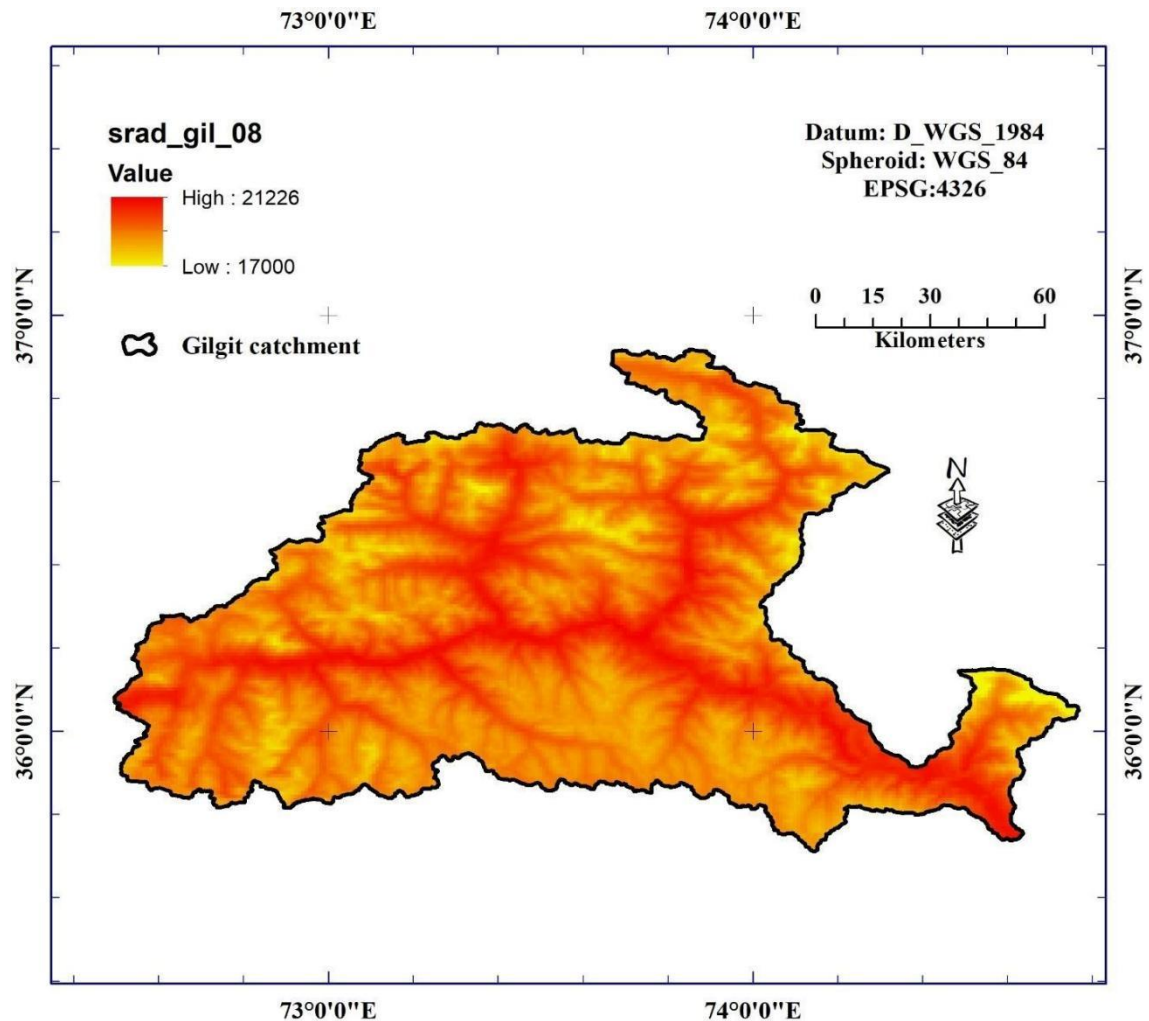


Figure 5.21 Spatial distribution of monthly averaged Solar radiation (in kJ m⁻² day⁻¹) for the month of August for Gilgit catchment

The interpolated solar radiation data processed from the point data from local stations, monthly averaged of 30 years, portrays a high value of 18315 kJ m⁻² day⁻¹ and a low value of 15446 kJ m⁻² day⁻¹ across watershed for the month of September. Normally higher latitudes receive less solar radiation. Hence, the values at 36°N are higher than those at 37°N as shown in the following figure 5.22. The low values of

solar radiation at the higher altitudes on Northern side may also be associated with the significant amount of cloud cover often present at high mountains. Normally, under clear sky conditions the solar radiation increases with altitude.

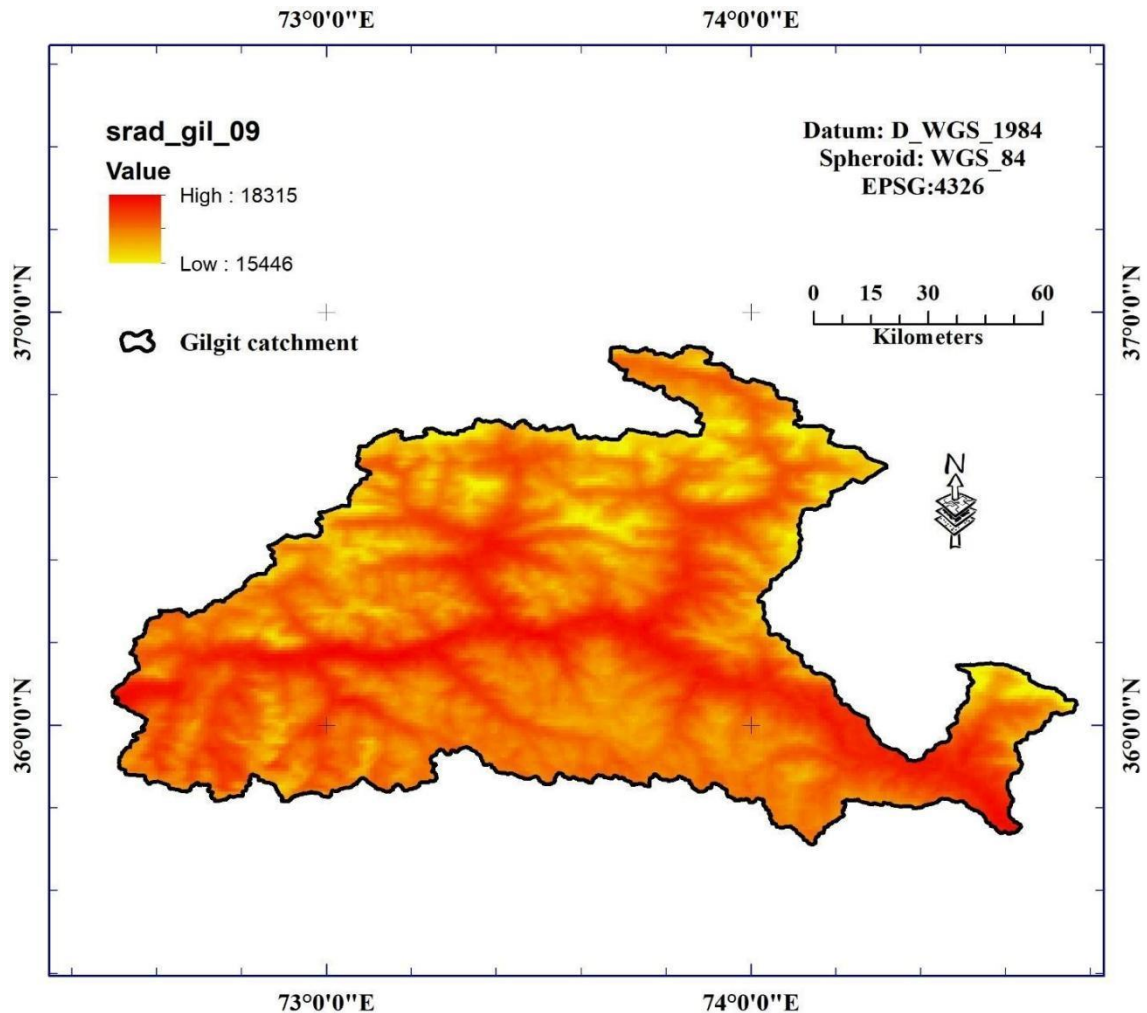


Figure 5.22 Spatial distribution of monthly averaged Solar radiation (in $\text{kJ m}^{-2} \text{day}^{-1}$) for the month of September for Gilgit catchment

The interpolated solar radiation data processed from the point data from local stations, monthly averaged of 30 years, portrays a high value of $14666 \text{ kJ m}^{-2} \text{day}^{-1}$ and a low value of $12108 \text{ kJ m}^{-2} \text{day}^{-1}$ across watershed for the month of October. Normally higher latitudes receive less solar radiation. Hence, the values at 36°N are higher than those at 37°N as shown in the following figure 5.23. The low values of solar radiation at the higher altitudes on Northern side may also be associated with the significant amount

of cloud cover often present at high mountains. Normally, under clear sky conditions the solar radiation increases with altitude.

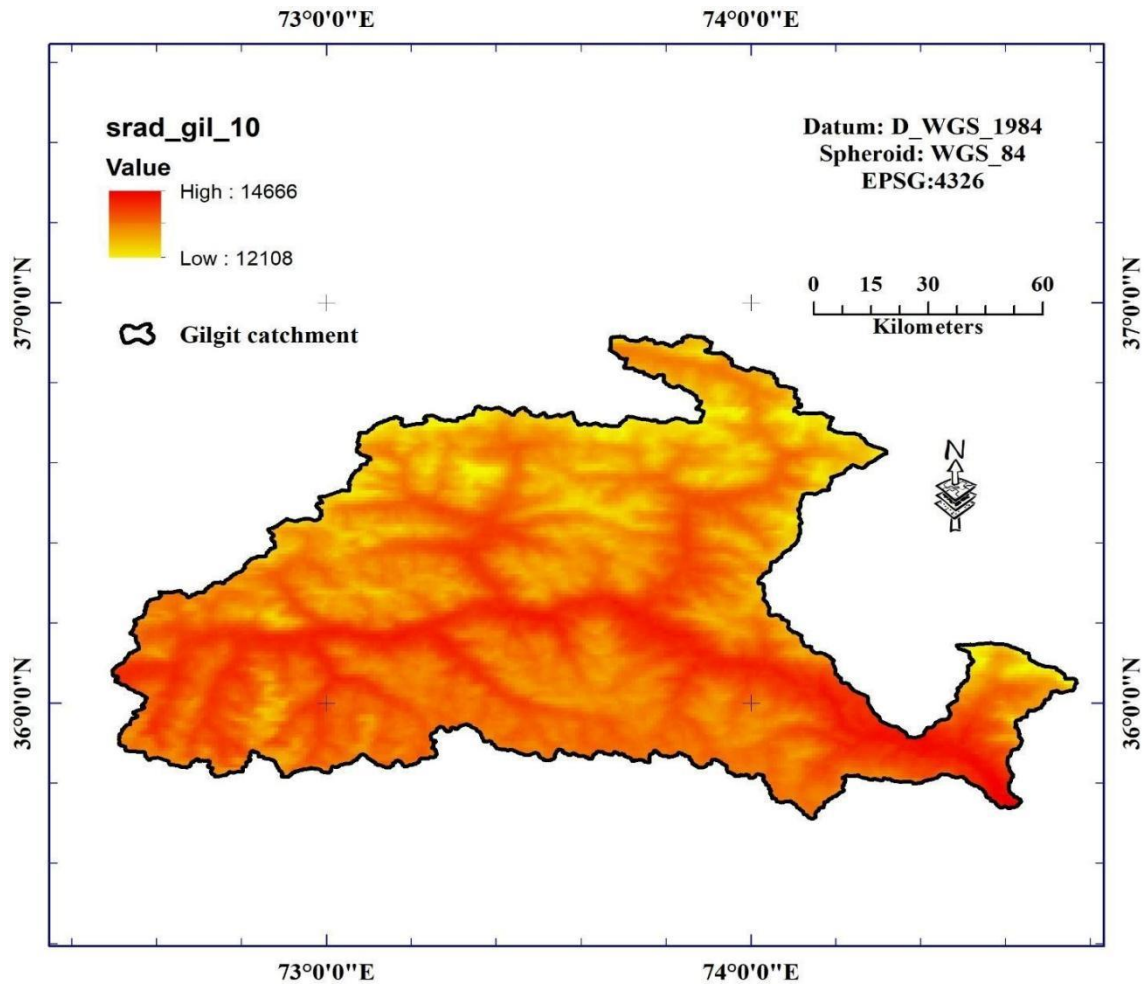


Figure 5.23 Spatial distribution of monthly averaged Solar radiation (in $\text{kJ m}^{-2} \text{day}^{-1}$) for the month of October for Gilgit catchment

The interpolated solar radiation data processed from the point data from local stations, monthly averaged of 30 years, portrays a high value of $10765 \text{ kJ m}^{-2} \text{day}^{-1}$ and a low value of $7994 \text{ kJ m}^{-2} \text{day}^{-1}$ across watershed for the month of November. Normally higher latitudes receive less solar radiation. Hence, the values at 36°N are higher than those at 37°N as shown in the following figure 5.24. The low values of solar radiation at the higher altitudes on Northern side may also be associated with the significant amount of cloud cover often present at high mountains. Normally, under

clear sky conditions the solar radiation increases with altitude.

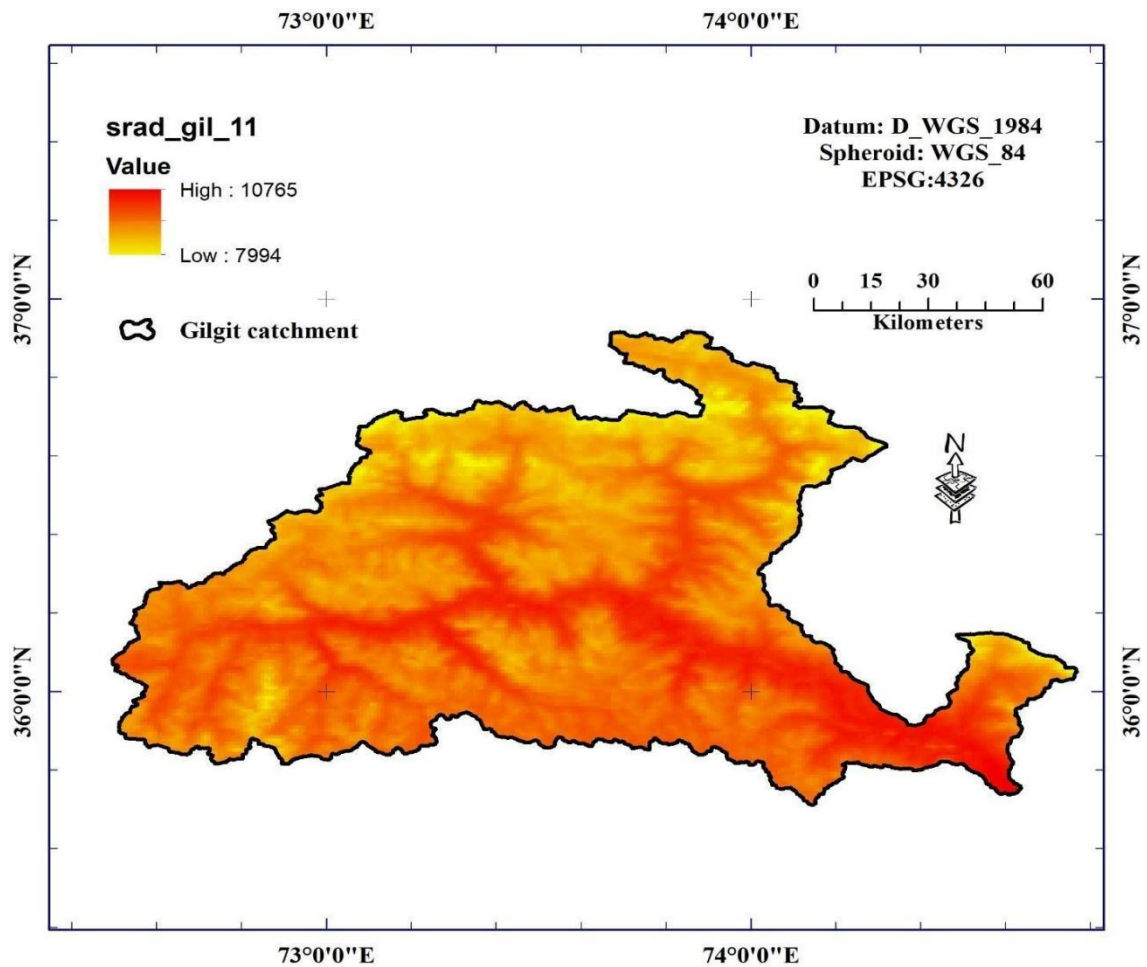


Figure 5.24 Spatial distribution of monthly averaged Solar radiation (in $\text{kJ m}^{-2} \text{day}^{-1}$) for the month of November for Gilgit catchment

The interpolated solar radiation data processed from the point data from local stations, monthly averaged of 30 years, portrays a high value of $7602 \text{ kJ m}^{-2} \text{day}^{-1}$ and a low value of $5436 \text{ kJ m}^{-2} \text{day}^{-1}$ across watershed for the month of December. Normally higher latitudes receive less solar radiation. Hence, the values at 36°N are higher than those at 37°N as shown in the following figure 5.25. The low values of solar radiation at the higher altitudes on Northern side may also be associated with the significant amount of cloud cover often present at high mountains. Normally, under clear sky conditions the solar radiation increases with altitude.

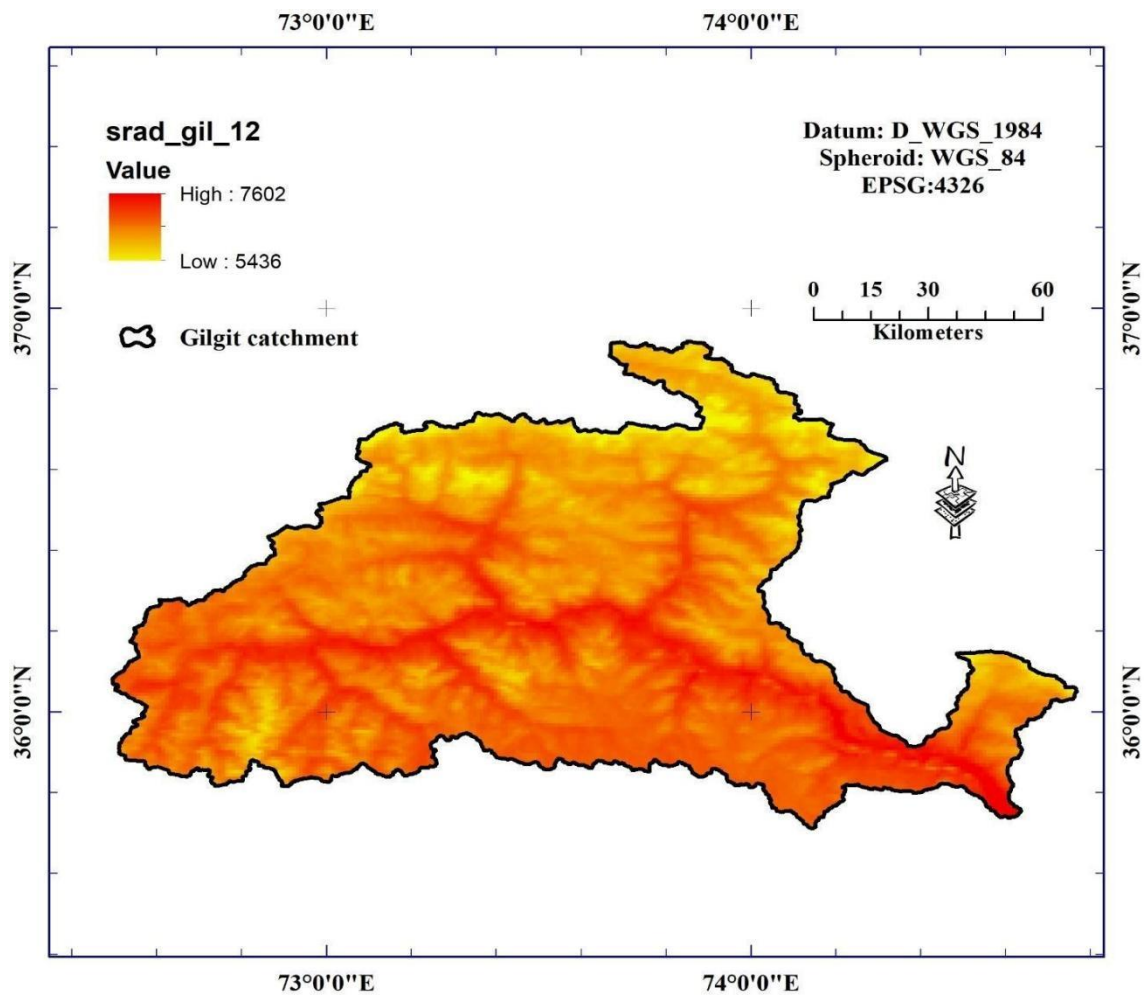


Figure 5.25 Spatial distribution of monthly averaged Solar radiation (in $\text{kJ m}^{-2} \text{day}^{-1}$) for the month of December for Gilgit catchment

Table 5.2 Yearly Low and High values for solar radiation (in kJ m⁻² day⁻¹) in Gilgit watershed

Sr.	Month	Srad (Low)	Srad (High)	Srad (Ave)
1	January	5641	7545	6593
2	February	8176	10093	9135
3	March	11721	14075	12898
4	April	16793	18065	17429
5	May	20422	21560	20991
6	June	21927	24790	23359
7	July	18612	22605	20609
8	August	17000	21226	19113
9	September	15446	18315	16881
10	October	12108	14666	13387
11	November	7994	10765	9380
12	December	5436	7602	6519

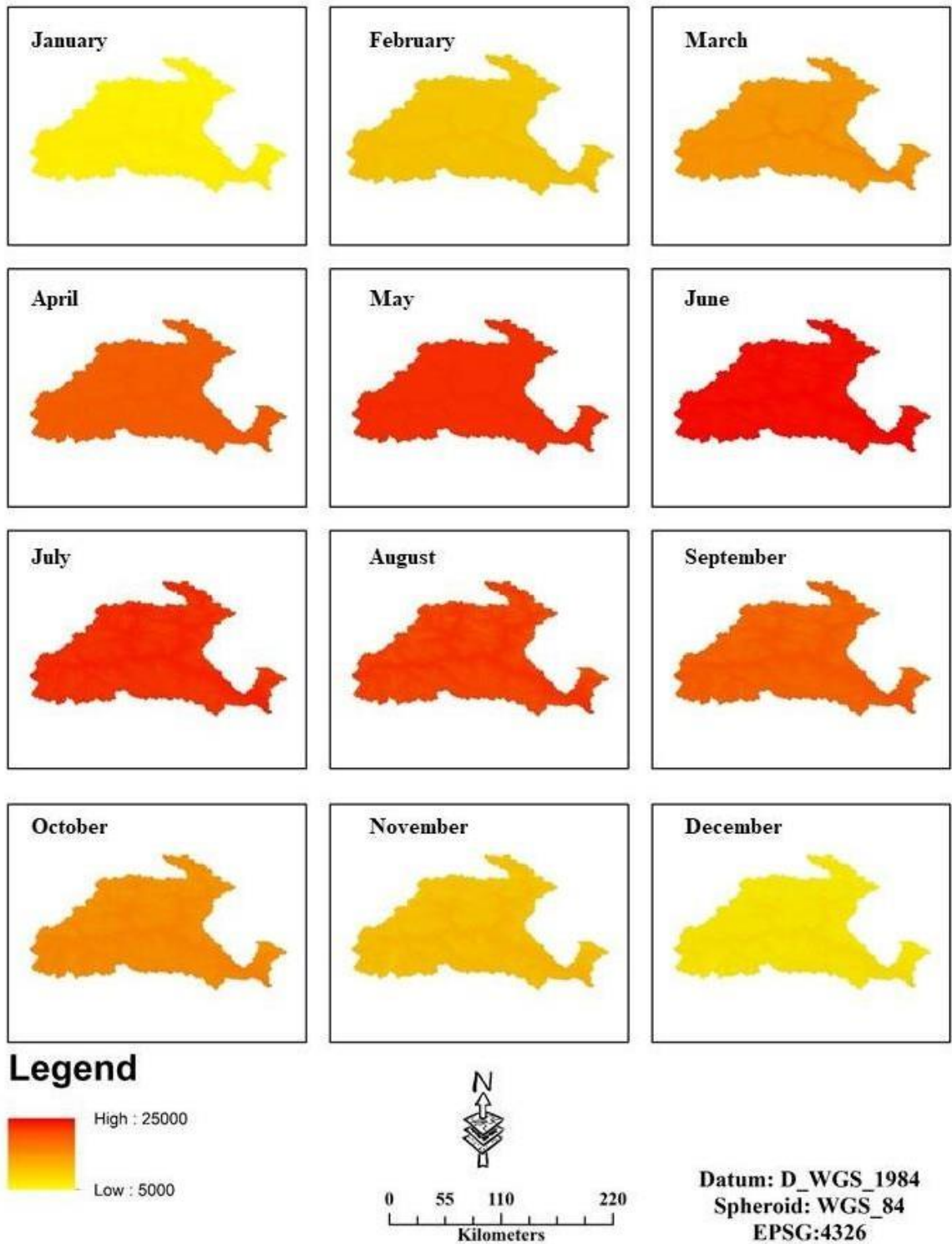


Figure 5.26 Spatial distribution of monthly averaged Solar radiation (in $\text{kJ m}^{-2} \text{day}^{-1}$) normalized matrix for yearly profile for Gilgit catchment

Following inference may be drawn from the analysis of solar radiation energy effect on Gilgit watershed:

- a. The solar radiation carries energy to the surface of the glacier.
- b. A part of the solar radiation is absorbed into the glacier ice and increases the temperature of the snow pack and hence becomes responsible for glacier shrinkage.
- c. The other part of the solar radiation is returned back in the air in the form of solar albedo which is higher for fresh snow.
- d. Solar radiation values provide better estimate of the energy budget of glaciers.
- e. In the months of May, June and July, the glaciers receive max energy in the form of solar radiation and hence accelerate melting / glacier retreat. Whereas solar radiation is at min in the winter months. During the winter months the glacier melting is further condensed by the presence of cloud cover and presence of fresh snow which is responsible for more reflectance on the high-altitude region in the higher area of the glaciers in particular and on overall extent of the glacier in general.

5.3 Precipitation in the Gilgit Watershed

There are four rainy seasons in the study area viz., wintertime, pre- monsoon, monsoon (rainy and cloud burst season) and post monsoon precipitation. The town of Gupis is known to have the lowest rainfall in the GB region (Javed et al., 2020). Javed et al., (2020) have analyzed the 90-years ground based point measurements from meteorological observatories operated by the Pak Meteorological Department.

However, the study lacks the interpolated analysis at the spatial extent. It is shown that Gupis station gets approx. 13 rainy days in the whole year excluding the solid precipitation in the form of snow at upper elevations.

The data of observation / measurement of precipitation are known to contain many inaccuracies owing to its spatial and temporal pattern in quantity and intensity. The interpolated precipitation data processed from the point data from local stations, monthly averaged of 30 years, portrays a high value of 57 mm and a low value of 4 mm across watershed for the month of January.

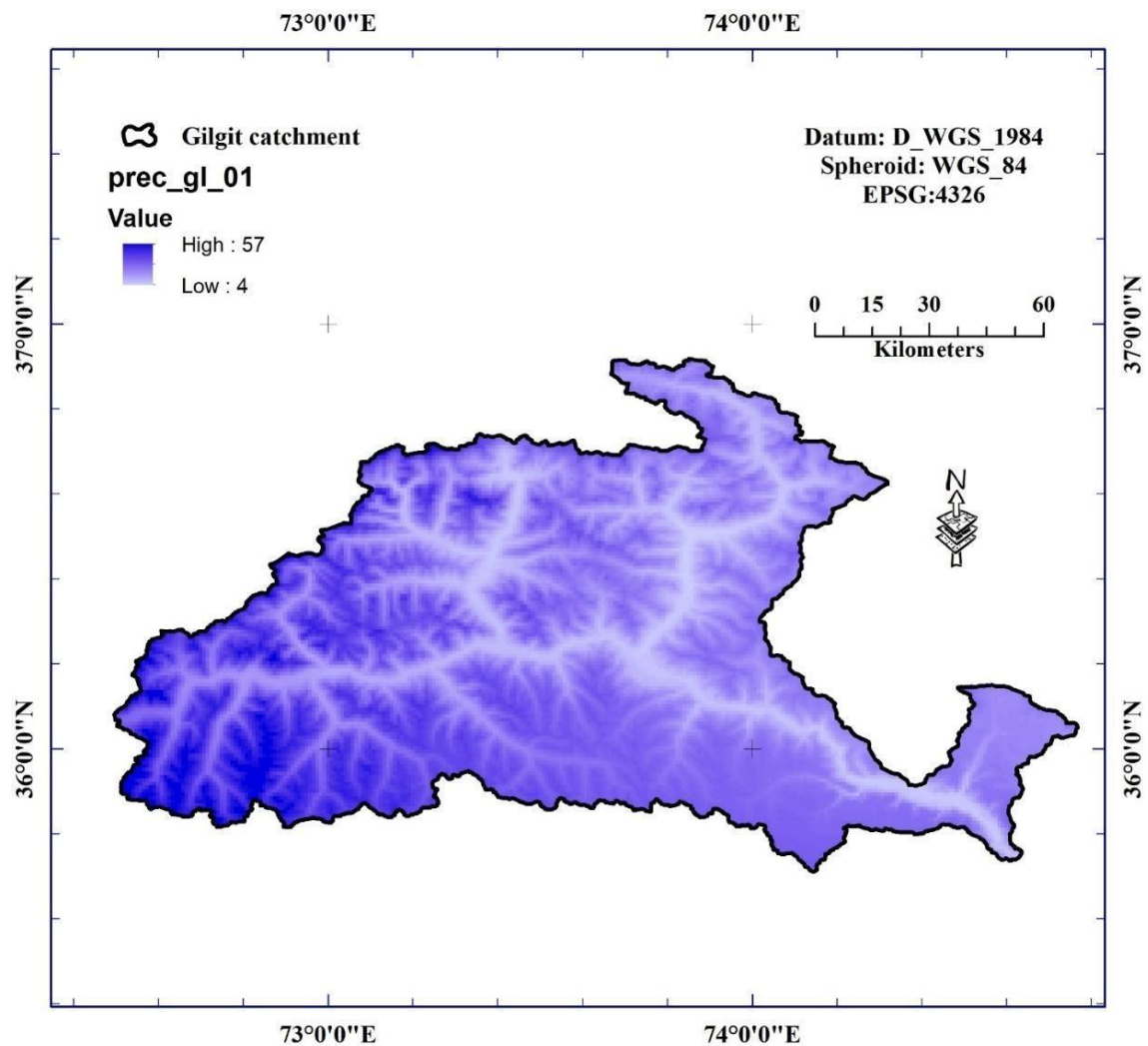


Figure 5.27 Spatial distribution of monthly precipitation (in mm) for the month of January for Gilgit catchment

The interpolated precipitation data processed from the point data from local stations, monthly averaged of 30 years, portrays a high value of 72 mm and a low value of 5 mm across watershed for the month of February.

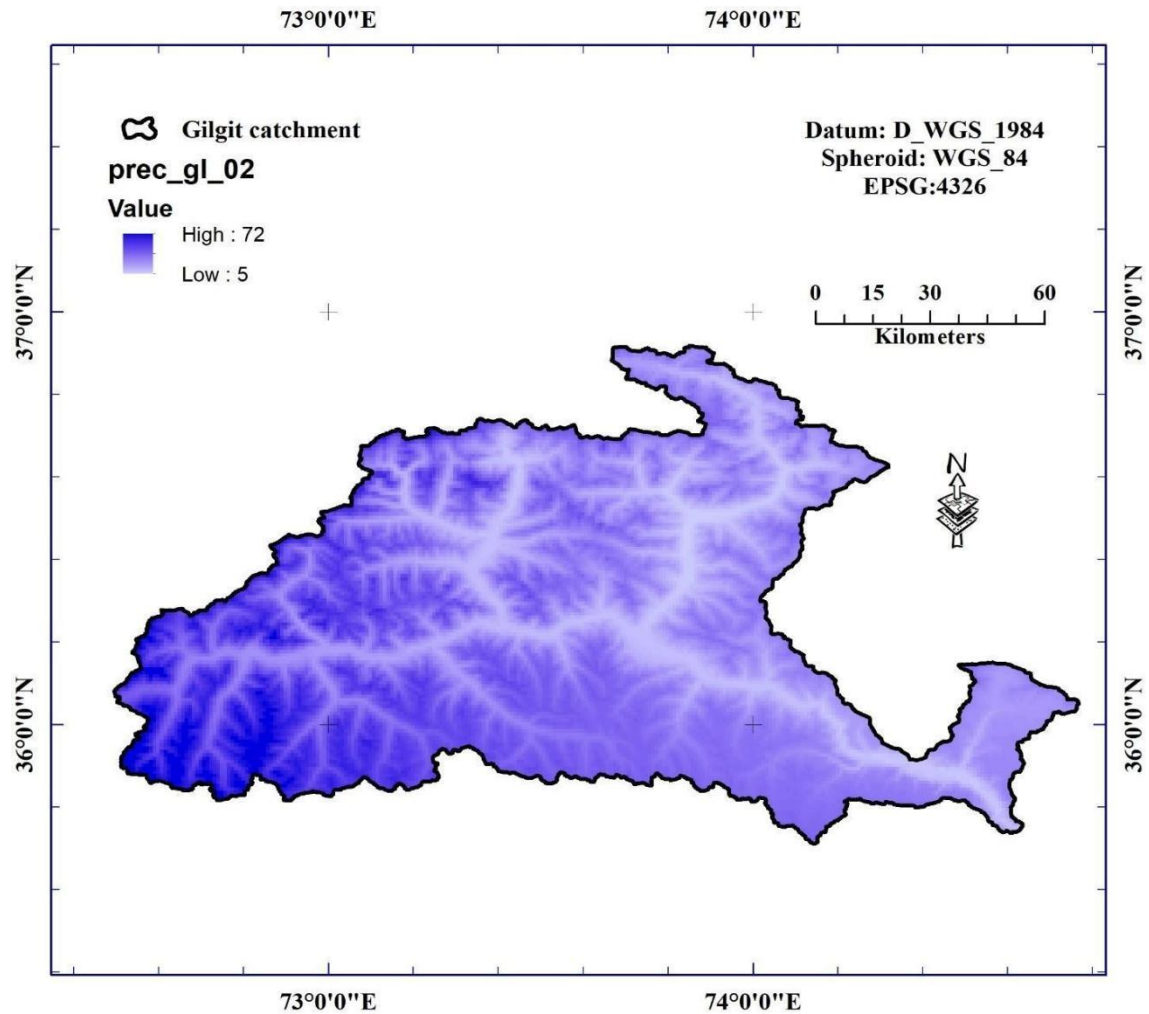


Figure 5.28 Spatial distribution of monthly precipitation (in mm) for the month of February for Gilgit catchment

The interpolated precipitation data processed from the point data from local stations, monthly averaged of 30 years, portrays a high value of 89 mm and a low value of 8 mm across watershed for the month of March.

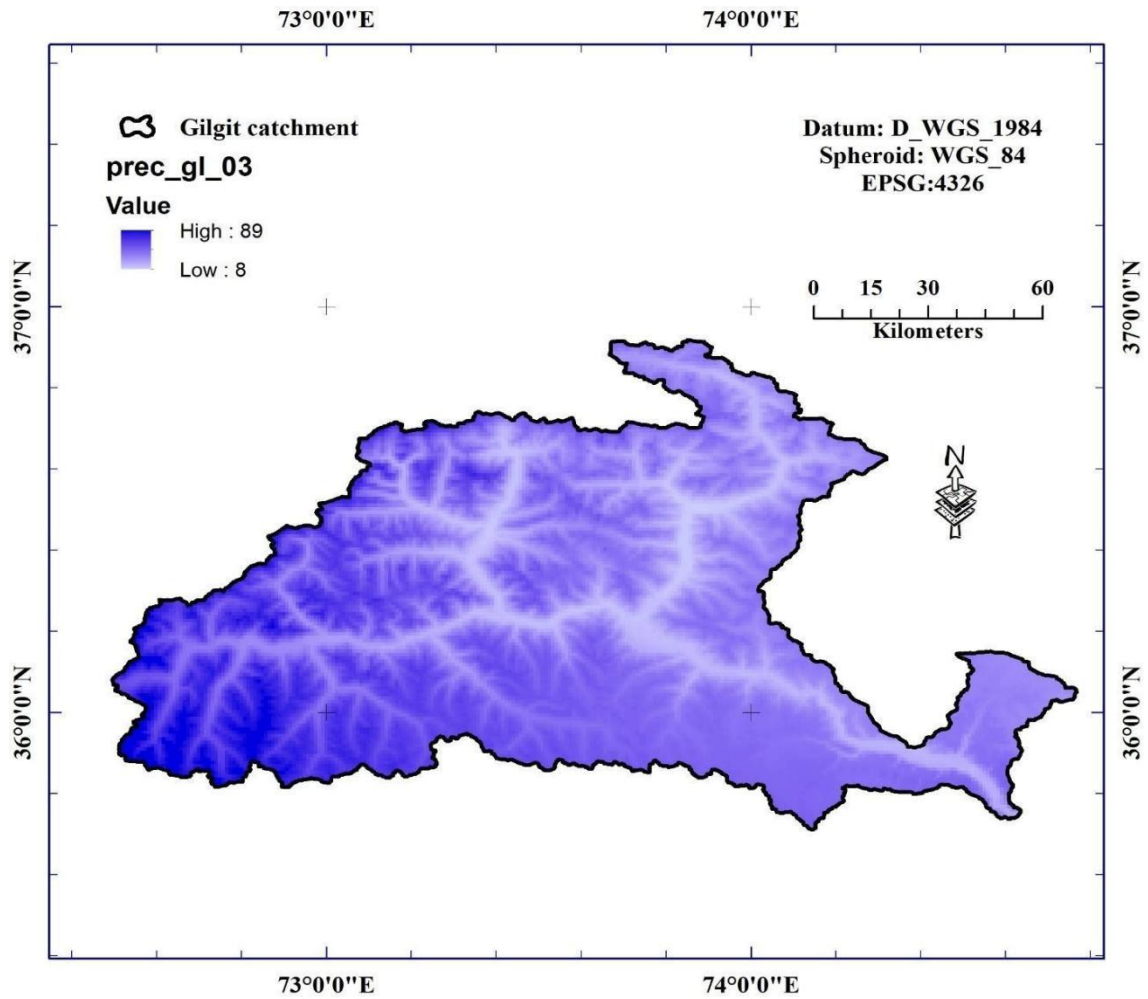


Figure 5.29 Spatial distribution of monthly precipitation (in mm) for the month of March for Gilgit catchment

The interpolated precipitation data processed from the point data from local stations, monthly averaged of 30 years, portrays a high value of 95 mm and a low value of 16 mm across watershed for the month of April.

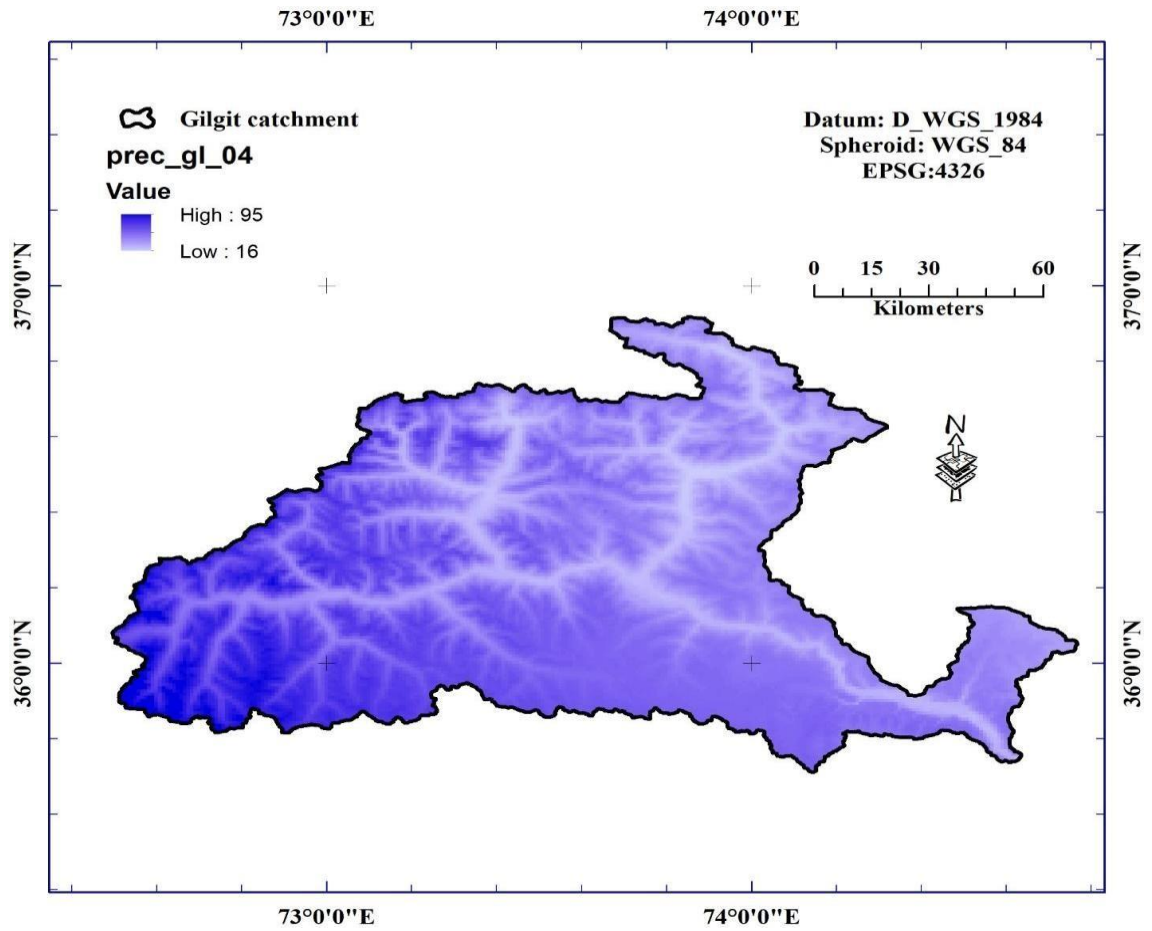


Figure 5.30 Spatial distribution of monthly precipitation (in mm) for the month of April for Gilgit catchment

The interpolated precipitation data processed from the point data from local stations, monthly averaged of 30 years, portrays a high value of 70 mm and a low value of 24 mm across watershed for the month of May.

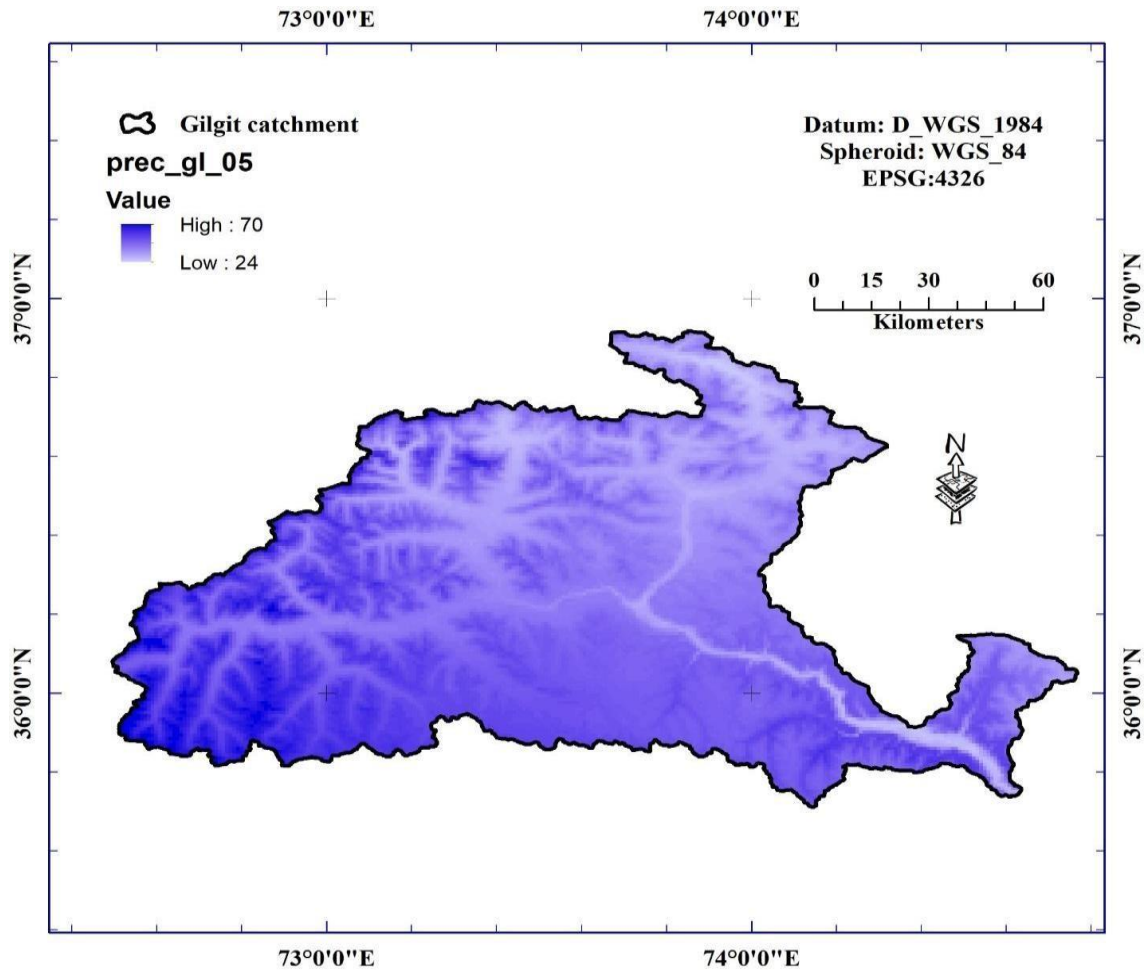


Figure 5.31 Spatial distribution of monthly precipitation (in mm) for the month of May for Gilgit catchment

The interpolated precipitation data processed from the point data from local stations, monthly averaged of 30 years, portrays a high value of 28 mm and a low value of 9 mm across watershed for the month of June.

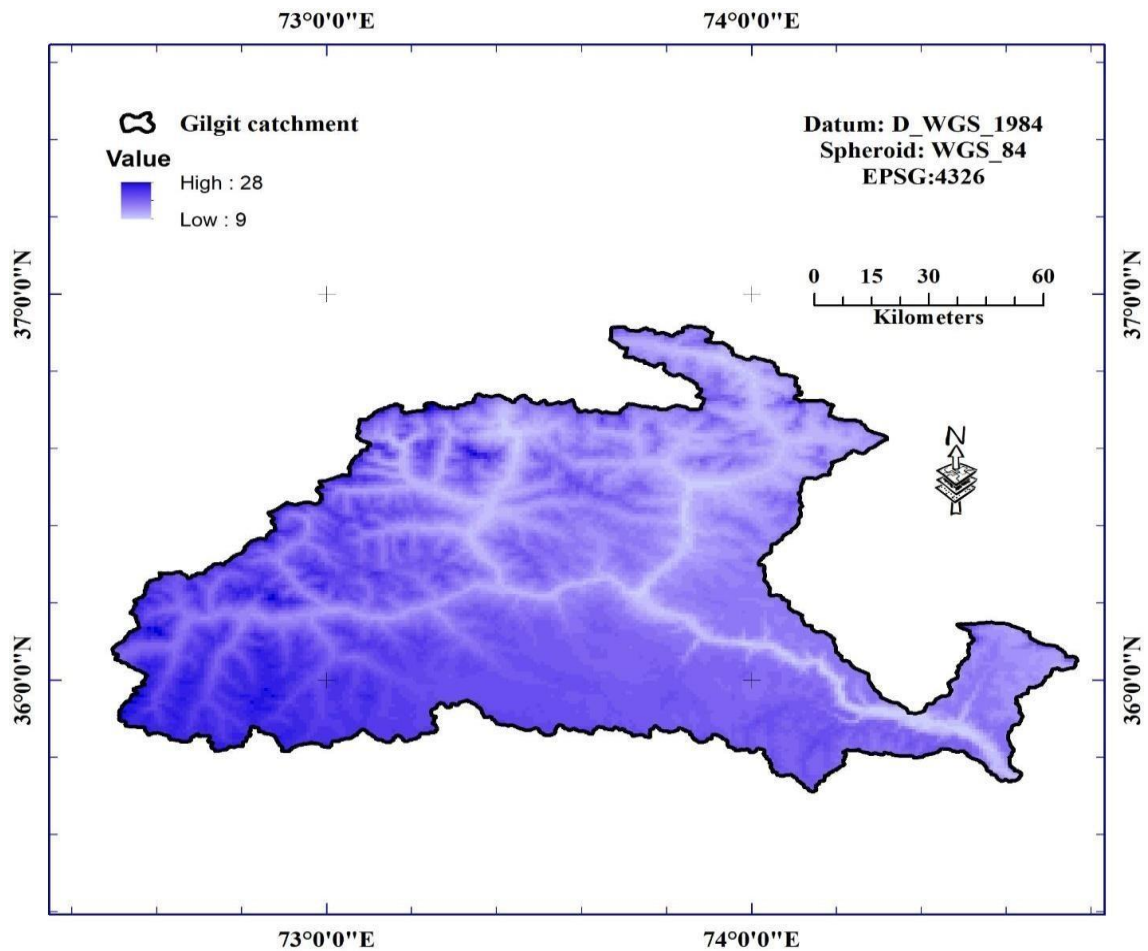


Figure 5.32 Spatial distribution of monthly precipitation (in mm) for the month of June for Gilgit catchment

The interpolated precipitation data processed from the point data from local stations, monthly averaged of 30 years, portrays a high value of 111 mm and low value of 9 mm across watershed for the month of July.

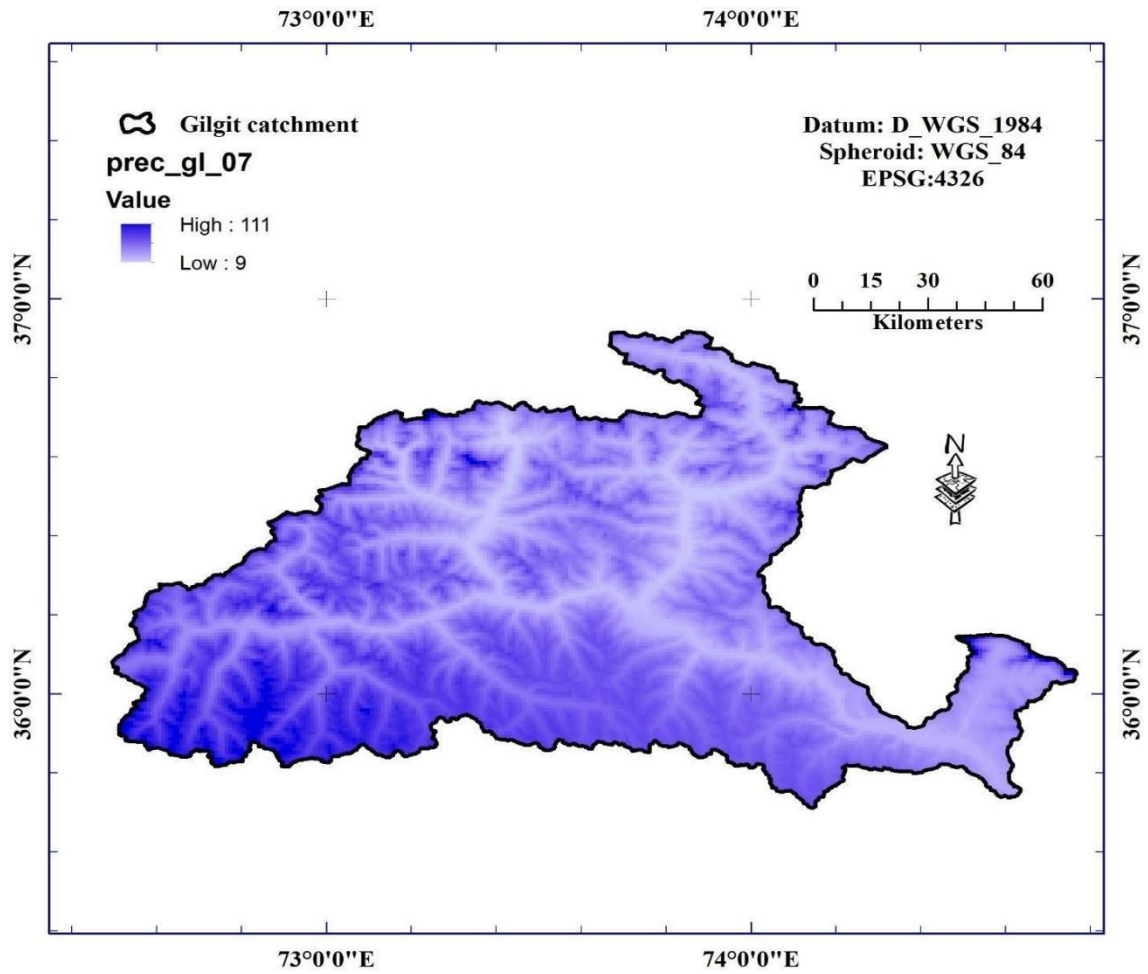


Figure 5.33 Spatial distribution of monthly precipitation (in mm) for the month of July for Gilgit catchment

The interpolated precipitation data processed from the point data from local stations, monthly averaged of 30 years, portrays a high value of 91 mm and a low value of 11 mm across watershed for the month of August.

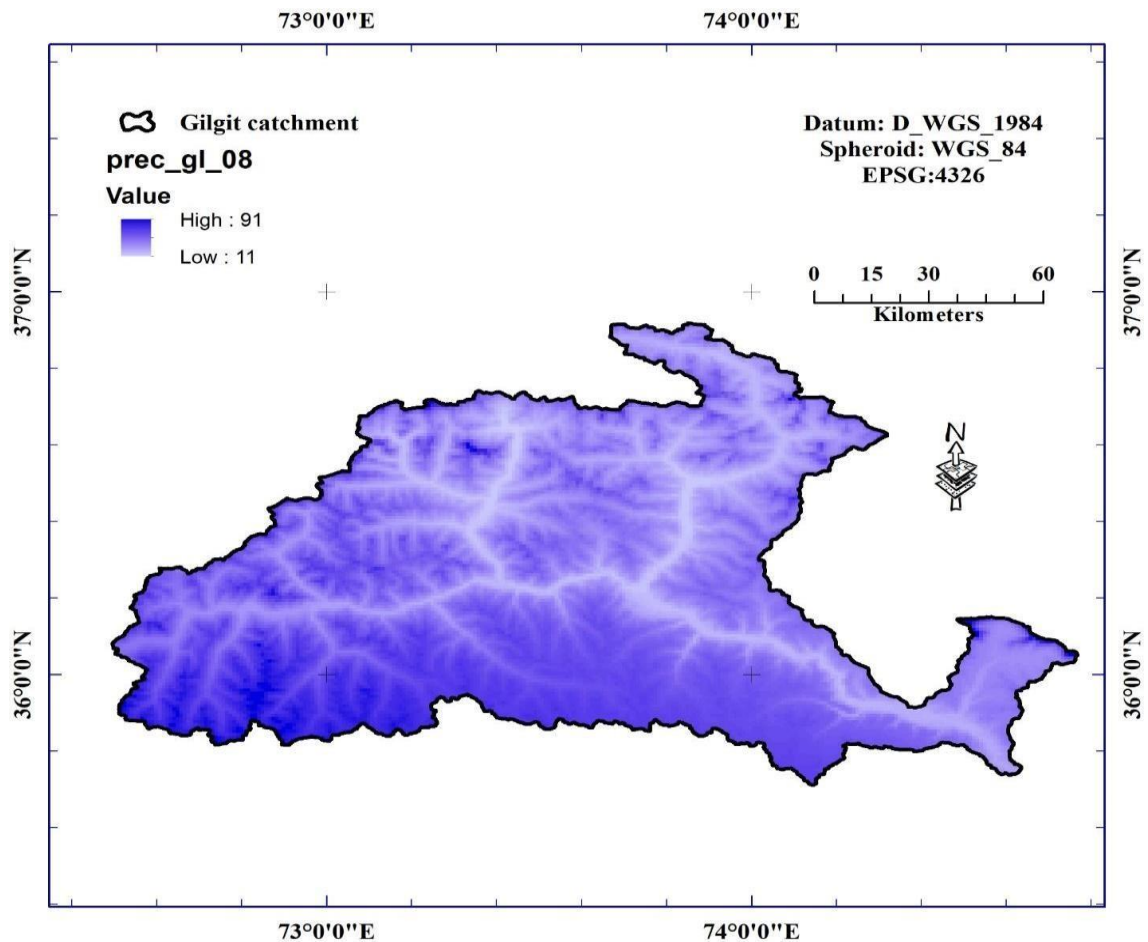


Figure 5.34 Spatial distribution of monthly precipitation (in mm) for the month of August for Gilgit catchment

The interpolated precipitation data processed from the point data from local stations, monthly averaged of 30 years, portrays a high value of 52 mm and a low value of 8 mm across watershed for the month of September.

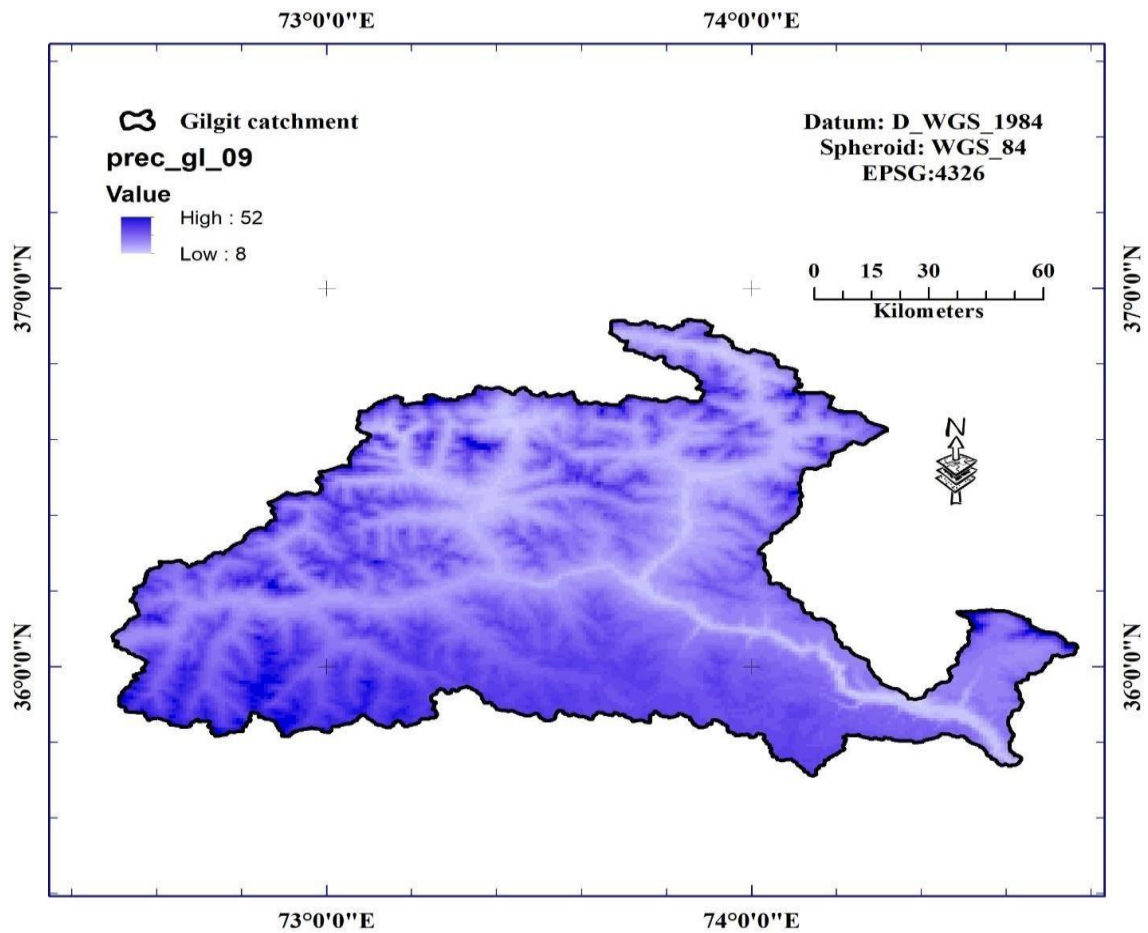


Figure 5.35 Spatial distribution of monthly precipitation (in mm) for the month of September for Gilgit catchment

The interpolated precipitation data processed from the point data from local stations, monthly averaged of 30 years, portrays a high value of 43 mm and a low value of 5 mm across watershed for the month of October.

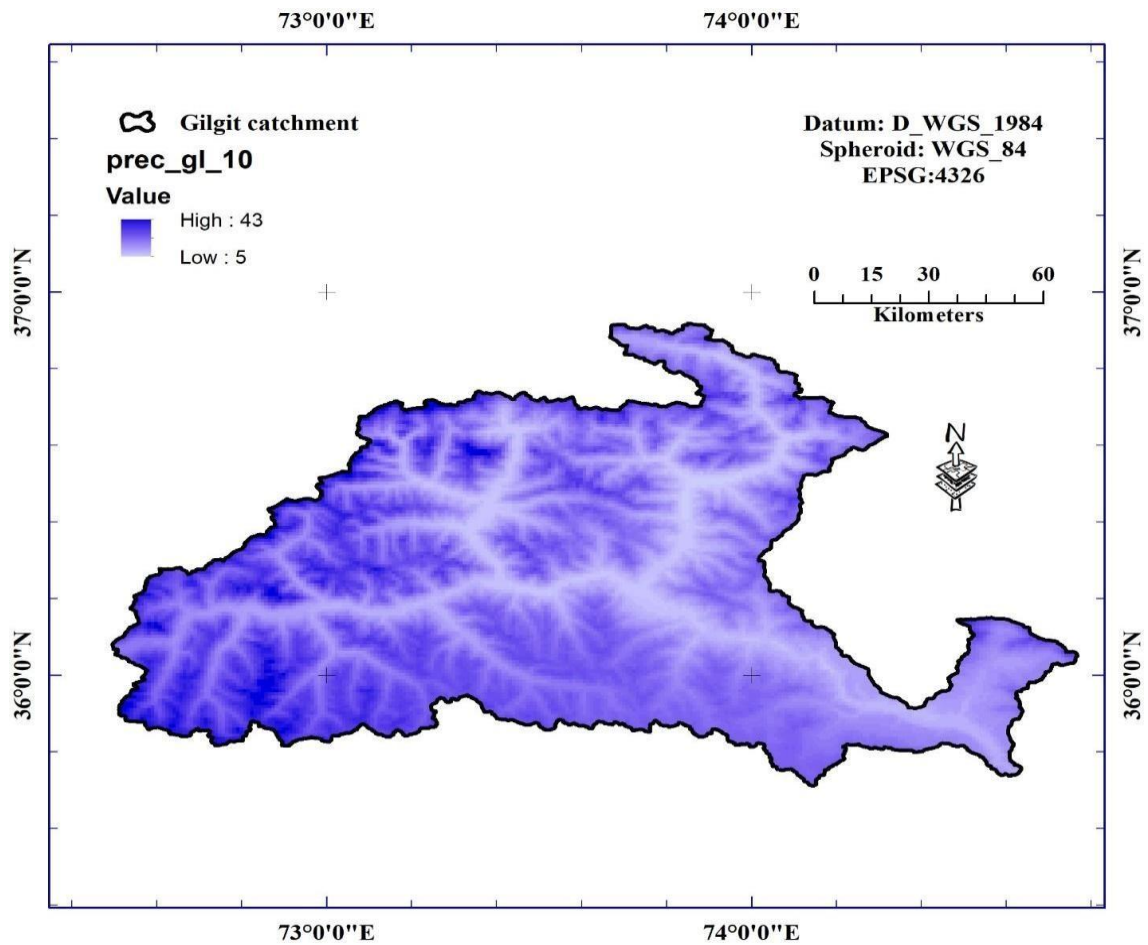


Figure 5.36 Spatial distribution of monthly precipitation (in mm) for the month of October for Gilgit catchment

The interpolated precipitation data processed from the point data from local stations, monthly averaged of 30 years, portrays a high value of 29 mm and a low value of 1 mm across watershed for the month of November.

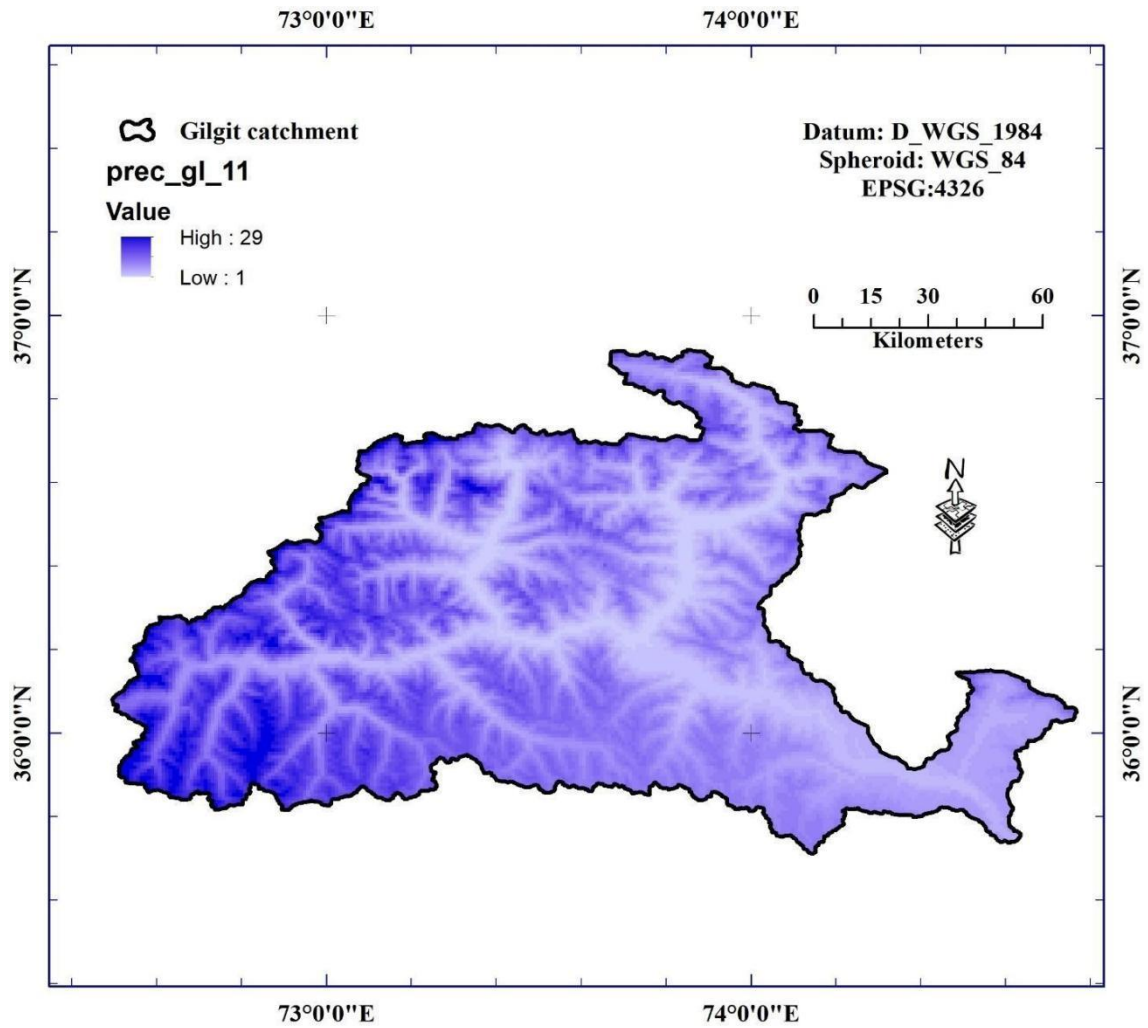


Figure 5.37 Spatial distribution of monthly precipitation (in mm) for the month of November for Gilgit catchment

The interpolated precipitation data processed from the point data from local stations, monthly averaged of 30 years, portrays a high value of 58 mm and a low value of 2 mm across watershed for the month of December.

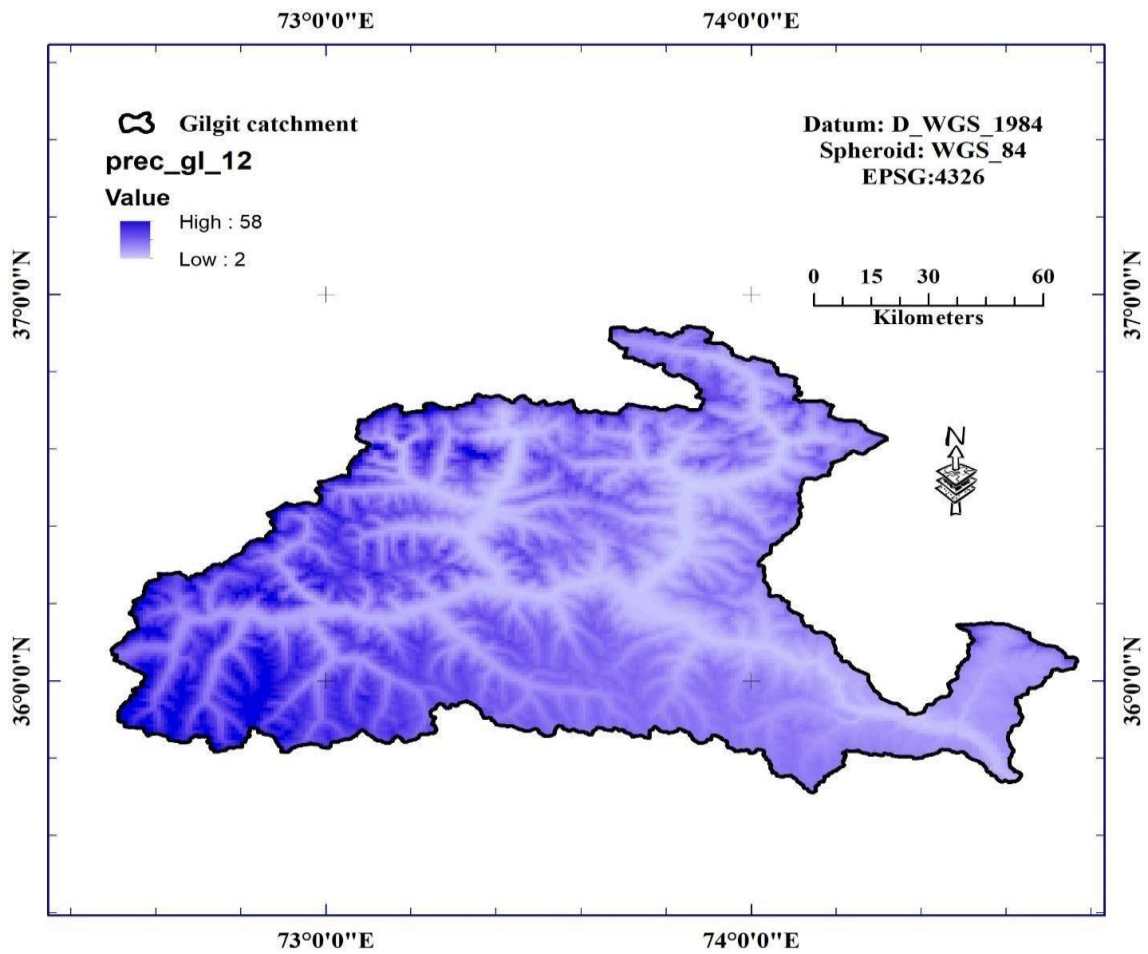


Figure 5.38 Spatial distribution of monthly precipitation (in mm) for the month of December for Gilgit catchment

Table 5.3 Yearly precipitation profile (in mm) of Gilgit Watershed

Sr.	Month	Precip (Low)	Precip (High)	Precip (Ave)
1	January	4	57	31
2	February	5	72	39
3	March	8	89	49
4	April	16	95	56
5	May	24	70	47
6	June	9	28	19
7	July	9	111	60
8	August	11	91	51
9	September	8	52	30
10	October	5	43	24
11	November	1	29	15
12	December	2	58	30

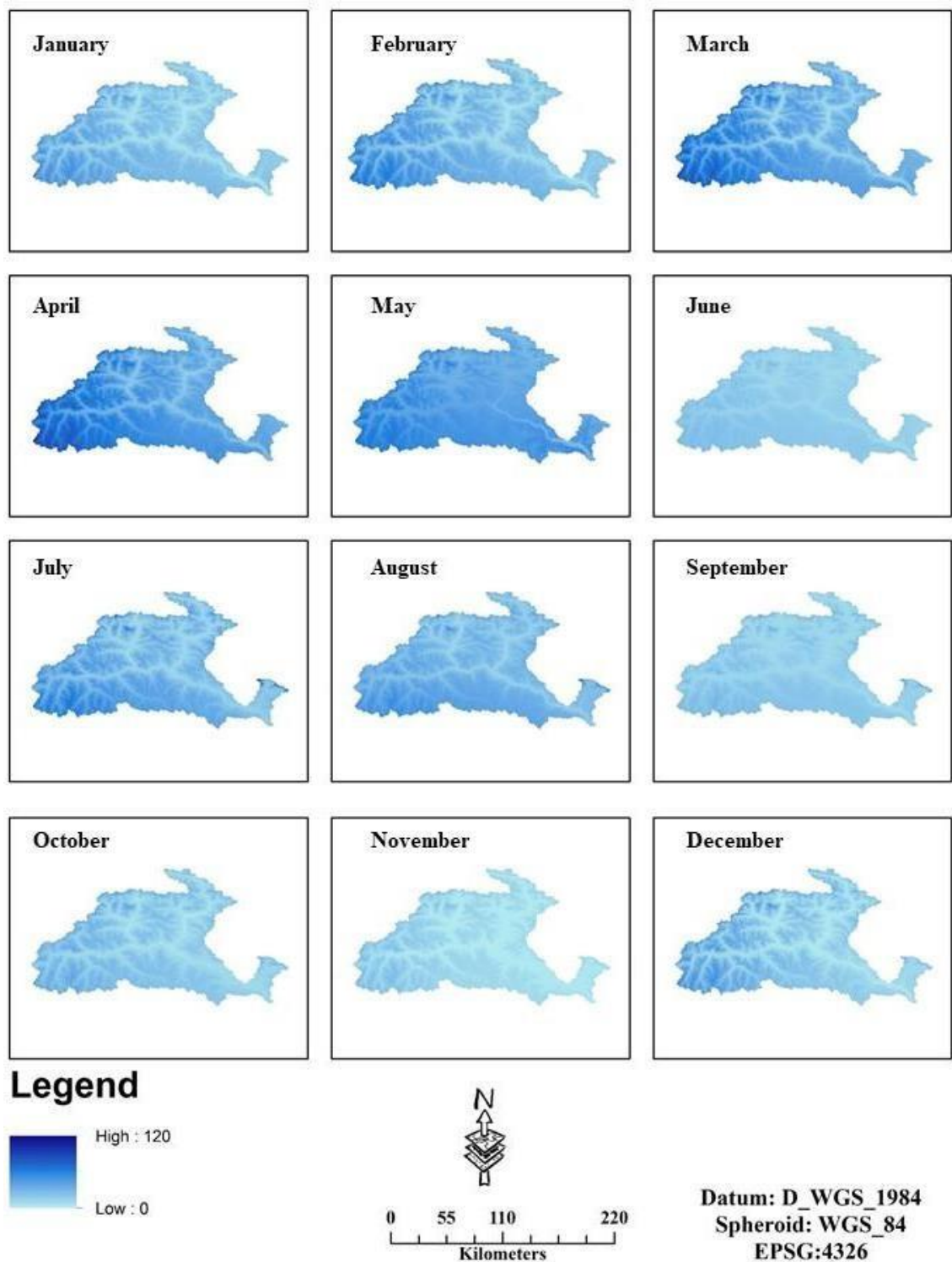


Figure 5.39 Spatial distribution of monthly precipitation (in mm) normalized matrix of yearly profile for Gilgit catchment

5.4 Temperature (Maximum) Profile of Gilgit Watershed

The highest temperature of the day is called as maximum temperature. The global grids of monthly averaged 30-years data were obtained and the subset of the study area was extracted to obtain the regional temperature values. The interpolated maximum surface temperature processed from the point data from local stations, monthly average of 30 years portrays a high value of 10.7 degree Celsius and a low value of -24.7 degree Celsius for the month of January.

The low values of temperature are mainly observed at higher altitudes on Northern side and high values of temperature on the lower altitudes on southeast of Gilgit watershed, respectively. The scale range is 60 km as shown in Figure 5.40. Moreover, January being the severe winter month has a more projecting T_{\min} (low) as compare to T_{\max} (high). January is the frosty winter coldest month in Gilgit.

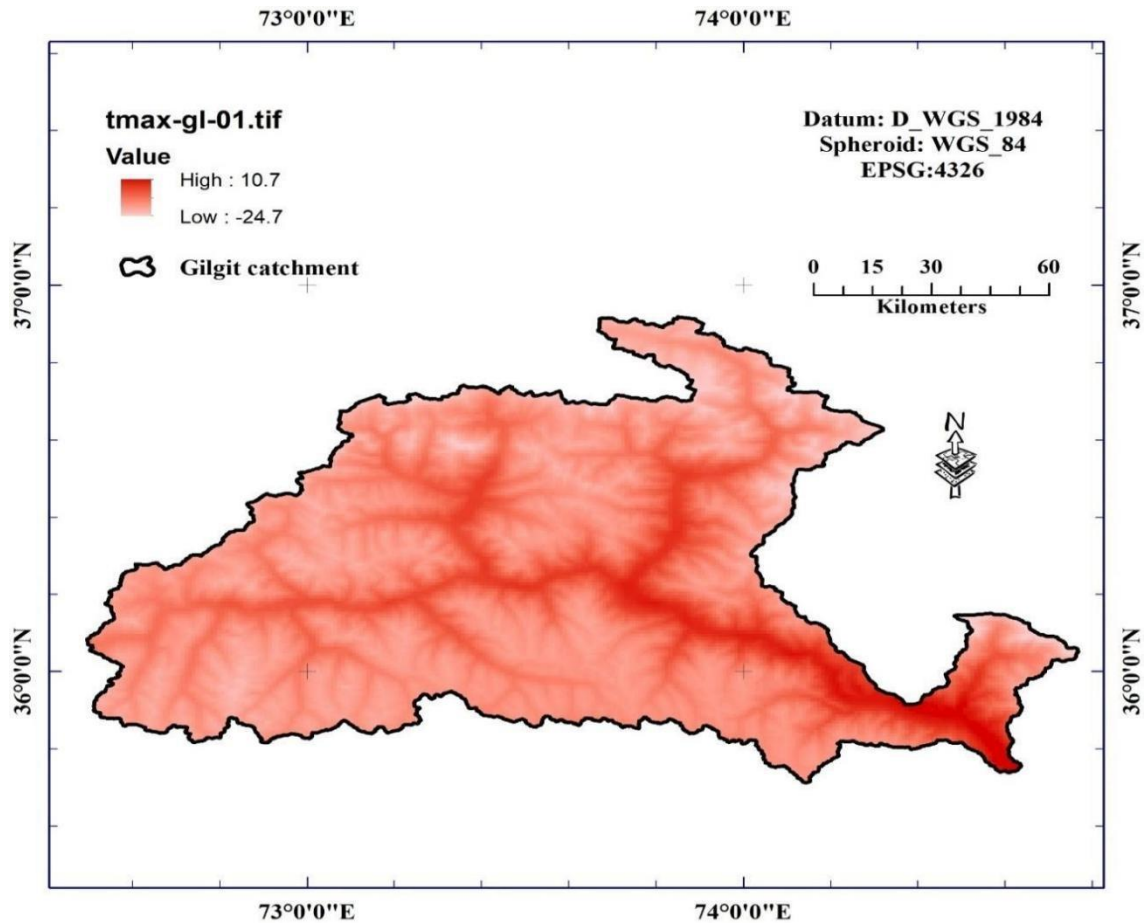


Figure 5.40 Spatial distribution of monthly averaged Maximum Temperature (in degrees Celsius) for the month of January for Gilgit catchment

The interpolated maximum surface temperature processed from the point data from local stations, monthly average of 30 years portrays a high value of 13.4 degree Celsius and a low value of -24.6 degree Celsius for the month of February. The low values of temperature are mainly observed at higher altitudes on Northern side and high values of temperature on the lower altitudes on southeast of Gilgit watershed, respectively. Moreover, February being the winter month has a more projecting T_{\min} (low) as compare to T_{\max} (high). The last month of the winter, February, is a unruffled month in Gilgit. The average high-temperature slightly increases from a frosty January to a cool February.

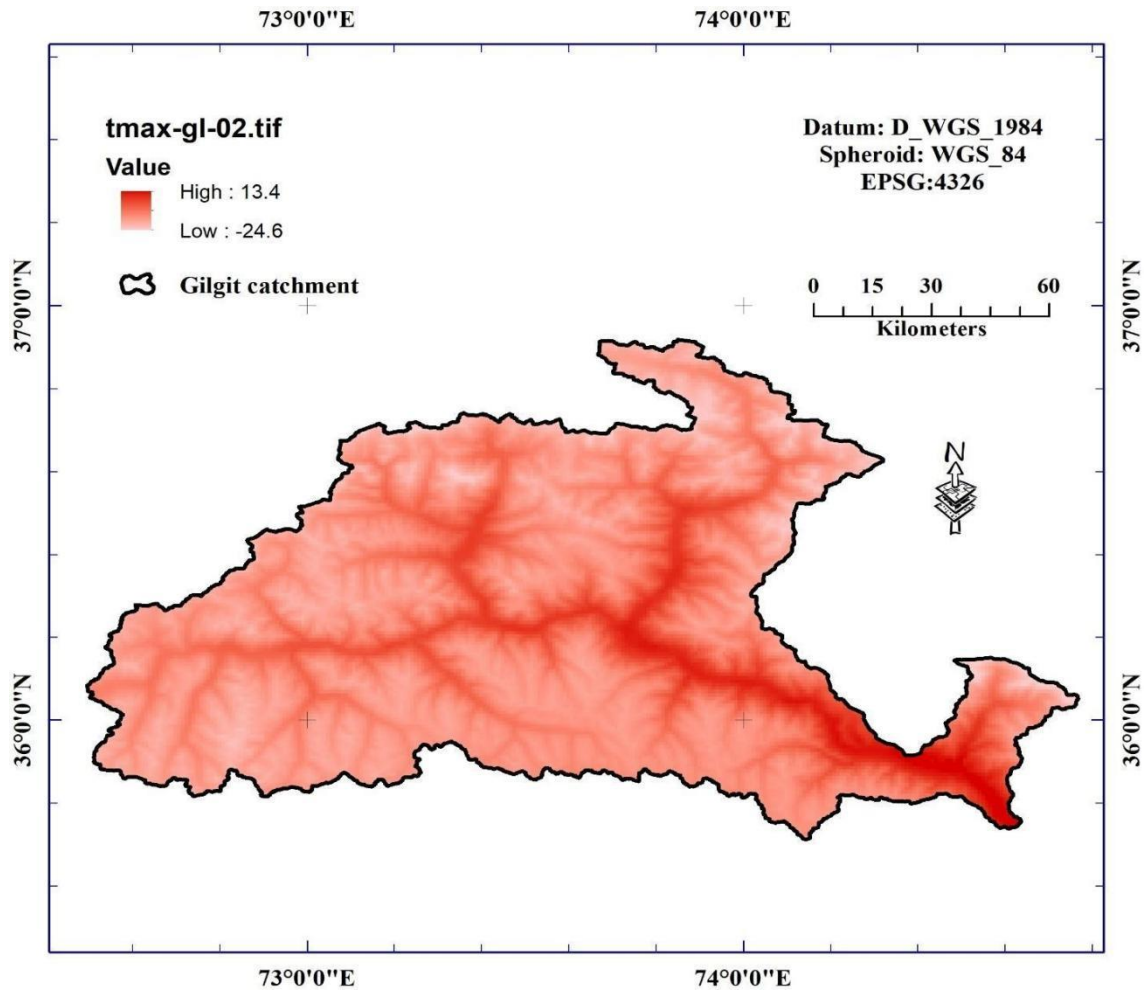


Figure 5.41 Spatial distribution of monthly averaged Maximum Temperature (in degrees Celsius) for the month of February for Gilgit catchment

The interpolated maximum surface temperature processed from the point data from local stations, monthly average of 30 years portrays a high value of 19 degrees Celsius and a low value of -21.8 degree Celsius for the month of March. The low values of temperature are mainly observed at higher altitudes on Northern side and high values of temperature on the lower altitudes on southeast of Gilgit watershed, respectively. The first month of the spring, March, is a relaxed month in Gilgit with average temperature ranging between -1.4 degree Celsius and max 19 degree Celsius. In Gilgit, the average high-temperature rises, from a fresh 13.4 degree Celsius in February, to an enjoyable 19.0 degree Celsius in March

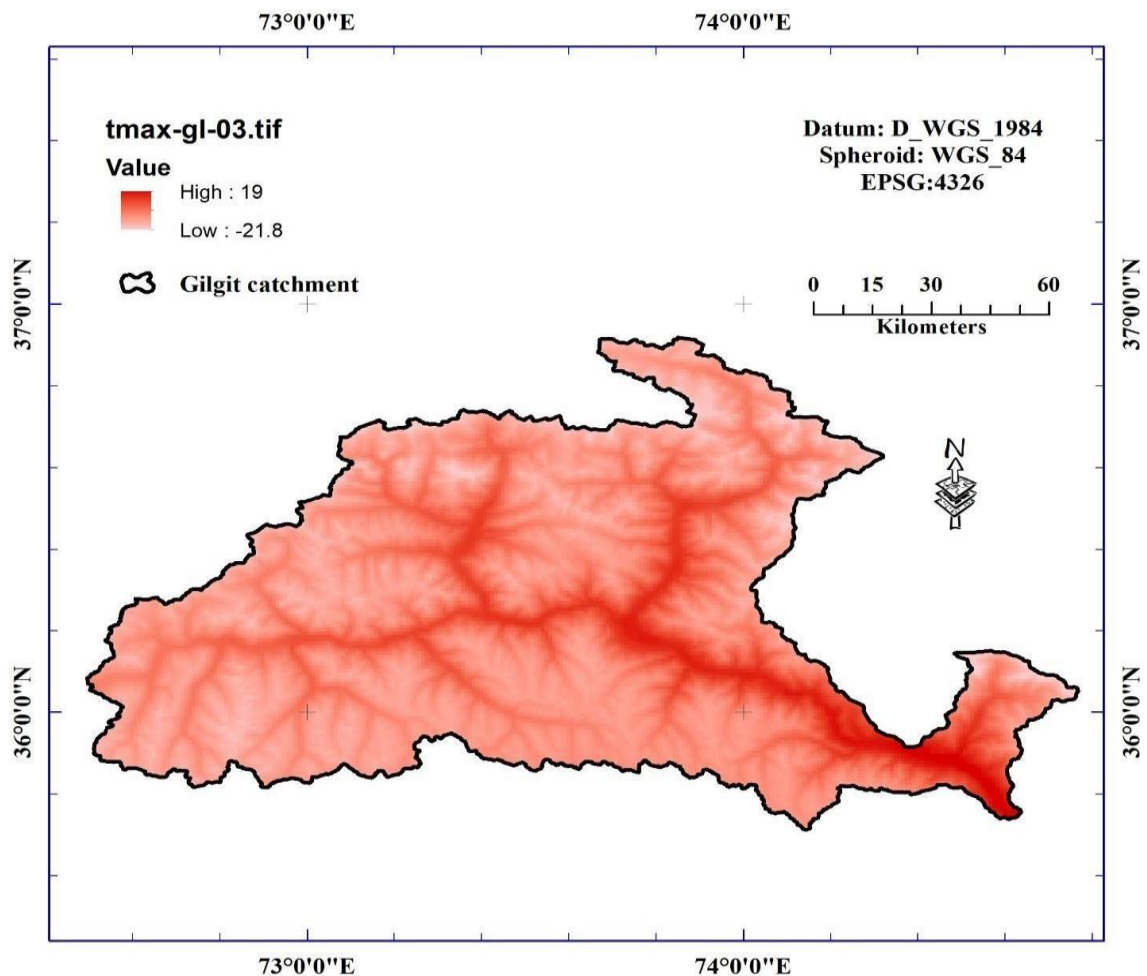


Figure 5.42 Spatial distribution of monthly averaged Maximum Temperature (in degrees Celsius) for the month of March for Gilgit

The interpolated maximum surface temperature processed from the point data from local stations, monthly averaged of 30 years portrays a high value of 25 degrees Celsius and a low value of -18.2 degree Celsius for the month of April. The low values of temperature are mainly observed at higher altitudes on Northern side and high values of temperature on the lower altitudes on southeast of Gilgit watershed, respectively. April is a warm spring month in Gilgit with average valley temperature changing between 9.2°C and 25.0 degree Celsius. In April, the average high-temperature rises, from a relaxed 19 degree Celsius in March, to a warm 25 degree Celsius.

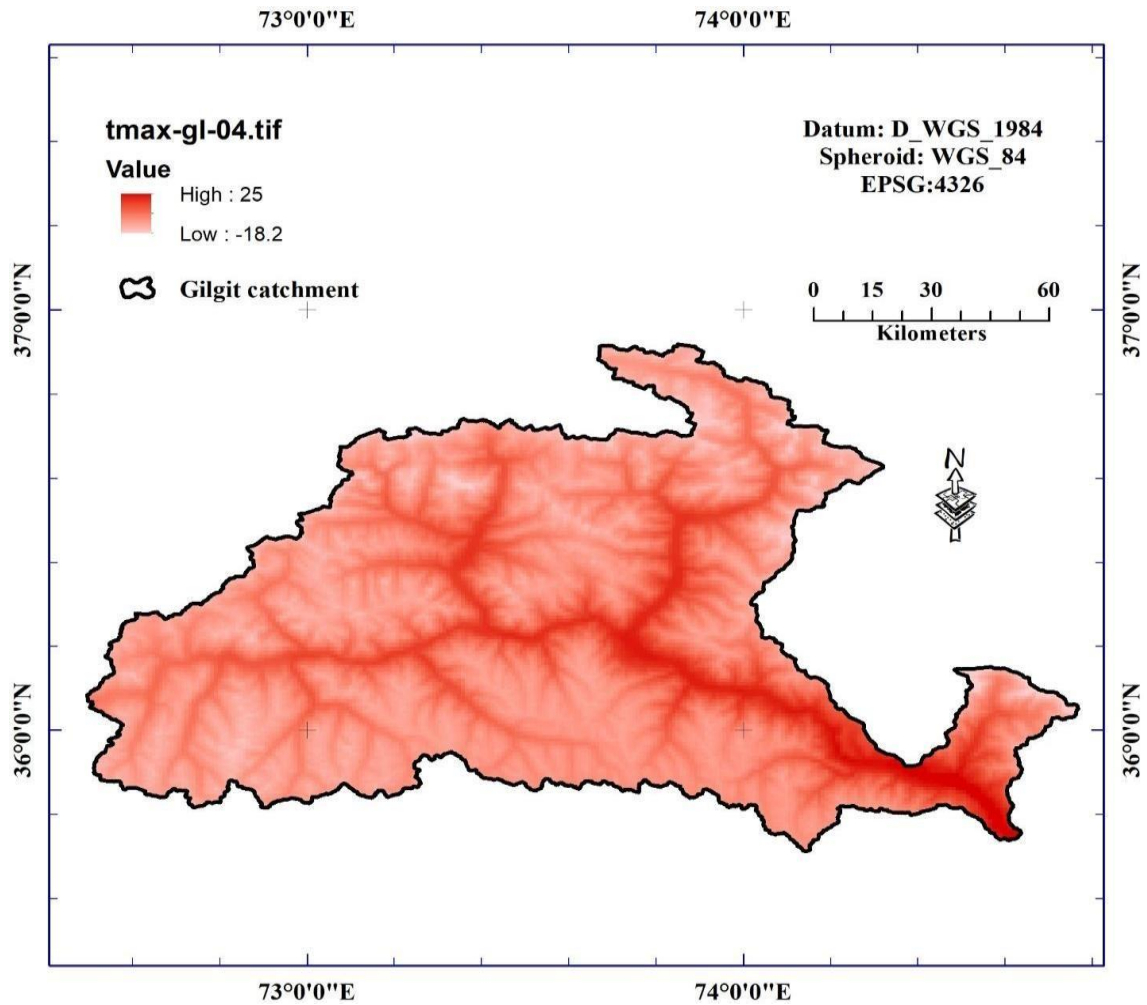


Figure 5.43 Spatial distribution of monthly averaged Maximum Temperature (in degrees Celsius) for the month of April for Gilgit catchment

The interpolated maximum surface temperature processed from the point data from local stations, monthly averaged of 30 years portrays a high value of 30.2 degrees Celsius and a low value of -13.4 degree Celsius across watershed for the month of May. The low values of temperature are mainly observed at higher altitudes on Northern side and high values of temperature on the lower altitudes on southeast of Gilgit watershed, respectively. May, the last month of the spring, in Gilgit is another warm month with average valley temperature fluctuating between 8 degree Celsius and 30 degree Celsius. In Gilgit, the average high-temperature marginally rises from a reasonably hot in April to a much warm in May.

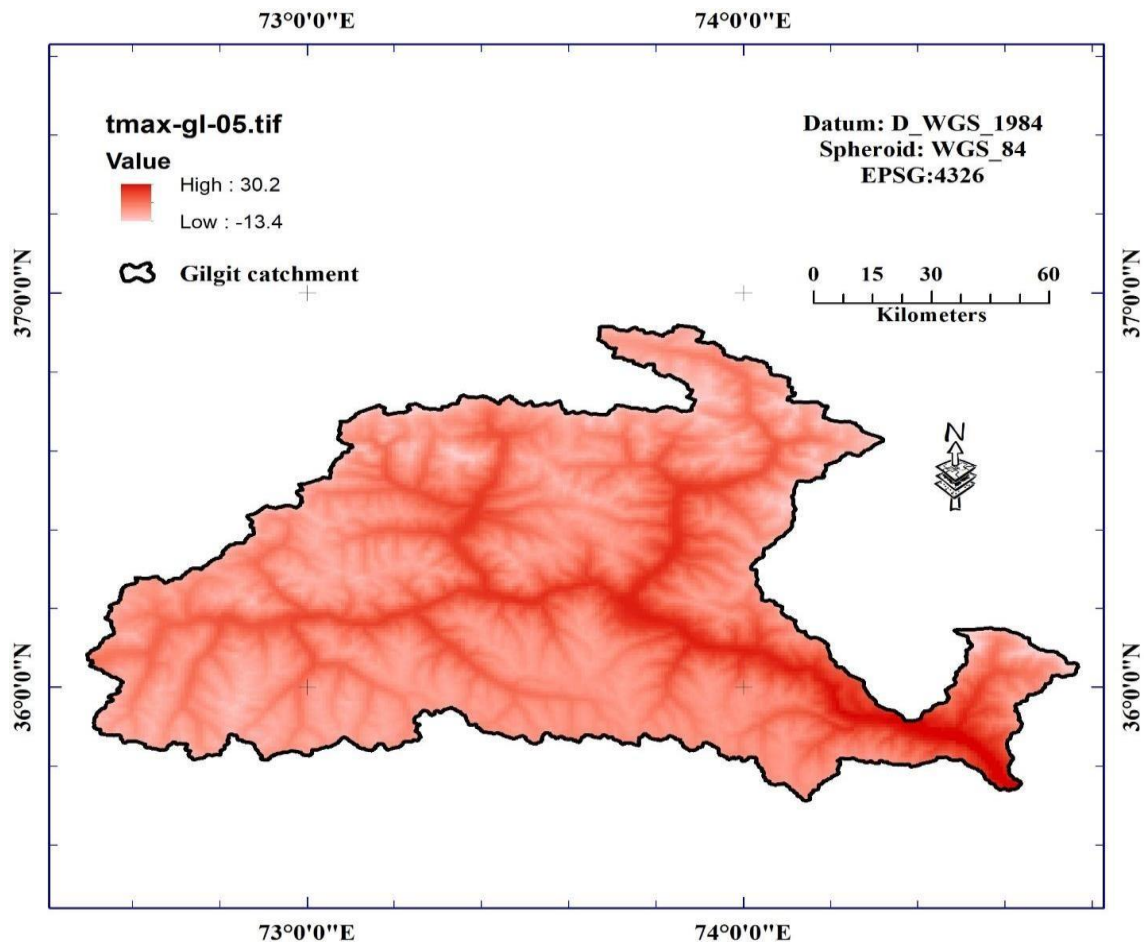


Figure 5.44 Spatial distribution of monthly averaged Maximum Temperature (in degrees Celsius) for the month of May for Gilgit catchment

The interpolated maximum surface temperature processed from the point data from local stations, monthly averaged of 30 years portrays a high value of 35.3 degrees Celsius and a low value of -8.8 degree Celsius across watershed for the month of June. The low values of temperature are mainly observed at higher altitudes on Northern side and high values of temperature on the lower altitudes on southeast of Gilgit watershed, respectively. June, the first month of the summer, in Gilgit, is a hot month, with average valley temperature fluctuating between 14 degree Celsius and max 35 degree Celsius. In June, the average high-temperature rises, from warming May.

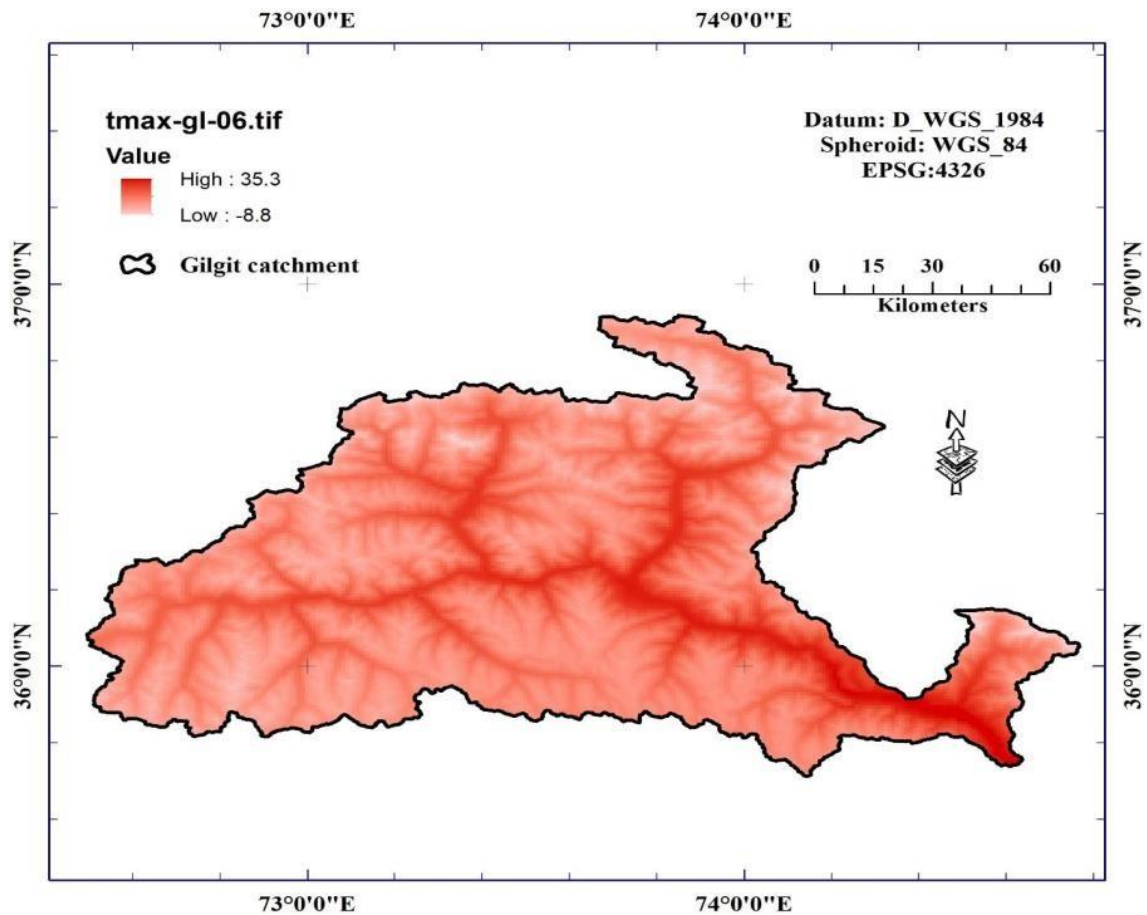


Figure 5.45 Spatial distribution of monthly averaged Maximum Temperature (in degrees Celsius) for the month of June for Gilgit catchment

The interpolated maximum surface temperature processed from the point data from local stations, monthly averaged of 30 years portrays a high value of 37.2 degrees Celsius and a low value of -3.9 degree Celsius across watershed for the month of July. The low values of temperature are mainly observed at higher altitudes on Northern side and high values of temperature on the lower altitudes on southeast of Gilgit watershed, respectively. July is a sweltering summer month in Gilgit with average valley temperature varying between 16.6 degree Celsius and 37.2 degree Celsius. The hottest month is July, with an average high-temperature of 37.2 degree Celsius and an average low-temperature of 20.5°C . In July, the average relative humidity remains approx. 30%.

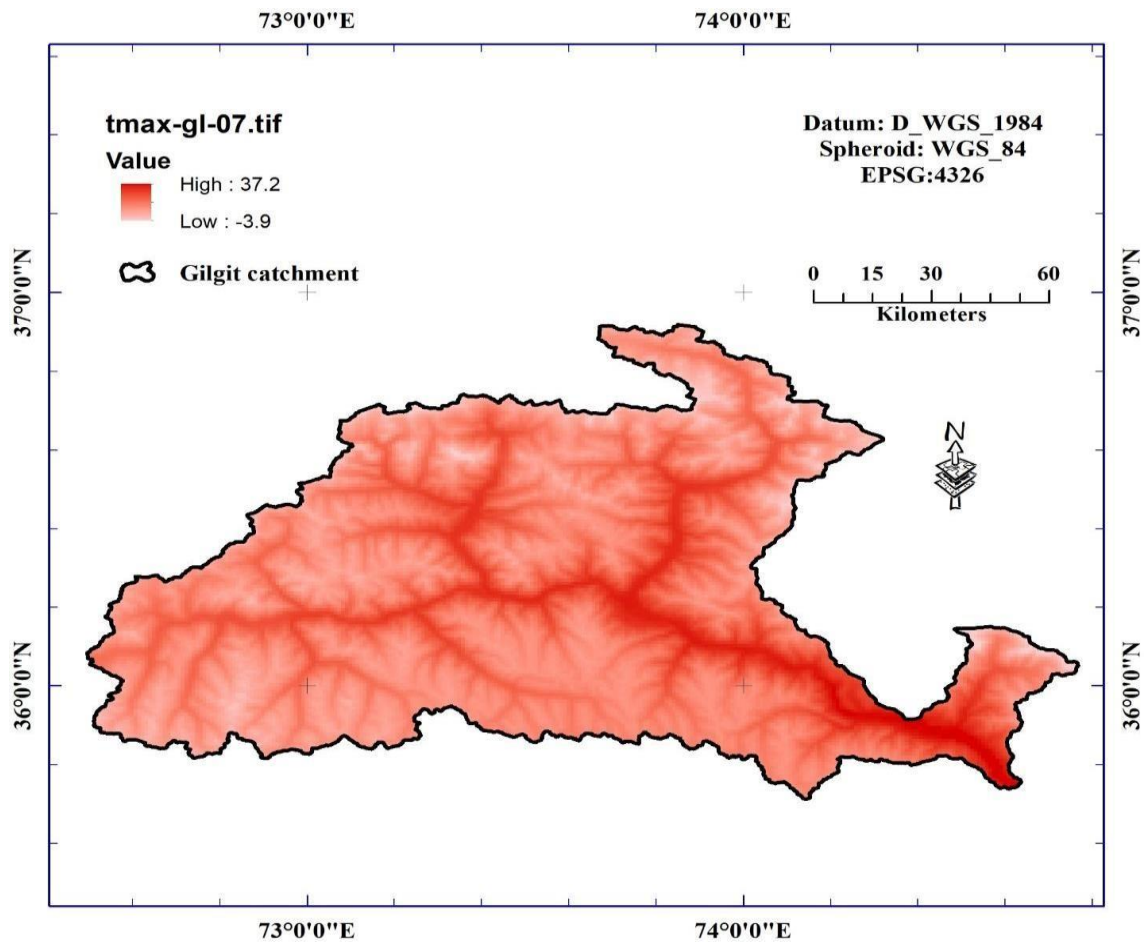


Figure 5.46 Spatial distribution of monthly averaged Maximum Temperature (in degrees Celsius) for the month of July for Gilgit catchment

The interpolated maximum surface temperature processed from the point data from local stations, monthly averaged of 30 years portrays a high value of 36.3 degrees Celsius and a low value of -4.1 degree Celsius across watershed for the month of August. The low values of temperature are mainly observed at higher altitudes on Northern side and high values of temperature on the lower altitudes on southeast of Gilgit watershed, respectively. August, the end month of the summer, is another scorching month in Gilgit, with average temperatures fluctuating from 16 to 36.3 degrees Celsius. The average maximum temperature in August is nearly as hot as it is in July.

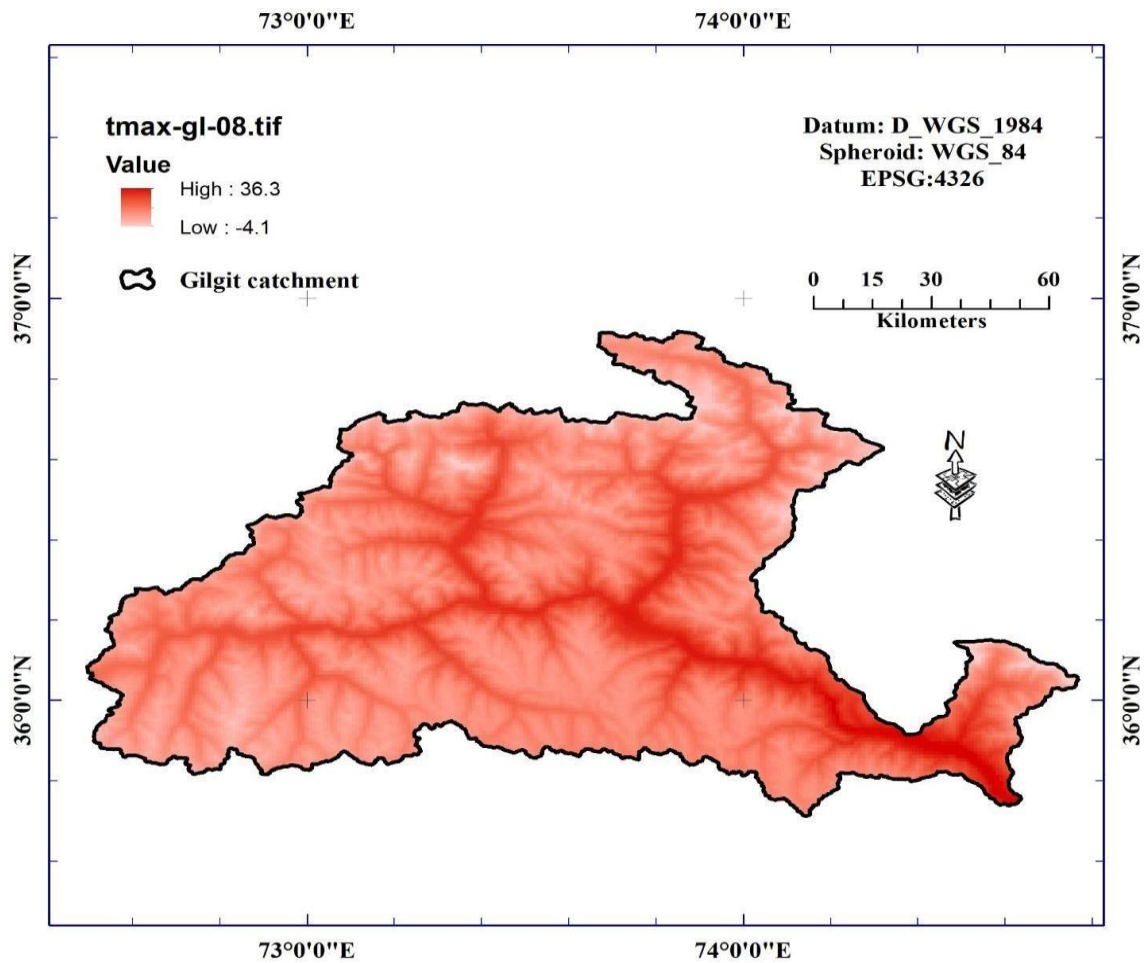


Figure 5.47 Spatial distribution of monthly averaged Maximum Temperature (in degrees Celsius) for the month of August for Gilgit catchment

The interpolated maximum surface temperature processed from the point data from local stations, monthly averaged of 30 years portrays a high value of 32.5 degrees Celsius and a low value of -8 degrees Celsius across watershed for the month of September. The low values of temperature are mainly observed at higher altitudes on Northern side and high values of temperature on the lower altitudes on southeast of Gilgit watershed, respectively. September is the leading month of the autumn and is even hot month in Gilgit with average temperature fluctuating between 12.25 degree Celsius and an average low of ~33 degree Celsius. In September, the average high-temperature slightly drops from a torrid value to a low hot value.

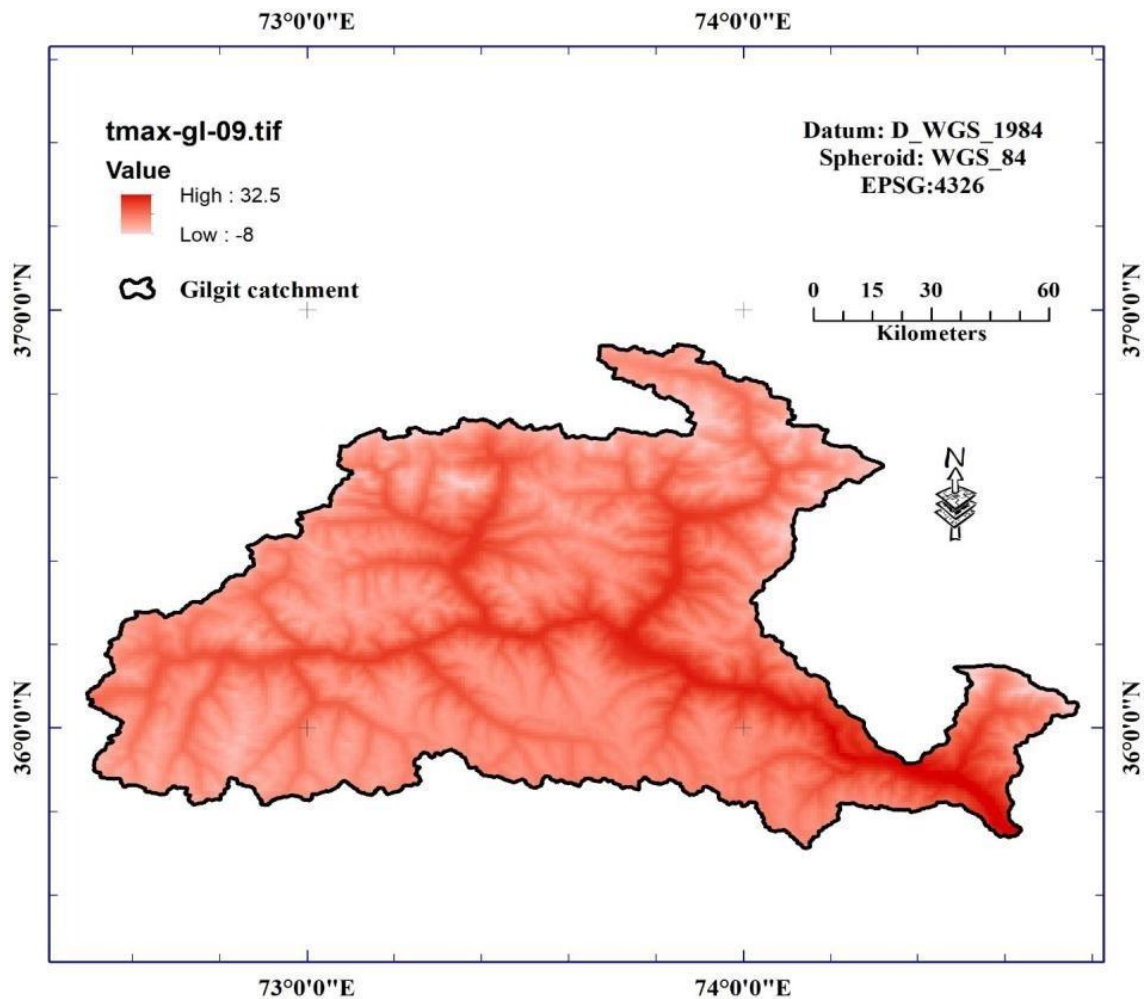


Figure 5.48 Spatial distribution of monthly averaged Maximum Temperature (in degrees Celsius) for the month of September for Gilgit catchment

The interpolated maximum surface temperature processed from the point data from local stations, monthly averaged of 30 years portrays a high value of 36.5 degrees Celsius and a low value of -14.4 degrees Celsius across watershed for the month of October. The low values of temperature are mainly observed at higher altitudes on Northern side and high values of temperature on the lower altitudes on southeast of Gilgit watershed, respectively. October, like September, in Gilgit is another warm autumn month, with average temperature fluctuating between 6 degree Celsius and 26.5 degree Celsius. In Gilgit, the average high-temperature in October drops from a tropical value to a still warm value.

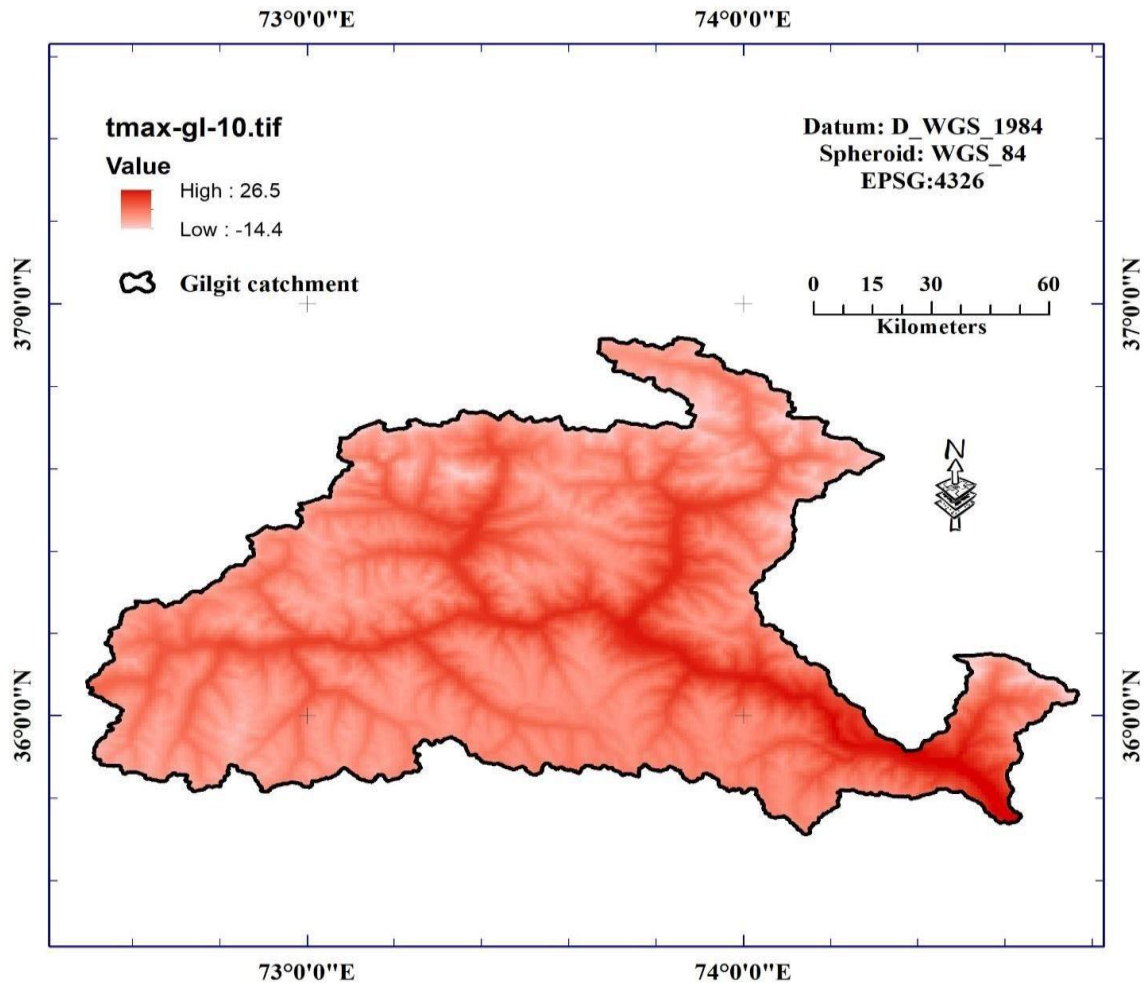


Figure 5.49 Spatial distribution of monthly averaged Maximum Temperature (in degrees Celsius) for the month of October for Gilgit catchment

The interpolated maximum surface temperature processed from the point data from local stations, monthly averaged of 30 years portrays a high value of 19.7 degrees Celsius and a low value of -19.3 degrees Celsius across watershed for the month of November. The low values of temperature are mainly observed at higher altitudes on Northern side and high values of temperature on the lower altitudes on southeast of Gilgit watershed, respectively. November is the last month of the autumn and slightly cool month in Gilgit. It is another relaxed month with temperature in the reach of an average high of 19.7 degree Celsius and an average low of 0.2 degree Celsius. In November, the average high-temperature drops, from a soberly hot value to cool value.

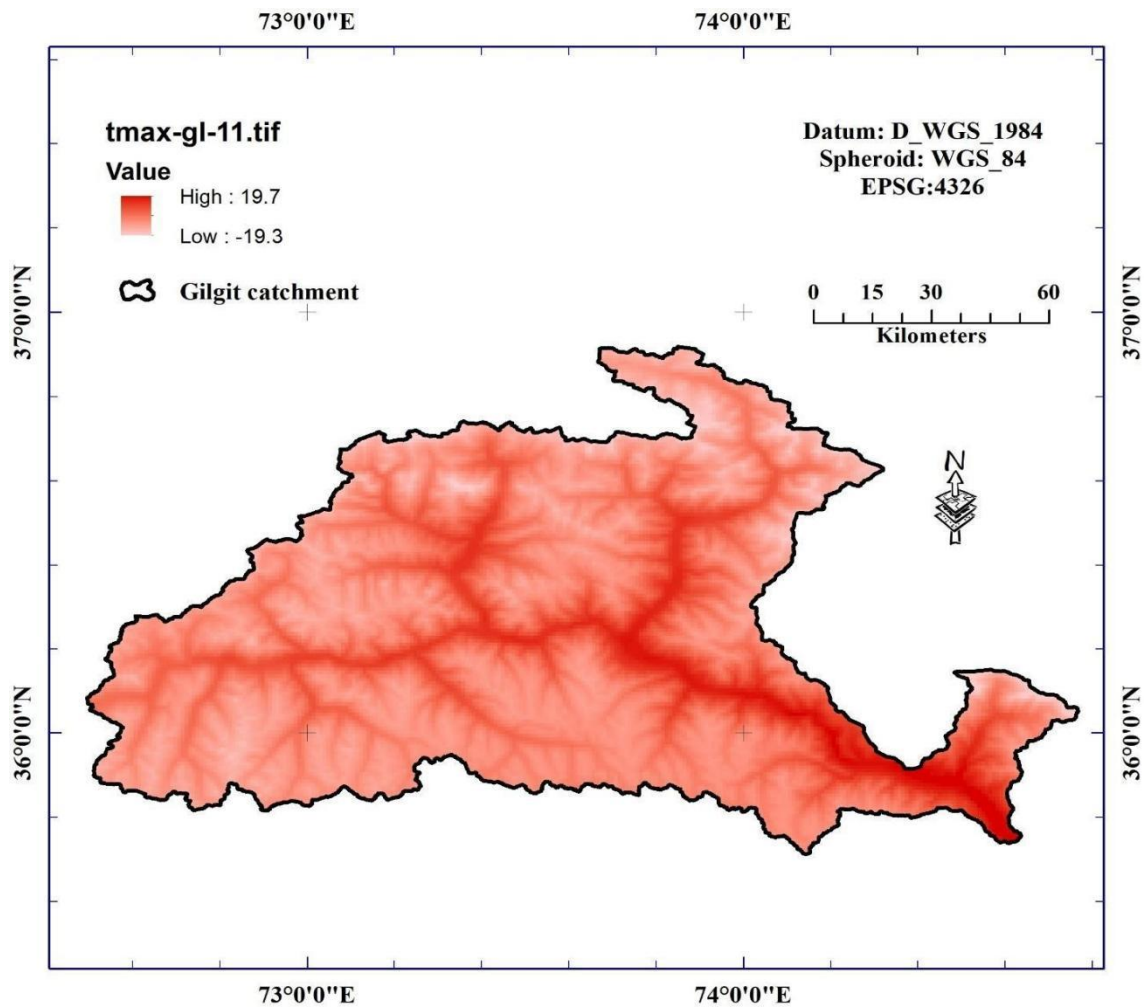


Figure 5.50 Spatial distribution of monthly averaged Maximum Temperature (in degrees Celsius) for the month of November for Gilgit catchment

The interpolated maximum surface temperature processed from the point data from local stations, monthly averaged of 30 years portrays a high value of 13 degrees Celsius and a low value of -21.8 degrees Celsius across watershed for the month of December. The low values of temperature are mainly observed at higher altitudes on Northern side and high values of temperature on the lower altitudes on southeast of Gilgit watershed, respectively. December, the first month of the winter, is a chilly month in Gilgit, with average temperatures fluctuating from -4.4 to 13 degrees Celsius. The average maximum temperature in Gilgit drops from a pleasant 19.7 degrees Celsius in November to a crisp 13 degrees Celsius in December.

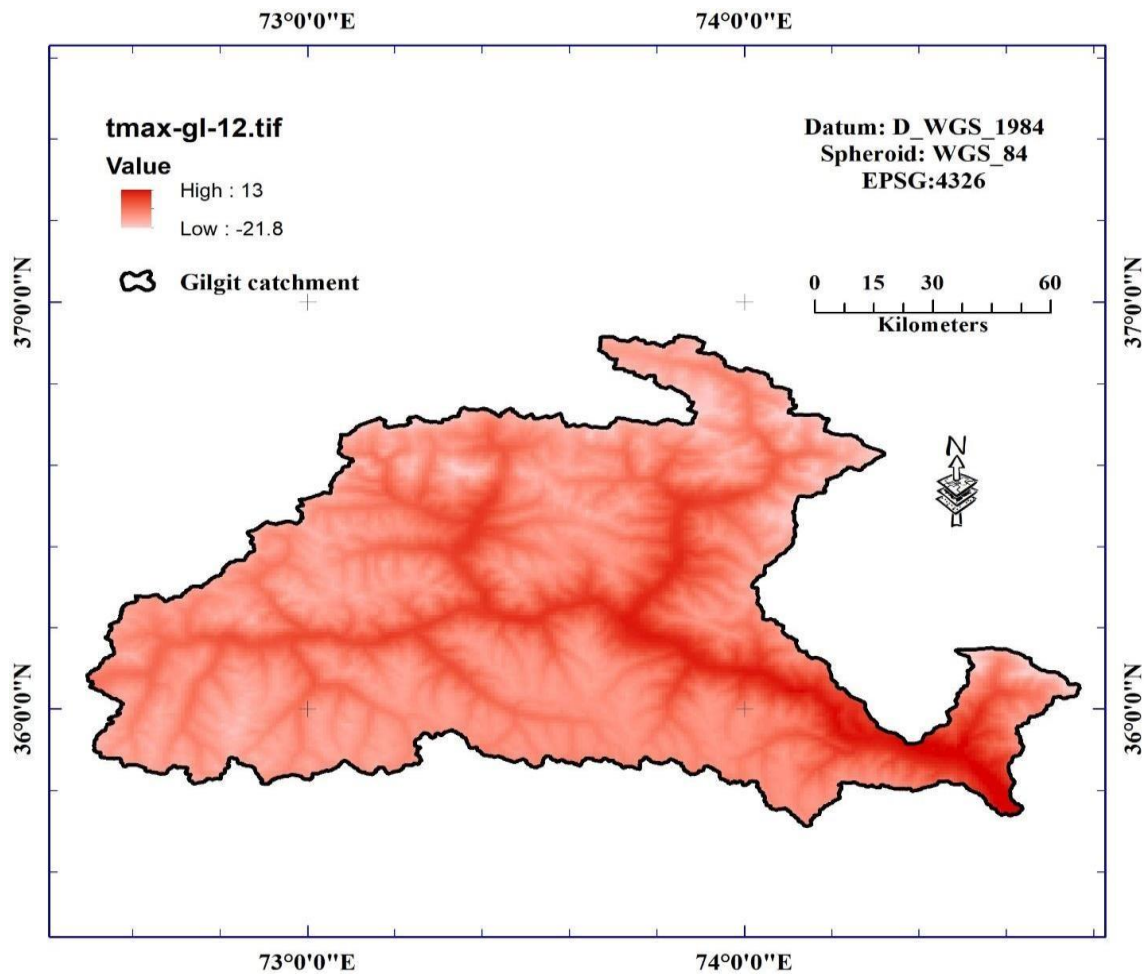


Figure 5.51 Spatial distribution of monthly averaged Maximum Temperature (in degrees Celsius) for the month of December for Gilgit catchment

Table 5.4 Monthly Low and High values for Maximum Temperature in degree Celsius in Gilgit watershed

Sr.	Month	T_{Max} (Low)	T_{Max} (High)	T_{Max} (Ave)
1	January	-24.7	10.7	-7
2	February	-24.6	13.4	-5.6
3	March	-21.8	19	-1.4
4	April	-18.2	25	3.4
5	May	-13.4	30.2	8.4
6	June	-8.8	35.3	13.25
7	July	-3.9	37.2	16.65
8	August	-4.1	36.3	16.1
9	September	-8	32.5	12.25
10	October	-14.4	26.5	6.05
11	November	-19.3	19.7	0.2
12	December	-21.8	13	-4.4

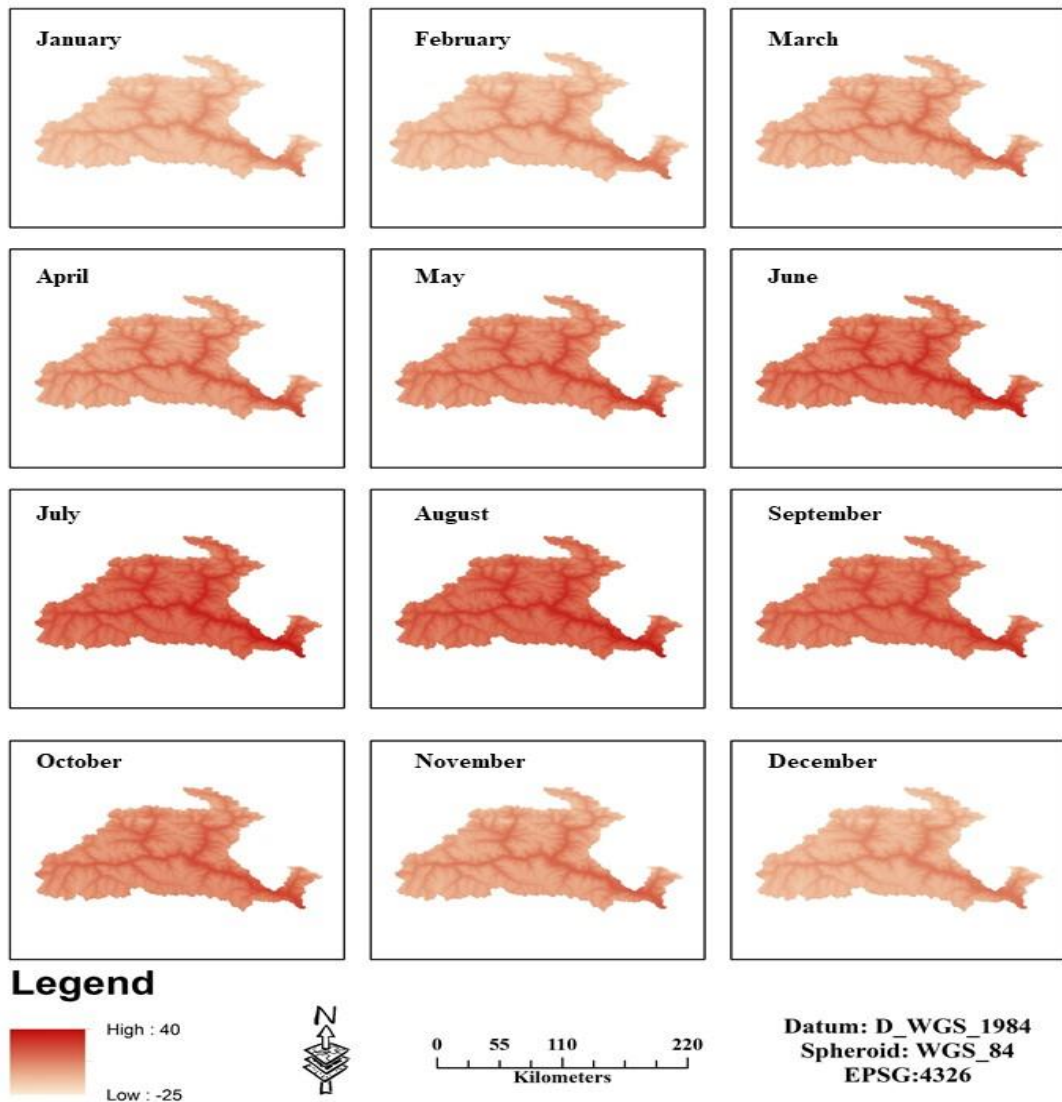


Figure 5.52 Spatial Distribution of Monthly Averaged maximum Temperature - Normalized Matrix for Yearly Profile

CHAPTER 6

RESULT AND DISCUSSION WATERSHED EXTRACTION

A catchment, watershed or drainage system is the hydrological unit together by drainage lying upslope from a pour point or specific outlet. The watershed extracting characteristics is important for water resource management and hydrological analysis in GIT/ GIS including catchment delineation and stream network.

Converging on the difficulties of ridges mismatch in watershed delineation in the mountainous regions, this study has introduced DEM-based delineation's comparison from multi-sensor, multi-mission DEM datasets at multi-resolution viz., SRTM, ASTER GDEM and GTOPO30 using the predefined method to complete watershed delineation. This is important to note that no manual editing was used to amend the extracted drainage structure in GIS environment. The comparative analysis was employed to the delineation of drainage and watershed at the basin level and further at the sub-catchments for five large glaciers viz, Karamber, Phakor, Bhort, Bad-e-Swat and East Gammu. The outlined watersheds have been visually studied in contradiction of the optical Landsat 8 OLI imagery for mountainous ridge matching. The SRTM 30m radar based has also resolved the additional precision for this basin delineation issue.

The extracted Gilgit watershed based on ASTER GDEM 30 m is shown in Figure 6.1, with an area approx. 12,757.446 km² with altitude distribution ranges from 1388 m to 7104 m. This watershed has an average of heights at an elevation of 4051.94 m. Furthermore, Figure 6.2, 6.3, 6.4, 6.5 and 6.6 displays the delineated watersheds (in red polygons) of Bad-e-Swat, Bhort, East Gammu, Karamber and Phakor glaciers having areas 49.410 km², 54.698 km², 42.730 km², 223.916 km² and 20.356 km² respectively. The locations of the watersheds of individual glaciers shown at Figure 6.2, 6.3, 6.4, 6.5 and 6.6 are merged in the Gilgit watershed in Figure 6.1.

The extracted Gilgit watershed based on SRTM 30 m is shown in Figure 6.7, which covers a total area of about 12760.996 km² with elevation allocation ranges from 1405 m to 7114 m. This watershed has an average of peaks at an elevation of 4046.626 m. Furthermore, Figure 6.8, 6.9, 6.10, 6.11 and 6.12 displays the delineated watersheds (in red polygons) of Bad-e-Swat, Bhort, East Gammu, Karamber and Phakor glaciers having areas 45.914 km², 57.781 km², 57.781 km², 223.807 km² and 24.077 km² respectively. The comparison of computed area from different DEM datasets is shown in Table 6.1.

The differences of the watersheds from different DEMs are shown in Figure 6.13. Here red polygon represents watershed from SRTM (1 arc sec) and black polygon represents watershed from ASTER-GDEM. There are many mismatches highlighted in circles along the watershed of Bhort glacier. However, outcomes revealed that, the SRTM 30m radar based showed additional correctness amongst these DEMs as of its additional accurate delineation.

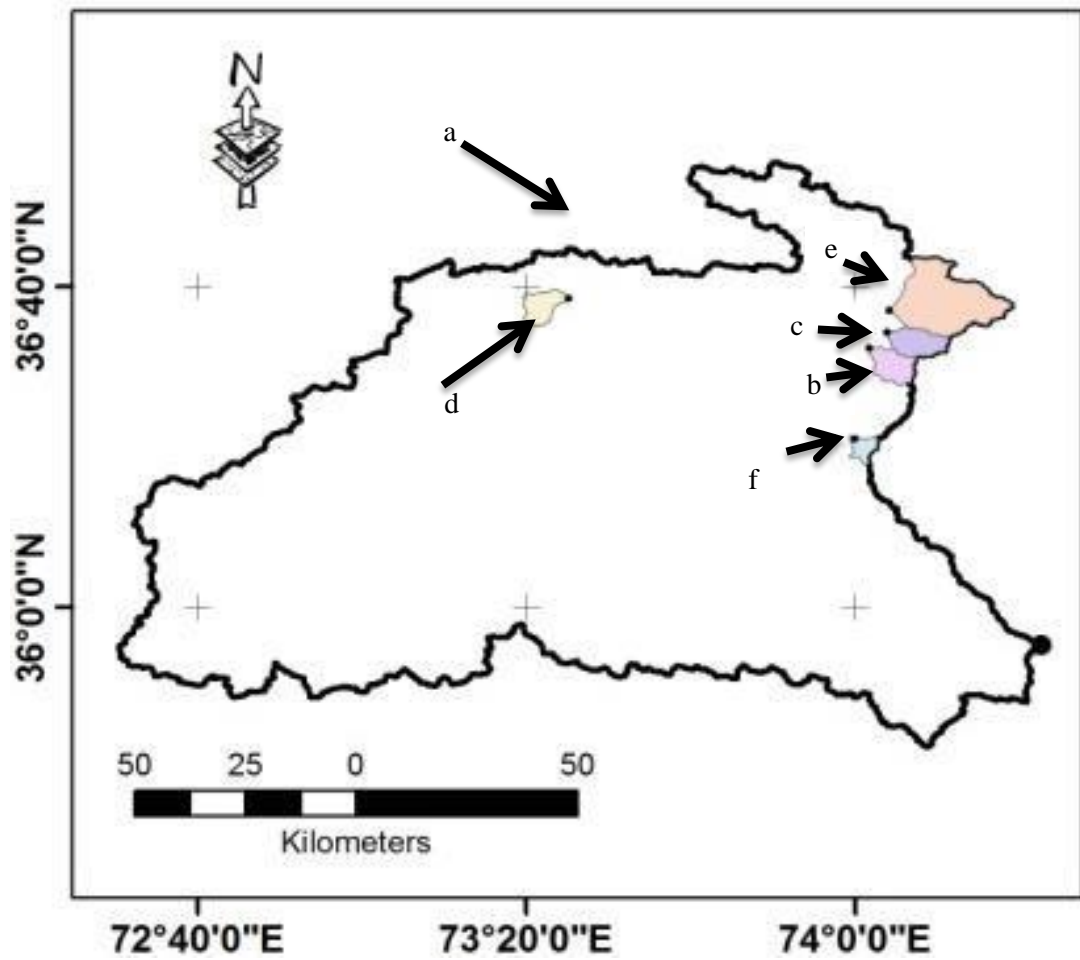


Figure 6.1 Delineated watersheds based on ASTER GDEM 30 m (a) Gilgit basin, (b) Bad-e-Swat glacier, (c) Bhort glacier, (d) East Gammu glacier, (e) Karamber glacier, (f) Phakor glacier

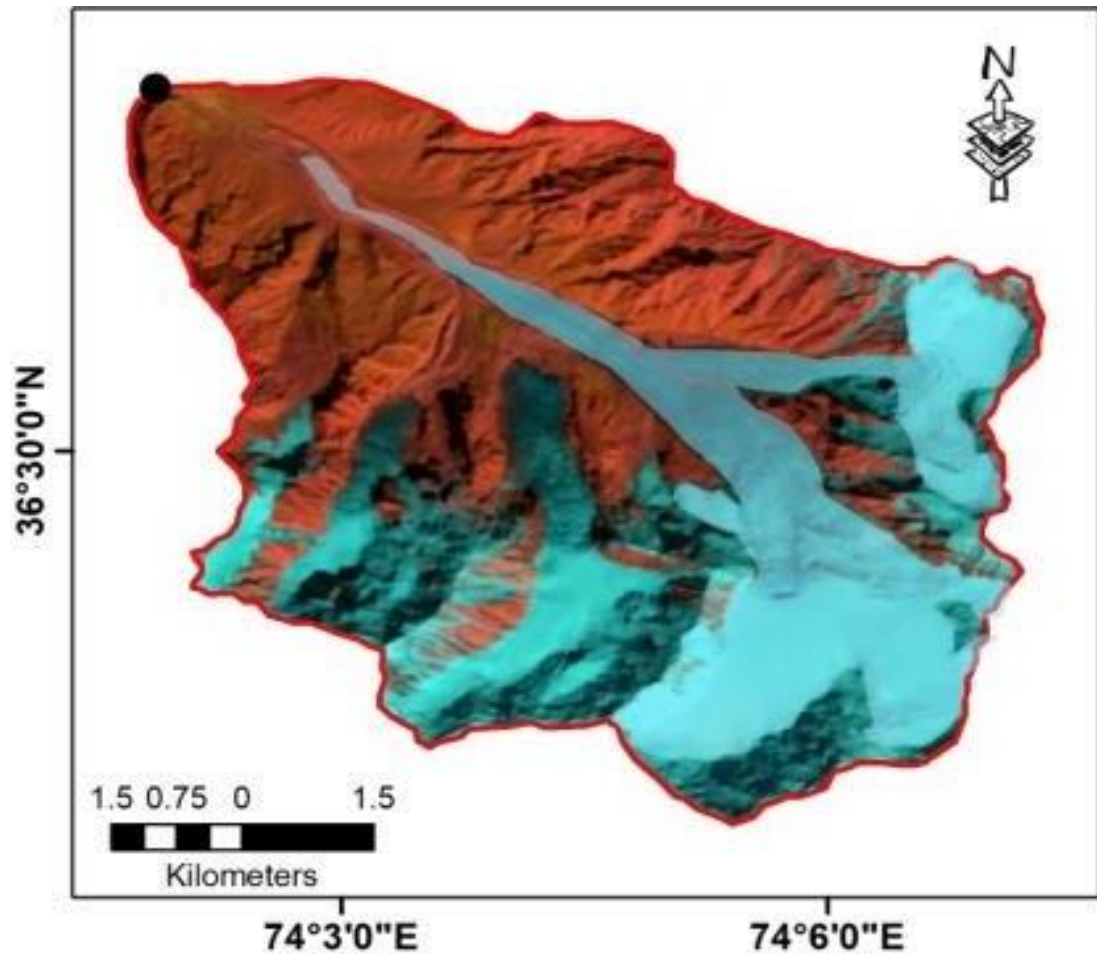


Figure 6.2 Delineated watersheds extracted from ASTER GDEM 30 m shown with Landsat-8 background False Color Composite (FCC) images (R:G:B::7:6:4) of Bad-e-Swat glacier

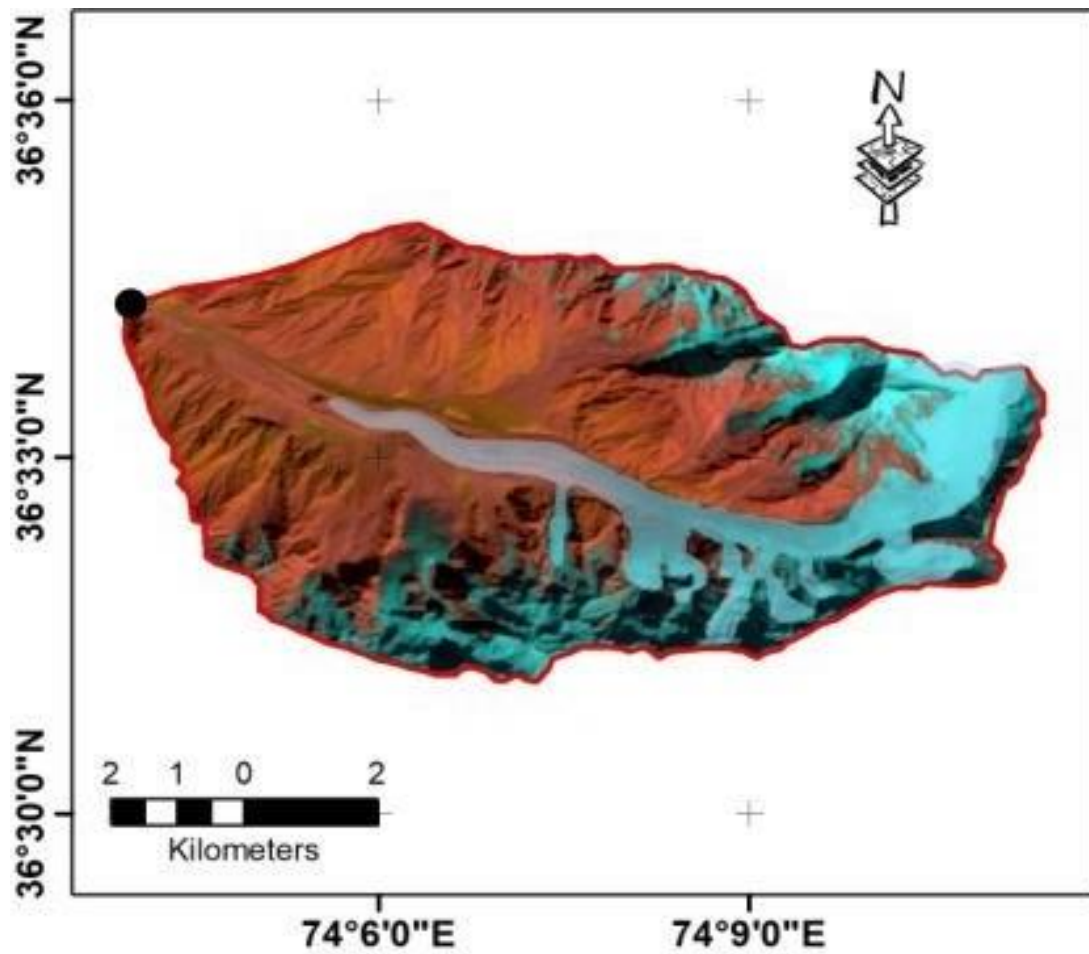


Figure 6.3 Delineated watersheds extracted from ASTER GDEM 30 m, shown with Landsat-8 background False Color Composite (FCC) images (R:G:B::7:6:4) of Bhorth glacier

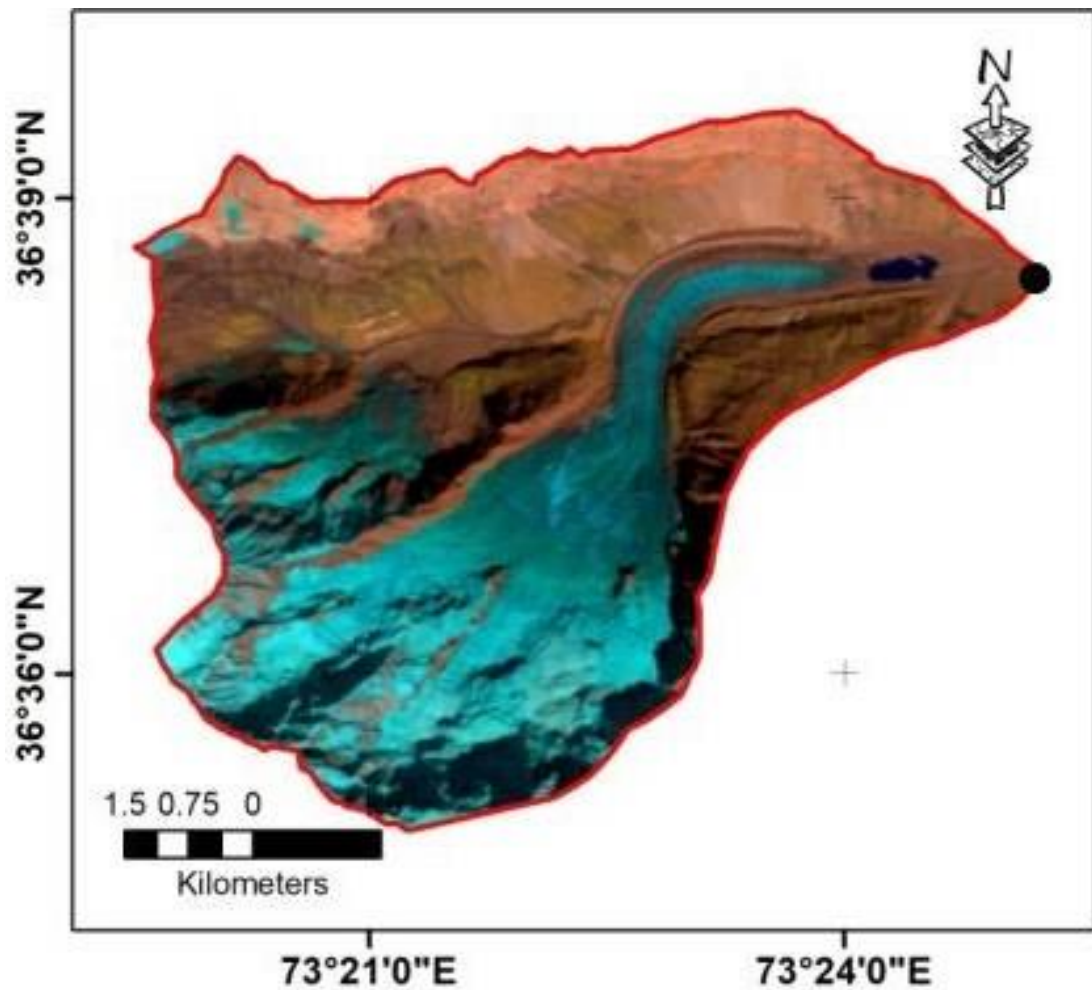


Figure 6.4 Delineated watersheds extracted from ASTER GDEM 30 m East Gammu glacier shown with Landsat-8 background False color Composite (FCC) images (R:G:B::7:6:4)

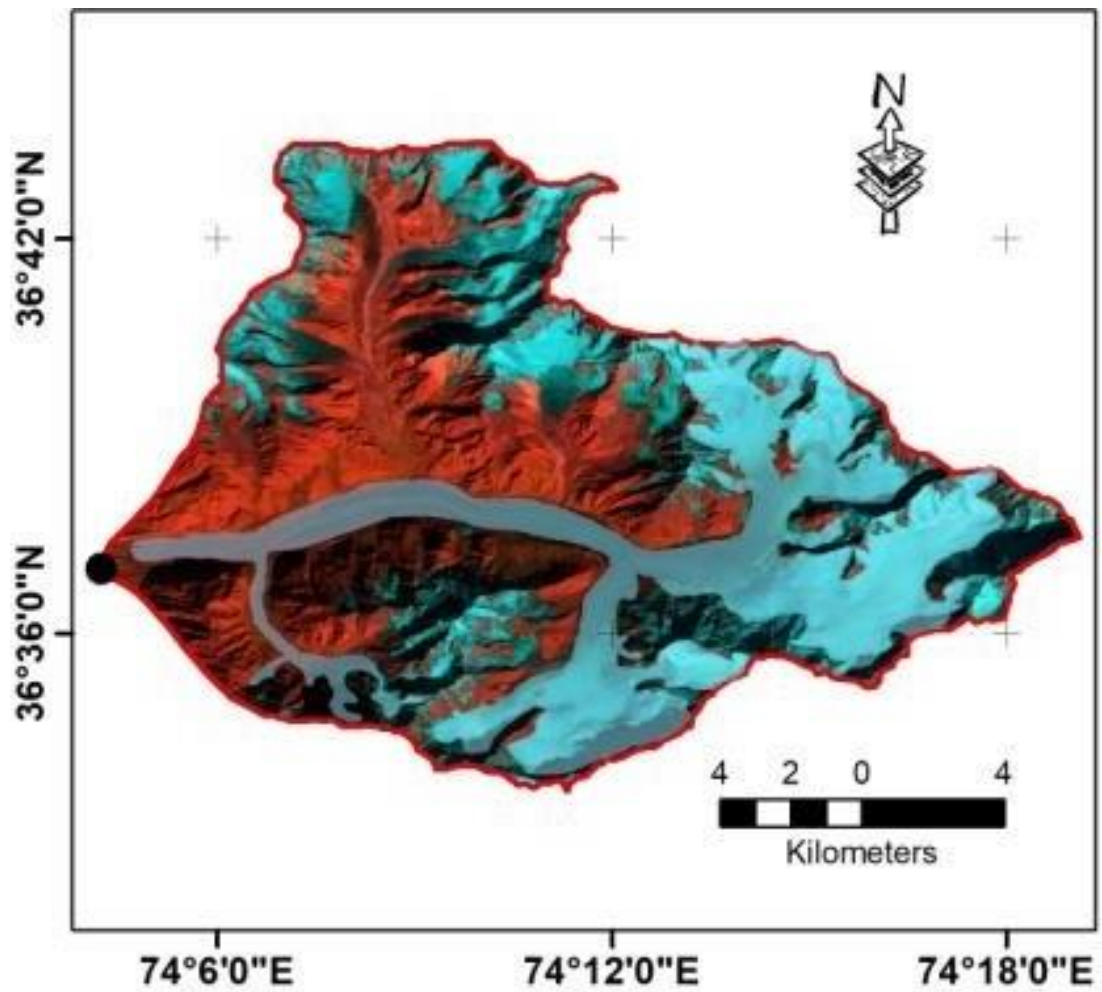


Figure 6.5 Delineated watersheds extracted from ASTER GDEM 30 m Karamber glacier shown with Landsat-8 background False color Composite (FCC) images (R:G:B::7:6:4)

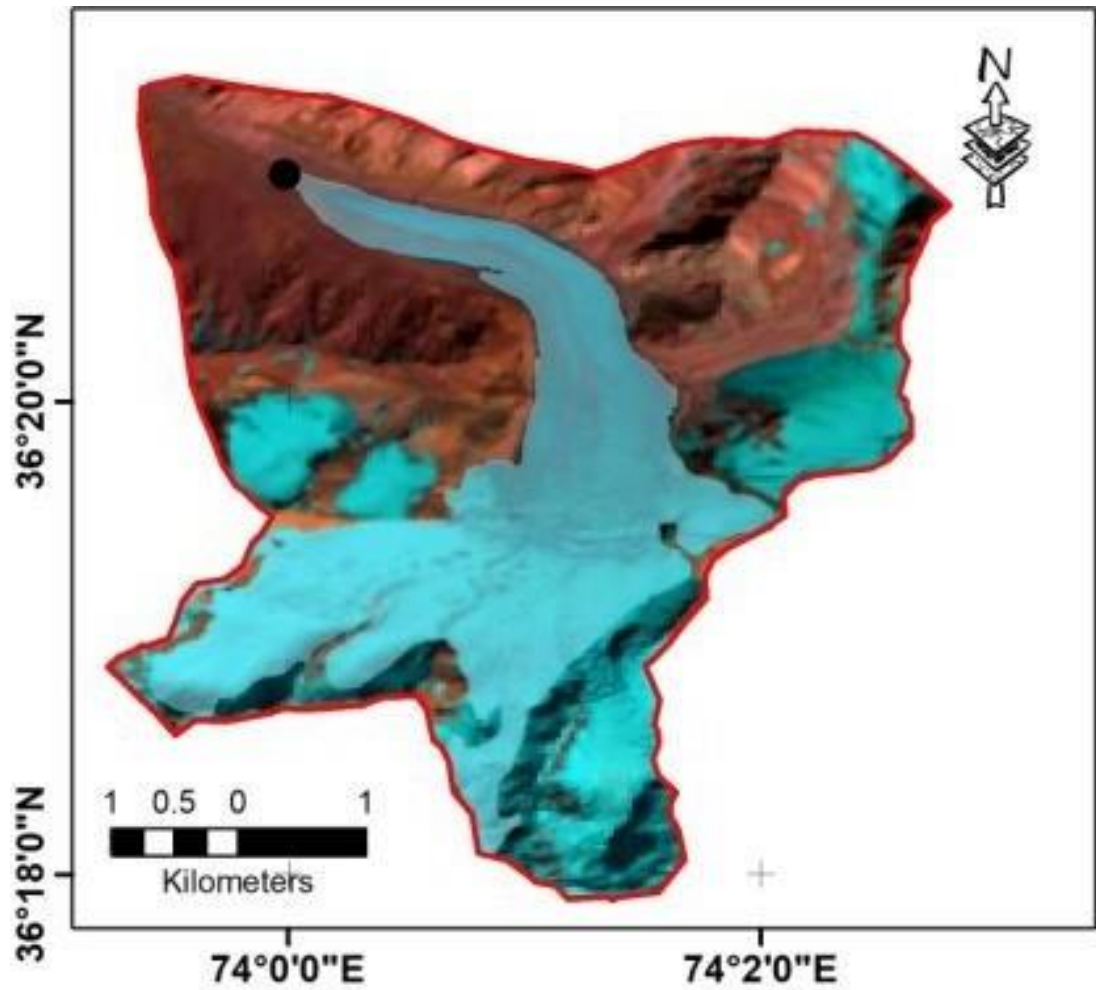


Figure 6.6 Delineated watersheds extracted from ASTER - GDEM 30 m Phakor glacier shown with Landsat-8 background False Color Composite (FCC) images (R:G:B::7:6:4)

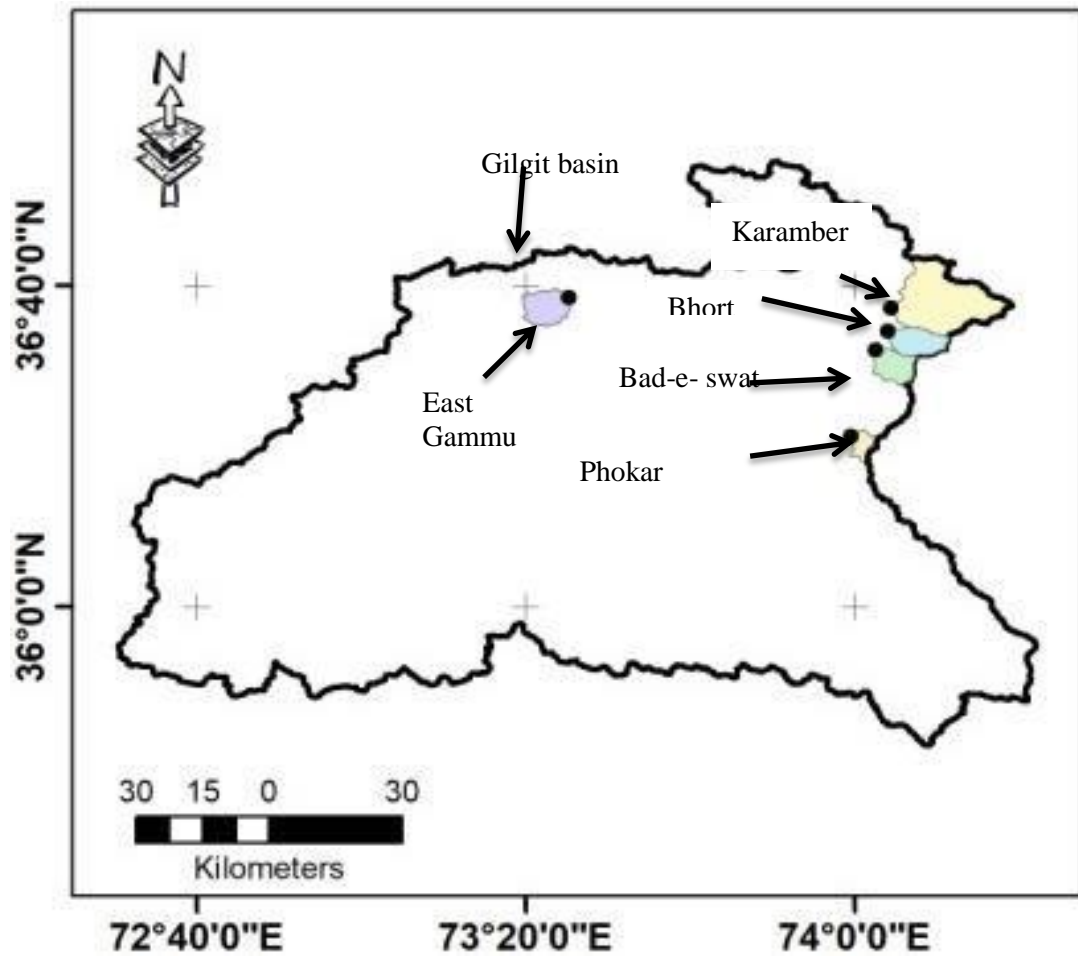


Figure 6.7 Delineated watersheds extracted from SRTM 30 m Gilgit basin

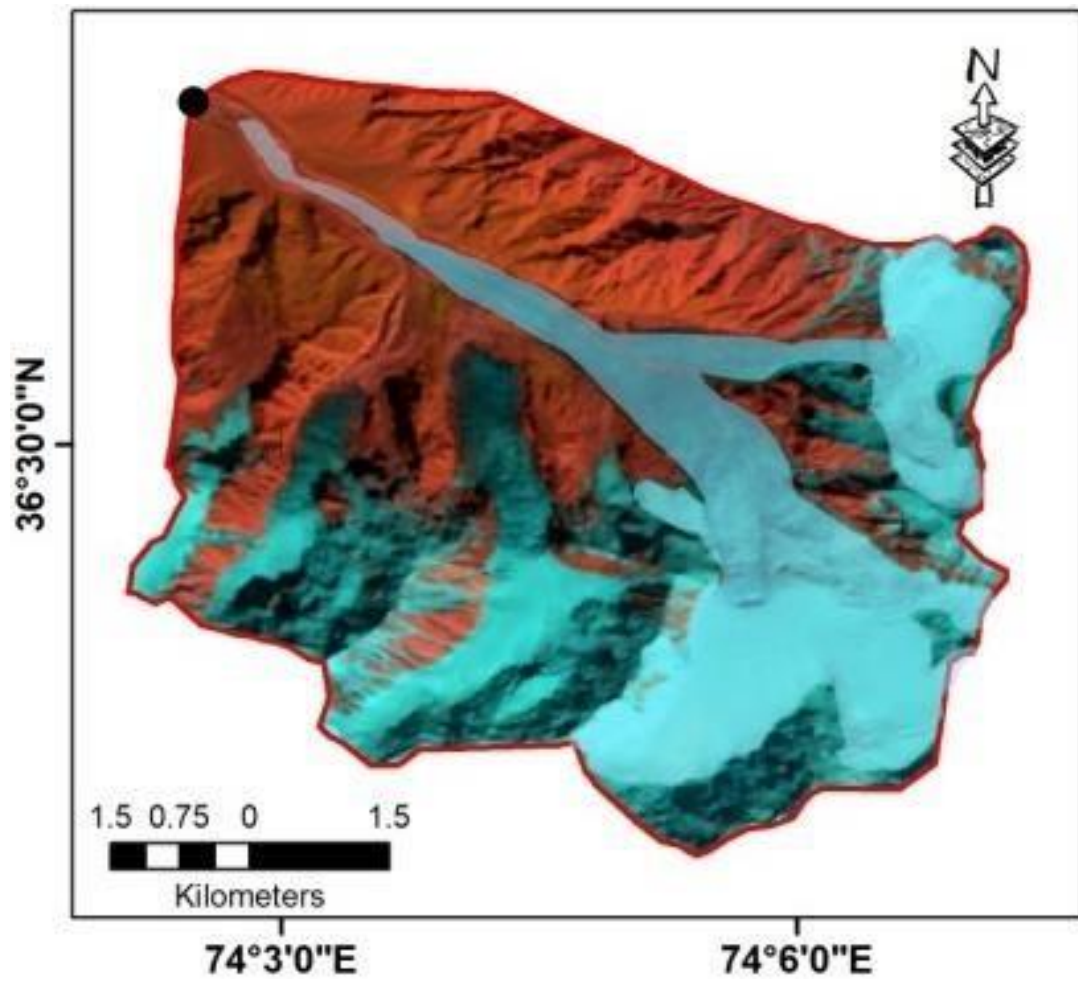


Figure 6.8 Delineated watersheds extracted from SRTM 30 m shown with Landsat-8 background False color Composite (FCC) images (R:G:B::7:6:4) of Bad-e-Swat glacier

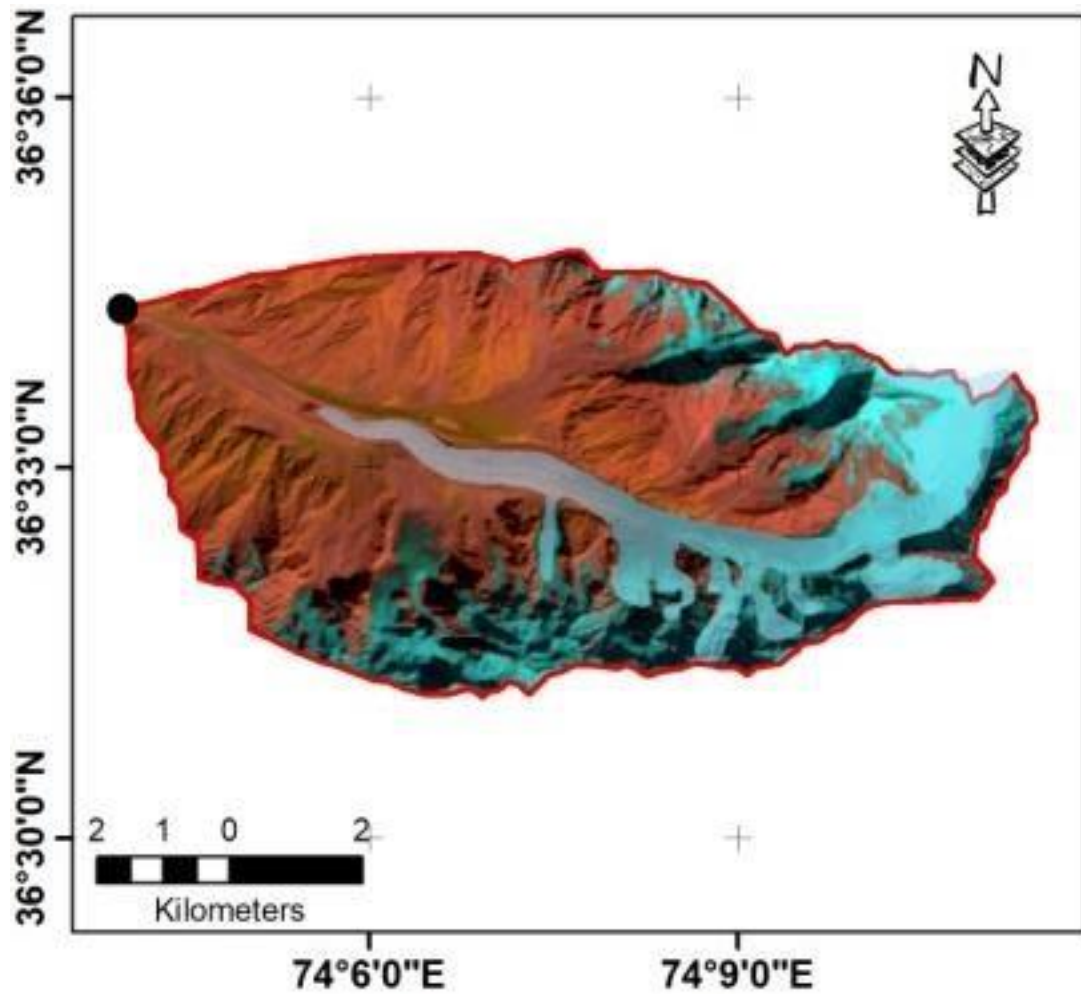


Figure 6.9 Delineated watersheds extracted from SRTM 30 m shown with Landsat-8 background False color Composite (FCC) images (R: G: B: 7:6:4) of Bhorth glacier

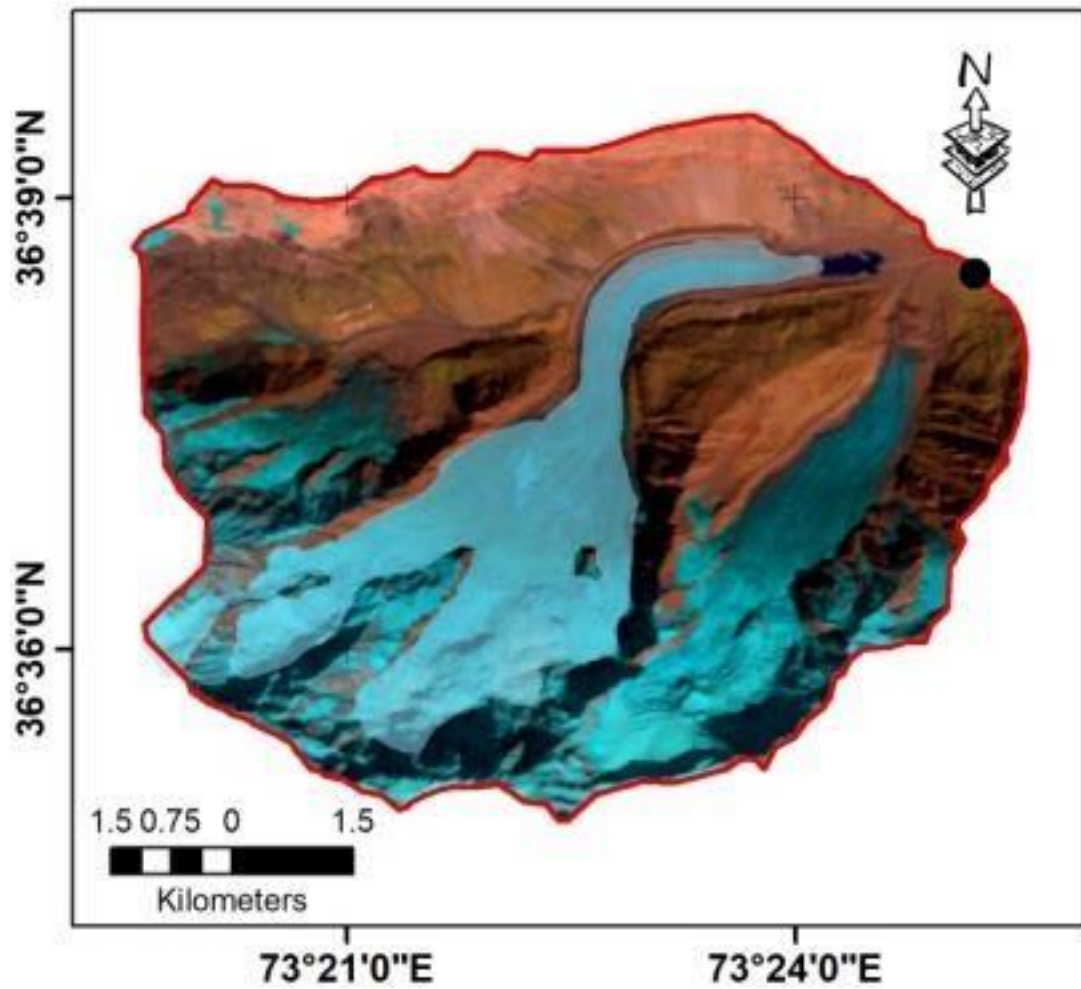


Figure 6.10 Delineated watersheds extracted from SRTM 30 m shown with Landsat-8 background False color Composite (FCC) images (R:G:B:7:6:4) of East Gammu glacier

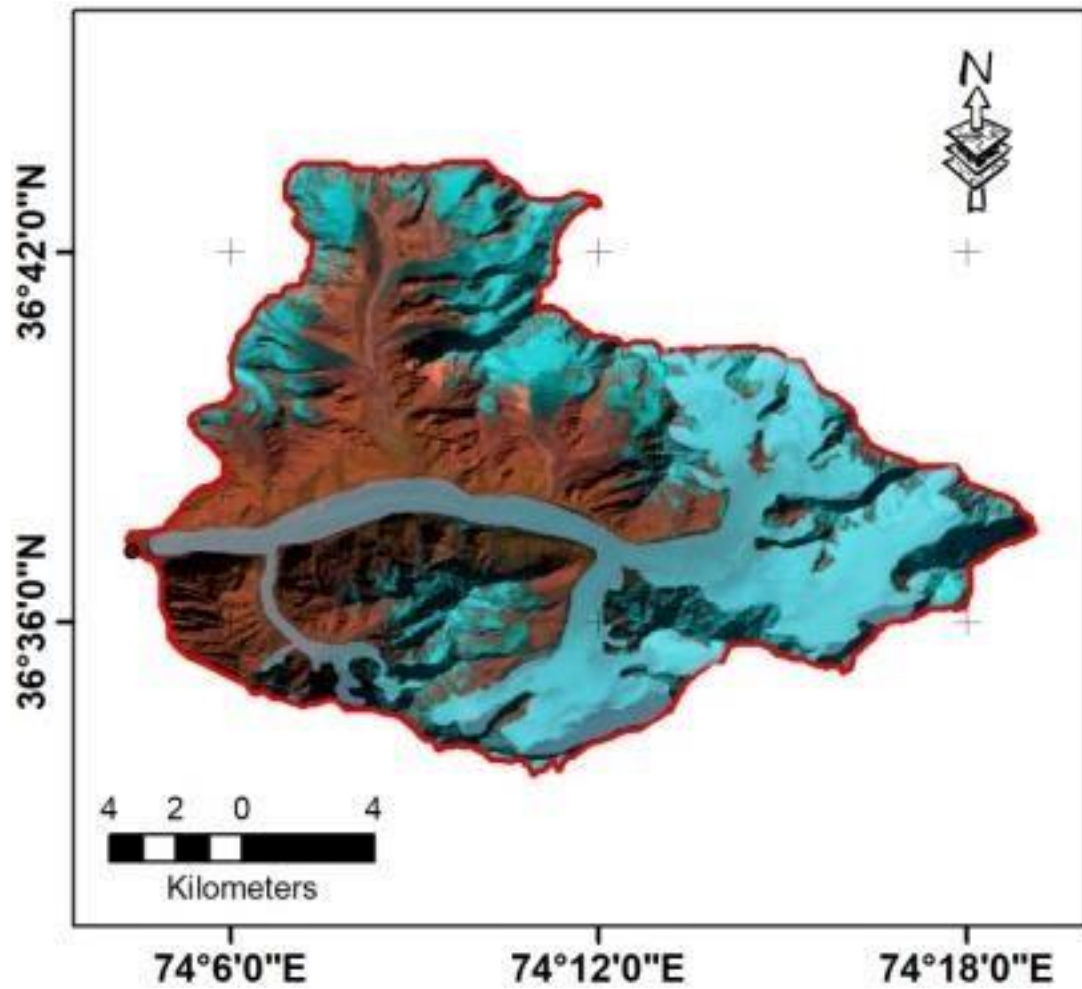


Figure 6.11 Delineated watersheds extracted from SRTM 30 m shown with Landsat-8 background False color Composite (FCC) images (R:G:B:7:6:4) of Karamber glacier

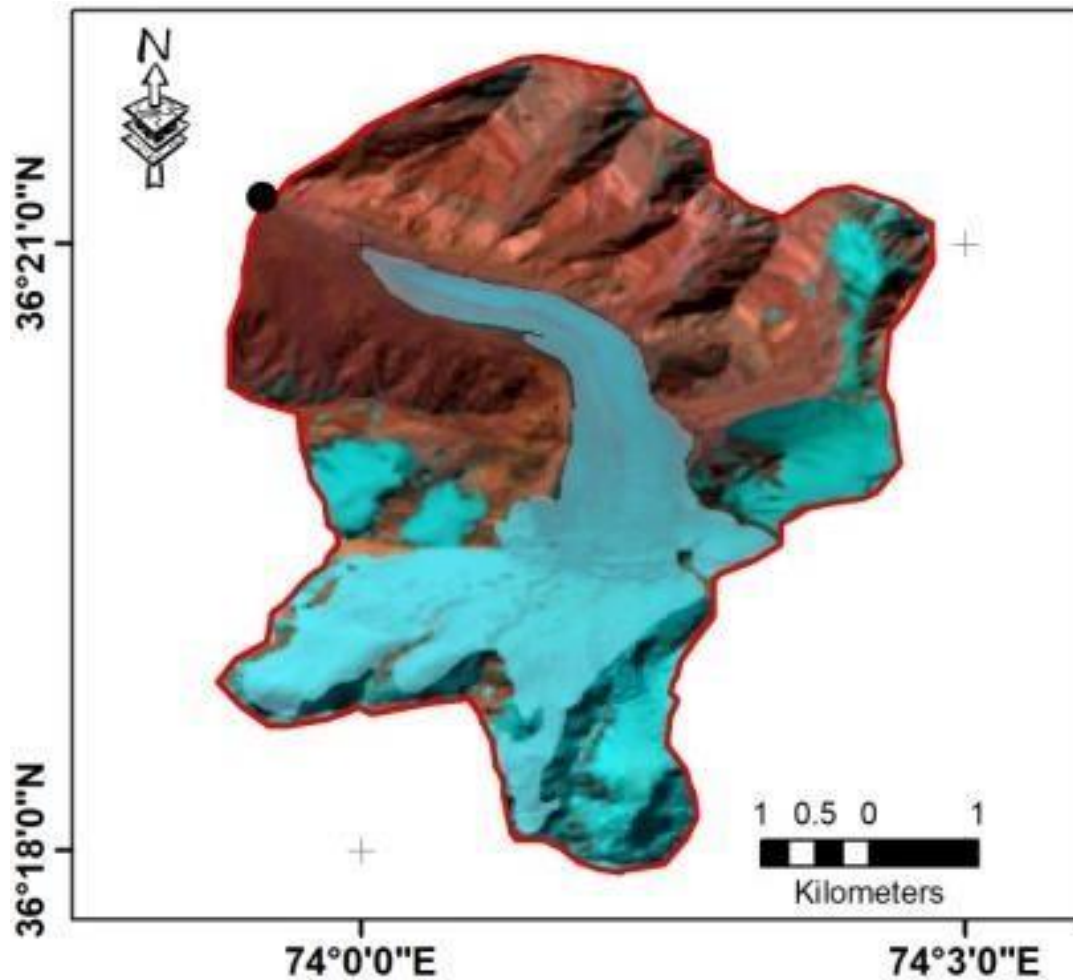


Figure 6.12 Delineated watersheds extracted from SRTM 30 m shown with Landsat-8 background False color Composite (FCC) images (R:G:B:7:6:4) of Phakor glacier.

Table 6.1 Comparison analysis of DEMs

DEM dataset	Gilgit basin	Bad-e-Swat	Bhort	East Gammu	Karamber	Phakor
SRTM	12760.996	45.914	53.857	57.781	223.807	24.077
ASTER GDEM	12757.446	49.410	54.698	42.730	223.916	20.356
GTOPO30	12711.14	-	-	-	-	-

A thirty arc second DEM equivalent to 1000 m spatial resolution has been used for the extraction of watershed of Gilgit basin namely GTOPO30. This DEM used for performing the correction and calibration applying with SPOT derived DEMS and the SRTM. It has been used in many research training and still being used in present days also (Endreny et al., 2000; Denker 2005). Being of low resolution its use limited to Gilgit watershed only. Individual glaciers inside the watershed not extracted.

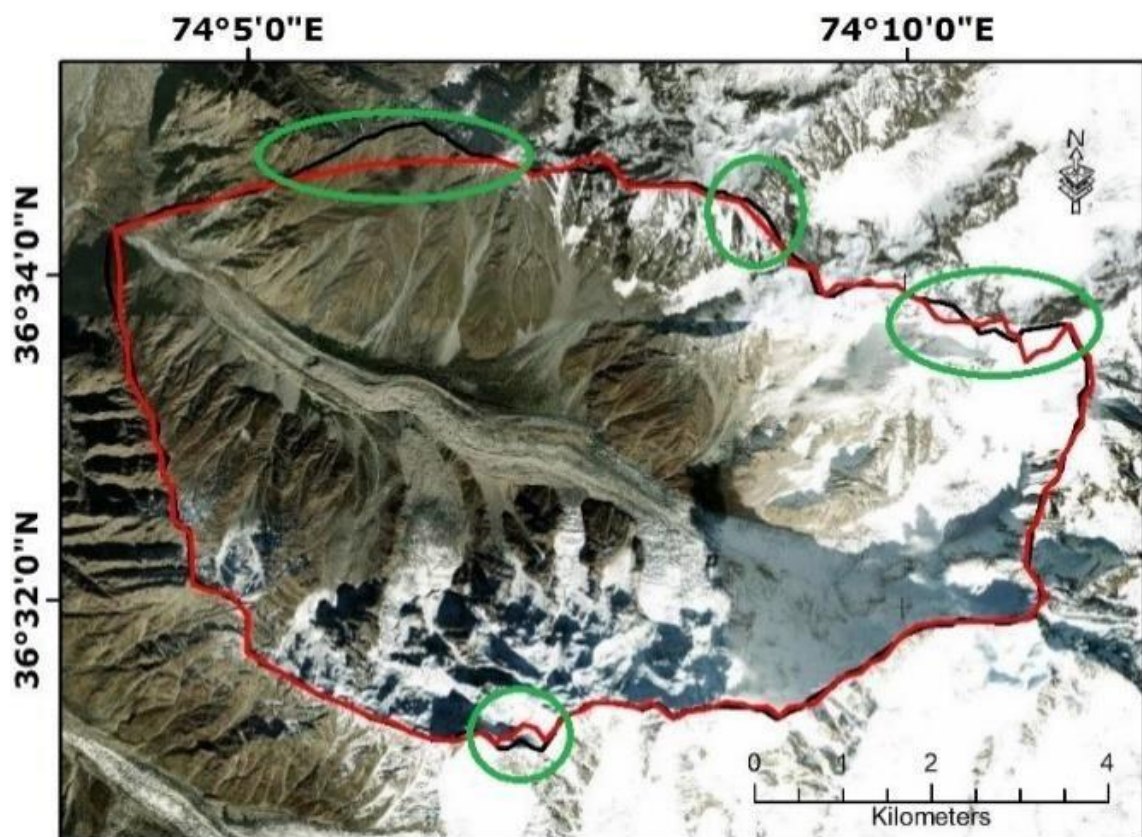


Figure 6.13 Bhort glacier – Polygons from Figure 6.3 and Figure 6.9 are combined to highlight mismatches) for the comparison of watersheds derived from SRTM (Red) and ASTER-GDEM (Black) shown with background Natural Color Composite images of Landsat-8

The comparison analysis between SRTM and ASTER GDEM has been done by matching the extracted area of watershed for Gilgit basin and different glaciers. The results of data showed that, the SRTM 30 m radar based demonstrated the additional precision amid such DEMs due to its particular delineation in the sub-basin of Gilgit as

analyzed in combination with optical remote sensing imagery. However, it is appropriate to say that attributes and features for both DEMs generally show close agreement to each other.

CHAPTER 7

RESULT AND DISCUSSION GLACIER CHANGE ANALYSIS

7.1 Discussions on Glacier Changes

The object-based classification is quicker in calculation and effective due to their unique feature and spectral patterns consideration. Literature reveals that, object-based classification gives better and accurate results as compare to pixel based classification. Temporal satellite images of Landsat for the year of 1988 to 2018 were acquired and analyzed. Glacier-wise change detected in all five selected glaciers has been shown and discussed in ensuing paragraphs. On ground picture, glacier extent and elevation profile of each selected glacier have been shown and discussed.

7.1.1 Bhort Glacier

Bhort is among one of the largest glacier in the region of Gilgit with a significant part under the debris cover. The debris cover comprise of small and large rocks as shown in Figure 7.1. The extent of the glacier is shown in Figure 7.2. Its terminus starts at 3000 m above sea level, located geographically at 36° 33'52"N and

74° 04'28"E. The extent coordinates of the Bhort glacier are from 74° 04'40"E to 74° 11'10"E and from 36° 31'12"N to 36° 34'04"N.



Figure 7.1 On way to Bhort glacier (24 Oct 2020)

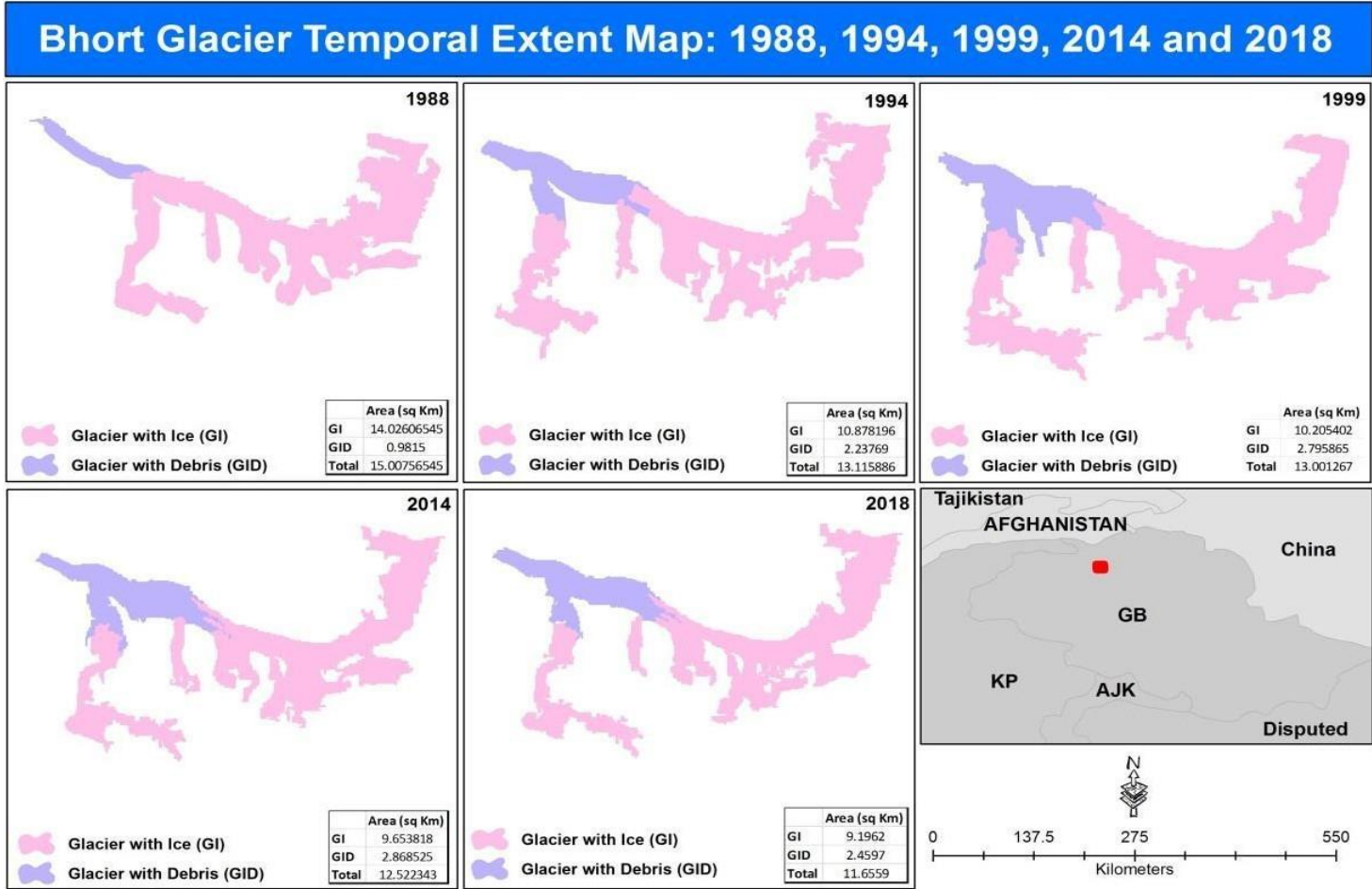


Figure 7.2 Bhort glacier temporal change extent for the years 1988, 1994, 1999, 2014 and 2018.

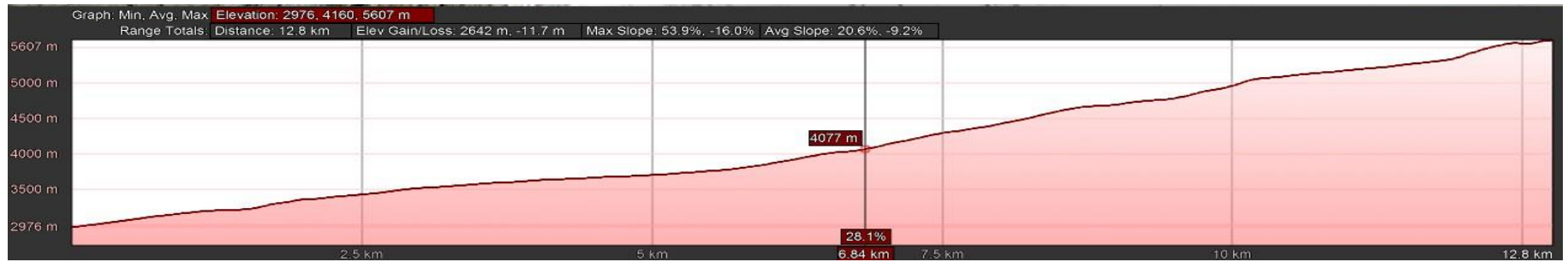


Figure 7.3 Elevation profile of Bhorth glacier

It was observed that the ice-covered areas are 14.02, 10.87, 10.20, 9.65 and 9.19 km² for the years 1988, 1994, 1999, 2014 and 2018 respectively. However, the debris-covered areas were 0.98, 2.23, 2.79, 2.86 and 2.45 km² for the years 1988, 1994, 1999, 2014 and 2018 respectively. Furthermore, the overall glacier changes are 15.00, 13.11, 13.00, 12.52 and 11.65 km² for the years 1988, 1994, 1999, 2014 and 2018 respectively. The results revealed that, the overall ice-covered area from 1988 to 2018 has reduced to 4.11 sq. km. However, from 1988 to 2018 the overall debris-covered area has increased to 1.47sq. km.

7.1.2 Bad-e-Swat Glacier

Bad-e-Swat glacier is one of the main glaciers in Gilgit region as shown in Figure 7.3. Its terminus starts at 2802 m above sea level, located geographically at 36° 32'20"N and 74° 02'15"E. The extent coordinates of the Bad-e-Swat glacier are from 74° 02'15"E to 74°06'35"E and from 36°28'15"N to 36° 32'20"N. It was observed that the ice-covered areas are 11.76, 14.13, 11.52, 12.72 and 11.67 sq. km for the years 1988, 1994, 1999, 2014 and 2018 respectively.

However, the debris-covered areas were 0.48, 0.57, 1.007, 1.06 and 1.001 sq km for the years 1988, 1994, 1999, 2014 and 2018 respectively. Furthermore, the overall glacier changes are 12.24, 14.70, 12.52, 13.78 and 12.67 sq km for the years 1988, 1994, 1999, 2014 and 2018 respectively. The results revealed that, the overall ice-covered area for 30 years has been reduced in all years except 1988 that may be due to the climatic changes. However, from 1988 to 2018 the debris covered area has increased to 0.52 sq. km.



Figure 7.4 Bad-e-e Swat glacier and lake (25 October 2020)

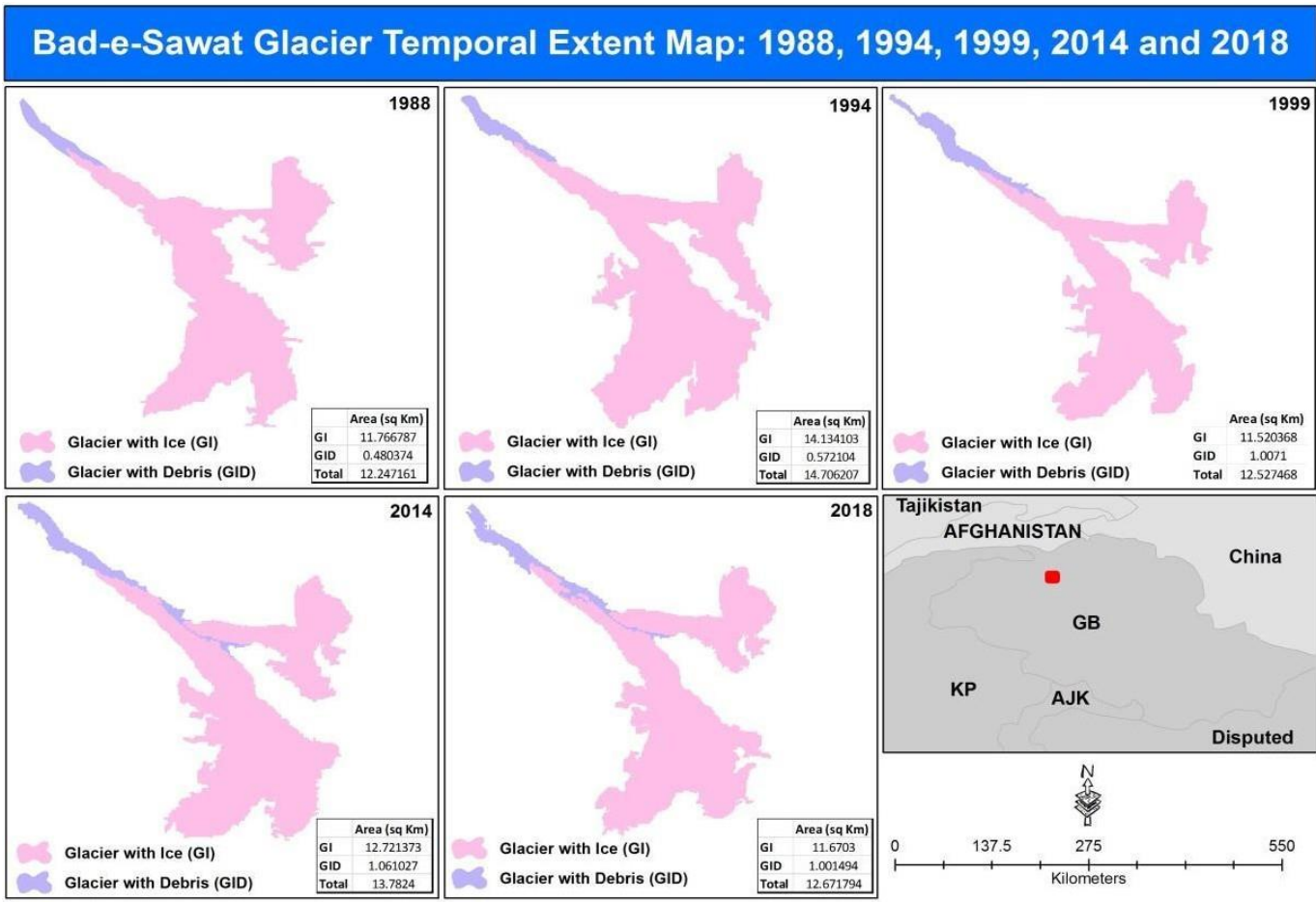


Figure 7.5 Bad-e-Swat glacier temporal glacier change extent for the years 1988, 1994, 1999, 2014 and 2018.

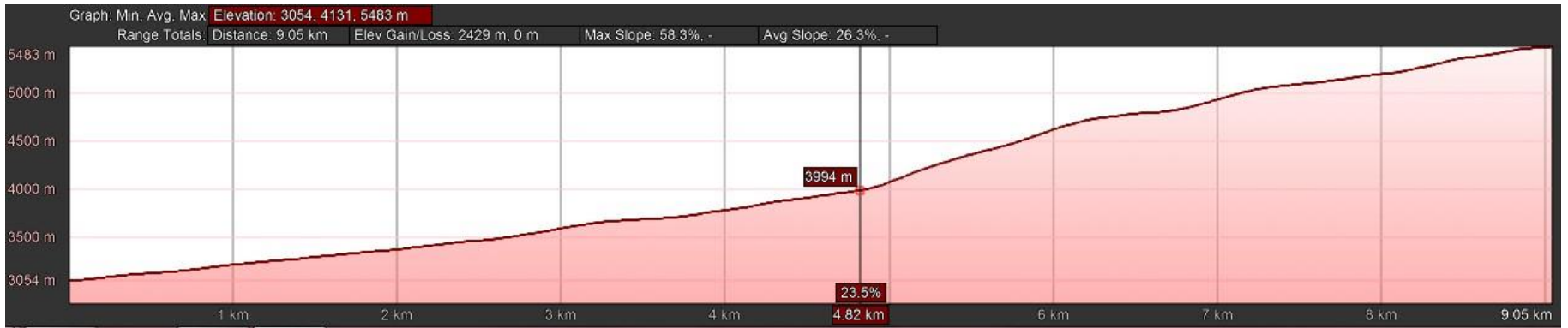


Figure 7.6 Elevation profile of Bad-e-Swat glacier

7.1.3 East Gammu Glacier

East Gammu glacier is one of the major glaciers in Gilgit watershed, as shown in Figure 7.5. It's terminus starts at 2800 masl, located geographically at $36^{\circ} 38'30''\text{N}$ and $73^{\circ} 24'10''\text{E}$. The extent coordinates of the East Gammu glacier are from $73^{\circ} 19'30''\text{E}$ to $73^{\circ} 24'10''\text{E}$ and from $36^{\circ} 35'10''\text{N}$ to $36^{\circ} 38'30''\text{N}$.

It was observed that the ice-covered areas are 9.02, 12.38, 11.47, 9.97 and 9.77 sq. km for the years 1988, 1994, 1999, 2014 and 2018 respectively. However, the debris-covered areas were 0.68, 0.63, 0.37, 0.47 and 0.32 sq. km for the years 1988, 1994, 1999, 2014 and 2018 respectively. Furthermore, the overall glacier changes are 9.71, 13.02, 11.84, 10.44 and 10.09 sq. km for the years 1988, 1994, 1999, 2014 and 2018 respectively. The results revealed that, the overall ice-covered area for 30 years has been reduced in all years except 1988 that may be due to the climatic changes. Moreover, from 1988 to 2018 the debris-covered area has decreased to 0.37 sq. km.



Figure 7.7 East Gammu glacier and lake (25 October 2020)

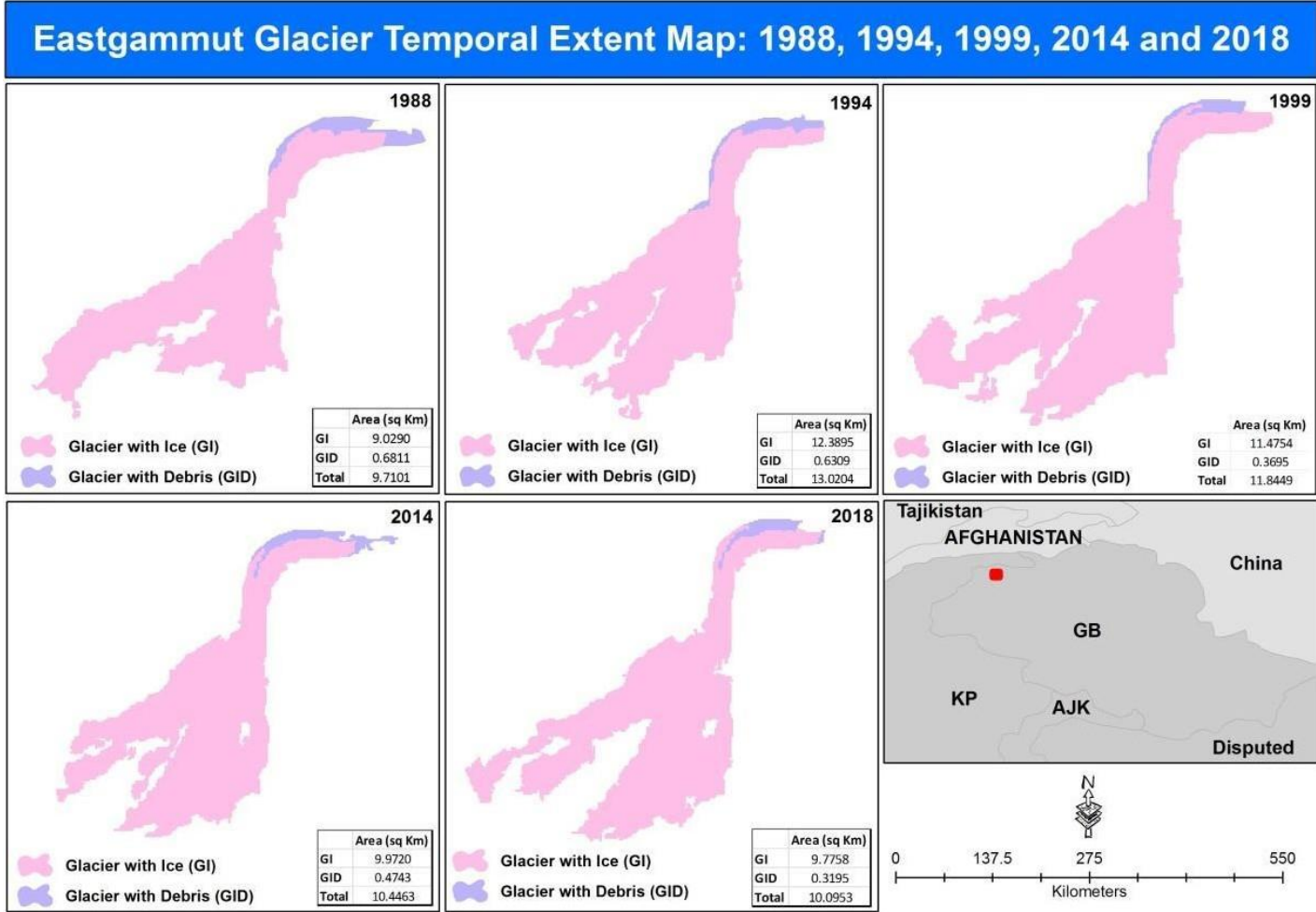


Figure 7.8 East Gammu glacier temporal changes for the years 1988, 1994, 1999, 2014 and 2018.

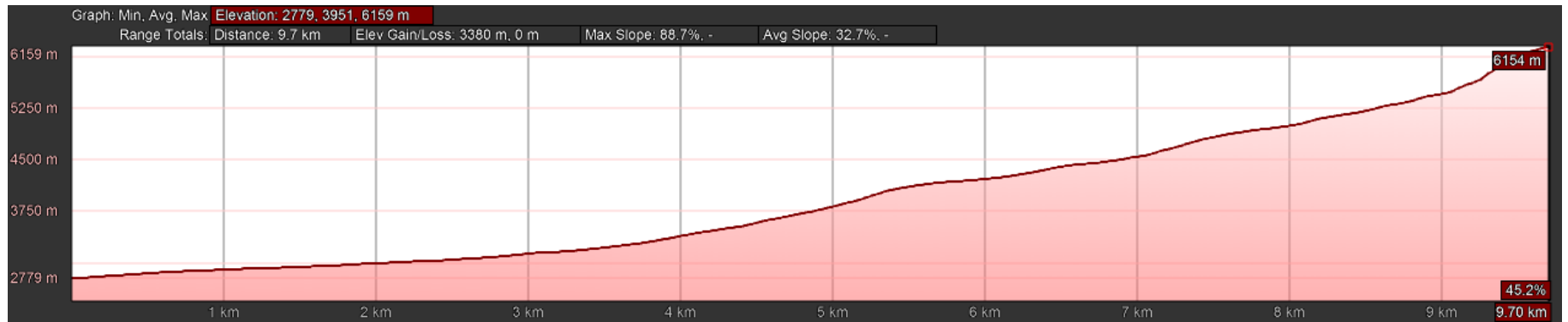


Figure 7.9 Elevation Profile of East Gammu glacier

7.1.4 Karamber Glacier

Karamber glacier is one of the biggest glaciers in Gilgit watershed as shown in Figure 7.8. Its terminus starts at 2850 meters above sea level, located geographically at $36^{\circ} 36'55''\text{N}$ and $74^{\circ} 04'10''\text{E}$. The extent coordinates of the Karamber glacier are from $74^{\circ}04'10''\text{E}$ to $74^{\circ}17'50''\text{E}$ and from $36^{\circ}33'45''\text{N}$ to $36^{\circ}40'22''\text{N}$. It was observed that the ice-covered areas are 57.92, 58.03, 51.36, 51.26 and 52.18 sq. km for the years 1988, 1994, 1999, 2014 and 2018 respectively.

However, the debris-covered areas were 5.33, 5.00, 8.00, 7.38 and 8.03 sq. km for the years 1988, 1994, 1999, 2014 and 2018 respectively. Furthermore, the overall glacier changes are 63.26, 63.04, 59.36, 58.60 and 61.21 sq. km for the years 1988, 1994, 1999, 2014 and 2018 respectively. The results revealed that, from 1988 to 2018 the overall ice-covered area has reduced to 4.74 sq. km. However, from 1988 to 2018 the overall debris-covered area has increased to 2.7 sq. km.



Figure 7.10 Karamber glacier (25 Oct 2020)

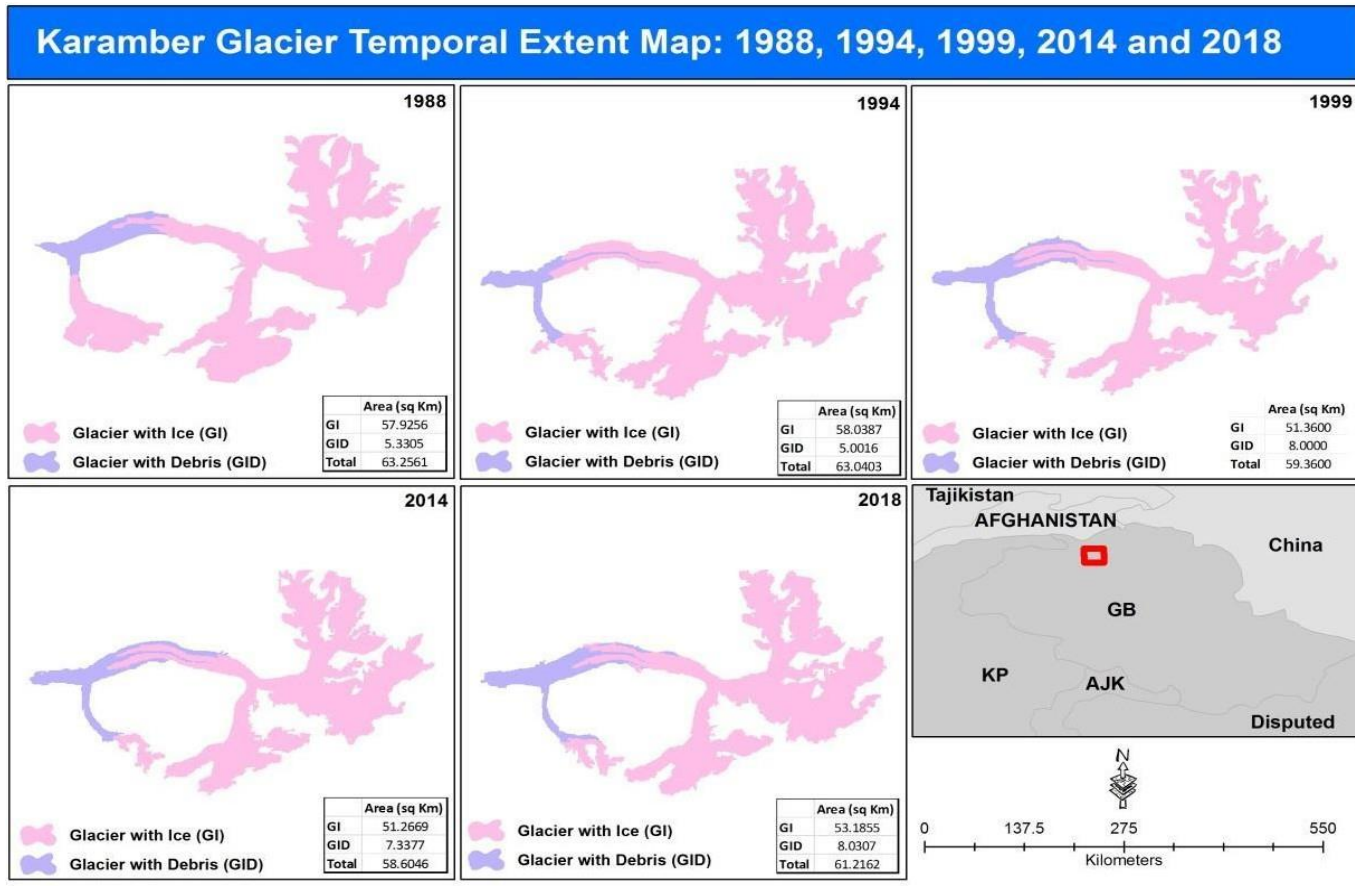


Figure 7.11 Karamber glacier temporal glacier change extent for the years 1988, 1994, 1999, 2014 and 2018.



Figure 7.12 Elevation Profile of Karamber glacier

7.1.5 Phakor Glacier

Phakor glacier is one of the major glaciers in Gilgit region as shown in Figure 7.9. Its terminus starts at 4010 masl, located geographically at $36^{\circ} 20'55''\text{N}$ and $74^{\circ} 00'05''\text{E}$. The extent coordinates of the Phakor glacier are from $73^{\circ}59'26''\text{E}$ to $74^{\circ}02'03''\text{E}$ and from $36^{\circ}18'02''\text{N}$ to $36^{\circ}20'55''\text{N}$. It was observed that the ice-covered areas are 7.27, 7.02, 6.89, 6.32 and 6.14 sq. km for the years 1988, 1994, 1999, 2014 and 2018 respectively. Moreover, no debris is found in the year of 1988 due non availability of imagery.

However, the debris-covered areas were 0.48, 0.16, 0.37 and 0.33 sq. km for the years 1994, 1999, 2014 and 2018 respectively. Furthermore, the overall glacier changes are 7.27, 7.50, 7.06, 6.70 and 6.47 sq. km for the years 1988, 1994, 1999, 2014 and 2018 respectively. The results revealed that, from 1988 to 2018 the overall ice-covered area has reduced to 1.17 sq. km. interestingly, debris covered area also reduced to 0.15 sq. km.



Figure 7.13 Phakor glacier (25 October 2020)

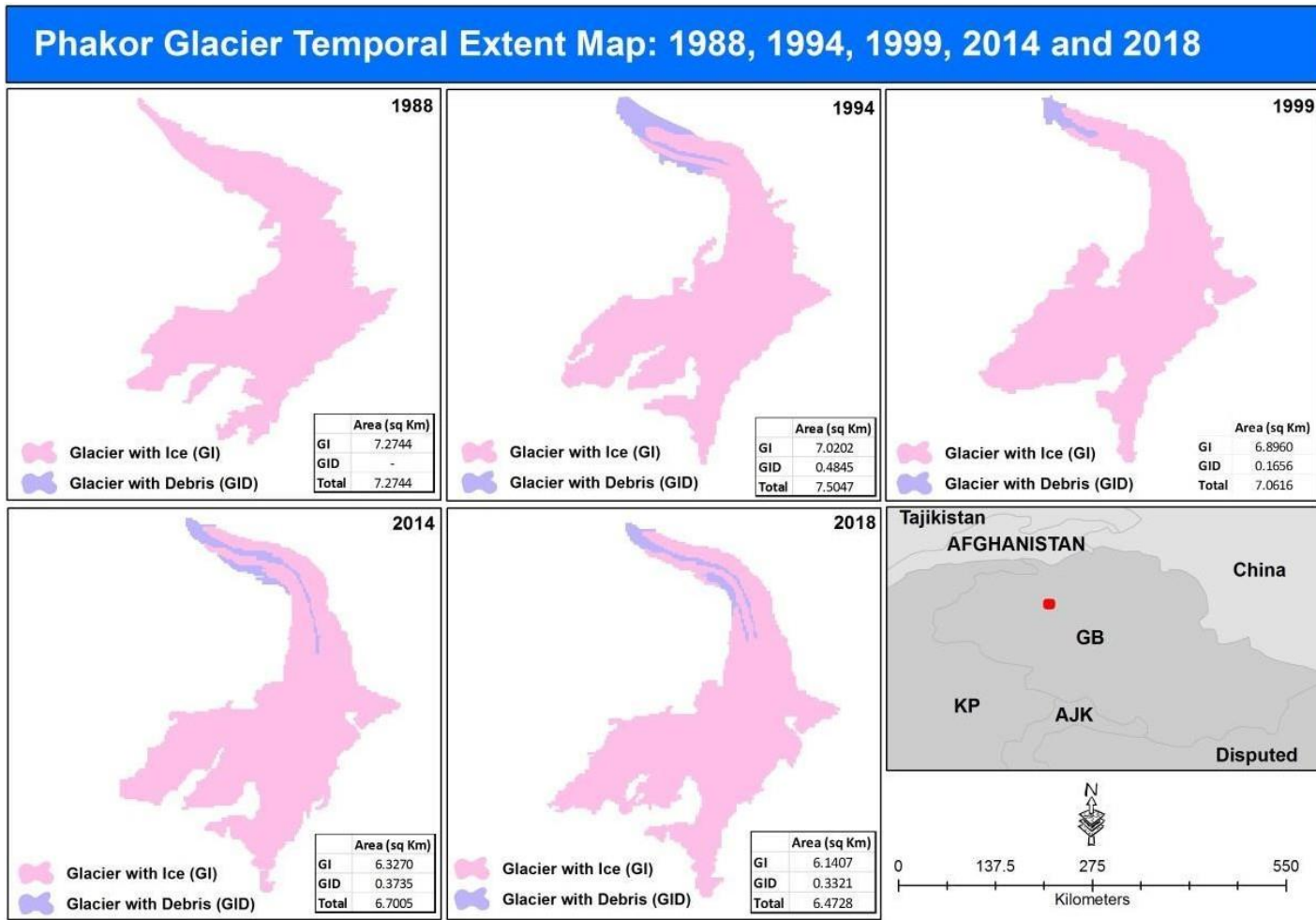


Figure 7.14 Phakor glacier temporal glacier change extent for the years 1988, 1994, 1999, 2014 and 2018.



Figure 7.4 Elevation profile of Phakor glacier

For many glaciological applications Glacier center lines play a crucial part. For example, center lines are significant for formative glacier length variations over time period, analyzing velocity fields estimating glacier volumes and one-dimensional modeling of glaciers. Also, glacier length, resulting from center lines, is a vital factor for glacier accounts. Center lines of each glacier are based on digital elevation model (DEM) and frameworks of specific glaciers. The center lines are splits into key outlets and major streams of a set of glaciers and classify them according to a geometry order starting from the glacier terminus. A natural way of identifying the glacier terminus is by taking out the lowermost glacier cell. The center lines of 5x glaciers are shown in the Figure 7.16.

Glacier Centre Lines - Top View

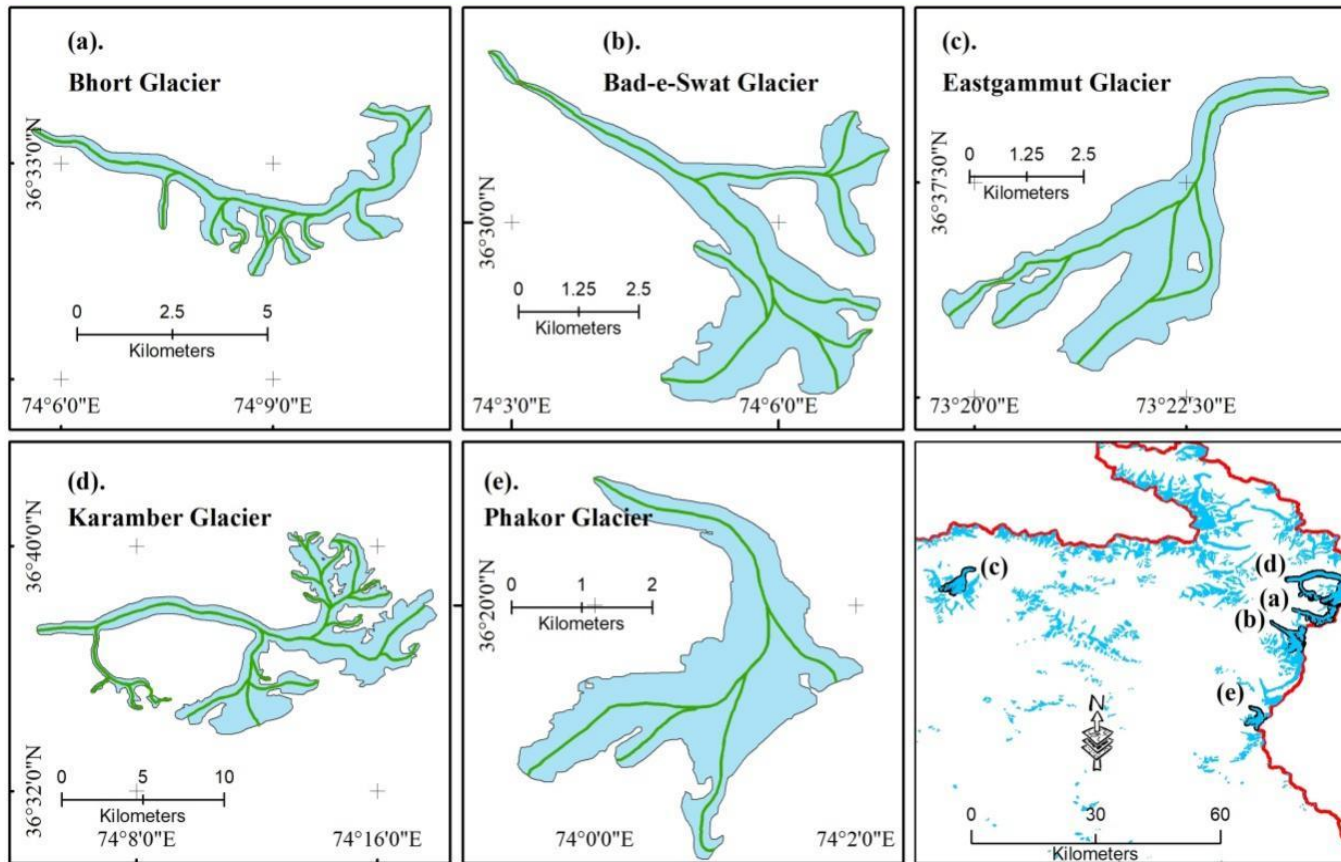


Figure 7.5 Centre lines of 5x glaciers

7.1.6 Tabular Presentation of Clean Ice Glacier Area

Table 7.1 Computed temporal glacier cover area (clean ice) in square kilometers

Glacier Name /Year	2018	2014	1999	1994	1988
Bhort	9.1962	9.6538	10.2054	10.8782	14.0261
Bad-e-Swat	11.6703	12.7214	11.5204	14.1341	11.7668
East-Gammu	9.7758	9.9720	11.4754	12.3895	9.0290
Karamber	53.1855	51.2669	51.3600	58.0387	57.9256
Phakor	6.1407	6.3270	6.8960	7.0202	7.2744

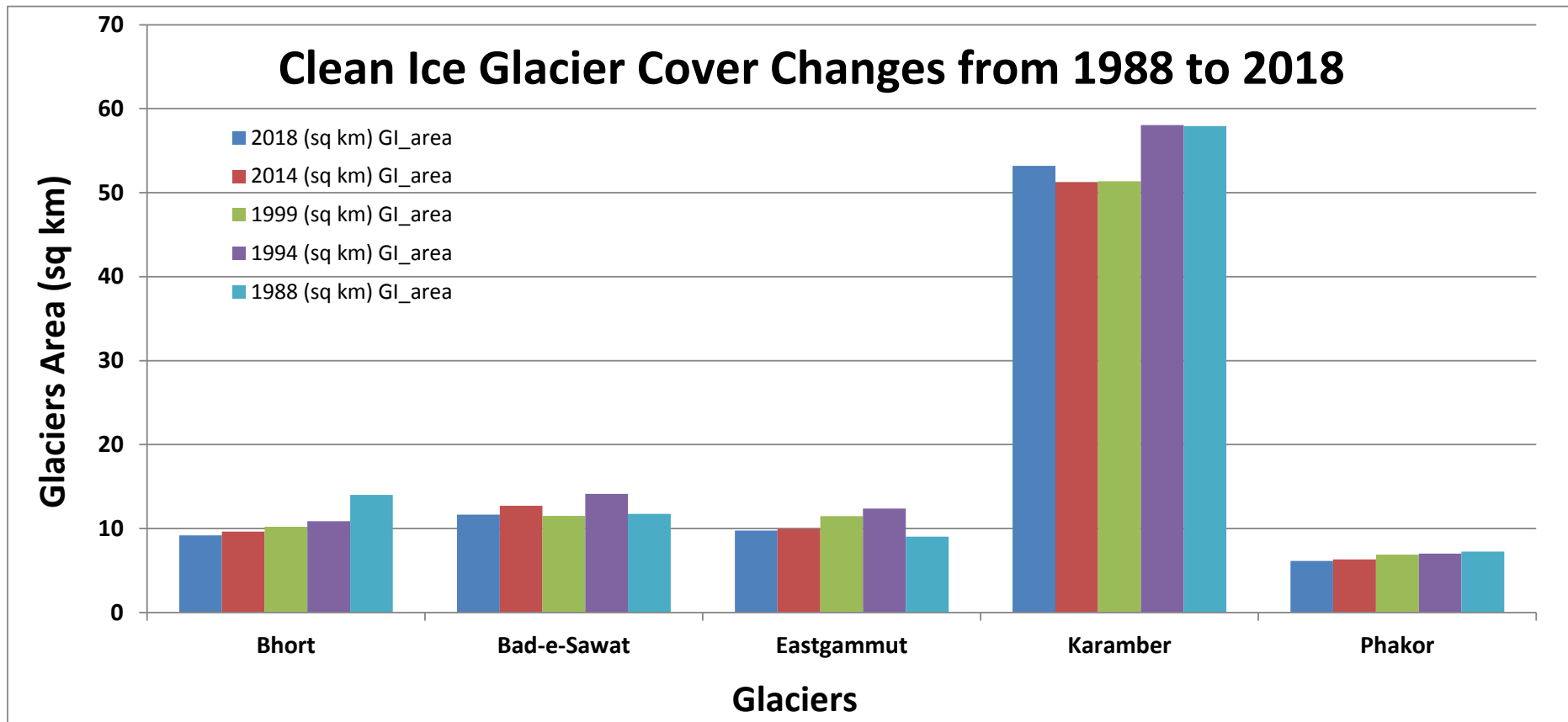


Figure: 7.17 Glacier-wise change trends for clean ice

7.1.7 Tabular Presentation of Debris Cover Glacier Area

Table 7.2 Computed temporal glacier cover area (debris cover) in square kilometers

Glacier Name /Year	2018 (sq km)	2014 (sq km)	1999 (sq km)	1994 (sq km)	1988 (sq km)
Bhort	2.4597	2.8685	2.7959	2.2377	0.9815
Bad-e-Swat	1.0015	1.0610	1.0071	0.5721	0.4804
East-Gammu	0.3195	0.4743	0.3695	0.6309	0.6811
Karamber	8.0307	7.3377	8.0000	5.0016	5.3305
Phakor	0.3321	0.3735	0.1656	0.4845	-

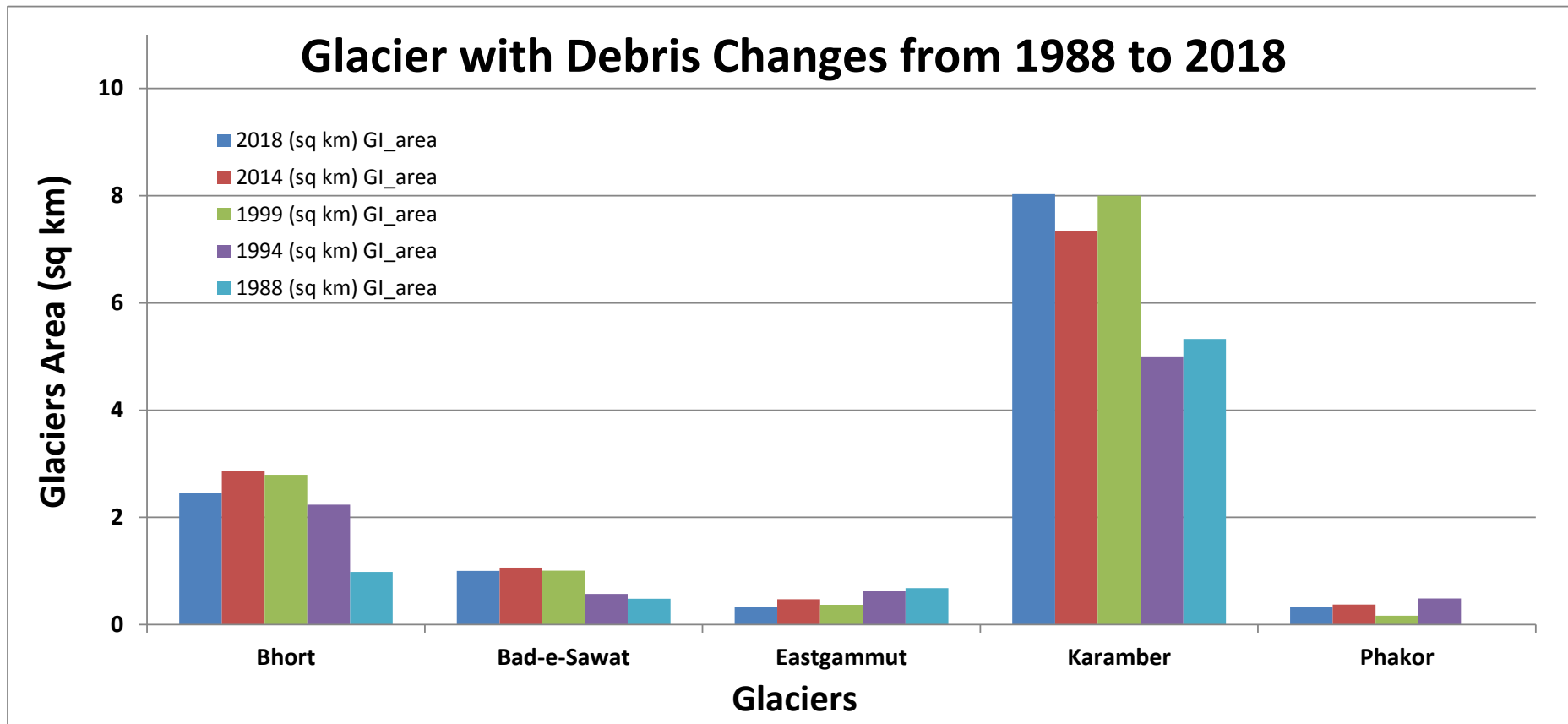


Figure: 7.18 Glacier-wise change trends for debris covered ice

7.1.8 Tabular Presentation of Glacier Cover Area (GCA)

Table 7.3 Computed temporal glacier cover area (combined) in square kilometers

Glacier Name /Year	2018 (sq. km)	2014 (sq. km)	1999 (sq. km)	1994 (sq.km)	1988 (sq. km)
Bhort	11.6559	12.5223	13.0013	13.1159	15.0076
Bad-e-Swat	12.6718	13.7824	12.5275	14.7062	12.247
East-Gammu	10.0953	10.4463	11.8449	13.0204	9.7101
Karamber	61.2162	58.6046	59.3600	63.0403	63.256
Phakor	6.4728	6.7005	7.061615	7.50469	7.2743

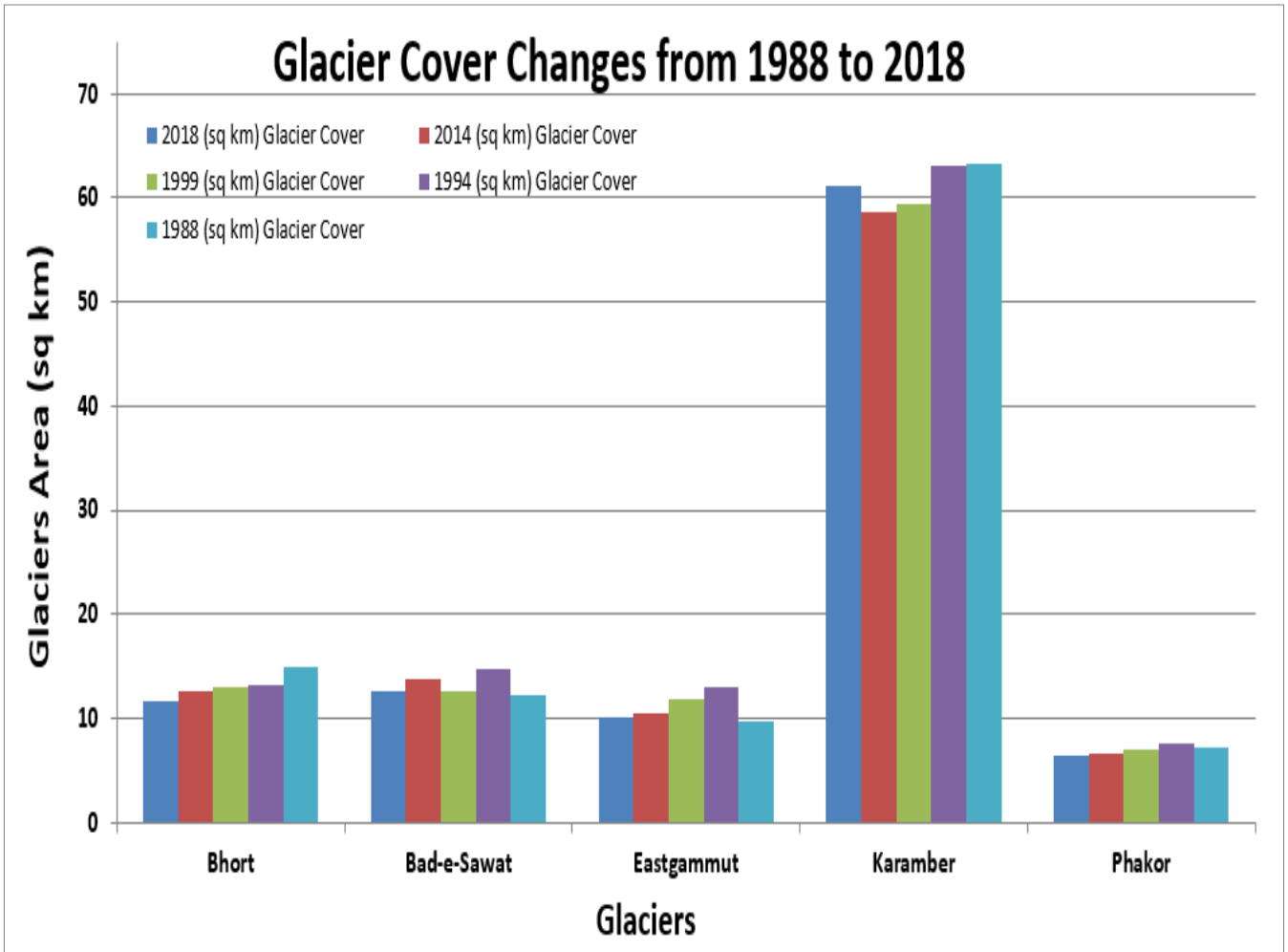


Figure: 7.6 Glacier-wise change trends combined ice and debris cover

The glacier mapping outlines the change detection for the five glaciers of the Gilgit watershed detecting that mostly glaciers are rather stable, specifically the under study glaciers in the Gilgit watershed. Some glaciers are receding but that is not at alarming rate if compare them with eastern Himalaya glaciers.

7.2 Accuracy Assessment on Mapping of Glaciers

7.2.1 Error Matrix

Any classification system used to comprehend a remotely sensed image will always produce some level of inaccuracy. The simplest technique to assess inaccuracies is to use a graphical inspection. We can see mistakes and estimate their size by equating the image with the results of its interpretation. However, numerical methods of valuation must be used in order to obtain a reliable accuracy assessment.

A confusion matrix (or error matrix) is a common quantitative tool for determining picture categorization accuracy. It's a table that demonstrates in what way the categorization outcome and a reference image resemble. The ground veracity data gathered during the field survey was used to build the error matrix. These files contain (a) cartographic data and (b) ground survey findings acquired using a GPS device. Table 7.4 shows the error matrix that was computed. The ground truth classes are in the table's columns, and the classes of the categorized image to be assessed are in the table's rows. The number of pixels for all conceivable correlations between the ground truth and the categorized image are shown in the table's cells.

Table 7.4 Error matrix

Class	Glc	Debris	Water bodies	Other (rocks etc)	Row Total	User Accuracy (UsAc) [on a scale of 0 – 1]
Glacier Cover	133	6	0	3	142	0.937
Debris Cover	8	35	0	0	43	0.814
Water Bodies	0	0	20	1	21	0.952
Other (rocks etc)	4	0	2	38	44	0.864
Col Total	145	41	22	42	250	
Producer Accuracy (PrAc) [on a scale of 0 – 1]	0.917	0.854	0.909	0.905		

The matrix's diagonal essentials have been shaded and highlighted. The number of accurately detected pixels is contained in diagonal cells. The entire number of pixels has been divided by the sum of these pixels to get the overall classification accuracy 'p_a', which is 87.50 percent.

7.2.2 Overall Accuracy

The overall accuracy is calculated by apportioning the diagonal sum with the entire number of data points.

$$\text{Overall Accuracy} = \frac{\text{Diagonal Sum}}{\text{Total number of Sample Points}}$$

$$\text{Overall Accuracy} = \frac{226}{250}$$

$$\text{Overall Accuracy} = 0.904$$

$$\text{Overall Accuracy} = 90.4\%$$

7.2.3 Kappa Coefficient

The classification findings similarity to random values is gauged by the Kappa coefficient. Its possible values fall between 0 and 1. If the kappa coefficient is 0, the

reference image and the classified image have no covenant at all. If the Kappa coefficient is 1, the categorize image and the real image are perfect and on same position. As a consequence, the classification is better, the greater the Kappa coefficient.

The accuracy of class identification has been tested in addition to overall accuracy. Classification mistakes are found in the non-diagonal cells of the matrix, which are instances where the reference picture and the classified image do not match.

Under estimation (omission errors, omission) and over estimation (commission errors, commission) are two forms of errors. Over estimation errors occur when a classification algorithm assign pixels to a class that do not belong to it. The number of pixels incorrectly assigned to a class can be detected in column cells above and below the main diagonal of the class. The totality of these cell pixels is the complete value of the class over- estimation, which is equal to 12 pixels in the first column on glacier class. Moreover, if we do division this amount by the total number of class pixels, the relative over-estimation error (OvEr) is obtained. For class glacier denoted by G' in Table 7.4:

$$\text{OvEr} = (bG + cG + dG) / \sum G$$

$$\text{OvEr} = (4 + 0 + 8) / 145$$

$$\text{OvEr} \approx 0.083$$

The amount of over estimation mistakes is also defined by the Producer's Accuracy (PrAc) sign. It's the total number of pixels in the reference image separated

by the number of accurately recognized pixels. Table 7.4 shows the class 'glacier,' designated by the letter 'G.'

$$\text{PrAc} = a_G / \sum G$$

$$\text{PrAc} = 133 / 145$$

$$\text{PrAc} \approx 0.917$$

OvEr and PrAc values are connected:

$$\text{PrAc} = 1 - \text{OvEr}$$

Pixels that fit in one class are encompassed in other classes, resulting in under-estimation mistakes for any class. The number of missed pixels is established in the row cells to the left and right of the main diagonal in the error matrix. Omission errors are highlighted in class G. The absolute (total) value of the class omission is the sum of these cells.

In addition, we can calculate the relative (comparative) omission error (OmEr) by dividing this total by the total number of class pixels in the classified image:

$$\text{OmEr} = (a_D + a_W + a_O) / \sum a$$

$$\text{OmEr} = (6 + 0 + 3) / 142$$

$$\text{OmEr} \approx 0.063$$

One more index that processes the quantity of omission mistakes is the user's accuracy (UsAc) (under-estimation). It's the number of successfully identified pixels in a class divided by the total number of pixels in the categorized image for that class.

Table 7.4 gives the following values for class G:

$$UsAc = aG / \sum G$$

$$UsAc = 133 / 142$$

$$UsAc \approx 0.937$$

OmEr and UsAc values are connected:

$$UsAc = 1 - Om$$

The overall accuracy of classification is represented by the Kappa Coefficient by including the values of OvEr and OmEr.

It is vital to highlight that the accuracy values of the producer and user cannot be utilized separately as a measure of categorization accuracy because these values do not represent the entire picture. Therefore, the user accuracy and producer accuracy are combined together into a random accuracy value (also termed as chance agreement value by some researchers). The random accuracy value is calculated to be 0.395.

Finally, the kappa coefficient is calculated from the following relationship.

$$Kappa\ Coefficient = \frac{Overall\ Accuracy - Random\ Accuracy}{1 - Random\ Accuracy}$$

$$Kappa\ Coefficient = \frac{0.904 - 0.395}{1 - 0.395}$$

$$Kappa\ Coefficient = 0.8414$$

$$Kappa\ Coefficient = 84.14\%$$

To recap the technique, the 250 ground truth reference data points were obtained utilizing the error matrix approach and stratified random sampling. Tables 7.5, 7.6, 7.7,

7.8, and 7.9 contain a complete list of all the points. For category matching, these ground truth locations were superimposed on the land use land cover map. According to Maitima et.al, (2009) methodology, the created error matrix and associated ground truth category membership are placed in rows, while categorized cover type is placed in columns.

Correct values fall along the matrix's primary diagonal when it is arranged this manner (Morgado et al., 2012). If the reported values are wrongly classified then classified values are incorrectly placed in the off diagonal sections of the matrix, making it obvious which class they belong to (Mundia and Murayama 2009).

Table 7.5 List of Randomly Sampled Ground Truth Reference Data Points for Bhort Glacier

Sampling point	Name	Lat, Long and elevation		
Point Nr.01	Bhort Glacier	36°33'17.06"N	74° 9'52.31"E	5685m
Point Nr.02	Bhort Glacier	36°33'4.27"N	74°10'9.30"E	5346m
Point Nr.03	Bhort Glacier	36°32'57.13"N	74° 9'59.43"E	5144m
Point Nr.04	Bhort Glacier	36°33'11.30"N	74°10'8.58"E	5553m
Point Nr.05	Bhort Glacier	36°32'47.63"N	74° 9'53.32"E	4864m
Point Nr.06	Bhort Glacier	36°32'32.79"N	74° 9'44.28"E	4710m
Point Nr.07	Bhort Glacier	36°32'28.84"N	74° 9'29.24"E	4597m
Point Nr.08	Bhort Glacier	36°32'41.02"N	74° 8'28.99"E	4108m
Point Nr.09	Bhort Glacier	36°32'29.38"N	74° 9'19.90"E	4519m
Point Nr.10	Bhort Glacier	36°32'52.46"N	74° 8'3.47"E	3894m
Point Nr.11	Bhort Glacier	36°32'39.20"N	74° 9'35.98"E	4915m
Point Nr.12	Bhort Glacier	36°33'9.21"N	74° 7'27.92"E	3680m
Point Nr.13	Bhort Glacier	36°33'14.75"N	74° 7'2.66"E	3646m
Point Nr.14	Bhort Glacier	36°33'15.97"N	74° 6'51.03"E	3614m
Point Nr.15	Bhort Glacier	36°33'23.48"N	74° 6'20.76"E	3504m
Point Nr.16	Bhort Glacier	36°33'26.05"N	74° 6'3.73"E	3466m
Point Nr.17	Bhort Glacier	36°33'28.82"N	74° 5'48.22"E	3368m

Point Nr.18	Bhort Glacier	36°33'34.51"N	74° 5'33.87"E	3310m
Point Nr.19	Bhort Glacier	36°33'39.17"N	74° 5'21.72"E	3233m
Point Nr.20	Bhort Glacier	36°33'47.08"N	74° 4'51.95"E	3076m
Point Nr.21	Bhort Glacier	36°33'34.23"N	74° 5'8.24"E	3189m
Point Nr.22	Bhort Glacier	36°33'23.22"N	74° 5'16.54"E	3246m
Point Nr.23	Bhort Glacier	36°32'56.86"N	74° 6'11.76"E	3667m
Point Nr.24	Bhort Glacier	36°32'39.55"N	74° 6'22.81"E	3784m
Point Nr.25	Bhort Glacier	36°32'13.87"N	74° 6'20.06"E	4121m
Point Nr.26	Bhort Glacier	36°32'56.61"N	74° 4'46.99"E	3857m
Point Nr.27	Bhort Glacier	36°32'36.63"N	74° 5'17.59"E	4076m
Point Nr.28	Bhort Glacier	36°32'8.16"N	74° 4'45.97"E	4883m
Point Nr.29	Bhort Glacier	36°31'39.35"N	74° 5'25.75"E	4969m
Point Nr.30	Bhort Glacier	36°31'29.25"N	74° 5'56.97"E	5073m
Point Nr.31	Bhort Glacier	36°31'43.98"N	74° 6'6.32"E	4651m
Point Nr.32	Bhort Glacier	36°31'36.16"N	74° 6'31.79"E	5001m
Point Nr.33	Bhort Glacier	36°31'45.42"N	74° 6'47.82"E	4940m
Point Nr.34	Bhort Glacier	36°31'52.05"N	74° 6'40.84"E	4630m
Point Nr.35	Bhort Glacier	36°31'58.74"N	74° 7'14.23"E	4781m
Point Nr.36	Bhort Glacier	36°31'41.70"N	74° 7'6.61"E	5251m
Point Nr.37	Bhort Glacier	36°32'3.20"N	74° 7'1.07"E	4600m

Point Nr.38	Bhort Glacier	36°31'35.84"N	74° 6'58.85"E	5231m
Point Nr.39	Bhort Glacier	36°32'13.88"N	74° 7'46.72"E	4301m
Point Nr.40	Bhort Glacier	36°31'47.97"N	74° 7'39.75"E	5030m
Point Nr.41	Bhort Glacier	36°31'36.55"N	74° 7'22.38"E	5420m
Point Nr.42	Bhort Glacier	36°31'23.87"N	74° 6'49.31"E	5391m
Point Nr.43	Bhort Glacier	36°32'36.55"N	74° 5'54.40"E	3883m
Point Nr.44	Bhort Glacier	36°32'23.58"N	74° 5'43.36"E	4104m
Point Nr.45	Bhort Glacier	36°33'14.57"N	74° 7'49.13"E	4017m
Point Nr.46	Bhort Glacier	36°33'8.36"N	74° 8'13.14"E	4442m
Point Nr.47	Bhort Glacier	36°33'20.57"N	74° 8'2.40"E	4357m
Point Nr.48	Bhort Glacier	36°33'29.23"N	74° 7'33.61"E	3961m
Point Nr.49	Bhort Glacier	36°33'32.73"N	74° 7'16.43"E	3842m
Point Nr.50	Bhort Glacier	36°33'46.22"N	74°11'39.72"E	5498m

Table 7.6 List of Randomly Sampled Ground Truth Reference Data Points for Bad e Swat Glacier

Sr	Glacier name	Latitude	Longitude	Elev
Point Nr1	Bad e Swat Glacier	36°31'0.47"N	74° 5'47.86"E	4894m
Point Nr.2	Bad e Swat Glacier	36°31'21.49"N	74° 5'21.16"E	4987m
Point Nr.3	Bad e Swat Glacier	36°29'46.96"N	74° 4'59.45"E	4549m
Point Nr.4	Bad e Swat Glacier	36°30'27.26"N	74° 3'3.66"E	4406m
Point Nr.5	Bad e Swat Glacier	36°30'46.31"N	74° 5'57.12"E	4788m
Point Nr.6	Bad e Swat Glacier	36°31'10.32"N	74° 5'0.20"E	4412m
Point Nr.7	Bad e Swat Glacier	36°30'55.42"N	74° 6'21.90"E	5203m
Point Nr.8	Bad e Swat Glacier	36°31'31.19"N	74° 5'3.09"E	4767m
Point Nr.9	Bad e Swat Glacier	36°29'49.01"N	74° 4'20.03"E	4510m
Point Nr.10	Bad e Swat Glacier	36°29'58.83"N	74° 2'39.99"E	4731m
Point Nr.11	Bad e Swat Glacier	36°30'35.73"N	74° 2'47.27"E	4257m
Point Nr.12	Bad e Swat Glacier	36°31'27.01"N	74° 4'35.78"E	4286m
Point Nr.13	Bad e Swat Glacier	36°31'47.30"N	74° 4'8.98"E	4094m
Point Nr.14	Bad e Swat Glacier	36°32'1.77"N	74° 4'34.34"E	4670m
Point Nr.15	Bad e Swat Glacier	36°32'1.18"N	74° 4'16.68"E	4430m
Point Nr.16	Bad e Swat Glacier	36°31'11.66"N	74° 4'22.39"E	3870m
Point Nr.17	Bad e Swat Glacier	36°31'13.54"N	74° 4'0.96"E	3527m

Point Nr.18	Bad e Swat Glacier	36°30'54.44"N	74° 2'21.13"E	4335m
Point Nr.19	Bad e Swat Glacier	36°31'12.53"N	74° 2'21.24"E	3883m
Point Nr.20	Bad e Swat Glacier	36°30'50.82"N	74° 2'48.65"E	3987m
Point Nr.21	Bad e Swat Glacier	36°31'1.04"N	74° 2'33.67"E	3888m
Point Nr.22	Bad e Swat Glacier	36°31'9.82"N	74° 2'59.01"E	3684m
Point Nr.23	Bad e Swat Glacier	36°30'55.23"N	74° 3'17.29"E	3826m
Point Nr.24	Bad e Swat Glacier	36°31'16.11"N	74° 2'41.71"E	3656m
Point Nr.25	Bad e Swat Glacier	36°31'6.26"N	74° 2'4.83"E	4213m
Point Nr.26	Bad e Swat Glacier	36°31'24.72"N	74° 2'11.02"E	3712m
Point Nr.27	Bad e Swat Glacier	36°31'36.18"N	74° 1'59.72"E	3580m
Point Nr.28	Bad e Swat Glacier	36°31'34.96"N	74° 2'30.26"E	3249m
Point Nr.29	Bad e Swat Glacier	36°31'48.13"N	74° 2'15.05"E	3145m
Point Nr.30	Bad e Swat Glacier	36°31'56.46"N	74° 1'57.08"E	3086m
Point Nr.31	Bad e Swat Glacier	36°31'26.41"N	74° 4'18.03"E	3985m
Point Nr.32	Bad e Swat Glacier	36°31'37.76"N	74° 3'59.64"E	3772m
Point Nr.33	Bad e Swat Glacier	36°31'57.57"N	74° 3'54.20"E	3988m
Point Nr.34	Bad e Swat Glacier	36°32'4.09"N	74° 3'38.26"E	3795m
Point Nr.35	Bad e Swat Glacier	36°31'42.29"N	74° 3'44.92"E	3553m
Point Nr.36	Bad e Swat Glacier	36°32'1.24"N	74° 3'6.86"E	3271m
Point Nr.37	Bad e Swat Glacier	36°32'5.63"N	74° 2'51.00"E	3131m

Point Nr.38	Bad e Swat Glacier	36°32'7.45"N	74° 3'0.88"E	3321m
Point Nr.39	Bad e Swat Glacier	36°32'13.64"N	74° 3'19.68"E	3598m
Point Nr.40	Bad e Swat Glacier	36°32'17.01"N	74° 3'3.43"E	3460m
Point Nr.41	Bad e Swat Glacier	36°30'55.42"N	74° 5'26.31"E	4512m
Point Nr.42	Bad e Swat Glacier	36°32'16.76"N	74° 2'50.50"E	3271m
Point Nr.43	Bad e Swat Glacier	36°32'16.45"N	74° 2'33.96"E	2984m
Point Nr.44	Bad e Swat Glacier	36°32'0.10"N	74° 2'28.02"E	2907m
Point Nr.45	Bad e Swat Glacier	36°32'8.45"N	74° 2'13.18"E	2802m
Point Nr.46	Bad e Swat Glacier	36°32'15.08"N	74° 2'2.25"E	2736m
Point Nr.47	Bad e Swat Glacier	36°32'19.25"N	74° 1'50.99"E	2679m
Point Nr.48	Bad e Swat Glacier	36°31'52.31"N	74° 2'56.53"E	3098m
Point Nr.49	Bad e Swat Glacier	36°32'5.85"N	74° 2'32.12"E	2925m
Point Nr.50	Bad e Swat Glacier	36°32'23.87"N	74° 2'1.73"E	2748

Table 7.7 List of Randomly Sampled Ground Truth Reference Data Points for East Gammu Glacier

Point Nr1	East Gammu Glacier	36°35'59.85"N	73°19'56.48"E	6110m
Point Nr.2	East Gammu Glacier	36°36'5.36"N	73°20'12.19"E	5558m
Point Nr.3	East Gammu Glacier	36°36'30.11"N	73°20'18.59"E	5479m
Point Nr.4	East Gammu Glacier	36°35'47.35"N	73°20'3.14"E	5614m
Point Nr.5	East Gammu Glacier	36°36'8.90"N	73°20'31.27"E	5223m
Point Nr.6	East Gammu Glacier	36°36'19.22"N	73°20'58.15"E	4863m
Point Nr.7	East Gammu Glacier	36°35'29.06"N	73°20'42.80"E	6022m
Point Nr.8	East Gammu Glacier	36°35'39.70"N	73°20'57.93"E	5448m
Point Nr.9	East Gammu Glacier	36°36'50.36"N	73°21'0.83"E	4677m
Point Nr.10	East Gammu Glacier	36°35'52.29"N	73°21'2.68"E	5500m
Point Nr.11	East Gammu Glacier	36°35'45.03"N	73°21'7.38"E	5296m
Point Nr.12	East Gammu Glacier	36°35'34.34"N	73°21'31.38"E	5166m
Point Nr.13	East Gammu Glacier	36°36'0.85"N	73°21'25.18"E	4970m
Point Nr.14	East Gammu Glacier	36°35'35.38"N	73°21'13.29"E	5177m
Point Nr.15	East Gammu Glacier	36°35'12.52"N	73°21'22.87"E	5880m
Point Nr.16	East Gammu Glacier	36°35'17.16"N	73°20'55.12"E	5943m
Point Nr.17	East Gammu Glacier	36°35'6.21"N	73°22'18.46"E	6091m

Point Nr.18	East Gammu Glacier	36°35'41.46"N	73°21'43.47"E	5093m
Point Nr.19	East Gammu Glacier	36°35'41.12"N	73°22'3.23"E	5013m
Point Nr.20	East Gammu Glacier	36°35'15.29"N	73°22'25.27"E	5690m
Point Nr.21	East Gammu Glacier	36°36'38.96"N	73°21'26.19"E	4468m
Point Nr.22	East Gammu Glacier	36°35'41.74"N	73°22'42.16"E	4773m
Point Nr.23	East Gammu Glacier	36°35'29.64"N	73°22'32.88"E	5332m
Point Nr.24	East Gammu Glacier	36°36'13.87"N	73°21'49.16"E	4570m
Point Nr.25	East Gammu Glacier	36°36'7.72"N	73°22'12.35"E	4522m
Point Nr.26	East Gammu Glacier	36°36'49.27"N	73°21'51.53"E	4222m
Point Nr.27	East Gammu Glacier	36°36'41.64"N	73°22'10.90"E	4202m
Point Nr.28	East Gammu Glacier	36°36'20.47"N	73°22'27.94"E	4381m
Point Nr.29	East Gammu Glacier	36°36'1.64"N	73°22'44.65"E	4600m
Point Nr.30	East Gammu Glacier	36°37'18.54"N	73°22'3.12"E	3840m
Point Nr.31	East Gammu Glacier	36°36'50.69"N	73°22'21.49"E	4032m
Point Nr.32	East Gammu Glacier	36°36'35.04"N	73°21'14.89"E	4631m
Point Nr.33	East Gammu Glacier	36°37'23.78"N	73°22'14.05"E	3639m
Point Nr.34	East Gammu Glacier	36°36'52.80"N	73°22'31.37"E	3650m
Point Nr.35	East Gammu Glacier	36°36'27.52"N	73°22'43.10"E	4198m
Point Nr.36	East Gammu Glacier	36°36'33.03"N	73°22'52.98"E	4195m
Point Nr.37	East Gammu Glacier	36°36'29.84"N	73°20'33.64"E	5059m

Point Nr.38	East Gammu Glacier	36°37'6.36"N	73°22'38.32"E	3555m
Point Nr.39	East Gammu Glacier	36°36'9.26"N	73°20'3.39"E	4142m
Point Nr.40	East Gammu Glacier	36°37'15.53"N	73°22'42.92"E	3506m
Point Nr.41	East Gammu Glacier	36°37'51.28"N	73°22'43.40"E	3172m
Point Nr.42	East Gammu Glacier	36°38'15.79"N	73°23'1.21"E	3006m
Point Nr.43	East Gammu Glacier	36°36'6.96"N	73°21'37.11"E	4692m
Point Nr.44	East Gammu Glacier	36°38'24.93"N	73°23'12.85"E	2960m
Point Nr.45	East Gammu Glacier	36°38'27.19"N	73°23'22.13"E	2944m
Point Nr.46	East Gammu Glacier	36°35'0.14"N	73°22'24.12"E	6110m
Point Nr.47	East Gammu Glacier	36°35'55.37"N	73°22'8.90"E	4792m
Point Nr.48	East Gammu Glacier	36°35'40.47"N	73°20'46.96"E	5930m
Point Nr.49	East Gammu Glacier	36°36'29.05"N	73°24'55.06"E	2873m
Point Nr.50	East Gammu Glacier	36°38'30.06"N	73°23'54.01"E	2861m

Table 7.8 List of Randomly Sampled Ground Truth Reference Data Points for Karamber Glacier

Point Nr. 1	Karamber Glacier	36°34'18.54"N	74° 9'17.25"E	5012m
Point Nr.2	Karamber Glacier	36°34'7.79"N	74° 9'50.55"E	5155m
Point Nr.3	Karamber Glacier	36°34'1.43"N	74°10'31.40"E	4944m
Point Nr.4	Karamber Glacier	36°34'13.11"N	74°10'55.44"E	4821m
Point Nr.5	Karamber Glacier	36°33'46.22"N	74°11'39.72"E	3934m
Point Nr.6	Karamber Glacier	36°34'35.51"N	74°10'27.96"E	4898m
Point Nr.7	Karamber Glacier	36°34'19.05"N	74°11'23.25"E	4885m
Point Nr.8	Karamber Glacier	36°35'1.46"N	74°11'39.69"E	4514m
Point Nr.9	Karamber Glacier	36°35'25.71"N	74°11'30.72"E	4446m
Point Nr.10	Karamber Glacier	36°34'58.24"N	74°12'4.68"E	4658m
Point Nr.11	Karamber Glacier	36°36'0.87"N	74°11'50.60"E	4357m
Point Nr.12	Karamber Glacier	36°35'14.82"N	74°10'25.80"E	4746m
Point Nr.13	Karamber Glacier	36°35'27.93"N	74° 9'59.62"E	5250m
Point Nr.14	Karamber Glacier	36°35'28.81"N	74°12'17.78"E	4849m
Point Nr.15	Karamber Glacier	36°35'5.20"N	74°12'39.78"E	5091m
Point Nr.16	Karamber Glacier	36°35'25.36"N	74°11'56.93"E	4617m
Point Nr.17	Karamber Glacier	36°35'34.23"N	74°11'42.15"E	4429m

Point Nr.18	Karamber Glacier	36°35'33.90"N	74°12'39.77"E	5204m
Point Nr.19	Karamber Glacier	36°35'31.61"N	74°12'34.65"E	5076m
Point Nr.20	Karamber Glacier	36°35'18.17"N	74°12'51.99"E	5016m
Point Nr.21	Karamber Glacier	36°35'20.30"N	74°12'38.73"E	5061m
Point Nr.22	Karamber Glacier	36°35'13.71"N	74°12'35.95"E	5025m
Point Nr.23	Karamber Glacier	36°35'6.68"N	74°10'45.43"E	4547m
Point Nr.24	Karamber Glacier	36°36'1.01"N	74° 9'40.21"E	5928m
Point Nr.25	Karamber Glacier	36°35'59.29"N	74° 9'53.42"E	5478m
Point Nr.26	Karamber Glacier	36°35'59.54"N	74°10'8.35"E	5137m
Point Nr.27	Karamber Glacier	36°35'34.10"N	74°10'44.49"E	4631m
Point Nr.28	Karamber Glacier	36°35'20.29"N	74°11'3.49"E	4856m
Point Nr.29	Karamber Glacier	36°34'36.97"N	74° 9'44.61"E	4816m
Point Nr.30	Karamber Glacier	36°35'49.36"N	74°11'34.38"E	4387m
Point Nr.31	Karamber Glacier	36°36'15.39"N	74°11'40.47"E	4294m
Point Nr.32	Karamber Glacier	36°36'44.74"N	74°12'14.05"E	4115m
Point Nr.33	Karamber Glacier	36°36'42.92"N	74°12'2.24"E	4103m
Point Nr.34	Karamber Glacier	36°37'4.99"N	74°13'9.39"E	4218m
Point Nr.35	Karamber Glacier	36°35'33.48"N	74°13'20.73"E	5479m
Point Nr.36	Karamber Glacier	36°37'37.97"N	74°14'19.28"E	4233m
Point Nr.37	Karamber Glacier	36°37'13.81"N	74°16'46.23"E	5082m

Point Nr.38	Karamber Glacier	36°36'44.71"N	74°15'51.89"E	4979m
Point Nr.39	Karamber Glacier	36°37'3.99"N	74°15'24.91"E	5065m
Point Nr.40	Karamber Glacier	36°37'50.03"N	74°18'27.05"E	6073m
Point Nr.41	Karamber Glacier	36°37'57.56"N	74°17'57.34"E	5639m
Point Nr.42	Karamber Glacier	36°36'17.93"N	74°16'19.18"E	4982m
Point Nr.43	Karamber Glacier	36°40'14.00"N	74°13'18.21"E	5825m
Point Nr.44	Karamber Glacier	36°40'7.76"N	74°14'48.82"E	5694m
Point Nr.45	Karamber Glacier	36°39'54.81"N	74°13'57.85"E	5230m
Point Nr.46	Karamber Glacier	36°39'17.77"N	74°15'2.01"E	5077m
Point Nr.47	Karamber Glacier	36°38'51.26"N	74°14'15.76"E	4723m
Point Nr.48	Karamber Glacier	36°37'8.07"N	74°14'7.76"E	4392m
Point Nr.49	Karamber Glacier	36°37'31.92"N	74°11'30.96"E	3731m
Point Nr.50	Karamber Glacier	36°37'48.97"N	74° 9'54.43"E	3469m

Table 7.9 List of Randomly Sampled Ground Truth Reference Data Points for Phakor Glacier

Point Nr.1	Phakor Glacier	36°18'3.15"N	74° 1'35.27"E	5586m
Point Nr.2	Phakor Glacier	36°18'7.54"N	74° 1'39.07"E	5494m
Point Nr.3	Phakor Glacier	36°18'12.98"N	74° 1'36.48"E	5344m
Point Nr.4	Phakor Glacier	36°18'12.76"N	74° 1'43.42"E	5371m
Point Nr.5	Phakor Glacier	36°18'17.08"N	74° 1'37.63"E	5278m
Point Nr.6	Phakor Glacier	36°18'19.26"N	74° 1'34.05"E	5198m
Point Nr.7	Phakor Glacier	36°18'24.56"N	74° 1'32.25"E	5082m
Point Nr.8	Phakor Glacier	36°18'30.91"N	74° 1'32.36"E	5020m
Point Nr.9	Phakor Glacier	36°18'17.19"N	74° 1'43.43"E	5259m
Point Nr.10	Phakor Glacier	36°18'22.88"N	74° 1'38.05"E	5147m
Point Nr.11	Phakor Glacier	36°18'37.46"N	74° 1'33.18"E	4967m
Point Nr.12	Phakor Glacier	36°18'44.62"N	74° 1'31.97"E	4921m
Point Nr.13	Phakor Glacier	36°18'50.31"N	74° 1'34.25"E	4899m
Point Nr.14	Phakor Glacier	36°18'55.78"N	74° 1'35.64"E	4867m
Point Nr.15	Phakor Glacier	36°19'2.51"N	74° 1'39.08"E	4849m
Point Nr.16	Phakor Glacier	36°19'6.70"N	74° 1'44.51"E	4826m
Point Nr.17	Phakor Glacier	36°19'15.15"N	74° 1'45.46"E	4708m
Point Nr.18	Phakor Glacier	36°19'21.13"N	74° 1'47.69"E	4680m

Point Nr.19	Phakor Glacier	36°19'24.42"N	74° 1'54.60"E	4570m
Point Nr.20	Phakor Glacier	36°19'33.14"N	74° 2'4.58"E	4749m
Point Nr.21	Phakor Glacier	36°19'36.02"N	74° 1'58.03"E	4683m
Point Nr.22	Phakor Glacier	36°19'38.51"N	74° 1'53.51"E	4644m
Point Nr.23	Phakor Glacier	36°19'42.13"N	74° 1'46.59"E	4550m
Point Nr.24	Phakor Glacier	36°19'45.18"N	74° 1'44.62"E	4506m
Point Nr.25	Phakor Glacier	36°19'49.99"N	74° 1'47.51"E	4508m
Point Nr.26	Phakor Glacier	36°19'53.88"N	74° 1'51.79"E	4493m
Point Nr.27	Phakor Glacier	36°18'26.66"N	74° 1'42.86"E	5058m
Point Nr.28	Phakor Glacier	36°18'32.98"N	74° 1'41.91"E	4957m
Point Nr.29	Phakor Glacier	36°19'17.71"N	74° 2'6.70"E	4517m
Point Nr.30	Phakor Glacier	36°19'38.21"N	74° 2'1.92"E	4753m
Point Nr.31	Phakor Glacier	36°19'44.21"N	74° 1'57.31"E	4681m
Point Nr.32	Phakor Glacier	36°19'45.08"N	74° 2'8.14"E	4685m
Point Nr.33	Phakor Glacier	36°19'46.35"N	74° 1'52.51"E	4616m
Point Nr.34	Phakor Glacier	36°19'50.09"N	74° 1'57.32"E	4605m
Point Nr.35	Phakor Glacier	36°19'56.46"N	74° 1'46.21"E	4409m
Point Nr.36	Phakor Glacier	36°19'53.96"N	74° 1'43.38"E	4427m
Point Nr.37	Phakor Glacier	36°19'59.66"N	74° 1'41.53"E	4397m
Point Nr.38	Phakor Glacier	36°20'4.24"N	74° 1'37.56"E	4396m

Point Nr.39	Phakor Glacier	36°20'1.30"N	74° 1'38.82"E	4400m
Point Nr.40	Phakor Glacier	36°20'20.60"N	74° 1'34.19"E	4410m
Point Nr.41	Phakor Glacier	36°20'28.96"N	74° 1'29.17"E	4334m
Point Nr.42	Phakor Glacier	36°20'30.45"N	74° 1'36.20"E	4445m
Point Nr.43	Phakor Glacier	36°20'47.64"N	74° 1'10.88"E	4443m
Point Nr.44	Phakor Glacier	36°20'49.43"N	74° 1'2.47"E	4339m
Point Nr.45	Phakor Glacier	36°20'54.72"N	74° 0'52.55"E	4324m
Point Nr.46	Phakor Glacier	36°21'1.22"N	74° 0'31.03"E	4273m
Point Nr.47	Phakor Glacier	36°21'6.86"N	74° 0'15.45"E	4207m
Point Nr.48	Phakor Glacier	36°19'43.64"N	74° 0'39.92"E	4559m
Point Nr.49	Phakor Glacier	36°19'56.68"N	74° 0'43.86"E	4505m
Point Nr.50	Phakor Glacier	36°20'21.40"N	74° 0'38.43"E	4349m

CHAPTER 8

RESULT AND DISCUSSION COMPUTATION OF GLACIER VELOCITIES

Key research problems in glaciology is to determine in what way glaciers react animatedly to changing climate and how it differs provincially is one of the burning research question. Inter annual fluctuations in ice velocity result from mass-balance forcing that modifies the geometry of glacier and corresponding driving stress. The mass flux over a cross-section for a glacier that is moving toward steady-state equivalent the mass balance upstream of the cross-section. Therefore, mass loss frequently causes glaciers to halt pace. A varying climate can, however, also have an influence on the likelihood of sliding and alter a glacier's thermal regime and borderline practices (ice-ocean, ice-lake and ice-bed interactions). Therefore, it is difficult to envisage how glacier flow will retort to climate change. Mass loss paired with higher melt water output or a change to a temperate regime could result in a faster flow rate. In the end, glaciers react to changes in mass balance in a delayed dynamical manner depending on their unique response times. The aforementioned research question has been addressed at regional scales in a number of recent papers that examined decadal variations in stream speed in connection to glacial mass loss. However, only a small number of local studies have taken up the issue in the background of recorded variations

between real and balance velocities. It is now possible to discourse the unresolved research questions from a local to global perspective thanks to the available database due to current age band of diverse global glacier datasets, including the Randolph Glacier Inventory-RGI, Go LIVE and ITS LIVE ice speed, globally- distributed and thickness datasets like data of mass balance by WGMS and companion ground measurements as well. The variance between the calculated glacier velocities, resulting from obtainable Go LIVE and ITS-LIVE datasets, and additional speckle tracking from SAR scenes, and the balance velocity, resulting from mass balance outlines, hypsometry, and ice thickness datasets, will be compared for the first time for glaciers in various RGI sub regions. In order to deal with size and prototypical suspicions, the conventional method of calculating balance flux along a flow line was employed. (Cooley, J., Van Wychen, W., DeJong, H., Jiskoot, H. 2014).

Sea level rise is being considered as a worldwide task of the modern age and is attributed with the faster melting of glaciers and ice sheets. The main causes of this sea level rise and faster melting of glaciers probably are exponential rise in the concentration of greenhouse gases such as CO₂, NO_x, and H₂O etc. found in the troposphere alongwith global warming. The concentration of atmospheric carbon dioxide (CO₂) Over the last century due burning of fossil fuels like coal and oil has increased.

Since the turn of the 20th century, several glaciers have been melting quickly all across the world. This phenomenon is mostly the result of human activity. Even if we drastically reduce emissions in the upcoming decades, more than a third of the world's surviving glaciers would disappear before the year 2100. Ninety-five percent of the oldest and thickest sea ice in the Arctic has already disappeared. Scientists predicted

that the Arctic may be free of ice as early as 2040 if emissions continue to increase uncontrolled due to the fast rise in air and ocean temperatures. Due to the industrial revolution, temperatures have increased due to the production of greenhouse gases such as carbon dioxide and have even risen in both poles. Resultantly, melting ice causes more warming. The ocean and land grip more incoming solar radiation, and then release the heat to the atmosphere as their color is murkier. With this state, more warming generated by the melted ice and ultimately further ice melts. This causes more global warming. IPCC estimate that accelerating melting and solid ice discharge is due to enhanced flow of glaciers and ice sheet mass. Both optical and radar imagery can be used for surface velocities measurement. Multiple techniques from pairs of radar images used for deriving surface velocities. Synthetic Aperture Radar Interferometry is the utmost precise method that is for Sentinel-1 in cm level to measure changes in range from repeat-pass observations. Regional ice velocity mappings are released yearly by several satellites. The main satellites for determining glacier and ice sheet velocities are optical (Landsat 4/5/6/7/8 and Sentinel-2) and SAR (Sentinel-1) satellite data, according to Gardner et al. (2018). Inter-mission Time Series of Land Ice Velocity and Elevation (ITS_LIVE) is NASA MEaSUREs project which has released 45 ice velocity products (image-pair granules, data cubes, and regional mosaics). ITS_LIVE project provide automated low latency, global glacier elevation change datasets.

The computation of glacier mass flow, numerical ice dynamic modeling, and time series studies all depend on glacier surface velocity which should have reliable and unbroken records. The Copernicus program of the EU (European Union) and ESA (European Space Agency) being collaborators in satellite imagery, the Sentinel-1 satellite constellation has been collecting repeat-pass synthetic aperture radar (SAR) data since 2014. Regardless of weather, season, or time of day, it provides worldwide,

nearly actual duration/period scenario along with totally programmed analysis of up to 6 day temporal resolution field analysis on glacier surface velocity. The NASA MEaSURES project present a fresh worldwide dataset of glacier surface velocities with 200 m spatial resolution, monthly and yearly averaged velocity mosaics, and scene-pair velocity fields that are updated continuously. A well- known intensity offset tracking approach is used to extract the velocity information from both old and new Sentinel-1 SAR recordings. At the University of Erlangen-Nuremberg in HPC (high-performance computing) atmosphere the data collection was performed. It contains twelve significant regions of snow and ice on mountains that are well apart from the ice sheets of the polar ice regions. The velocity products can be downloaded for free and used for quick online analysis through this interactive website: <http://retreat.geographie.uni-erlangen.de>. By comparing the velocity products to that produced from very extraordinary resolution Terra SAR-X SAR and Landsat-8 optical (ITS LIVE, Go LIVE) data, the program demonstrates the probable of the products time series analyses for velocity at exact extraordinary progressive resolution for the example region of Svalbard. The program also evaluates the quality of the velocity products. The GFZ Potsdam Data Services make the subdivision of Sentinel-1 velocities for Svalbard that were used to analyze this work available using the DOI <https://doi.org/10.5880/fidgeo.2021.016> (Friedl et al., 2021). It was noted that the annual velocity mosaics produced by Landsat-8 and Sentinel-1 are generally in good covenant, although speckle tracking on Sentinel-1, 6 days repeat attainments yields additional accurate velocity extents than optical data across featureless and slowly moving regions. Additionally, uncertainties computed for 16 days repeat Landsat-8 data (0.17–0.18 m d1) are fewer than half (0.08 m d1) of the uncertainties of 12 days repeat Sentinel-1 mid-glacier scene-pair velocities.

By utilizing Normalized Cross Correlation on matching path-row Landsat

Collection L1T and L1GT image pairings in the panchromatic Band 8 (15 m pixel size), glacier velocities were calculated. Examining multiple velocity mosaics derived from two distinct dispensation methods created by NSIDC (National Snow and Ice Data Centre) allowed researchers to determine how sensitive consequences were to changes in Landsat processing methodology (such as search template size, spatial resolution, geolocation offset correction, data filtering, image-pair date separation, and compositing).

The glacier speed vectors in the northern Pakistani Karakorum region are displayed in Figure 8.1 using data from the ITS_ LIVE project portal run by NSIDC. It should be noted that in this chapter, the phrases "glacier velocity" and "glacier speed" have been used interchangeably. Figure 8.1 displays an overview of the glacier velocities for the entire region.



Figure 8.1 Glacier velocity vectors in the Karakorum region

By comparing the velocities estimated by Landsat and SAR at flux-gate nodes for sinks with little variation in ice release basins where velocity discrepancies are considered to be analytical extent reservations in velocities were identified. Locally, velocity uncertainty can reach 20–30 m yr⁻¹, but on basin scales (> 1000 km), it is

largely uncorrelated. All velocity mosaics are available for acquisition and validation and can be downloaded without any cost. These were acquired and data of the relevant ROI was extracted for regional analysis. The key differences between the JPL and NSIDC processing chains are in how the image-pair data are adjusted for geolocation inaccuracies, how the imagery is searched for matching features, and the selection of search parameters such as pattern extent and typography.

8.1 Bad-e-Swat Glacier

The point data of three marked places (shown in Figure 8.4) on the Bad e Swat Glacier have been plotted in Figure 8.2 and 8.3. The trend lines for the scattered data have been drawn for all three points' viz., green, orange and blue. The trends show that the peak value of the velocity of the glacier was ~250-300 meters per year which has increased to ~300-350 meters per year as shown in Figure 8.2. This figure also shows a sharp decrease in glacier velocities in 2016 and 2021. Higher glacier velocity translates into higher ablation of the glacier in the summer season whereas lower glacier velocity indicates firmness and strong accumulation of the glacier as shown in Figure 8.3 where a closer insight into seasonal fluctuations is shown.

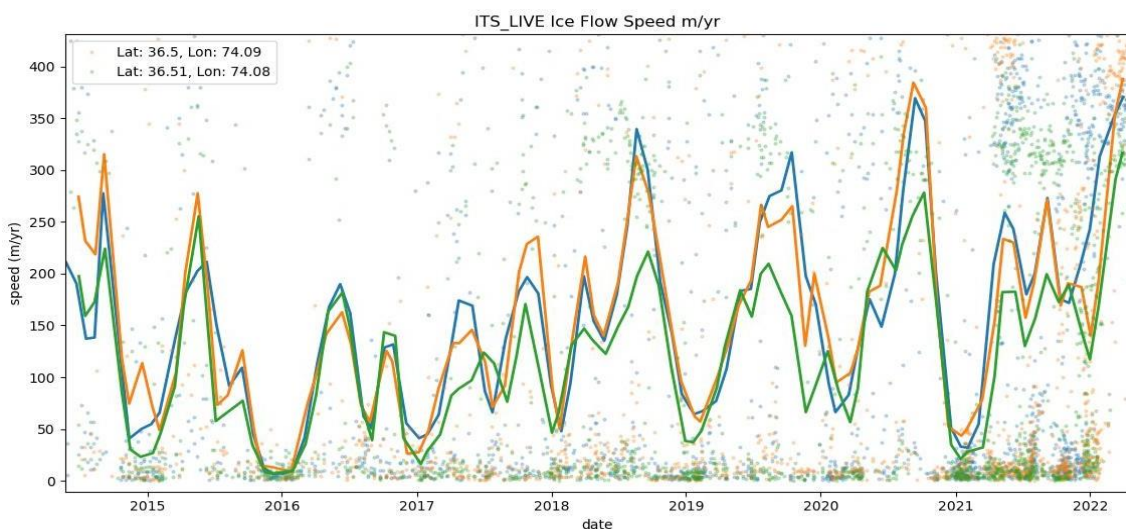


Figure 8.2 Glacier velocities at the marked locations of Bad-e- Swat glacier from 2015-22

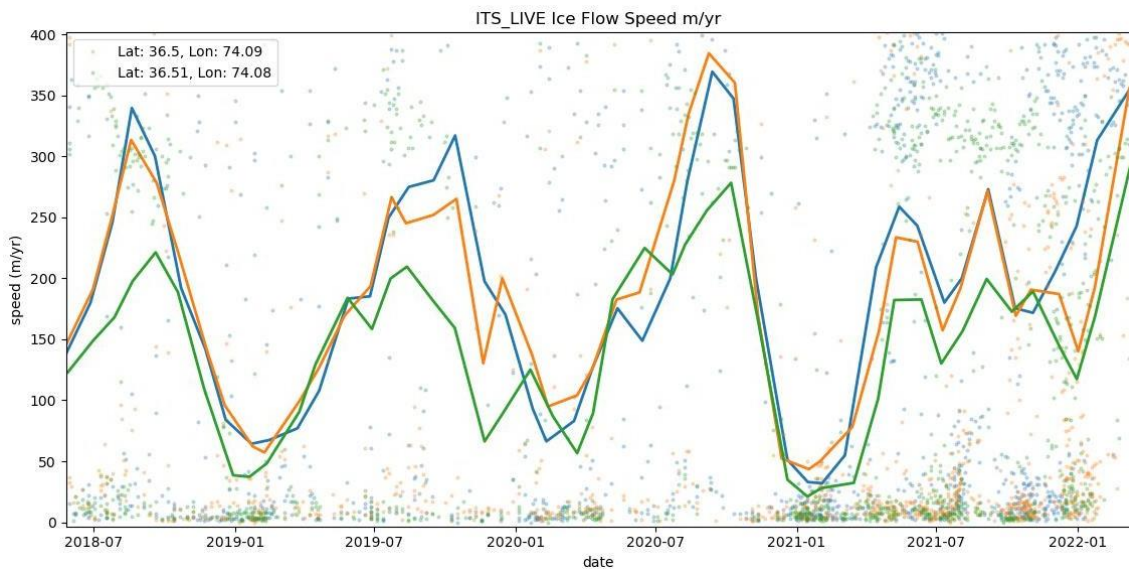


Figure 8.3 Glacier velocities at the marked locations of Bad-e-Swat glacier from 2018-22

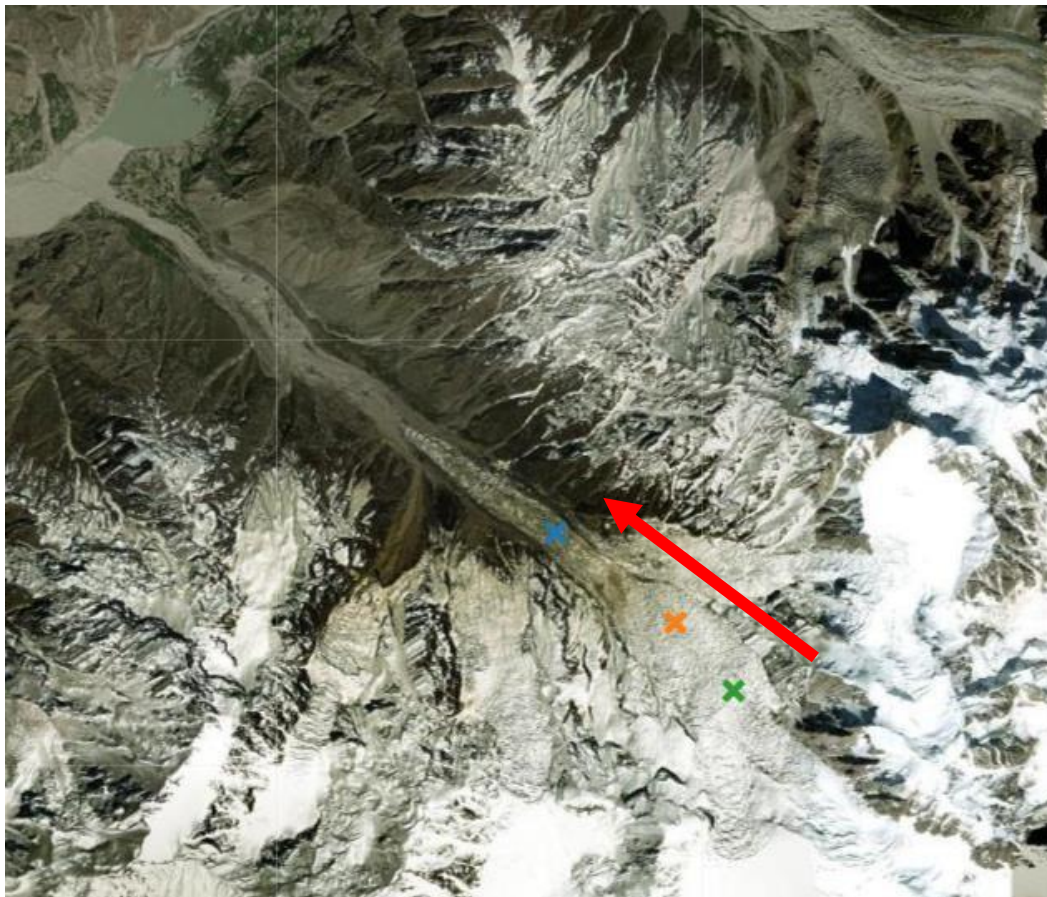


Figure 8.4 Marked locations of Bad e Swat glacier and flow direction

8.2 Karambar Glacier

The point data of three marked places (shown in Figure 8.7) on the Karambar Glacier have been plotted in Figure 8.5 and 8.6. The trend lines for the scattered data have been drawn for all three points' viz., Green, Orange and Blue. The trends show that the peak value of the velocity of the glacier was ~200-350 meters per year which has increased to ~300-400 meters per year as shown in Figure 8.5. Figure 8.5 also shows a sharp decrease in glacier velocities in 2016 and 2022. Higher glacier velocity translates into higher ablation of the glacier in the summer season whereas lower glacier velocity indicates firmness and strong accumulation of the glacier as shown in Figure 8.6 where a closer insight into seasonal fluctuations is shown.

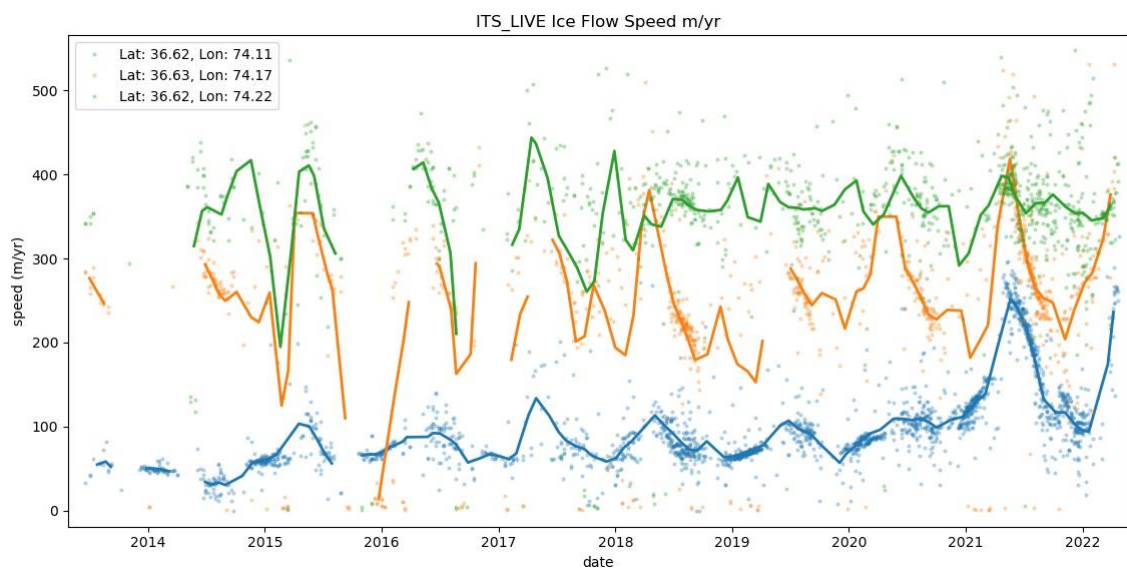


Figure 8.5 Glacier velocity at the marked locations of Karambar glacier from 2014-22.

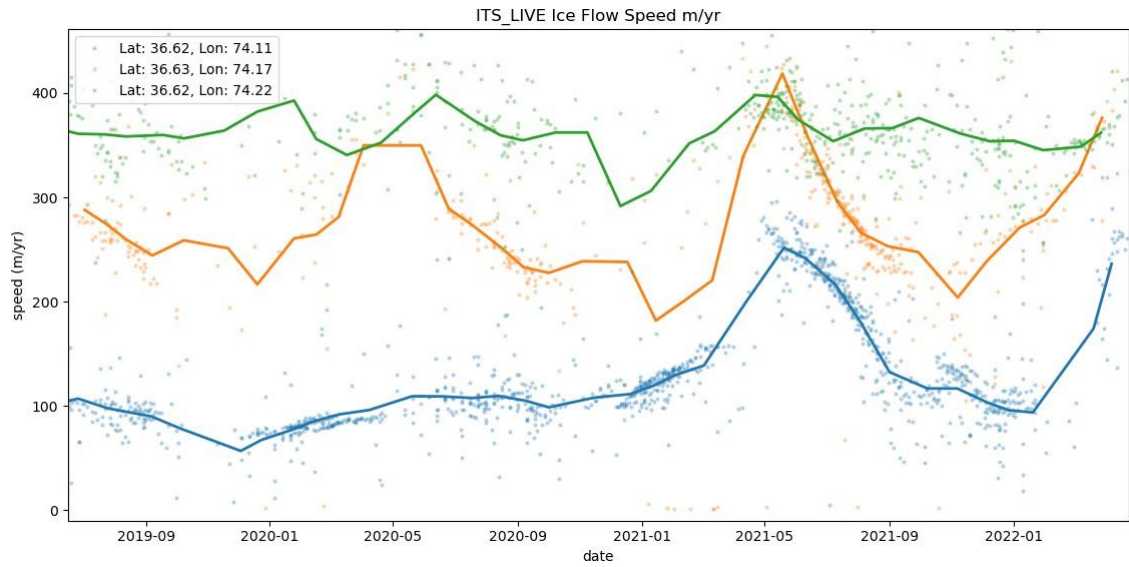


Figure 8.6 Glacier velocity at the marked locations of Karambar glacier 2019 to 2022

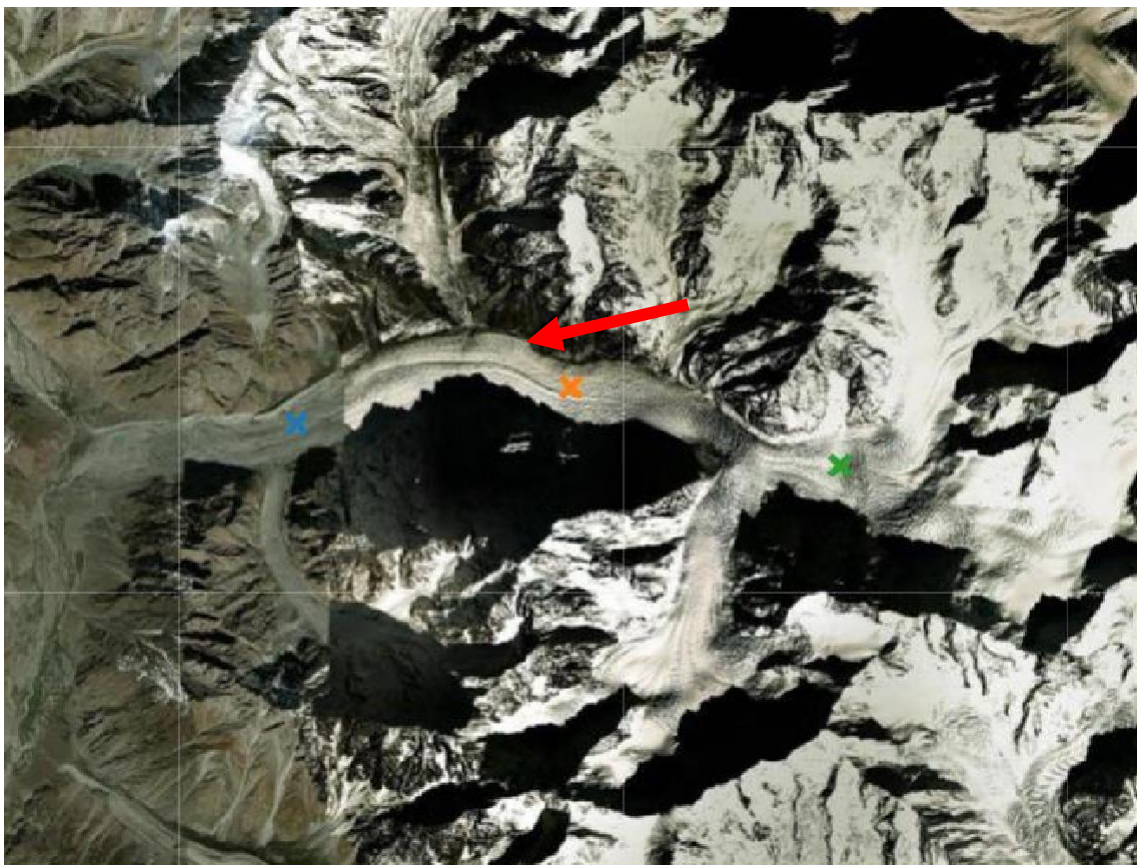


Figure 8.7 Marked location of Karambar glacier and flow direction

8.3 Bhort Glacier

The point data of three marked places (shown in Figure 8.10) on the Bhort Glacier have been plotted in Figure 8.8 and 8.9. The trend lines for the scattered data have been drawn for all three points' viz., Green, Orange and Blue. The trends show that the peak value of the velocity of the glacier was ~100-150 meters per year which has increased to ~100-175 meters per year as shown in Figure 8.8. Figure 8.8 also shows a sharp decrease in glacier velocities in 2016 and 2021. Higher glacier velocity translates into higher ablation of the glacier in the summer season whereas lower glacier velocity indicates firmness and strong accumulation of the glacier as shown in Figure 8.9 where a closer insight into seasonal fluctuations is shown.

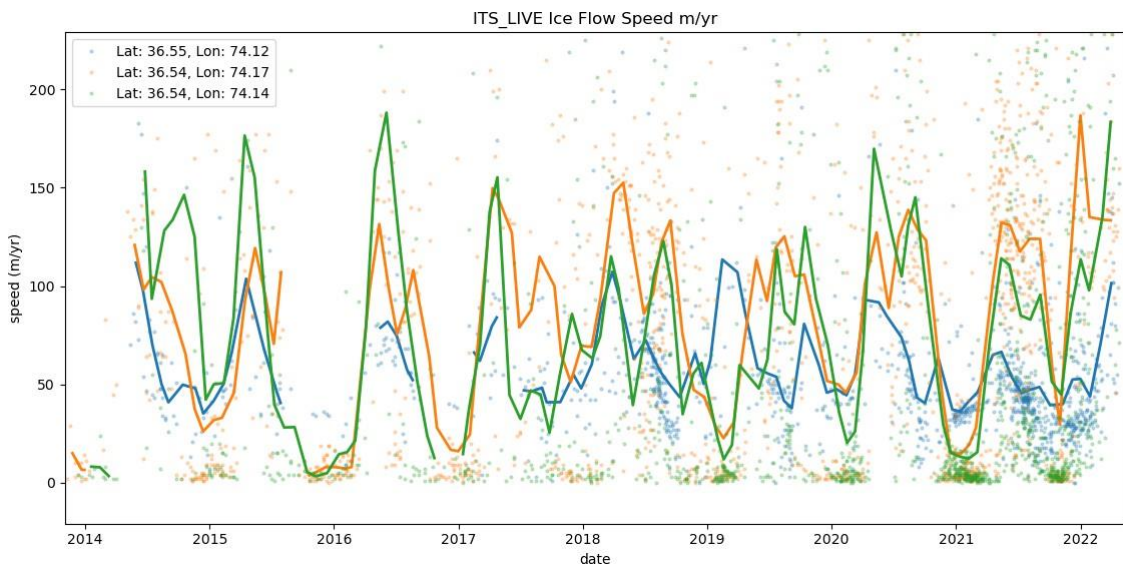


Figure 8.8 Glacier velocity at the marked locations of Bhort glacier from 2014-22

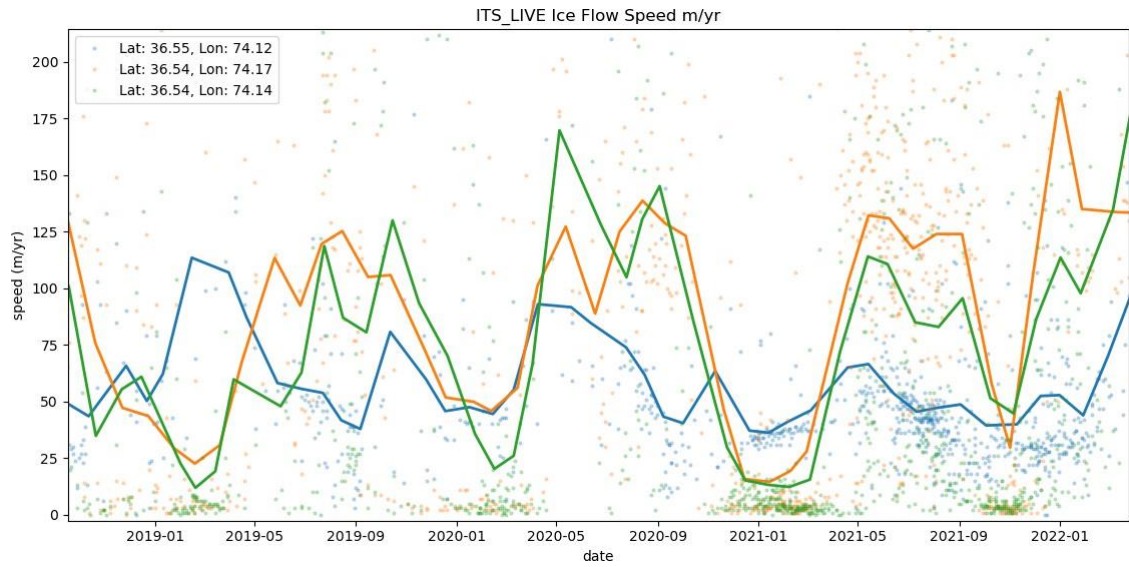


Figure 8.9 Glacier velocity at the marked locations of Bhorth glacier 2019 to 2022



Figure 8.10 Marked locations of Bhorth Glacier and flow direction

8.4 Phakor Glacier

The point data of three marked places (shown in Figure 8.13) on the Phakor Glacier have been plotted in Figure 8.11 and 8.12. The trend lines for the scattered data have been drawn for all three points' viz., Green, Orange and Blue. The trends show that the peak value of the velocity of the glacier was ~100-150 meters per year which has increased to ~100-175 meters per year as shown in Figure 8.11. Figure 8.11 also shows a sharp decrease in glacier velocities in 2016 and 2021. Higher glacier velocity translates into higher ablation of the glacier in the summer season whereas lower glacier velocity indicates firmness and strong accumulation of the glacier as shown in Figure 8.12 where a closer insight into seasonal fluctuations is shown.

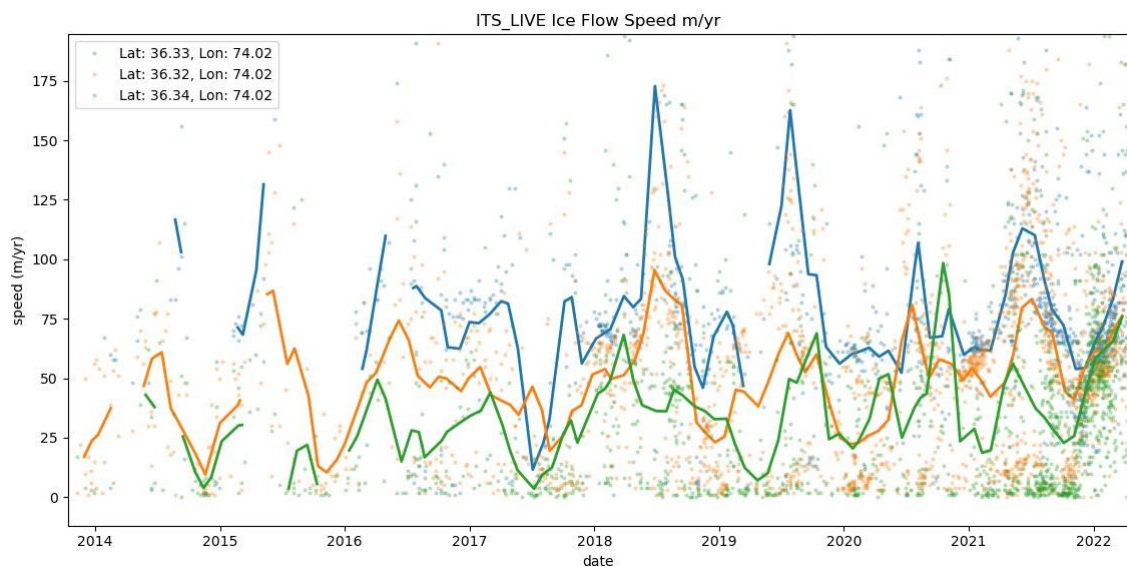


Figure 8.11 Glacier velocity at the marked locations of Phakor glacier from 2014-22

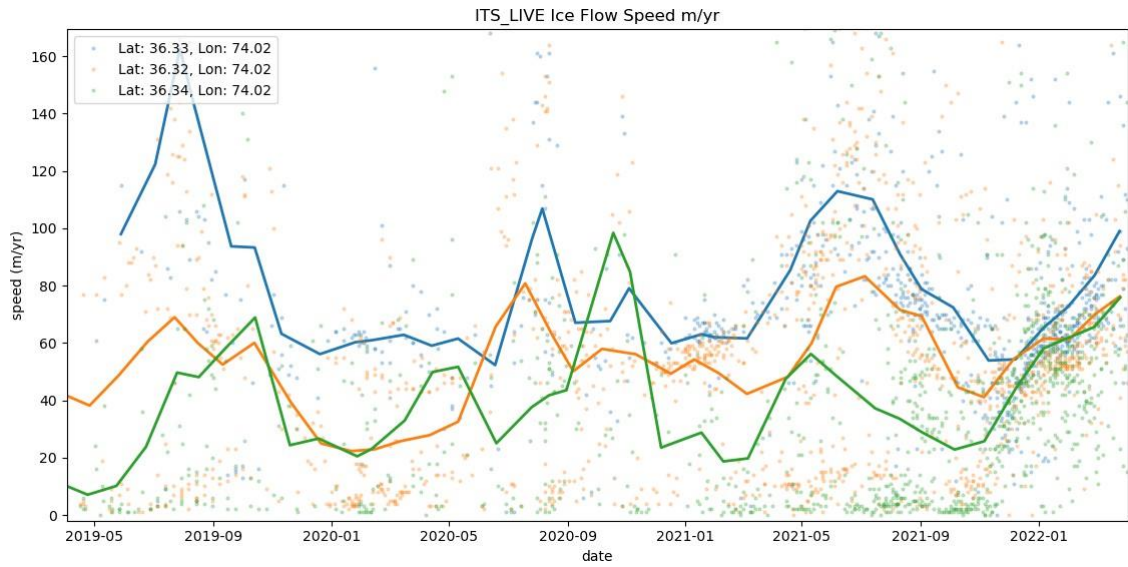


Figure 8.12 Glacier velocity at the marked locations of Phakor glacier 2019 to 2022



Figure 8.13 Marked location of Phakor glacier and flow direction

8.5 East Gammu Glacier

The point data of three marked places (shown in Figure 8.16) on the East Gammu Glacier have been plotted in Figure 8.14 and 8.15. The trend lines for the scattered data have been drawn for all three points' viz., Green, Orange and Blue. The trends show that the peak value of the velocity of the glacier was ~100-200 meters per year which has increased to ~100-300 meters per year as shown in Figure 8.14. Figure 8.14 also shows a sharp decrease in glacier velocities in 2016 and 2021. Higher glacier velocity translates into higher ablation of the glacier in the summer season whereas lower glacier velocity indicates firmness and strong accumulation of the glacier as shown in Figure 8.15 where a closer insight into seasonal fluctuations is shown.

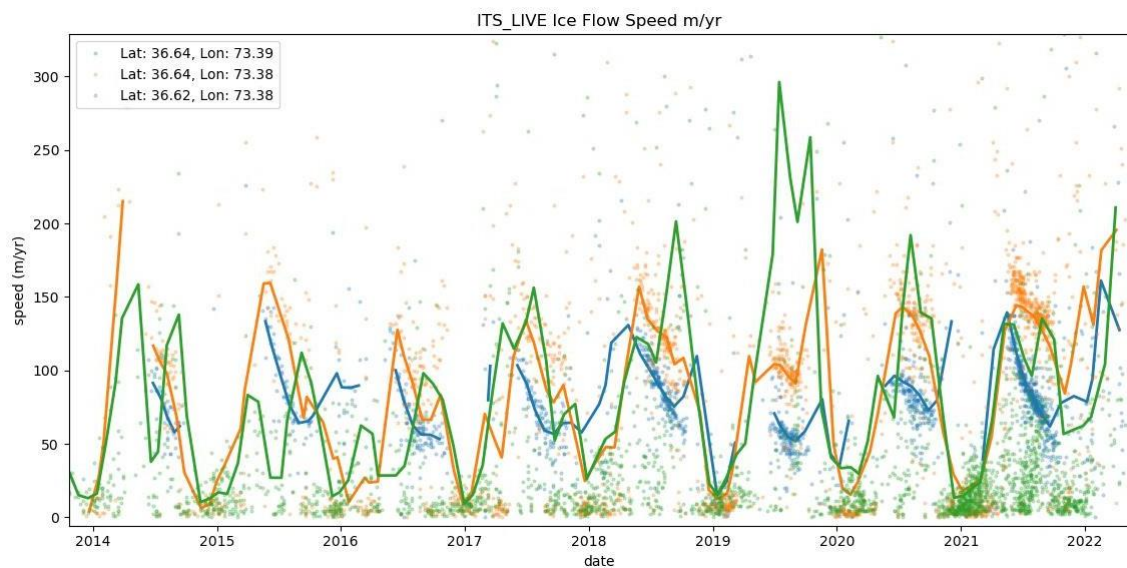


Figure 8.14 Glacier velocity at the marked locations of East Gammu glacier from 2014-22

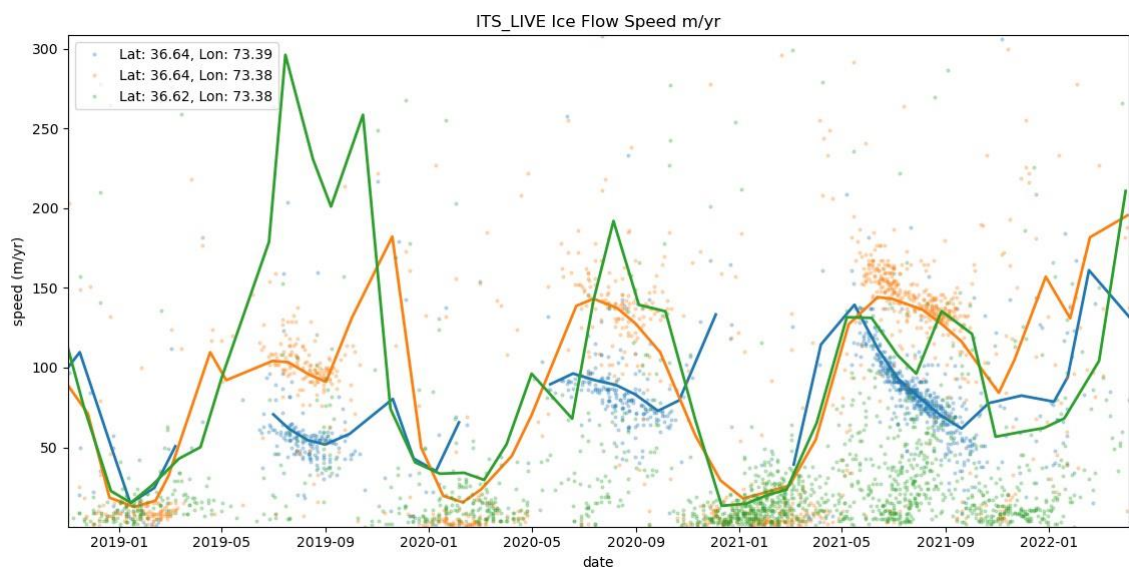


Figure 8.15 Glacier velocity at the marked locations of East Gammu glacier 2019 to 2022

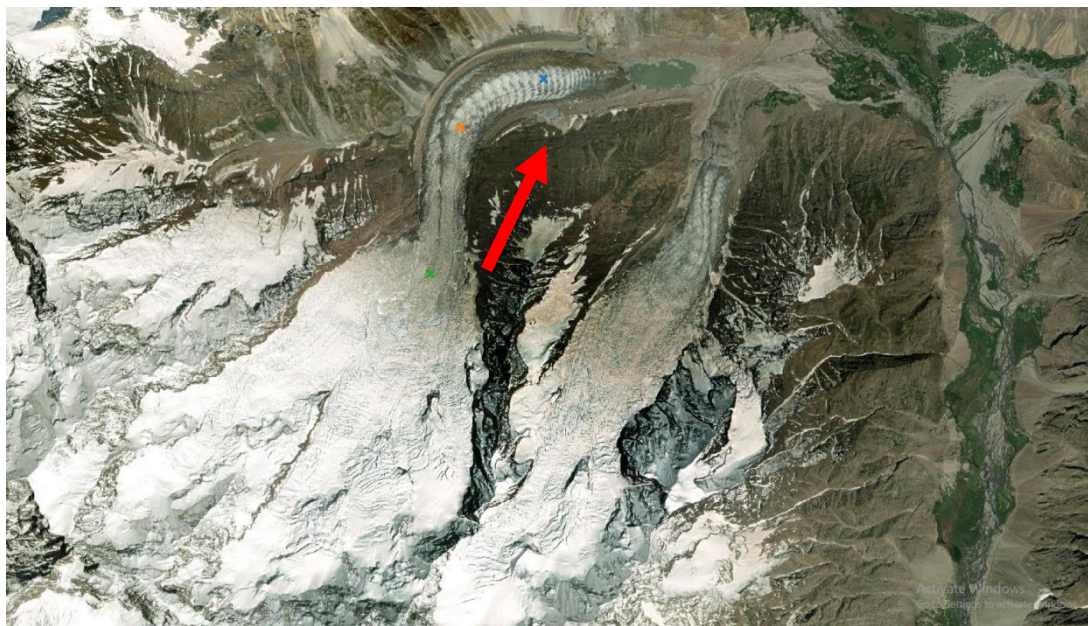


Figure 8.16 Marked locations of East Gammu Glacier and flow direction

8.6 Discussion

An overview of velocity changes in the five selected glaciers described above show that understudy glaciers are in unchanging state. Glacier velocities vary from 25 m/year to 450 m/year in the summer season at the time when glacier melt is expected. The glaciers that are on higher elevation, devouring lower temperatures have low velocities whereas the glaciers at low elevation have higher velocities.

This section describes the MEaSURES ITS_LIVE Sentinel-1 Image-Pair Glacier and Ice Sheet Surface Velocities and the related visualizations. The dataset is delivered for all bulky glacierized areas. To validate the data eminence and algorithms I show 5 Sentinel-1 image pairs over 5 different sites in Gilgit watershed in areas of medium to fast and medium to slow flow. Little positive variations in the velocity and little negative variations in the velocity points demonstrate the stability of the glaciers.

CHAPTER 9

CONCLUSION

A large volume of water, from the global, water cycle, is stored in the mountain glaciers; the variation in the glacier size greatly reliance's on the rainfall in the form of snow and waterfall. It is also highlighted that the meteorological station density is very less in the Upper Indus Basin (UIB) in general and Gilgit River basin in particular which needs to be substantially increased for better thoughtfulness of the hydrological cycle.

This study highlights extraction of watersheds from the DEM data. Further it takes one more step to compare the DEM datasets in the research area and compare the outcomes of delineation. This is the first time that author has known about the stability of the glaciers that they are not fast melting. The result provides a significant contribution to advancing knowledge in the glacier/snow hydrology and is not a mere replication of elements from any previously published research.

The results showed that the watershed extracting characteristics are important for effective water resource management and the hydrological analysis for catchment

delineation and stream network. Focusing, the problem of ridges mismatch in watershed delineation in the mountainous regions is paramount for concluding real time watershed condition. This study uses unique approach involving the delineation of watersheds in order to access the accuracy of the open sources DEMs that are multi-sensor, multi-mission datasets at multi-resolution viz., SRTM, ASTER GDEM and GTOPO30. The pre-defined methods to complete watershed delineation are used.

The comparative analysis was employed for the demarcation of drainage and watershed at the basin level and further at the sub-catchments of five large glaciers viz, Bad-e-Swat, Karamber, Phakor, East Gammu, Bhort and Karamber. The delineated watersheds studied against the optical Landsat 8 OLI imagery visually for rugged crest alike.

The outcomes indicated that the SRTM 30 m (radar based) is further accurate for this region. Other portion of the thesis treats with the change detection of the glacier area in the last 30 years. In order to, accomplish the task the satellite imageries from year 1988, 1994, 1999, 2014 and 2018 have been used to map and monitor the five large glaciers in the Gilgit watershed.

At first the unsupervised classification techniques were applied, the results obtained were not so much precise with visible misclassification of several glacier cover areas. However, with supervised classification the results were improved. The additional benefit was obtained by using object based image analysis, which provides a better way through partitioning and segmentation of the pixels of similar spectral characteristics.

The glacier mapping using the object based classification techniques, thus, has been used to delineate the glacier area. It was observed from the overall results that, mostly glaciers are rather stable in Karakorum region specifically in the Gilgit watershed. Due to these glaciers geographic condition, altitude, topography, orientation and climate conditions small inconsistency in them was observed. In order to assess the accurateness of the glacier mapping the accuracy assessment was carried out using the error matrix approach with a calculated kappa coefficient value that comes out to be 84.14%.

This study has presented a generalized relationship for glaciers ablation and accumulation; alongwith remote-sensing workflow synchronizations validate this association from time series of optical satellite imageries. The new remote-sensing workflow described in the chapter 8 has allowed us to combine surface velocity time series, calculated from two dissimilar satellites systems viz, Landsat-8 and Sentinel-2 and attain a high spatiotemporal resolution.

The combined dataset is then improved by after processing phases that considerably increase data eminence. It is expected that this remote sensing workflow may be applied in the future to the surge-type glaciers in Pakistan's Karakorum, and obtain a predominantly thorough image of the active variations foremost to and during the anticipated surges.

In accordance with the aims and objectives of this dissertation, outlined in chapter 1, the following statements may be concluded relating to the advancement of knowledge in the research region of this study.

1. As mentioned at objective at para 1.4.1, the five large glaciers in the Gilgit river watershed have been mapped using time series of satellite remote sensing data from years 1988, 1994, 1999, 2014 and 2018. The results offer a better understanding into the glacier status in the study area, as the health of the glacier over 30 years has been monitored and the result suggest an inverse pattern as to the concepts of rapid glacier melting which does not exist here in this region.
2. As mentioned at objective's para 1.4.2, assessment of diverse remote sensing products / datasets by the computation of hydrological watershed of the Gilgit sub-basin has been made. Different remote sensing products / datasets have been compared viz., SRTM, ASTER and GTOPO for watershed delineation. These multi-sensor DEM data have been used for the extraction of watersheds/catchments and the accuracy of the results has been analyzed in this region. This provides the confidence level about the addressing the most important question that which satellite product is suitable and precise in this study area for delineation of Gilgit watershed.
3. As mentioned at objective's para 1.4.3, advanced satellite data processing techniques such as image classification including Object Based Classification has been opted in this study. Long-term climate data comprising of 30 years monthly averages have been studied for the research area showing the effects of temperature, precipitation and thermal radiant energy on glacier melt or stability.
4. As mentioned at objective para 1.4.4, the evaluation of time series of

areal extents of the glaciers has been made. The areal extents of five large glaciers in the Gilgit river watershed have been mapped using time series of satellite remote sensing data from years 1988, 1994, 1999, 2014 and 2018.

5. As mentioned at objective's para 1.4.5, the areal extents of the five large glaciers have been analyzed to conclude the absence of any major surge, retreat or stability of the selected glaciers. Since there is not strong depletion of glaciers over three decade's time, this suggests that the winter accumulation on the glaciers in the Gilgit river basin has strong influence that is of the order of ablation in the summer season.
6. As mentioned at objective's para 1.4.6, the comparison of multi-sensor DEM data for the extraction of watersheds / catchments of 5x glaciers has been made.
7. As mentioned at objective's para 1.4.7, the delineation of velocity of the 5x selected glaciers has been computed.

REFERENCES

- Aboelnour, M., & Engel, B. A. (2018). Application of remote sensing techniques and geographic information systems to analyze land surface temperature in response to land use/land cover change in Greater Cairo Region, Egypt. *Journal of Geographic Information System*, *10*(1), 57–88.
- Abu El-Magd, S. A., Orabi, H. O., Ali, S. A., Parvin, F., & Pham, Q. B. (2021). An integrated approach for evaluating the flash flood risk and potential erosion using the hydrologic indices and morpho-tectonic parameters. *Environmental Earth Sciences*, *80*, 1-17.
- Adnan M., Liu S., Sifullah M., Iqbal M., Ali A. F., Mukhtar M. A. (2022). Spatiotemporal variations in runoff and runoff components in response to climate change in a glacierized subbasin of the Upper Indus Basin, Pakistan. *Frontiers in Earth Science*. Vol 10, DOI=10.3389/feart.2022.970349. <https://www.frontiersin.org/10.3389/feart.2022.970349>.
- Adnan, M., Nabi, G., Kang, S., Zhang, G., Adnan, R. M., Anjum, M. N. Ali, A. F. (2017). Snowmelt Runoff Modelling under Projected Climate Change Patterns in the Gilgit River Basin of Northern Pakistan. *Polish Journal of Environmental Studies*, *26* (2), 525-542. <https://doi.org/10.15244/pjoes/66719>.
- Adnan, M., Nabi, G., Poomee, M. S., & Ashraf, A. (2017). Snowmelt runoff prediction under changing climate in the Himalayan cryosphere: A case of Gilgit River Basin. *Geoscience Frontiers*, *8*(5), 941-949.

- Afsar, S., Abbas, N., & Jan, B. (2013). Comparative study of temperature and rainfall fluctuation in Hunza-nagar District. *Journal of Basic and applied sciences*, **9**, 151-156.
- Afzal, Muhammad Mannan, et al. "Hydrological and dynamical response of glaciers to climate change based on their dimensions in the Hunza Basin, Karakoram." *Journal of Hydrology* 617 (2023): 128948.
- Ahmad S., Israr M., Liu S., Hayat H., Gul J., Wajid S., Ashraf M., Baig S. U. & Ahmad A. T. (2020) Spatio-temporal trends in snow extent and their linkage to hydro-climatological and topographical factors in the Chitral River Basin (Hindukush, Pakistan), *Geocarto International*, 35:7, 711-734, DOI: 10.1080/10106049.2018.1524517.
- Ahmad, S., Israr, M., Liu, S., Hayat, H., Gul, J., Wajid, S., et al. (2018). Spatio-temporal trends in snow extent and their linkage to hydro-climatological and topographical factors in the Chitral River Basin (Hindu Kush, Pakistan). *Geocarto International*, 1-24.
- Ahsan, S., Bhat, M. S., Alam, A., Farooq, H., & Shiekh, H. A. (2021). Evaluating the impact of climate change on extreme temperature and precipitation events over the Kashmir Himalaya. *Climate Dynamics*, *1*(0123456789).
- Ali, K., Bajracharya, R. M., Chapagain, N. R., Raut, N., Sitaula, B. K., Begum, F., et al. (2019). Analyzing Land Cover Change Using Remote Sensing and GIS: A Case Study of Gilgit River Basin, North Pakistan. *International Journal of Economic and Environmental Geology*, **10**(1), 100- 105.

- Ali, K., Bajracharya, R. M., Sitaula, B. K., Raut, N., and Koirala, H. L. (2017). Morphometric Analysis of Gilgit River Basin in Mountainous Region of Gilgit-Baltistan Province, Northern Pakistan. *Journal of Geoscience and Environment Protection*, **5**(07), 70.
- Ali, S.H.; Bano, I.; Kayastha, B.R.; Shrestha, (2017). A Comparative Assessment of Runoff and its Components in Two Catchments of Upper Indus Basin by Using a Semi Distributed Glaciohydrological Model; The International Archives of the Photogrammetry, Remote Sensing and Spatial Information Sciences; ISPRS Geospatial Week: Wuhan, China; Volume XLII-2/W7.
- Ali, Nahida, and Shakil A. Romshoo. "Stream Flow Changes and Glacier Recession in the Upper Indus Basin." *Geostatistical and Geospatial Approaches for the Characterization of Natural Resources in the Environment: Challenges, Processes and Strategies*. Springer International Publishing, 2016.
- Al-qaysi, N. H. H. (2016). Delineation of the Watersheds Basin in the Konya City and Modeling by Geographical Information System. *Journal of International Environmental Application and Science*, **11**(3), 303-311.
- Rajeevan, M., Pai, D. S., Anil Kumar, R., & Lal, B. (2007). New statistical models for long-range forecasting of southwest monsoon rainfall over India. *Climate Dynamics*, **28**, 813-828.
- Aroengbinang, B. W., & Kaswanto. (2015). Driving Force Analysis of Land use and Cover Changes in Cimandiri and Cibuni Watersheds. *Procedia Environmental Sciences*, **24**, 184–188.

- Ashraf, A., Naz, R., & Roohi, R. (2012). Monitoring and estimation of glacial resource of Azad Jammu and Kashmir using remote sensing and GIS techniques. *Pakistan Journal of Meteorology*, **816**(3).
- Atif, I., Iqbal, J., & Mahboob, M. A. (2018). Investigating Snow Cover and Hydro meteorological Trends in Contrasting Hydrological Regimes of the Upper Indus Basin. *Atmosphere*, **9**(5), 162.
- Awan, S. A. (2002). The climate and flood risk potential of northern areas of Pakistan. *Science Vision*, **7**(3-4), 100-109.
- Ayub, S., Akhter, G., Ashraf, A., & Iqbal, M. (2020). Snow and glacier melt runoff simulation under variable altitudes and climate scenarios in Gilgit River Basin, Karakoram region. *Modeling Earth Systems and Environment*, **6**(3), 1607-1618.
- Azam, Mohammad Nurul, et al. "Environmental concern: assessment of meteorological drought." *International Journal of Environment and Sustainable Development* 16.2 (2017): 156-166.
- Azam, M. F., Wagon, P., Berthier, E., Vincent, C., Fujita, K., & Kargel, J. S. (2018). Review of the status and mass changes of Himalayan-Karakoram glaciers. *Journal of Glaciology*, **64**(243), 61-74.
- Baig, Siddique Ullah, Humaira Khan, A. D. (2018). Spatio-temporal analysis of glacial ice area distribution of Hunza River Basin , Karakoram region of Pakistan. *Hydrological Processes*, (March), 1–11.
- Bajracharya, S. R., Maharjan, S. B., Shrestha, F., Guo, W., Liu, S., Immerzeel, W., & Shrestha, B. (2015). The glaciers of the Hindu Kush Himalayas: current status and observed changes from the 1980s to 2010. *International Journal of Water Resources Development*, **31**(2), 161-173.
- Bazai, Nazir Ahmed, et al. "Increasing glacial lake outburst flood hazard in response to

- surge glaciers in the Karakoram." *Earth-Science Reviews* 212 (2021): 103432.
- Bhambri, R., et al. (2011). "Mapping of debris-covered glaciers in the Garhwal Himalayas using ASTER DEMs and thermal data." *International Journal of Remote Sensing* 32(23): 8095-8119.
- Bhambri, R., Watson, C. S., Hewitt, K., Haritashya, U. K., Kargel, J. S., Pratap Shahi, A., ... & Govil, H. (2020). The hazardous 2017–2019 surge and river damming by Shispare Glacier, Karakoram. *Scientific reports*, 10(1), 1- 14.
- Bhat, S. A., Meraj, G., & Pandit, A. K. (2016). Assessing the influence of stream flow and precipitation regimes on water quality of the major inflow stream of Wular Lake in Kashmir Himalaya. *Arabian Journal of Geosciences*, 9(1), 1–15.
- Bhatti, Muhammad Tousif, Arif A. Anwar, and Muhammad Azeem Ali Shah. "Revisiting telemetry in Pakistan's Indus basin irrigation system." *Water* 11.11 (2019): 2315.
- Bilal, H., Chamhuri, S., Mokhtar, M.B. *et al.* Recent snow covers variation in the Upper Indus Basin of Gilgit Baltistan, Hindukush Karakoram Himalaya. *J. Mt. Sci.* 16, 296–308 (2019). <https://doi.org/10.1007/s11629-018-5201-3>.
- Bishop, M. P., Shroder Jr, J. F., & Ward, J. L. (1995). SPOT multispectral analysis for producing supraglacial debris- load estimates for Batura glacier, Pakistan. *Geocarto International*, 10:4, 81-90
- Blaschke, T. (2010). "Object based image analysis for remote sensing." *ISPRS journal of photogrammetry and remote sensing* 65(1): 2-16.
- Bolch T, Pieczonka T, Benn D (2011). Multi-decadal mass loss of glaciers in the Everest area (Nepal Himalaya) derived from stereo imagery. *The Cryosphere* 5:349-358.
- Bolch, T. (2007). Climate change and glacier retreat in northern Tien Shan

- (Kazakhstan/Kyrgyzstan) using remote sensing data. *Global and Planetary Change*, **56**(1-2), 1-12.
- Bolch, T. and U. Kamp. (2006). Glacier mapping in high mountains using DEMs, Landsat and ASTER data. In Kaufmann, V. and W. Sulzer, eds. *Proceedings of the 8th International Symposium on High Mountain Remote Sensing Cartography*. Graz, KarlFranzens University, 13–24. (Grazer Schriften der Geographieund Raumforschung 41.)
- Bolch, T., Kulkarni, A., Kääb, A., Huggel, C., Paul, F., Cogley, J.G., Frey, H., Kargel, J.S., Fujita, K., Scheel, M. and Bajracharya, S., (2012). The state and fate of Himalayan glaciers.*Science* 336:310-314
- Bolch, T., Pieczonka, T., Mukherjee, K., & Shea, J. (2017). Brief communication: Glaciers in the Hunza catchment (Karakoram) have been nearly in balance since the 1970s. *The Cryosphere*, *11*, 531–539.
- Chen J, Wilson C, Tapley B. (2006). Satellite gravity measurements confirm accelerated melting of Greenland ice sheet.*Science*,**313**:1958-1960
- Chevallier, P., et al. (2011). "Snow cover dynamics and hydrological regime of the Hunza River basin, Karakoram Range, Northern Pakistan." *Hydrology and Earth System Sciences* **15**(7): 2259-2274.
- Cuffey, K. M. and Paterson, W. S. B. (2010) *The Physics of Glaciers*, Butterworth-Heinemann, Burlington, MA, USA, Forth edn. ISBN 9780123694614
- Dagnachew, M., Kebede, A., Moges, A., & Abebe, A. (2020). Land use land cover changes and its drivers in gibe river catchment, omo gibe basin, Ethiopia. *Journal of Agriculture and Environment for International Development*, **114**(1), 33–56
- Dagnachew, melku phd, et al. understanding soil quality, land use changes and climate

variability for effective watershed management, the case of gojeb river catchment, omo-gibe basin, ethiopia. diss. haramya university, 2020.

- Dahri Z. H., Ludwig F., Moors E., Ahmad S., Ahmad B., Ahmad S., Riaz M., Kabat P. (2021). Climate change and hydrological regime of the high-altitude Indus basin under extreme climate scenarios. *Science of The Total Environment*, Vol (768), 144467, ISSN 0048-9697, <https://doi.org/10.1016/j.scitotenv.2020.144467>.
- Denker, H. (2005). Evaluation of SRTM3 and GTOPO30 terrain data in Germany. *Gravity, Geoid and Space Missions* (pp. 218-223). Springer, Berlin, Heidelberg.
- Din, K., Tariq, S., Mahmood, A., & Rasul, G. (2014). Temperature and precipitation: GLOF triggering indicators in Gilgit-Baltistan, Pakistan. *Pakistan Journal of Meteorology*, **10**(20).
- Ebabu, K., Tsunekawa, A., Haregeweyn, N., Adgo, E., Meshesha, D. T., Aklog, D., Masunaga, T., Tsubo, M., Sultan, D., & Fenta, A. A. (2019). Effects of land use and sustainable land management practices on runoff and soil loss in the Upper Blue Nile basin, Ethiopia. *Science of the Total Environment*, **648**, 1462–1475.
- Endreny, T. A., Wood, E. F., & Hsu, A. (2000). Correction of errors in SPOT- Derived DEM's using GTOPO30 data. *IEEE transactions on geoscience and remote sensing*, **38**(3), 1234-1241.
- ERDENETUYA, M., et al. (2002). "Glacier change estimation using Landsat TM data."
- Evans, David JA, and Ian S. Evans. "Glacial processes and landforms." (2022).
- Farhan S. B., Zhang Y., Aziz A., Gao H., Ma Y., Kazmi J., Shahzad A., Hussain I., Mansha M., Umar M., Nasir J., Shafiq M., Farhan Y., Shaikh S., Zamir U. B., Asad F., Ahmed R. (2020). Assessing the impacts of climate change on the high altitude snow- and glacier-fed hydrological regimes of Astore and Hunza, the sub-catchments of Upper Indus Basin. *Journal of Water and Climate Change* 1

June 2020; 11 (2): 479–490. doi: <https://doi.org/10.2166/wcc.2018.107>.

- Farhan SB, Zhang Y, Ma Y, Guo Y, Ma N (2015). Hydrological regimes under the conjunction of westerly and monsoon climates: a case investigation in the Astore Basin, Northwestern Himalaya *Climate Dynamics* **44**:3015-3032.
- Farr, T.G., Rosen, P.A., Caro, E., Crippen, R., Duren, R., Hensley, S., Kobrick, M., Paller, M., Rodriguez, E., Roth, L. and Seal, D., (2007). The shuttle radar topography mission. *Reviews of geophysics*, **45**(2).
- Fenta, A. A., Yasuda, H., Haregeweyn, N., Belay, A. S., Hadush, Z., Gebremedhin, M. A., & Mekonnen, G. (2017). The dynamics of urban expansion and land use/land cover changes using remote sensing and spatial metrics: the case of Mekelle City of northern Ethiopia. *International Journal of Remote Sensing*, **38**(14), 4107–4129
- Fey, C., Wichmann, V., & Zangerl, C. (2017). Reconstructing the evolution of a deep seated rockslide (Marzell) and its response to glacial retreat based on historic and remote sensing data. *Geomorphology*, **298**, 72-85.
- Fick, S.E. and R.J. Hijmans (2017). WorldClim 2: new 1km spatial resolution climate surfaces for global land areas. *International Journal of Climatology* **37** (12): 4302-4315.
- Findell, K. L., Berg, A., Gentine, P., Krasting, J. P., Lintner, B. R., Malyshev, S., Santanello, J. A., & Shevliakova, E. (2017). The impact of anthropogenic land use and land cover change on regional climate extremes. *Nature Communications*, **8**(1), 1–10.
- Fowler, H. J., & Archer, D. R. (2005). Hydro-climatological variability in the Upper Indus Basin and implications for water resources. *Regional Hydrological Impacts of Climatic Change—Impact Assessment and Decision Making*, **295**,

131-138.

- Frauenfelder, R., & Kääb, A. (2009). Glacier mapping from multitemporal optical remote sensing data within the Brahmaputra river basin. In Proceedings of the 33rd International Symposium on Remote Sensing of Environment (pp. 4-8).
- Frey, H. (2011). Compilation and applications of glacier inventories using satellite data and digital terrain information, Geogr. Inst.
- Fujita K, Nuimura T (2011). Spatially heterogeneous wastage of Himalayan glaciers. Proceedings of the National Academy of Sciences *108*:14011-14014
- Gardelle J, Berthier E, Arnaud Y (2012). Slight mass gain of Karakoram glaciers in the early twenty-first century. Nature geoscience *5*:322-325
- Gardner, A. S., G. Moholdt, T. Scambos, M. Fahnestock, S. Ligtenberg, M. van den Broeke, and J. Nilsson (2018). Increased West Antarctic and unchanged East Antarctic ice discharge over the last 7 years, Cryosphere, **12**(2): 521–547
- Gardner, A., Fahnestock, M., and Scambos, T. (2019). ITS_LIVE regional glacier and ice sheet surface velocities, National Snow and Ice Data Center (NSIDC), <https://doi.org/10.5067/6II6VW8LLWJ7>.
- Garee K, Chen X, Bao A, Wang Y, Meng F. (2017). Hydrological Modeling of the Upper Indus Basin: A Case Study from a High-Altitude Glacierized Catchment Hunza. *Water*. *9*(1):17. <https://doi.org/10.3390/w9010017>.
- Gendreau, Madeline. "Using Remotely Sensed Data to Track Sít'Kusá (Turner Glacier) Surge Movement." (2022).
- Gong, B., Im, J., & Mountrakis, G. (2011). An artificial immune network approach to multi-sensor land use/land cover classification. Remote Sensing of Environment, **115**(2), 600–614.

- Gregory, I. N., Arts, and Service, H. D. S. H. D. (2003). A place in history: A guide to using GIS in historical research: Oxbow Oxford.
- Gubler, S., Hunziker, S., Begert, M., Croci-Maspoli, M., Konzelmann, T., Brönnimann, S., Schwierz, C., Oria, C. and Rosas, G., (2017). The influence of station density on climate data homogenization. *International journal of climatology*, **37**(13), 4670-4683.
- Haleem, Kashif & Ullah, Afed & Ahmad, Sohail & Khan, Ahmad & Khan, Wisal & Khan, Jehanzeb (2022). Hydrological impacts of climate and land-use change on flow regime variations in upper Indus basin. *Journal of Water and Climate Change*; 13 (2): 758–770. doi: <https://doi.org/10.2166/wcc.2021.238>.
- Harper, J. T. 1993: Glacier terminus fluctuations on Mount Baker, Washington, U.S.A., 1940-1990, and climatic variations. *Arctic and Alpine Research*, 25(4): 332-340.
- Hasson, S., Böhner, J., & Lucarin, V. (2017). Prevailing climatic trends and runoff response from Hindu Kush–Karakoram–Himalaya, upper Indus Basin. *Earth Syst Dyn* **8**: 337–355.
- Hasson, S.; Lucarini, V.; Khan, M.; Petitta, M.; Bolch, T.; Gioli, G. (2014). Early 21st century snow cover state over 5 the western river basins of the indus river system. *Hydrol. Earth Syst. Sci.*, 18, 4077–4100.
- Hayakawa, Yuichi S., Takashi Oguchi, and Zhou Lin. "Comparison of new and existing global digital elevation models: ASTER G-DEM and SRTM-3." *Geophysical Research Letters* 35.17 (2008).
- Herold, M., & Johns, T. (2007). Linking requirements with capabilities for deforestation monitoring in the context of the UNFCCC-REDD process. *Environmental Research Letters*, 2(4), 45025.

- Hewitt, Paul L., and Gordon L. Flett. "Perfectionism and depression: A multidimensional analysis." *Journal of social behavior and personality* 5.5 (1990): 423.
- Hewitt K (2005). The Karakoram anomaly? Glacier expansion and the elevation effect, *Karakoram Himalaya. Mountain Research and Development* 25:332-340
- Hewitt K (2011). Glacier change, concentration, and elevation effects in the Karakoram Himalaya, Upper Indus Basin. *Mountain Research and Development* 31:188-200
- Hewitt, K. (2009). Rock avalanches that travel onto glaciers and related developments, Karakoram Himalaya, Inner Asia. *Geomorphology*, **103**(1), 66-79.
- Hewitt, K., & Liu, J. (2010). Ice-dammed lakes and outburst floods, Karakoram Himalaya: historical perspectives on emerging threats. *Physical geography*, **31**(6), 528-551.
- Hijmans, R. J., Cameron, S. E., Parra, J. L., Jones, P. G., & Jarvis, A. (2005). Very high resolution interpolated climate surfaces for global land areas. *International Journal of Climatology: A Journal of the Royal Meteorological Society*, **25**(15), 1965-1978.
- Hoegh-Guldberg, O., D. Jacob, M. Taylor, M. Bindi, S. Brown, I. Camilloni, A. Diedhiou, R. Djalante, K.L. Ebi, F. Engelbrecht, J. Guiot, Y. Hijjoka, S. Mehrotra, A. Payne, S.I. Seneviratne, A. Thomas, R. Warren, and G. Zhou, 2018: Impacts of 1.5°C Global Warming on Natural and Human Systems. In: *Global Warming of 1.5°C*.
- Huggel, C., Käab, A., Haeberli, W., Teysseire, P., and Paul, F. (2002). Remote sensing based assessment of hazards from glacier lake outbursts: a case study in the Swiss Alps. *Canadian Geotechnical Journal*, **39**(2), 316-330.

- Hussain D., Kuo C.Y., Hameed A, Tseng K.H., Jan B., Abbas N., Kao H.C., Lan W.H., Imani M. (2019). Spaceborne Satellite for Snow Cover and Hydrological Characteristic of the Gilgit River Basin, Hindukush Karakoram Mountains, Pakistan. *Sensors (Basel)*. 2019 Jan 27;19(3):531. doi: 10.3390/s19030531.
- İkiel, C., & Ustaoglu, B. (2011). Sakarya Deltasının doğu kesiminde kıyı çizgisi değişiminin coğrafi bilgi sistemleri ve uzaktan algılama yöntemleriyle analizi. *Fiziki Coğrafya Araştırmaları*, 483–492
- IPCC, 2001: Thornes, J. E. (2002). Climate change 2001: impacts, adaptation and vulnerability, Contribution of Working Group II to the Third Assessment Report of the Intergovernmental Panel on Climate Change, edited by JJ
- McCarthy, OF Canziani, NA Jallat, H., Khokhar, M. F., Kudus, K. A., Nazre, M., Saqib, N. U., Tahir, U., & Khan, W. R. (2021). Monitoring carbon stock and land-use change in 5000-year-old juniper forest stand of ziarat, balochistan, through a synergistic approach. *Forests*, *12*(1), 1–15
- Mariye, Mehari, Melesse Maryo, and Jianhua Li. "The study of land use and land cover (LULC) dynamics and the perception of local people in Aykoleba, Northern Ethiopia." *African Journal of Environmental Science and Technology* 15.7 (2021): 282-297.
- Irfan M., Shafiq M., Khan M. (2020). Using Multi-Mission Satellite Elevation Data for Delineation of Gilgit Watershed in Pakistan in Geographical Information Technology Environment. *Int. J. Econ. Environ. Geol.* Vol. 11 (2) 19-24, 2020.
- Iverson, N. R. (2010). Shear resistance and continuity of subglacial till: hydrology rules. *Journal of Glaciology*, *56*(200), 1104-1114.
- Javed, ZH., Khan, S., Wahid, A., Ranjha, A. N., Hasan, M., (2020). Climate of the Gilgit-Baltistan Province, Pakistan. *International Journal of Economic and Environmental Geology*, *11*(3), 16-21.
- Jenson, S. K. (1991). Applications of hydrologic information automatically extracted from digital elevation models. *Hydrological Processes*, *5*(1), 31-44.
- Jenson, S. K., and Domingue, J. O. (1988). Extracting topographic structure from digital elevation data for geographic information system analysis. *Photogrammetric engineering and remote sensing*, *54*(11), 1593-1600.

- Jilani, R., Haq, M., & Naseer, A. Monitoring of Mountain Glacial Variations in Northern Pakistan, from 1992 to 2008 using Landsat and ALOS Data. Karachi: Pakistan Space & Upper Atmosphere Research Commission (SUPARCO).
- JPL-NASA (2014). U.S. Releases Enhanced Shuttle Land Elevation Data". JPL-Shuttle Radar Topography Mission. Retrieved 11 January 2020.
- Kanwal, S., Atif, S., and Shafiq, M. (2017). GIS based landslide susceptibility mapping of northern areas of Pakistan, a case study of Shigar and Shyok Basins. *Geometrics, Natural Hazards and Risk*, **8**(2), 348-366.
- Kargel JS, Cogley JG, Leonard GJ, Haritashya U, Byers A (2011). e. *Proceedings of the National Academy of Sciences* 108:14709-14710
- Karpilo Jr, R. D. (2009). "Glacier monitoring techniques." *Geological Monitoring: Boulder, Colorado, Geological Society of America.*—2009.—P: 141- 162.
- Khalid, S., et al. (2013). "Hydro-meteorological Characteristics of Indus River Basin at Extreme North of Pakistan." *J Earth Sci Clim Change* 5(1).
- Khattak, M. S., Babel, M. S., & Sharif, M. (2011). Hydro-meteorological trends in the upper Indus River basin in Pakistan. *Climate Research*, 46(2), 103–119. <http://www.jstor.org/stable/24872316>.
- Klare, M. T. (2020). Climate Change, Water Scarcity, and the Potential for Interstate Conflict in South Asia. *Journal of Strategic Security*, 13(4), 109-122.
- Kulkarni, A. V., Bahuguna, I. M., Rathore, B. P., Singh, S. K., Randhawa, S. S., Sood, R. K., & Dhar, S. (2007). Glacial retreat in Himalaya using Indian remote sensing satellite data. *Current science*, 69-74.
- Latif, Y., Ma, Y. & Ma, W. (2021). Climatic trends variability and concerning flow regime of Upper Indus Basin, Jehlum, and Kabul river basins Pakistan. *Theor Appl Climatol* 144, 447–468. <https://doi.org/10.1007/s00704-021-03529-9>.
- Latif, Y., Ma, Y., Ma, W., Muhammad, S., Adnan, M., Yaseen, M., & Fealy, R. (2020). Differentiating snow and glacier melt contribution to runoff in the Gilgit River basin via degree-day modeling approach. *Atmosphere*, **11**(10), 1023.
- Leary, DJ, Dokken and KS White (eds). Cambridge University Press, Cambridge, UK, and New York, USA, 2001. No. of pages: 1032. ISBN 0-521- 01500-6 (paperback), ISBN 0-521-80768-9 (hardback).
- Maitima, J.M., Mugatha, S.M., Reid, R.S., Gachimbi, L.N., Majule, A., Lyaruu, H., Pomery, D., Mathai, S. and Mugisha, S., (2009). The linkages between land use

- change, land degradation and biodiversity across East Africa. *African Journal of Environmental Science and Technology*, 3(10).
- Malinverni, E. S., Croci, C., & Sgroi, F. (2008). Glacier monitoring by remote sensing and GIS techniques in open source environment. *EARSeL eProceedings*, 7(2), 120.
- Mariye, M., Mariyo, M., Changming, Y., Teffera, Z. L., & Weldegebrial, B. (2020). Effects of land use and land cover change on soil erosion potential in Berhe district: A case study of Legedadi watershed, Ethiopia. *International Journal of River Basin Management*, 1–13
- Masson-Delmotte, V., P. Zhai, A. Pirani, S.L. Connors, C. Péan, S. Berger, N. Caud, Y. Chen, L. Goldfarb, M.I. Gomis, M. Huang, K. Leitzell, E. Lonnoy, J.B.R. Matthews, T.K. Maycock, T. Water field, O. Yelekçi, R. Yu, and B. Zhou (2021). IPCC, 2021: Summary for Policymakers. In: *Climate Change 2021: The Physical Science Basis. Contribution of Working Group I to the Sixth Assessment Report of the Intergovernmental Panel on Climate Change*. In Press.
- Matsuo K, Heki K (2010). Time-variable ice loss in Asian high mountains from satellite gravimetry. *Earth and Planetary Science Letters* 290:30-36.
- Mayer C, Lambrecht A, Mihalcea C, Belò M, Diolaiuti G, Smiraglia C, Bashir F (2010). Analysis of glacial meltwater in Bagrot Valley, Karakoram: based on short-term ablation and debris cover observationson Hinarche Glacier. *Mountain Research and Development* 30:169-177
- Mayer, C., Fowler, A. C., Lambrecht, A., & Scharrer, K. (2011). A surge of North Gasherbrum Glacier, Karakoram, China. *Journal of Glaciology*, 57(205), 904-916.
- Mayer, C., Lambrecht, A., Belo, M., Smiraglia, C., & Diolaiuti, G. (2006). Glaciological characteristics of the ablation zone of Baltoro glacier, Karakoram, Pakistan. *Annals of Glaciology*, 43, 123-131.
- Meraj, G., Romshoo, S. A., Ayoub, S., & Altaf, S. (2018). Geoinformatics based approach for estimating the sediment yield of the mountainous watersheds in Kashmir Himalaya, India. *Geocarto International*, 33(10), 1114–1138.
- Morello, Lauren. –Scientists Present a Complex Picture of Earth's 'Third Pole'. CIRUN - Environmental Change in the News, www.climateneeds.umd.edu/climatewire-09-14-12/article-26.php. Published: Thursday, September 13, 2012

- Morgado, P., Toger, M., Abrantes, P., & Fiegel, J. (2012). A bottom up approach to modeling habitat connectivity dynamics through networks analysis. *Sustainable Development—Authoritative and Leading Edge Content for Environmental Management*, 131-148.
- Mukhopadhyay, B., and Khan, A. (2015). A reevaluation of the snowmelt and glacial melt in river flows within Upper Indus Basin and its significance in a changing climate. *Journal of Hydrology*, 527, 119-132.
- Nabi G., Ullah S., Khan S., Ahmad, S., Kumar, S. (2018). China-Pakistan Economic Corridor (CPEC): melting glaciers –a potential threat to ecosystem and biodiversity. *Environmental Science and Pollution Research* 25: 3209 3210.
- Naeem, U. A., Shamim, M. A., Ejaz, N., ur Rehman, H., Mustafa, U., Hashmi, H. N., & Ghumman, A. R. (2016). Investigation of temporal change in glacial extent of Chitral watershed using Landsat data. *Environmental monitoring and assessment*, 188(1), 43.
- Ndegwa Mundia, C., & Murayama, Y. (2009). Analysis of land use/cover changes and animal population dynamics in a wildlife sanctuary in East Africa. *Remote Sensing*, 1(4), 952-970.
- New, M., Lister, D., Hulme, M., & Makin, I. (2002). A high-resolution data set of surface climate over global land areas. *Climate research*, 21(1), 1-25.
- Pareta, K., and Pareta, U. (2011). Quantitative morphometric analysis of a watershed of Yamuna basin, India using ASTER (DEM) data and GIS. *International journal of Geometrics and Geosciences*, 2(1), 248-269.
- Pareta, K., and Pareta, U. (2014). New watershed codification system for Indian river basins. *Journal of hydrology and environment research*, 2(1), 31- 40.
- Paul, F. (2000). Evaluation of different methods for glacier mapping using Landsat TM. *EARSel eProceedings*, 1(1), 239-245.
- Paul, F., Barrand, N.E., Baumann, S., Berthier, E., Bolch, T., Casey, K., Frey, H., Joshi, S.P., Konovalov, V., Le Bris, R. and Mölg, N. (2013). On the accuracy of glacier outlines derived from remote-sensing data. *Annals of Glaciology*, 54(63), pp.171-182.
- Paul, F., Strozzi, T., Schellenberger, T., & Kääb, A. (2017). The 2015 surge of Hispar Glacier in the Karakoram. *Remote Sensing*, 9(9), 888.

- Paul, F., Winsvold, S. H., Kääh, A., Nagler, T., & Schwaizer, G. (2016). Glacier remote sensing using Sentinel-2. Part II: Mapping glacier extents and surface faces, and comparison to Landsat 8. *Remote Sensing*, 8(7), 575.
- Qaisar, M., Shafiq, M., Ghauri, B. M. K., Younes, I., and Abuzar, M. K. (2019). Comparative Analysis of Different Remote Sensing Techniques for Mapping of Supraglacial Lakes on Hispar Glacier. *International Journal of Economic and Environmental Geology*, 9(2), 66-74.
- Quincey, D. J., et al. "Ice velocity and climate variations for Baltoro Glacier, Pakistan." *Journal of Glaciology* 55.194 (2009): 1061-1071.
- Racoviteanu, A. E., Armstrong, R., & Williams, M. W. (2013). Evaluation of an ice ablation model to estimate the contribution of melting glacier ice to annual discharge in the Nepal Himalaya. *Water Resources Research*, 49(9), 5117-5133.
- Rahim, I., Ali, S. M., and Aslam, M. (2018). GIS Based landslide susceptibility mapping with application of analytical hierarchy process in District Ghizer, Gilgit Baltistan Pakistan. *Journal of Geoscience and Environment Protection*, 6(2), 34-49.
- Rai, P. K., Mohan, K., Mishra, S., Ahmad, A., and Mishra, V. N. (2017). A GIS-based approach in drainage morphometric analysis of Kanhar River Basin, India. *Applied Water Science*, 7(1), 217-232.
- Rashid, I., & Abdullah, T. (2016). Investigation of temporal change in glacial extent of Chitral watershed using Landsat data: a critique. *Environmental monitoring & assessment*, 188(10), 1-5.
- Rasool, R., Fayaz, A., Shafiq, M. ul, Singh, H., & Ahmed, P. (2021). Land use land cover change in Kashmir Himalaya: Linking remote sensing with an indicator based DPSIR approach. *Ecological Indicators*, 125(January), 107447.
- Rasool, Umair, et al. "Evaluating the relationship between groundwater quality and land use in an urbanized watershed." *Environmental Science and Pollution Research* (2023): 1-20.
- Rasul, G., Chaudhry, Q. Z., Mahmood, A., & Hyder, K. W. (2011). Effect of temperature rise on crop growth and productivity. *Pak. J. Meteorology*, 8(15), 53-62.
- Rasul, G., Chaudhry, Q. Z., Mahmood, A., Hyder, K. W., & Dahe, Q. (2011). Glaciers and glacial lakes under changing climate in Pakistan. *Pakistan Journal of*

Meteorology, **8**(15), 01-08.

Rather, I. A., & Dar, A. Q. (2020). Assessing the impact of land use and land cover dynamics on water quality of Dal Lake, NW Himalaya, India. *Applied Water Science*, **10**(10), 1–18.

Rounce, David R., et al. "Global glacier change in the 21st century: Every increase in temperature matters." *Science* 379.6627 (2023): 78-83.

Raup, B., Kääb, A., Kargel, J.S., Bishop, M.P., Hamilton, G., Lee, E., Paul, F., Rau, F., Soltész, D., Khalsa, S.J.S. and Beedle, M. (2007). Remote sensing and GIS technology in the Global Land Ice Measurements from Space (GLIMS) project. *Computers & Geosciences*, **33**(1), pp.104-125.

Saary, J., et al. (2005). "A systematic review of contact dermatitis treatment and prevention." *Journal of the American Academy of Dermatology* 53(5): 845. e841- 845. e813.

Salomonson, V. V., & Appel, I. (2004). Estimating fractional snow cover from MODIS using the normalized difference snow index. *Remote sensing of environment*, **89**(3), 351-360.

Scherler D, Bookhagen B, Strecker MR (2011). Spatially variable response of Himalayan glaciers to climatechange affected by debris cover. *Nature geoscience* **4**:156-159

Schmidt S, Nüsser M (2012). Changes of high altitude glaciers from 1969 to 2010 in the Trans-HimalayanKang Yatze Massif, Ladakh, northwest India. *Arctic, Antarctic, and Alpine Research* **44**:107-121

Shafiq, M., Santos, B., Alexandra Perez, A., and Blank, C. (2011). Enhancing global climate data exchange to better monitor climate change and empower policy makers, scientists and the community. Paper presented at the 62nd International Astronautical Congress, Cape Town.

Shafiq, M., et al. "A geographical analysis of land use/land cover dynamics in Lolab watershed of Kashmir Valley, Western Himalayas using remote sensing and GIS." *J. Remote Sens. GIS* 6 (2017): 189.

Shafique, M., Faiz, B., Bacha, A. S., & Ullah, S. (2018). Evaluating glacier dynamics using temporal remote sensing images: a case study of Hunza Valley, northern Pakistan. *Environmental earth sciences*, **77**(5), 1-11.

- Shukla, A., et al. (2010). "Delineation of debris-covered glacier boundaries using optical and thermal remote sensing data." *Remote Sensing Letters* 1(1): 11-17.
- Sivalingam, Sivaranjani, et al. "Study of dynamics in surface ice flow rate of glaciers in Hunza basin, Karakoram." *Environmental Science and Pollution Research* 30.22 (2023): 62782-62802.
- Smith, T., Bookhagen, B., & Cannon, F. (2015). Improving semi-automated glacier mapping with a multi-method approach: applications in central Asia. *The Cryosphere*, 9(5), 1747-1759.
- Smith, Mark W., et al. "Aerodynamic roughness of glacial ice surfaces derived from high-resolution topographic data." *Journal of Geophysical Research: Earth Surface* 121.4 (2016): 748-766.
- SUPARCO, and ITP-CAS. (2017). Glacier Inventory of Pakistan (1st ed. Vol. 1): Pakistan Space and Upper Atmosphere Research Commission
- Tachikawa, T., Hato, M., Kaku, M., & Iwasaki, A. (2011). Characteristics of ASTER GDEM version 2. In 2011 IEEE international geoscience and remote sensing symposium (pp. 3657-3660). IEEE.
- Tahir, A. A. (2011). Impact of climate change on the snow covers and glaciers in the Upper Indus River basin and its consequences on the water reservoirs (Tarbela reservoir)–Pakistan, Montpellier 2.
- Tasseti, Nora, Annamaria Bernardini, and Eva Savina Malinverni. "Use of remote sensing data and GIS technology for assessment of landslide hazards in Susa valley, Italy." *EARSeL eProceedings* 7.1 (2008): 59-67.
- Taylor, R. G. (2016). A comparison of mixed integer programming and a heuristic approach for harvest blocking in Australia: Mississippi State University.
- USGS EROS (1996) Digital Elevation - Global 30 Arc-Second Elevation (GTOPO30), DOI number: 10.5066/F7DF6PQS Retrieved 11 January 2020.
- Usman Ali Naeem, Muhammad Ali Shamim, Naeem Ijaz, Abdul Razzaq Ghumman (2015). Investigation of temporal change in glacial extent of Chitral watershed using Landsat data. *Environmental Monitoring and Assessment*, 188, Article number: 43 (2016)
- Umar, Sheikh, M. A. Lone, and Narendra Kumar Goel. "Modeling of annual rainfall extremes in the Jhelum River basin, North Western Himalayas." *Sustainable Water Resources Management* 7 (2021): 1-13.

- Veettil, B. K. (2012). "A Remote sensing approach for monitoring debris- covered glaciers in the high altitude Karakoram Himalayas." *International Journal of Geometrics and Geosciences* 2(3): 833-841.
- Vuille, M., & Bradley, R. S. (2000). Mean annual temperature trends and their vertical structure in the tropical Andes. *Geophysical Research Letters*, **27**(23), 3885-3888.
- Vuille, M., Francou, B., Wagnon, P., Juen, I., Kaser, G., Mark, B. G., & Bradley, R. S. (2008). Climate change and tropical Andean glaciers: Past, present and future. *Earth-science reviews*, **89**(3-4), 79-96.
- Wakode, H. B., Dutta, D., Desai, V., Baier, K., and Azzam, R. (2013). Morphometric analysis of the upper catchment of Kosi River using GIS techniques. *Arabian Journal of Geosciences*, **6**(2), 395-408.
- Willhauck, G., Schneider, T., De Kok, R., & Ammer, U. (2000). Comparison of object oriented classification techniques and standard image analysis for the use of change detection between SPOT multispectral satellite images and aerial photos. In *Proceedings of XIX ISPRS congress* (Vol. 33, pp. 35-42). Amsterdam: IAPRS.
- Xu, Xiaoqian, et al. "Assessment of interannual and seasonal glacier mass changes in the Karakoram during 2018–2022 using ICESat-2 data." *Journal of Hydrology* 626 (2023): 130223.
- Yaduvanshi, A., & Ranade, A. (2015). Effect of global temperature changes on rainfall fluctuations over river basins across Eastern Indo- Gangetic plains. *Aquatic Procedia*, **4**, 721-729.
- Yang, C., Everitt, J. H., & Murden, D. (2011). Evaluating high resolution SPOT 5 satellite imagery for crop identification. *Computers and Electronics in Agriculture*, **75**(2), 347–354.
- Yao, T., Thompson, L., Yang, W., Yu, W., Gao, Y., Guo, X., ... & Joswiak, D. (2012). Different glacier status with atmospheric circulations in Tibetan Plateau and surroundings. *Nature climate change*, **2**(9), 663-667.
- Yi, Shuang, and Wenke Sun. "Evaluation of glacier changes in high-mountain Asia based on 10 year GRACE RL05 models." *Journal of Geophysical Research: Solid Earth* 119.3 (2014): 2504-2517.
- Zemp M, Hoelzle M, Haeberli W (2009). Six decades of glacier mass-balance

observations: a review of the world wide monitoring network. *Annals of Glaciology* 50:101-111.

Zhang, Yong, et al. "Distribution of debris thickness and its effect on ice melt at Hailuogou glacier, southeastern Tibetan Plateau, using in situ surveys and ASTER imagery." *Journal of Glaciology* 57.206 (2011): 1147-1157.

Zhen, X., and Li, J., (1998). Remote Sensing monitoring of glaciers, snow and lake ice in Qinghai-Xizang (Tibetan) Plateau and their Influence on Environments, edited by M. Tang, G. Cheng and Z. Lin (Guangzhou, China: Guangdong Sciences and Technology Press) pp.279-308.